

# Influence of Humic Acid on the Sorption of Uranium(VI) and Americium(III) onto Kaolinite

Adéla Křepelová

Juli 2007

Wissenschaftlich-Technische Berichte  
**FZD-475**  
Juli 2007

Adéla Křepelová

**Influence of Humic Acid on the Sorption  
of Uranium(VI) and Americium(III) onto Kaolinite**



**Forschungszentrum  
Dresden** Rossendorf

**Influence of Humic Acid on the Sorption of Uranium(VI)  
and Americium(III) onto Kaolinite**

DISSERTATION

Zur Erlangung des akademischen Grades

Doctor rerum naturalium

(Dr. rer. nat.)

vorgelegt:

der Fakultät Mathematik und Naturwissenschaften

der Technischen Universität Dresden

von

Dipl.-Ing. Adéla Křepelová

geboren am 02.10.1976 in Pelhřimov, Tschechische Republik

Gutachter: Prof. Dr. habil. Gert Bernhard

Prof. Dr. Tobias Reich

Prof. Ing. Petr Beneš, Dr.Sc.

Eingereicht am: 02.02.2007

Tag der Verteidigung: 18.06.2007







## ***Contents***

Index of Used Abbreviations and Symbols

Summary/Zusammenfassung

<b>1. INTRODUCTION</b> .....	<b>1</b>
<b>2. KAOLINITE</b> .....	<b>3</b>
<b>2.1. Clays and Clay Minerals</b> .....	<b>3</b>
<b>2.2. Kaolinite Properties</b> .....	<b>6</b>
<b>2.3. Characterization of Kaolinite KGa-1b</b> .....	<b>9</b>
2.3.1. Chemical Composition.....	9
2.3.2. Structural and Mineralogical Analysis.....	10
2.3.3. Cation Exchange Capacity .....	12
2.3.4. Surface Area.....	13
<b>3. HUMIC SUBSTANCES</b> .....	<b>14</b>
<b>3.1. Properties of Humic Substances</b> .....	<b>14</b>
<b>3.2. Characterization of Humic Acid Type M42</b> .....	<b>17</b>
<b>4. U(VI)-SPECIATION IN AQUEOUS SOLUTION</b> .....	<b>19</b>
<b>4.1. Chemical Properties of Uranium</b> .....	<b>19</b>
<b>4.2. U(VI) Speciation in Presence of Inorganic Ligands</b> .....	<b>20</b>
<b>4.3. U(VI) Speciation in Presence of Humic Acid</b> .....	<b>23</b>
<b>5. HUMIC ACID SORPTION ONTO KAOLINITE</b> .....	<b>26</b>
<b>5.1. Kinetics of Humic Acid Sorption onto Kaolinite</b> .....	<b>27</b>
<b>5.2. Sorption Capacity of Kaolinite for Humic Acid</b> .....	<b>28</b>
<b>5.3. Effect of pH and Humic Acid Concentration</b> .....	<b>28</b>
<b>5.4. Influence of Ionic Strength</b> .....	<b>31</b>
<b>5.5. Effect of CO<sub>2</sub>-Presence</b> .....	<b>32</b>
<b>5.6. Influence of U(VI)-Presence</b> .....	<b>33</b>
<b>5.7. Binding of Humic Acid on Kaolinite Surface</b> .....	<b>35</b>
<b>6. U(VI) SORPTION ONTO KAOLINITE</b> .....	<b>37</b>
<b>6.1. Actinide Interactions with Solid Surfaces</b> .....	<b>37</b>
<b>6.2. Kinetics of U(VI) Sorption onto Kaolinite</b> .....	<b>41</b>
<b>6.3. Effect of pH and U(VI) Concentration</b> .....	<b>42</b>

<b>6.4. Influence of Ionic Strength.....</b>	<b>43</b>
<b>6.5. Effect of CO<sub>2</sub>-Presence .....</b>	<b>44</b>
<b>6.6. Effect of Size Fractionation of Kaolinite.....</b>	<b>46</b>
<b>6.7. Effect of Sample Filtration on the Results.....</b>	<b>47</b>
<b>6.8. Effect of Conditioning on the Kaolinite .....</b>	<b>48</b>
<b>7. INFLUENCE OF HUMIC ACID ON THE U(VI) SORPTION ONTO KAOLINITE .....</b>	<b>52</b>
<b>7.1. Kinetics of U(VI) Sorption onto Kaolinite in Presence of Humic Acid.....</b>	<b>53</b>
<b>7.2. U(VI) Sorption in Presence of Humic Acid .....</b>	<b>55</b>
<b>8. STRUCTURE DETERMINATION OF U(VI)-KAOLINITE SURFACE COMPLEXES IN ABSENCE AND PRESENCE OF HUMIC ACID .....</b>	<b>59</b>
<b>8.1. U(VI)-Humic Acid-Kaolinite Surface Complexes Studied by EXAFS .....</b>	<b>59</b>
8.1.1. Principles of X-ray Absorption Spectroscopy.....	60
8.1.2. Sample Preparation.....	64
8.1.3. EXAFS Analysis .....	65
8.1.4. Effect of pH .....	72
8.1.5. Influence of CO <sub>2</sub> at pH 8.5 .....	73
8.1.6. Effect of Humic Acid Presence .....	74
8.1.7. Comparison of EXAFS Results of the Binary and the Ternary Systems .....	75
<b>8.2. U(VI) Surface Complexation in the Systems U(VI)-Kaolinite and U(VI)-Humic Acid-Kaolinite Studied by TRLFs.....</b>	<b>78</b>
8.2.1. Laser Fluorescence Spectroscopy.....	78
8.2.2. Sample Preparation and Data Evaluation .....	84
8.2.3. Surface Complexation of U(VI) on Kaolinite in Absence of Humic Acid.....	87
8.2.4. Surface Complexation of U(VI) on Kaolinite in Presence of Humic Acid .....	90
8.2.5. Comparison of Results of the Binary and the Ternary Systems.....	93
8.2.6. Comparison of Results with Model Systems.....	94
<b>8.3. Surface Speciation Model Development .....</b>	<b>96</b>
8.3.1. System U(VI)-Kaolinite .....	96
8.3.2. U(VI)-Humic Acid-Kaolinite System .....	97
8.3.3. Conclusions .....	98
<b>9. INFLUENCE OF HUMIC ACID ON THE AM(III) SORPTION ONTO KAOLINITE ....</b>	<b>99</b>
<b>9.1. Americium Chemistry in Solution.....</b>	<b>99</b>
<b>9.2. Kinetics of Am(III) Sorption onto Kaolinite.....</b>	<b>102</b>
<b>9.3. Am(III) Sorption onto Kaolinite in Absence and Presence of Humic Acid.....</b>	<b>102</b>
9.3.1. Comparison of Am(III) and U(VI) Sorption Results.....	105
<b>9.4. Surface Complexation of Am(III) on Kaolinite in Absence and Presence of Humic Acid.....</b>	<b>106</b>
9.4.1. Sample Preparation and Data Evaluation .....	108
9.4.2. Results of Fluorescence Measurements.....	109



<b>10. EXPERIMENTAL PART.....</b>	<b>113</b>
<b>10.1. Materials.....</b>	<b>113</b>
<b>10.2. Experimental Procedures.....</b>	<b>114</b>
10.2.1. Kinetic Experiments.....	114
10.2.2. Sorption Experiments.....	115
<b>10.3. Instruments and Methods.....</b>	<b>116</b>
10.3.1. Analysis of U(VI) Concentration.....	116
10.3.2. Analysis of Humic Acid and Am(III) Concentration.....	117
10.3.3. Speciation Calculations.....	117
10.3.4. Structure Analysis of Kaolinite by Infrared Spectroscopy.....	117
10.3.5. Structure Analysis of Kaolinite by X-Ray Diffraction Spectroscopy.....	117
10.3.6. X-Ray Photoelectron Spectroscopy Measurements.....	118
10.3.7. Cation Exchange Capacity Measurement.....	118
10.3.8. Kaolinite Surface Area Measurement.....	118
10.3.9. EXAFS Measurements.....	118
10.3.10. Laser Fluorescence Measurements.....	119
10.3.11. Measuring of pH.....	121
10.3.12. Experiments under CO <sub>2</sub> -Free Atmosphere.....	121
10.3.13. Shaking of the Samples.....	121
10.3.14. Centrifugation of the Samples.....	121
10.3.15. Filtration of the Samples.....	121
<b>11. REFERENCES.....</b>	<b>122</b>

## ***Index of Used Abbreviations and Symbols***

%	Percent
°C	Degree Celsius
Å	Angström
AFFFF	Asymmetrical Flow Field-Flow Fractionation
atm	Atmosphere
ATR	Attenuated Total Reflection
atom%	Atom percent
ax	Axial
BET	Brunauer-Emmet-Teller
BMWi	Federal Ministry of Economics and Technology
CEC	Cation Exchange Capacity
CLSM	Confocal Laser Scanning Microscopy
CMS	Clay Mineral Society
DDLm	Diffuse Double Layer Model
DLVO	Derjaguin-Landau-Verwey-Overbeek
$\Delta E_0$	Energy phase shift
EDTA	Ethylenediaminetetraacetic acid
e.g.	For example
ESRF	European Synchrotron Radiation Facility
eq	Equatorial
et al.	And others
etc.	And so on
eV	Electron volt
EXAFS	Extended X-ray Absorption Fine Structure
FA	Fulvic Acid(s)
Fig.	Figure

FT	Fourier Transform
FTIR	Fourier Transform Infrared Spectroscopy
fs-TRLFS	Time-resolved Laser-induced Fluorescence Spectroscopy with ultrafast pulses
FZK-INE	Forschungszentrum Karlsruhe – Institut für Nukleare Entsorgung
FZD	Forschungszentrum Dresden-Rossendorf
h	Hour(s)
HA	Humic Acid(s)
H-bonds	Hydrogen bonds
HS	Humic Substances
I	Ionic strength
ICP-MS	Inductively Coupled Plasma Mass Spectroscopy
i.e.	That is
IEP	Isoelectric Point
IR	Infrared spectroscopy
K <sub>d</sub>	Distribution coefficient
L <sub>III</sub>	Characteristic Roentgen line of L <sub>III</sub> -edge
LIBD	Laser-induced Breakdown Spectroscopy
LIPAS	Laser-induced Photoacoustic Spectroscopy
LSC	Liquid Scintillation Counting
M	Molarity
MBq/g	Megabequerel per gram
meq/g	Milliequivalent per gram
min	Minute(s)
m <sup>2</sup> /g	Square meter per gram
mg/L	Milligram per liter
MS	Multiple Scattering

N	Coordination number
nm	Nanometer
NOM	Natural Organic Matter
p.a.	pro analysi
PCA	Polycarboxylic Acids
pCO <sub>2</sub>	Partial pressure of CO <sub>2</sub>
PEC	Proton Exchange Capacity
pH	Negative logarithm (base 10) of H <sup>+</sup> activity in solution
PP	Polypropylene
ppm	Parts per million
p.z.c.	Point of zero charge
p.z.n.p.c.	Point of zero net proton charge
R	Interatomic distance
RDF	Radial Distribution Function
ROBL	Rosendorf Beamline
rpm	Rotations per minute
s	Second(s)
SCM	Surface Complexation Model
SEM	Scanning Electron Microscopy
S/L	Solid/Liquid ratio
t <sub>1/2</sub>	Decay half-life
Tab.	Table
TLSCM	Triple-Layer Surface Complexation Model
TRLFS	Time-Resolved Laser-Induced Fluorescence Spectroscopy
TOC	Total Organic Carbon
TOF-SIMS	Time-Of-Flight Secondary Ion Mass Spectroscopy
UV	Ultra-Violet

Vis	Visible
wt. %	Weight percent
XAS	X-ray Absorption Spectroscopy
XANES	X-ray Absorption Near-Edge Structure
XPS	X-ray Photoelectron Spectroscopy
XRD	X-Ray Diffraction
y	Year(s)
2SPNE SC/CE	2 Site Protolysis Non Electrostatic Surface Complexation and Cation Exchange
$\beta$	Complexation constant or equilibrium constant
$\mu\text{g}$	Microgram
$\mu\text{m}$	Micrometer
$\mu\text{l}$	Microliter
$\lambda$	Wavelength
$\pi$	Covalent bond
$\sigma$	Standard deviation
$\sigma^2$	Debye-Waller factor
$\tau$	Fluorescence life time
$\chi(k)$	EXAFS-function

## ***Summary***

The migration behavior of actinides in the environment is influenced by different materials and processes dependent on geochemical conditions. An important mechanism for retarding actinide migration in the natural environment is the sorption onto minerals present along groundwater flow path. By the sorption of humic acid (HA) onto minerals and by the formation of soluble complexes with actinides, HA can affect the transport behavior of these contaminants.

The aim of this work was to study the influence of HA on the sorption of U(VI) onto kaolinite. Therefore, the batch experiments were performed to determine the U(VI) sorption onto kaolinite in the absence and presence of HA. First of all, applied kaolinite KGa-1b was characterized. The X-ray diffraction spectrum showed typical reflections for kaolinite. From infrared spectroscopy, a typical IR-spectrum for well-crystallized kaolinite comparable to literature data resulted. From chemical analysis, the composition of kaolinite KGa-1b was calculated. The kaolinite contains mainly 47.85% Al<sub>2</sub>O<sub>3</sub>, 42.98% SiO<sub>2</sub> and trace abundance of TiO<sub>2</sub> (1.45%). The cation exchange capacity and the surface area measurements yielded the values of 1.83 meq/100 g and 11.8 m<sup>2</sup>/g, respectively.

Kinetic experiments were conducted to evaluate the time which U(VI) and HA required to reach the sorption steady state. It was shown that the sorption steady state was reached very fast in all studied systems. The contact time for batch experiments was set to 60 h. Also, in the system U(VI)-HA-kaolinite, the effect of the sequence of U(VI) and HA addition to the kaolinite suspension was studied, but no significant influence was observed.

The effects of different experimental parameters (i.e., pH, HA concentration, ionic strength, CO<sub>2</sub>-presence, and U(VI)-presence) on the HA sorption onto kaolinite were studied. The HA sorption decreases with increasing pH value because of electrostatic repulsions between deprotonated negatively charged carboxyl groups of HA and the negative charge of the kaolinite surface. The sorption of HA decreases with increasing initial concentration of HA due to saturation of binding sites of kaolinite. The dependence of HA sorption on CO<sub>2</sub>-presence and U(VI)-presence was observed and the influence of the ionic strength at lower HA concentration was identified. X-ray photoelectron spectroscopy (XPS) measurements of HA sorbed onto kaolinite gave an important result, namely that HA does not sorb as a homogenous layer onto kaolinite and, instead, is located between kaolinite particles.

The sorption of U(VI) onto kaolinite is influenced by the pH, presence of CO<sub>2</sub>, U(VI) concentration, and HA-presence. In the absence of CO<sub>2</sub> the U(VI) sorption increases with increasing pH up to pH ~ 6 and then with increasing pH value it remains constant. The formation of negatively charged uranyl-carbonato complexes causes a decrease of the U(VI) sorption onto the negatively charged surface of kaolinite above pH 8 in the presence of CO<sub>2</sub>. An increase of the U(VI) concentration from 1·10<sup>-6</sup> M to 1·10<sup>-5</sup> M resulted in a shift of the sorption edge in pH scale by one unit higher, whereas the ionic strength has only a slight influence on the U(VI) sorption onto kaolinite. HA influences the U(VI) sorption significantly. HA enhances the U(VI) uptake in the acidic pH range (pH 3 – pH 5.5) compared to the system without HA due to the formation of additional binding sites for U(VI) coming from HA adsorbed onto kaolinite. The formation of dissolved uranyl-humate complexes reduced the U(VI) sorption in the near-neutral pH range. The presence of HA can enhance the U(VI) migration under environmentally relevant conditions. Therefore, HA has to be involved in model calculations for the assessment of the long-term safety of nuclear waste repositories.

X-ray absorption spectroscopy and laser fluorescence spectroscopy were applied for the first time to characterize the formed U(VI)-HA-kaolinite surface complexes. Extended X-ray absorption fine structure (EXAFS) measurements with U(VI)-HA-kaolinite sorbates were performed to determine the influence of the HA, pH, and CO<sub>2</sub>-presence on the U(VI)-kaolinite surface complexes. The results were compared with literature data of the binary system U(VI)-kaolinite. The structural model for fitting the EXAFS oscillations was derived from EXAFS investigations of the binary system U(VI)-kaolinite. The best fits of the measured EXAFS oscillations in the studied ternary system were obtained considering two uranium-oxygen coordination shells with two axial and five equatorial coordinated oxygen atoms, multiple scattering along the uranyl unit and two coordination shells each with one Al/Si atom. The inner-sphere sorption of U(VI) by edge-sharing with aluminol octahedra and/or silicon tetrahedra in the binary as well as in the ternary system was identified. Contrary to the binary system, no influence of pH and CO<sub>2</sub> on the EXAFS structural parameters was observed in the studied ternary system. Equally, no effect of HA on the EXAFS structural parameters in the system U(VI)-HA-kaolinite was found. Furthermore, it was determined that, in spite of HA-presence, U(VI) prefers to adsorb onto kaolinite directly than via HA.

The time-resolved laser-induced fluorescence spectroscopy (TRLFS) was applied to study the kind of U(VI) surface complexes on kaolinite in the absence and presence of HA. The measurements were performed at four different pH values (5, 6, 7, 8). In the binary system U(VI)-kaolinite, two U(VI)-surface species were identified on kaolinite, which differ in the amount of water molecules in their coordination environment. The obtained fluorescence lifetimes of the binary system were compared with fluorescence lifetimes of the model systems U(VI)-gibbsite and U(VI)-silica gel. The values of fluorescence lifetimes of both U(VI)-surface species on kaolinite lie in the range between values obtained for both model systems. Nevertheless, the fluorescence lifetimes of species on kaolinite are closer to those on gibbsite than on silica gel. The aluminol binding sites are assumed to control the sorption of U(VI). HA decreases the fluorescence intensity and the fluorescence lifetimes of both identified species. In the presence of HA, the hydration shell of U(VI) is partly displaced by HA. TRLFS measurements confirmed the conclusion from the EXAFS measurements that U(VI) prefers to bind to kaolinite directly than via HA. No significant effect of pH values on the fluorescence lifetimes was observed.

The first sorption experiments to study the influence of pH value and HA-presence on Am(III) sorption onto kaolinite were performed. In the absence of HA, Am(III) exhibits a very strong sorption onto kaolinite under given experimental conditions. It is almost independent on the pH value. In the presence of HA, there are small differences in the Am(III) sorption in comparison to the system without HA. At pH values  $< 5$ , HA enhances very slightly the sorption of Am(III). Conversely, at pH values  $\geq 5.5$  the presence of HA decreases the sorption of Am(III) in comparison to the system without HA due to formation of Am(III)-humate complexes.

Laser fluorescence spectroscopy measurements were carried out in the systems Am(III)-kaolinite and Am(III)-HA-kaolinite to study the surface complexation of Am(III) on kaolinite at different pH values. In the binary system Am(III)-kaolinite, no influence of pH on the fluorescence intensity was observed, while in the ternary system Am(III)-HA-kaolinite, a reduction of the fluorescence intensity with increasing pH values was found. Similarly to the U(VI)-system, the fluorescence intensity of the samples of the ternary system decreased in comparison to the samples of the binary system. For both systems, binary and ternary, fluorescence spectra were measured, which differ from the fluorescence spectrum of Am(III) in solution. Further measurements are required to satisfactorily explain the obtained results.



The results obtained in this work contribute to a better understanding of the geochemical interactions of actinides (especially U(VI)) in the environment. Consequently, more reliable predictions of actinides migration, essential for the safety assessment of nuclear waste repository, can be made.

## **Zusammenfassung**

Das Migrationsverhalten der Actiniden in der Natur wird von unterschiedlichen Prozessen und Substanzen beeinflusst. Dazu gehören Sorptionsprozesse an Mineralien die eine Retardation der Actinidenmigration bewirken können. Huminsäuren (HS) sind in der Lage durch ihre Sorption an Mineralien und durch die Bildung gelöster Actinid-Humat-Komplexe das Transportverhalten der Actiniden zu beeinflussen.

Ziel dieser Arbeit war das Studium des Einflusses von HS auf die U(VI)-Sorption an Kaolinit. Dazu erfolgten Batchexperimente zur Bestimmung der U(VI)-Sorption an Kaolinit in Gegenwart und in Abwesenheit von HS. Der für die Experimente eingesetzte Kaolinit KGa-1b wurde hinsichtlich wesentlicher Eigenschaften charakterisiert. Das Röntgendiffraktionspektrum zeigte typische Reflexe für Kaolinit. Mittels Infrarot-Spektroskopie wurde ein IR-Spektrum gemessen, das typisch für einen gut-kristallisierten Kaolinit und vergleichbar zur Literatur ist. Die Zusammensetzung des Kaolinit KGa-1b wurde aus der chemischen Analyse ermittelt. Der Kaolinit enthält hauptsächlich 47.85%  $\text{Al}_2\text{O}_3$ , 42.98%  $\text{SiO}_2$  und Spuren Mengen an  $\text{TiO}_2$  (1.45%). Die Kationenaustauschkapazität beträgt 1.83 meq/100 g. Die spezifische Oberfläche wurde mit  $11.8 \text{ m}^2/\text{g}$  bestimmt.

Es wurden kinetische Experimente durchgeführt, um die Zeit zu bestimmen, in der die U(VI)- und HS-Sorption an Kaolinit einen stationären Zustand erreicht hat. Die Ergebnisse zeigten, dass sich ein stationärer Zustand in allen untersuchten Systemen sehr schnell einstellt. Die Kontaktzeit für Batchexperimente wurde auf 60 Stunden angesetzt. Für das System U(VI)-HS-Kaolinit wurde zusätzlich der Einfluss der Reihenfolge der U(VI)- und HS-Zugabe zur Kaolinit suspension untersucht. Es wurde festgestellt, dass diese jedoch keinen signifikanten Effekt auf den stationären Zustand ausübt.

Der Einfluss verschiedener experimenteller Parameter (pH, HS-Konzentration, Ionenstärke,  $\text{CO}_2$ -Gegenwart und U(VI)-Gegenwart) auf die HS-Sorption an Kaolinit wurde untersucht. Die HS-Sorption nimmt mit steigendem pH-Wert ab, was auf die elektrostatische Abstoßung zwischen den negativ geladenen Carboxylgruppen der HS und der negativ geladenen Kaolinitoberfläche zurückzuführen ist. Aufgrund der Sättigung der Bindungsstellen am Kaolinit, sinkt die Sorption von HS mit steigender HS-Ausgangskonzentration. Eine Abhängigkeit der HS-Sorption von der  $\text{CO}_2$ - und U(VI)-Gegenwart wurde beobachtet und ein Einfluss der Ionenstärke

auf die HS-Sorption bei niedriger HS-Konzentration wurde bestimmt. Photoelektronenspektroskopische Messungen ergaben, dass die HS nicht als homogene Schicht auf der Kaolinitoberfläche sorbiert ist, sondern sich auch zwischen den Kaolinitteilchen befindet.

Die U(VI)-Sorption an Kaolinit wird vom pH-Wert, der Gegenwart von CO<sub>2</sub>, der U(VI)-Konzentration und der Gegenwart von HS beeinflusst. Mit steigendem pH-Wert nimmt die U(VI)-Sorption in Abwesenheit von CO<sub>2</sub> bis pH ~ 6 zu und bleibt dann mit zunehmendem pH-Wert konstant. In Gegenwart von CO<sub>2</sub> und bei pH-Werten > 8 bewirkt die Bildung negativ geladener Uranyl-Carbonato-Komplexe eine Abnahme der U(VI)-Sorption an der negativ geladenen Kaolinitoberfläche. Die Zunahme der U(VI)-Konzentration von 1·10<sup>-6</sup> M auf 1·10<sup>-5</sup> M führte zur Verschiebung der Sorptionskante zu höheren pH-Werten, wobei die Ionenstärke nur einen leichten Einfluss auf die U(VI)-Sorption an Kaolinit hat. Die U(VI)-Sorption am Kaolinit wird durch HS beeinflusst. In Gegenwart von HS wurde eine Erhöhung der U(VI)-Sorption im sauren pH Bereich (pH 3 – pH 5.5) beobachtet, was auf die Bildung zusätzlicher U(VI)-Bindungsstellen durch die HS-Sorption am Kaolinit zurückzuführen ist. Die Ergebnisse zeigen, dass die Bildung gelöster Uranyl-Humat-Komplexe die U(VI)-Sorption im neutralen pH-Bereich verringern kann, was zu einer erhöhten Mobilität von U(VI) unter naturnahen Bedingungen führen kann. Aufgrund dessen sind Wechselwirkungsprozesse von HS in Modellrechnungen zur Beurteilung der Sicherheit von Endlagern für radioaktive Abfälle miteinzubeziehend.

Zur Charakterisierung von U(VI)-HS-Oberflächenkomplexen an Kaolinit wurden erstmals röntgenabsorptions- und laserfluoreszenzspektroskopische Untersuchungen durchgeführt. Mittels EXAFS-Spektroskopie wurde der Einfluss von HS, pH und CO<sub>2</sub>-Gegenwart auf die U(VI)-Kaolinit-Oberflächenkomplexe untersucht und die Ergebnisse mit denen des binären Systems U(VI)-Kaolinit verglichen. Das Strukturmodell zur Anpassung der EXAFS-Oszillationen wurde aus EXAFS-Messungen am binären System U(VI)-Kaolinit abgeleitet. Die beste Anpassung der EXAFS-Oszillationen im studierten ternären System erfolgte unter Berücksichtigung von zwei Uran-Sauerstoff-Koordinationsschale mit zwei axial und fünf äquatorial koordinierten Sauerstoffatomen, Mehrfachstreueffekten entlang der Uranyleinheit und zwei U-Si- oder U-Al-Koordinationsschalen mit jeweils einem Atom. Vergleichbar zum binären System wurde für das ternäre System eine inner-sphärische Sorption von U(VI) identifiziert, wobei das Uran mit der Kante eines Siliziumoktaeders und/oder Aluminiumtetraeders verknüpft ist. Im Gegensatz zum binären System wurde für das ternäre System kein Einfluss des pH-Wertes und der Gegenwart

von CO<sub>2</sub> auf die EXAFS-Strukturparameter beobachtet. Ebenso wurde kein Einfluss von HS auf die Strukturparameter gefunden. Die Ergebnisse deuten darauf hin, dass auch in Gegenwart von HS, U(VI) bevorzugt direkt am Kaolinit sorbiert und nicht über die HS gebunden wird.

Mittels zeitaufgelöster laser-induzierter Fluoreszenzspektroskopie (TRLFS) wurden U(VI)-Oberflächenkomplexe am Kaolinit in Abwesenheit und Gegenwart von HS bestimmt. Die Messungen erfolgten bei vier verschiedenen pH-Werten (pH 5, 6, 7, 8). Für das binäre System U(VI)-Kaolinit wurden zwei U(VI)-Oberflächenspezies detektiert, die sich in der Anzahl an Wassermolekülen in ihrer Koordinationsumgebung unterscheiden. Die bestimmten Fluoreszenzlebensdauern wurden mit Fluoreszenzlebensdauern der Modellsysteme U(VI)-Gibbsit und U(VI)-Kieselgel verglichen. Die im System U(VI)-Kaolinit gemessenen Fluoreszenzlebensdauern liegen zwischen den Werten für beide Modellsysteme, dennoch sind die Fluoreszenzlebensdauern der U(VI)-Oberflächenspezies am Kaolinit näher der Fluoreszenzlebensdauern der U(VI)-Oberflächenspezies am Gibbsit. Das weist darauf hin, dass die Aluminol-Bindungsstellen die U(VI)-Sorption am Kaolinit bestimmen. In Gegenwart von HS werden die Fluoreszenzintensität und die Fluoreszenzlebenszeiten von den beiden identifizierten U(VI)-Oberflächenspezies reduziert. Ursache dafür ist ein teilweiser Austausch von Wassermolekülen aus der Hydrathülle vom U(VI) gegen HS. Die TRLFS-Messungen bestätigten die Schlussfolgerung aus den EXAFS-Untersuchungen, dass U(VI) eine direkte Bindung am Kaolinit gegenüber eine Bindung über die HS bevorzugt. Es wurde kein signifikanter Einfluss des pH-Wertes auf die Fluoreszenzlebenszeiten beobachtet.

Erste Sorptionsuntersuchungen zum Einfluss von pH-Wert und HS-Gegenwart auf die Am(III)-Sorption an Kaolinit wurden durchgeführt. Bei den gewählten experimentellen Bedingungen zeigt Am(III) in Abwesenheit von HS eine sehr starke Sorption am Kaolinit, die fast unabhängig vom pH-Wert ist. In Gegenwart von HS wurden leichte Unterschiede in der Am(III)-Sorption im Vergleich zum HS-freien System beobachtet. Bei pH < 5 wurde eine schwache Erhöhung der Am(III)-Sorption an Kaolinit bestimmt, wohingegen bei pH ≥ 5.5 die Am(III)-Sorption an Kaolinit in Gegenwart von HS aufgrund der Bildung gelöster Am(III)-Humat-Komplexe leicht absinkt.

Zur Bestimmung der Oberflächenkomplexe von Am(III) am Kaolinit bei unterschiedlichen pH-Werten erfolgten laserfluoreszenzspektroskopische Messungen für die Systeme Am(III)-Kaolinit und Am(III)-HS-Kaolinit. Im binären System Am(III)-Kaolinit wurde kein Einfluss des

pH-Wertes auf die Fluoreszenzspektren beobachtet, während im ternären System eine Verringerung der Fluoreszenzintensität mit steigendem pH-Wert gefunden wurde. Ähnlich zum U(VI)-System nimmt die Fluoreszenzintensität im ternären System Am(III)-HS-Kaolinit im Vergleich zum binären System ab. Für beide Systeme, binäres und ternäres, wurden Fluoreszenzspektren gemessen, die sich vom Fluoreszenzspektrum des Am(III) in Lösung unterscheiden. Weitere Untersuchungen zur Aufklärung der Struktur der gebildeten Oberflächenkomplexe sind erforderlich.

Die in dieser Arbeit gewonnenen Ergebnisse liefern einen Beitrag zum besseren Verständnis der geochemischen Wechselwirkungsprozesse von Actiniden in der Natur und dienen zuverlässigeren Prognosen zur Actinidenmigration in der Umwelt, die für die Abschätzung der Langzeitsicherheit von Endlagern für radioaktive Abfälle erforderlich sind.









# 1. Introduction

Understanding the migration behavior of radioactive and non-radioactive toxic substances in geological environments is essential for a reliable long-term safety assessment of potential nuclear waste disposal sites, of facilities of former uranium mining and milling sites in Saxony and Thuringia (Germany), and of subsurface dumps and sites with radioactive and/or heavy metal containing inventory. Depending on prevailing geochemical conditions, different materials and processes can influence the behavior of such pollutants in natural aquifer systems. An important mechanism for retarding radionuclide migration in the natural environment is sorption onto minerals present along groundwater flow path. Thus, a quantitative understanding of actinide sorption behavior is important in evaluating the suitability of proposed geologic repositories for nuclear waste. However, this understanding is complicated by the possible dependence of sorption processes on various parameters including aqueous solution properties and sorption phase characteristics [1].

Humic acids (HA), organic macromolecules ubiquitous found in natural environments, play an important role in the interaction processes of metal ions in nature. They are soluble in the pH range of natural waters and possess the ability for complex and colloid formation. Due to their interactions with organic and inorganic pollutants produced by human activity, they play a significant role in the biochemical cycles of ecosystems. By the formation of soluble complexes with the range of more or less toxic metals, including radionuclides, HA can affect the transport behavior of these contaminants. The attention paid towards the chemical behavior of selected contaminants in the environment containing HA increases also due to their relation to storage of the radioactive waste which can become a source of contamination of natural waters. Natural organic matter (NOM, e.g., HA) is a component of clay formations or soils. In most aquatic systems, species of NOM constitute an important pool of ligands for complexing trace metals and may dominate metal speciation under some conditions [2].

Clay rocks are, together with salt and granite, considered as possible host rock formations for the potential nuclear waste repository in Germany. Therefore, detailed studies on the kinetics, thermodynamics, redox behavior, and speciation of actinides in these rock formations are

required to make a reliable decision on which of them is the most suitable. These days the research is focused on clay rocks.

The main goal of this thesis is to investigate the influence of HA on the sorption of U(VI) onto kaolinite as the model mineral and representative of clay formations. Therefore, the sorption of U(VI) was studied in the binary as well as in the ternary systems in batch experiments under different experimental conditions. The influence of HA on the U(VI) sorption on kaolinite is interpreted with respect to the sorption of HA itself. For characterization of the U(VI) surface complexes on kaolinite, two spectroscopic methods were applied. To study the influence of HA on the near-neighbor surrounding of U(VI) in the kaolinite surface complexes, extended X-ray fine structure (EXAFS) measurements were performed with U(VI)-HA-kaolinite sorbates under different experimental conditions. Results of the EXAFS measurements are interpreted and compared with literature results of the binary system without HA. Time-resolved laser-induced fluorescence spectroscopy (TRLFS) was used in order to characterize the species of U(VI) sorbed onto kaolinite in the absence of HA and, for the first time, in the presence of HA. For a better understanding of the sorption mechanism, the obtained results are compared with other model systems representing possible sorption sites of kaolinite.

The first comparative experiments were performed to study the Am(III) sorption onto kaolinite in the absence and presence of HA. The laser fluorescence spectroscopy was applied to determine the Am(III) surface complexation in the binary as well as in the ternary system. Results of these first measurements are described and an attempt is made to interpret the measured data.

The obtained results contribute to the extension of the sorption database and to improve the modeling of actinide migration in the environment. Thus, more accurate safety assessments of potential nuclear waste repositories can be made.

## 2. Kaolinite

The present work deals with actinide interactions with kaolinite and with the influence of humic acid (HA) on these interactions. Kaolinite was applied as the model mineral of possible host rock formation for the potential nuclear waste repository. For this purpose, kaolinite KGa-1b from Clay Mineral Society (CMS) was chosen and used in all experiments. In this chapter, clays and clay minerals, particularly kaolinite, are shortly introduced. Furthermore, the results of characterization of used kaolinite KGa-1b are described in comparison to literature data.

### *2.1. Clays and Clay Minerals*

**Clays** are the finest-grain particles in a sediment, soil, or rock characterized by a grain size of less than 4  $\mu\text{m}$ . The term clay can also refer to a rock or deposit containing a large component of clay-size material. Thus, clay can be composed of any inorganic materials such as clay minerals, quartz, and feldspar or iron hydroxides, that possess a sufficiently fine grain size. Most clays, however, are composed primarily of clay minerals [3].

Clays occur in many different geological environments: weathering crusts and soil, continental and marine sediments, volcanic deposits, geothermal fields, wall-rock alteration produced by intrusion of plutonic rocks and hydrothermal fluids, and very low-grade metamorphic rocks [4]. Clay has many uses today, e.g., pottery, ceramics, linings for landfills, computer chips, cosmetics, cement production, chemical filtering and pharmaceuticals [5].

Properties of the clays include plasticity when wet, hardening through drying or firing, shrinkage or swelling, the ability to form colloidal suspensions when dispersed in water, tendency to flocculate and settle out in saline water [3],[6].

**Clay minerals** are fine-grained, hydrous, layer silicates that belong to the larger class of sheet silicates known as phyllosilicates. Clay minerals mostly form from pre-existing minerals, primarily from rock-forming silicates by transformation, and/or neof ormation, where rocks are in contact with water, air, or steam [4].

The structure of clay minerals is composed of two basic units: tetrahedral and octahedral sheets. Each *tetrahedron* consists of a cation, T, coordinated to four oxygen atoms, and linked to

adjacent tetrahedra by sharing three corners (the *basal oxygen atoms*,  $O_b$ ), see **Fig. 2.1**. Common tetrahedral cations are  $Si^{4+}$ ,  $Al^{3+}$ , and  $Fe^{3+}$  [7].

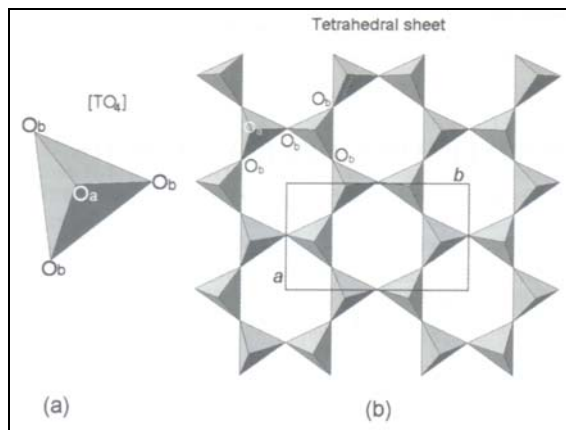


**Fig. 2.1:** (a) Tetrahedron  $[TO_4]$ , (b) tetrahedral sheet. Adopted from [7].

In the octahedral sheet, connections between each *octahedron* to neighboring octahedra are made by sharing edges. The edge-shared octahedra form sheets of hexagonal or pseudo-hexagonal symmetry. Octahedral cations are usually  $Al^{3+}$ ,  $Fe^{3+}$ ,  $Mg^{2+}$ , and  $Fe^{2+}$ . Octahedra show two different topologies related to (OH) position, i.e., the *cis*- and *trans*-orientation. The free corners (the tetrahedral *apical oxygen atoms*,  $O_a$ ) of all tetrahedra point to the same side of the sheet and connect the tetrahedral and octahedral sheets to form a common plane with octahedral anionic position  $O_{oct}$  ( $O_{oct} = OH, F, Cl, O$ ).  $O_{oct}$  anions lie near to the center of each tetrahedral 6-fold ring, but are not shared with tetrahedra [7].

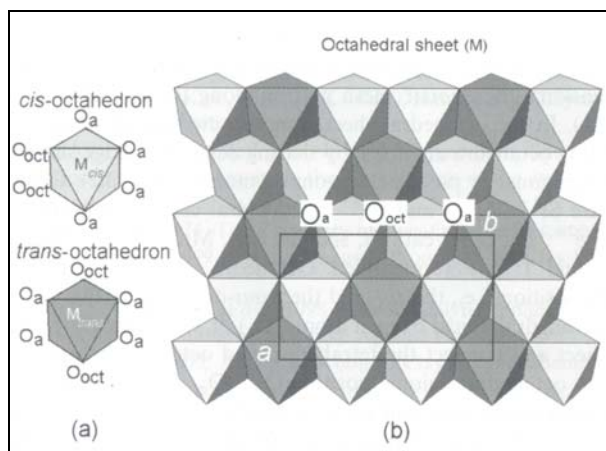


**Fig. 2.2:** (a)  $O_{oct}$  (OH, F, Cl) orientation in *cis*- and *trans*-octahedron, (b) location of *cis*- and *trans*-sites in the octahedral sheet. Adopted from [7].

Clay minerals are classified by their arrangement of tetrahedral and octahedral sheets. The 1:1 layer structure consists of the repetition of one tetrahedral and one octahedral sheet, while in the 2:1 layer structure one octahedral sheet is sandwiched between two tetrahedral sheets. Clay minerals and related phyllosilicates are classified further according to whether the octahedral sheet is dioctahedral or trioctahedral. In dioctahedral clays, two of three cation positions in the octahedral sheet are filled, every third position being vacant. This type of octahedral sheet is known as the gibbsite sheet. In trioctahedral clay minerals, all three octahedral positions are occupied [3]. Clay minerals include the following groups: *kaolinite group*, *smectite group*, *illite group*, and *chlorite group* [6].

### ***Organics in Clay Minerals***

The study of clay mineral organic interactions is an important part of the complex studies on the interaction processes in the natural systems. The surfaces of clay minerals in soil and subsurface environments can be coated by organic and inorganic polymers. Humic substances (HS, see chapter 3) and mineral surfaces do not function independent of each other, thus, the humic coating can have an impact on the sorption characteristics and it could be an important source of complexing mobile organic matter influencing the mobility of metal ions (e.g., radionuclides) in a nuclear waste repository. Therefore, the complex system including the clay mineral, HA and actinides is studied in this work.

Clay minerals, particularly kaolin species, can also adsorb specific types of neutral organic compounds between the layers. The penetration of organic molecules into the interlayer space of clay minerals is called intercalation. Intercalated guest molecules can be displaced by other suitable molecules. Almost all intercalated molecules can be displaced by other polar molecules, even by molecules that are not directly intercalated [8].

The organic guest compounds that are directly intercalated are divided into three groups: i) compounds that form hydrogen bonds (to break the H-bonds between the layers, the guest molecule must contain two separated groups to accept and donate H-bonds), ii) compounds with high dipole moments, iii) K-, Rb-, Cs- and  $\text{NH}_4^+$ -salts of short-chain fatty acids [8].

Claret et al. [9] reported a release of high concentrations of hydrophilic organic matter, characterized as HA and FA, after one and half years at high alkaline conditions from low-carbon containing clay. These results indicated that clay may be an important source of complexing

mobile organic matter influencing the mobility of radionuclides in a nuclear waste repository. Furthermore, by the study of the impact of alkaline solutions on the clay mineralogy of the Callovo-Oxfordian rock formation, Claret et al. [10] found the importance of clay organic coverage for the sorption of metal ions. They determined that the coverage of clay mineral outer surfaces, especially of the crystal edges, may be responsible for the low reactivity of the observed mineralogical transformation by blocking the access of the alkaline solution to these most reactive sites. At lower pH values such humic material may influence the sorption of metal ions, moreover, actinides.

## ***2.2. Kaolinite Properties***

Kaolinite can be formed by weathering (residual kaolins) and hydrothermal activity (hydrothermal kaolins), or occurs as an authigenic sedimentary mineral. Residual and hydrothermal kaolins, called primary kaolins, are formed in situ by surface and underground waters or hydrothermal fluids. Sedimentary kaolins, called secondary kaolins, are composed of kaolinized material from a source area that was eroded, transported, and deposited in a continental or coastal environment [4]. The structure of kaolinite is illustrated in **Fig. 2.3**. While individual hydrogen bonds have very low energy, the bonding energy is additive and the sum of the many hydrogen bonds results in the layers being very strongly bonded together and nearly impossible to separate. This bonding of the layers together results in kaolinite being a nonexpanding clay mineral [11].

The ideal composition of the kaolinite  $\text{Al}_2(\text{Si}_2\text{O}_5)(\text{OH})_4$  is 46.54 %  $\text{SiO}_2$ , 39.5 %  $\text{Al}_2\text{O}_3$ , 13.96 %  $\text{H}_2\text{O}$ , however, in nature, this exact composition is seldom, if ever, found.  $\text{Fe}_2\text{O}_3$ ,  $\text{TiO}_2$ ,  $\text{MgO}$  and  $\text{CaO}$  are nearly always present in kaolinite samples and  $\text{K}_2\text{O}$  and  $\text{Na}_2\text{O}$  are usually present. Most samples have an excess either of  $\text{SiO}_2$  or  $\text{Al}_2\text{O}_3$ . Mineral impurities such as quartz, anatase, rutile, pyrite, limonite, feldspar, mica, montmorillonite, and various iron and titanium oxides are commonly present in addition to a number of other minerals. Si and Al, in the form of hydroxides, apparently can occur as coating on the kaolinite layers. The amount of  $\text{TiO}_2$  ranges from 0.5 to 2.2 %. The ferric oxide content commonly ranges from 1 to 2 %. The minor components can affect the sorption of actinides onto minerals as reported, e.g., by Arnold et al. [12]. They found that U(VI) sorption onto phyllite is significantly influenced by ferrihydrite formed due to alteration reactions during the sorption experiments. Payne et al. [13] ascribe an

important role to  $\text{TiO}_2$ , present as a minor component in kaolinite, by U(VI) sorption onto kaolinite. Since kaolinite only has negative sites at the edges of the mineral that are not satisfied, the cation exchange capacity (CEC) is low, 3 – 15 meq/100 g [11].

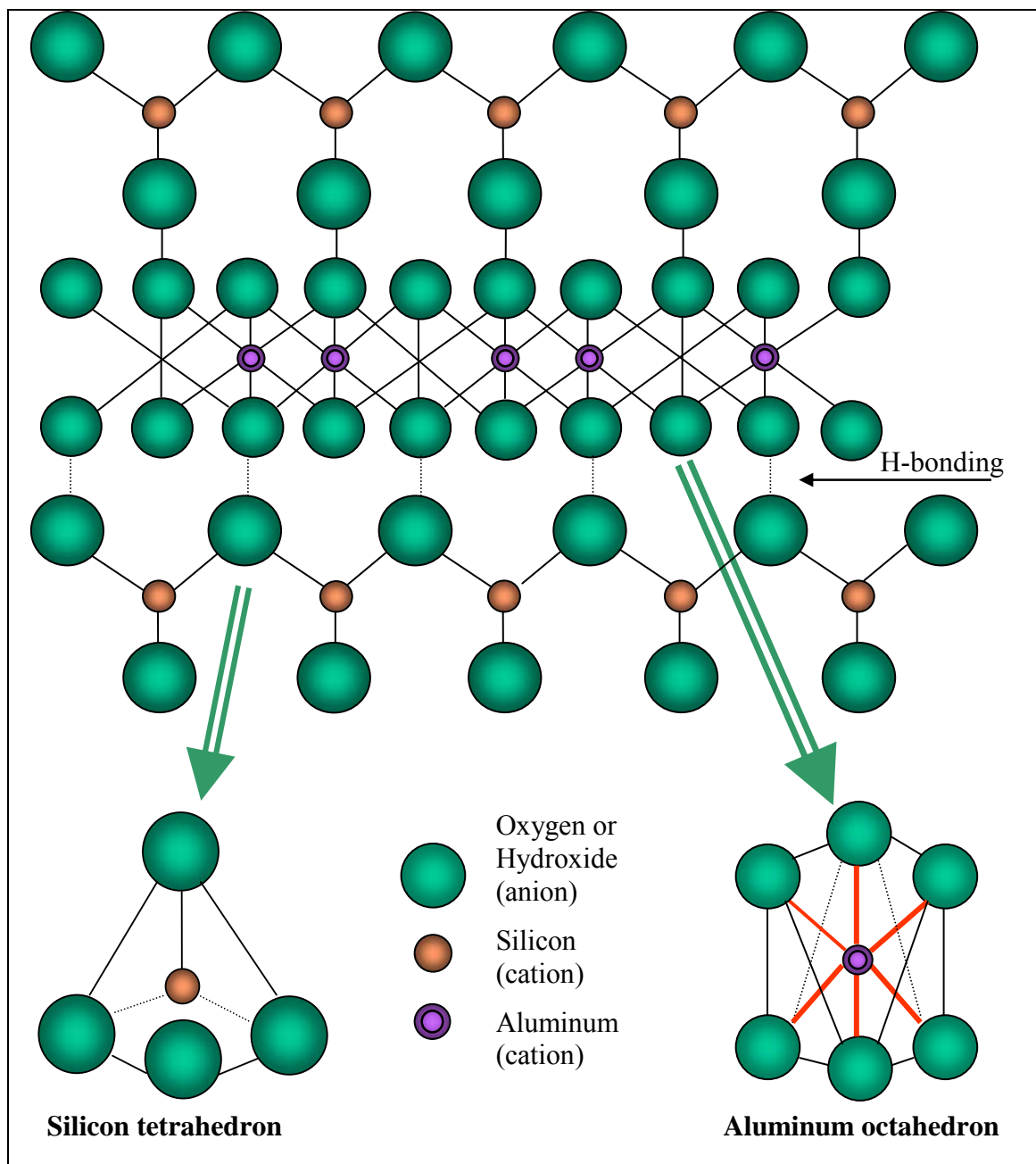


**Fig. 2.3:** Structure of kaolinite (two layer silicate clay 1:1) [5].

## **Surface Charge of Kaolinite**

One way in which surface charge can develop is by sorption of an ion, where the solid acts as an electrode (e.g.,  $H^+$  and  $OH^-$  on the surfaces of clays). In clay-aqueous systems, the potential of the surface is determined by the activity of ions (e.g.,  $H^+$ ) which react with the mineral surface. The simultaneous sorption of  $H^+$  and  $OH^-$  ions as well as other potential determining cations and anions leads to the concept of point of zero charge (p.z.c.), where the total charge from the cations and anions at the surface is equal to zero. The charge must be zero but this does not necessarily mean that the number of cations versus anions in the solution is equal. For clay minerals, the potential determining ions are  $H^+$  and  $OH^-$  and complex ions formed by bonding with  $H^+$  and  $OH^-$ . Kaolinite has a low  $pH_{pzc}$  between  $pH \sim 2$  and  $pH 6$  [11].

The surface charge of kaolinite influences the sorption of metal ions significantly. It has been ascribed to a variety of crystallographically distinct sites (**Fig. 2.4**). They include the following [14]:

- (1) **Edges** – Al and Si centers at kaolinite edges are terminated by hydroxyls and, in the case of aluminol, accept or donate protons. Since aluminum surfaces are positively charged at  $pH < 8.7$ , whereas silica groups are anionic to  $pH \sim 2$ , positive edge charge probably arises from gibbsite-like edge sites. Negative surface charge is thought to originate at high  $pH$  ( $pH > 9$ ) primarily from proton donor reactions on Si sites. Sorption of water onto aluminol sites also gives rise to Lewis acid sites.
- (2) **The Si basal plane** – Substitution of  $Al^{3+}$  or  $Fe^{3+}$  for Si in the tetrahedral sheet would cause a permanent (non-pH-dependent) negative charge on the Si basal plane.
- (3) **Basal plane hydroxyl groups** – Hydroxyl groups on the octahedral plane are coordinated with two underlying aluminum atoms and are thought to be appreciably less reactive than edge aluminols and silanols. Hydroxyl groups may exist locally on the siloxane sheet as well.

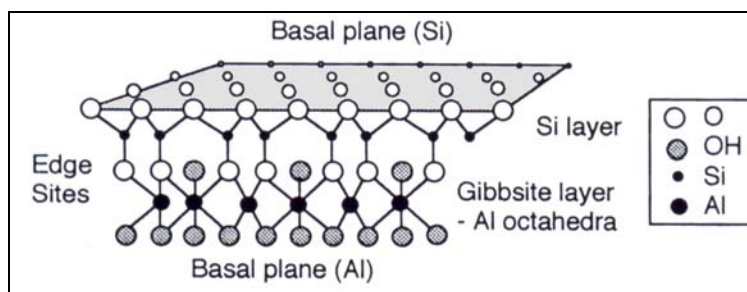


**Fig. 2.4:** Description of the kaolinite surface charge. Adopted from [14].



## **2.3. Characterization of Kaolinite KGa-1b**

Kaolinite KGa-1b is well described in literature [15]-[21]. Well-crystallized kaolin was selected to replace the exhausted stock of the kaolinite KGa-1. It was collected from a geographical location and stratigraphic position very close to KGa-1 [22]. Particle measurements indicated that the grain size of KGa-1b amounts to 57.8 % < 2  $\mu\text{m}$  and 32.0 % < 0.5  $\mu\text{m}$  and the total organic carbon content (TOC) for unprocessed KGa-1b was determined to be 231 ppm [22]. Kaolinite KGa-1b is moderately hydrophilic and has a large negative  $\xi$  potential (-49.2 mV at pH 7.3 – 7.5 and I: 0.015 M) [18]. The point of zero charge (p.z.c.) and point of zero net proton charge (p.z.n.p.c.) are reportedly 6.0 [23] and  $5.1 \pm 0.2$  [24] or  $4.99 \pm 0.03$  [25], respectively.

Before its use in this work, some characterization measurements of the kaolinite KGa-1b were performed. In the following chapters the results of FT-IR and XRD measurements, chemical analysis, CEC, and surface area measurements are introduced and the obtained results are compared with the data given in literature.

### **2.3.1. Chemical Composition**

The chemical composition of KGa-1b was measured by ICP-MS after acidic digestion (mixture of  $\text{HNO}_3$ ,  $\text{HCl}$  and  $\text{HF}$  3:1:1) in a microwave oven. **Tab. 2.1** summarizes the comparison of selected obtained data with results of chemical analyses reported for kaolinite KGa-1b in literature. In the size fractionated sample  $\text{SiO}_2$  prevails in the amount of 41.79 wt. %, the amount of  $\text{Al}_2\text{O}_3$  is 36.87 wt. %, while in the untreated sample the opposite phenomenon was observed.  $\text{Al}_2\text{O}_3$  prevails with 47.85 wt. %, the amount of  $\text{SiO}_2$  corresponds to 42.98 wt. %. Thus, it becomes evident that by the size fractionation (for details, see chapter 10.1(1)) mainly  $\text{Al}_2\text{O}_3$  is removed from the sample. From the minor components, the highest content of 1.45 wt. % has  $\text{TiO}_2$  in both samples. Small amounts of  $\text{Fe}_2\text{O}_3$ ,  $\text{CaO}$  and  $\text{K}_2\text{O}$  were found in both samples. The data obtained in this work are comparable to those reported in literature. In **Tab. 2.2** the abundances of trace and rare earth elements determined by means of ICP-MS for the kaolinite KGa-1b [20] are presented. It becomes evident that kaolinite contains 3.7 ppm of uranium. This amount is negligible in comparison to the amount of U(VI) applied in the sorption and kinetic experiments (cf. chapter 6) and, therefore, it was not considered in the experiments evaluations.

**Tab. 2.1:** Chemical composition of kaolinite KGa-1b and the comparison with literature.

Compound/ Element	This work		Literature [22]
	Size-fractionated ( $< 2 \mu\text{m}$ ) (wt. %)	Untreated (wt. %)	( $< 44 \mu\text{m}$ ) (wt. %)
Al <sub>2</sub> O <sub>3</sub>	36.87	47.85	39.2
SiO <sub>2</sub>	41.79	42.98	45.1
TiO <sub>2</sub>	1.45	1.45	1.66
Fe <sub>2</sub> O <sub>3</sub>	0.2	0.27	0.21
CaO	$< 0.06$	$< 0.06$	0.03
K <sub>2</sub> O	0.01	0.01	0.02
U	3.73 ppm	3.69 ppm	1.96 ppm <sup>[20]</sup>
TOC		$< 200 \text{ ppm}$ <sup>[26]</sup>	231 ppm <sup>[22]</sup>

**Tab. 2.2:** Abundances of some selected nuclides in kaolinite KGa-1b according to [20].

Nuclide	Concentration (ppm)	Nuclide	Concentration (ppm)	Nuclide	Concentration (ppm)
Co 59	3.27	La 139	33.73	Ho 165	0.369
Ni 60	17.87	Ce 140	77.12	Er 166	0.717
Cu 63	25.24	Pr 141	9.28	Tm 169	0.048
Rb 85	1.32	Nd 146	40.07	Yb 174	0.462
Sr 88	41.69	Sm 147	9.91	Lu 175	0.071
Y 89	6.95	Eu 151	2.510	Pb 208	32.5
Mo 95	2.020	Gd 157	10.43	Th 232	37.15
Sn 118	5.74	Tb 159	1.15	U 238	1.96
Sb 121	0.299	Dy 162	3.74		

### 2.3.2. Structural and Mineralogical Analysis

Two spectroscopic methods – XRD and FT-IR – were applied to characterize the structure of kaolinite KGa-1b. **Fig. 2.5** illustrates the XRD pattern obtained for size-fractionated ( $< 2 \mu\text{m}$ ) and untreated ( $< 44 \mu\text{m}$ ) kaolinite KGa-1b. The spectra show typical reflections for kaolinite and they are comparable with those reported in literature [17].

Pruett and Webb [22] reported that KGa-1b contains well-ordered kaolinite with a trace abundance of anatase. In both XRD spectra there is a peak observed at the diffraction angle 25. It belongs to TiO<sub>2</sub> in the form of anatase. From this it can be concluded that anatase is concentrated in the finer fractions of kaolinite KGa-1b. From the XRD analysis, the mean value of the grain size of kaolinite was estimated to be  $38 \pm 5 \text{ nm}$  and  $35 \pm 15 \text{ nm}$  for the size-fractionated and untreated kaolinite, respectively.

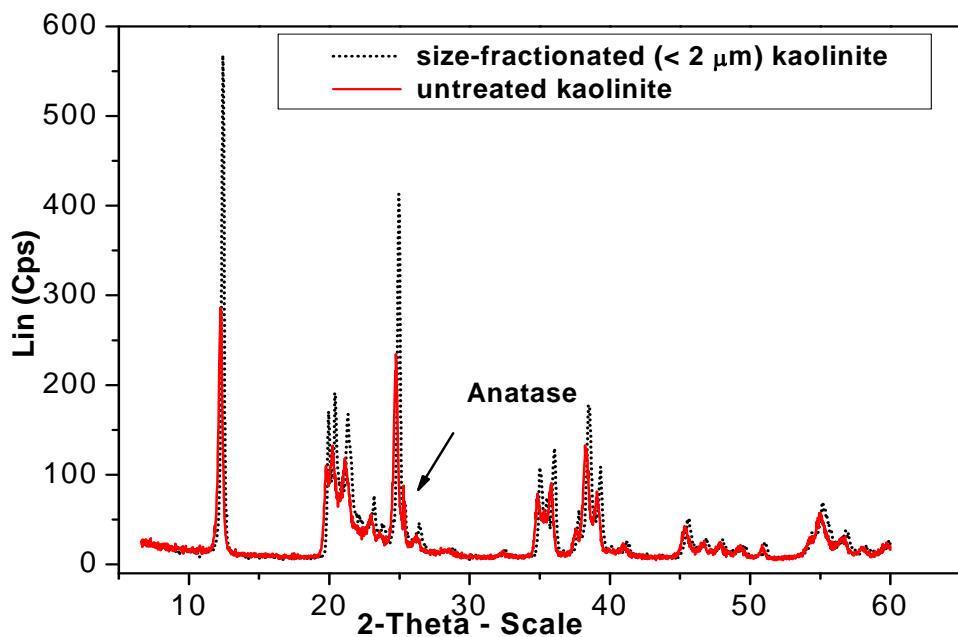


**Fig. 2.5:** XRD patterns of size-fractionated and untreated kaolinite KGa-1b.

The IR spectrum of kaolinite KGa-1b is shown in **Fig. 2.6**. It is a typical spectrum for well-crystallized kaolinite and it matches the literature data [19] very well. **Tab. 2.3** summarizes the assignment of the bands for the kaolinite KGa-1b according to [19].

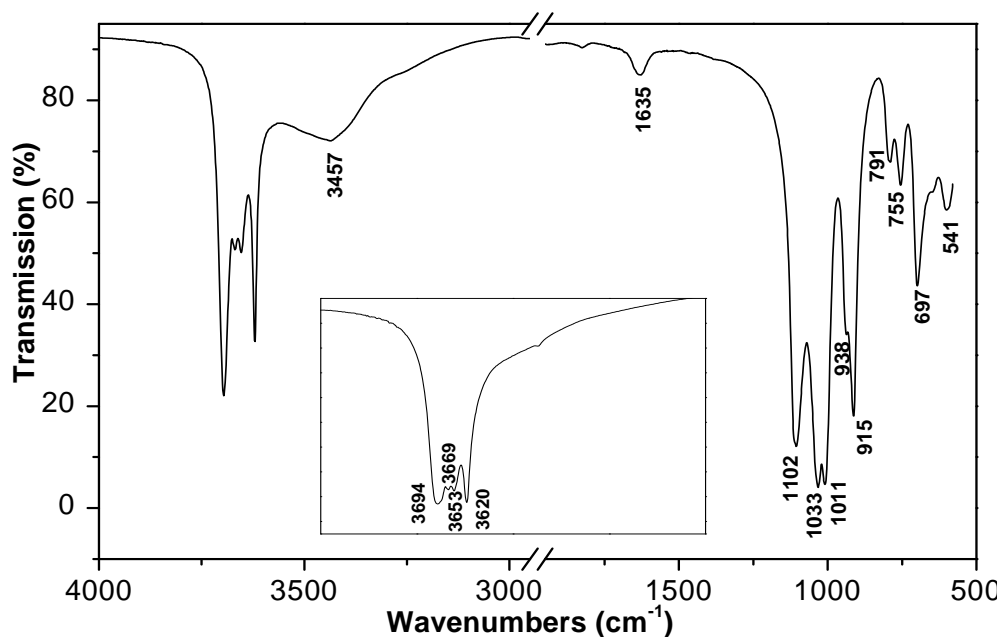


**Fig. 2.6:** IR spectrum of KGa-1b using 0.5 mg sample/200 mg KBr for 4000 - 400  $\text{cm}^{-1}$ . Inserted: 2.0 mg sample/200 mg KBr. Disk heated overnight at 150  $^{\circ}\text{C}$ .

**Tab. 2.3:** The assignments of the IR bands for KGa-1b.

<b>Position (cm<sup>-1</sup>)</b>	<b>Assignment</b>
3694, 3669, 3653	OH stretching of inner-surface hydroxyl groups
3620	OH stretching of inner hydroxyl groups
3457	OH stretching of water
1635	OH deformation of water
1102	perpendicular Si-O stretching
1033, 1011	in-plane Si-O stretching
938	OH deformation of inner-surface hydroxyl group
915	OH deformation of inner hydroxyl groups
791	Si-O
755, 697	Si-O, perpendicular
541	Al-O-Si deformation
472	Si-O-Si deformation
432	Si-O deformation

### 2.3.3. Cation Exchange Capacity

The cation exchange capacity (CEC) of clay minerals is a fundamental property of these materials and can be determined routinely. Methods of the measurements are based on a determination of the quantity of a particular exchangeable cation, by a variety of means, expressed per 100 g of dry clay. The CEC of a clay mineral is generally understood to be equivalent with the layer charge. In this work, the CEC of kaolinite was measured by the compulsive exchange method, for details see section 10.3.7.

The value determined in this work amounts to 1.83 meq/100 g and is slightly lower than that in the work of Borden et al. [21], see **Tab. 2.4**. This could be caused by using another method. Furthermore, due to the omnipresent impurities, it is generally difficult to determine true CEC values of clay minerals.

**Tab. 2.4:** CEC of kaolinite KGa-1b.

<b>Kaolinite</b>	<b>CEC (meq/100 g)</b>	<b>Source</b>
KGa-1b	1.83 ± 0.10	This work
KGa-1b	3.0	[21]

### **2.3.4. Surface Area**

The most commonly used procedure for determining surface area of a powder is to derive the amount of adsorbed nitrogen (or other inert gas) at monolayer coverage from a BET plot of sorption isotherm data. Knowing the projected cross sectional area per molecule in a monolayer, the surface area is calculated from the monolayer coverage. In this work, the surface area of kaolinite KGa-1b was determined by above described BET measurement and it amounts to 11.8 m<sup>2</sup>/g. This value agrees very well with literature data, see **Tab. 2.5**.

**Tab. 2.5:** Surface area of kaolinite KGa-1b.

<b>Kaolinite</b>	<b>Surface area (m<sup>2</sup>/g)</b>	<b>Source</b>
KGa-1b	11.8	This work
KGa-1b	11.7	[22]
KGa-1b	11.9	[27]

## 3. Humic Substances

### *3.1. Properties of Humic Substances*

Humic substances (HS) are ubiquitous in the environment, occurring in soils, water, and sediments in the geosphere. An important source of HS can also be clays (e.g., [9]) which are present in many soils. HS arise from decomposition of plant and animal tissues yet are more stable than their precursors. Their size, molecular weight, elemental composition, structure, and the number and position of functional groups vary depending on the origin and age of material. The humic content of soils varies between 0 – 10 %. In deep groundwaters the humic content, expressed as dissolved organic carbon (DOC), varies from 0.1 to 10 ppm [28].

There are three major fractions of HS operationally defined in terms of their solubilities:

- (1) **Humic**: This fraction of HS is insoluble at any pH value.
- (2) **Humic acid (HA)**: The fraction of HS, which is not soluble under acidic conditions (below pH 1), but becomes soluble at higher pH ( $\text{pH} > 3$ ).
- (3) **Fulvic acid (FA)**: This fraction of HS is soluble under all pH conditions [29].

All three classes are brown substances which cannot be defined chemically as they possess a variety of functional groups arranged in non-repetitive patterns. The humic type polyelectrolytes are relatively large macromolecules and may exhibit colloidal behavior. Their structures are random coils which expand and shrink in reaction to the pH, to the ionic strength, and to the binding of cations [30].

The range of the elemental composition of humic materials is relatively narrow, being approximately 40 – 60 % C, 30 – 50 % O, 4 – 5 % H, 1 – 4 % N, 1 – 2 % S, and 0.03 % P [31]. HA contain more hydrogen, carbon, nitrogen, and sulfur and less oxygen than FA. Humic materials consist of a skeleton of aliphatic and aromatic units cross-linked mainly by oxygen and nitrogen groups with the major functional groups being carboxylic acid, phenolic and alcoholic hydroxyls, ketone, and quinone groups. The structures of FA are somewhat more aliphatic and less aromatic than HA. FA are richer in carboxylic acid, phenolic and ketonic groups. This is responsible for their higher solubility in water at all pH values. HA, being more aromatic, become insoluble when the carboxylate groups are protonated at low pH values. The total

acidities of FA 890 – 1420 meq/100 g are clearly higher than those of HA 485 – 870 meq/100 g. This structure allows the humic materials to function as complexants with the ability to bind both hydrophilic and hydrophobic materials. This function, in combination with their colloidal properties, makes HS effective agents in transporting both organic and inorganic contaminants in the environment [28].

Numerous suggestions of the HS structure have been postulated. In **Fig. 3.1**, the model of a macromolecular structure of HA, developed by Schulten and Schnitzer on the basis of pyrolytic and spectroscopic analysis is introduced [32].

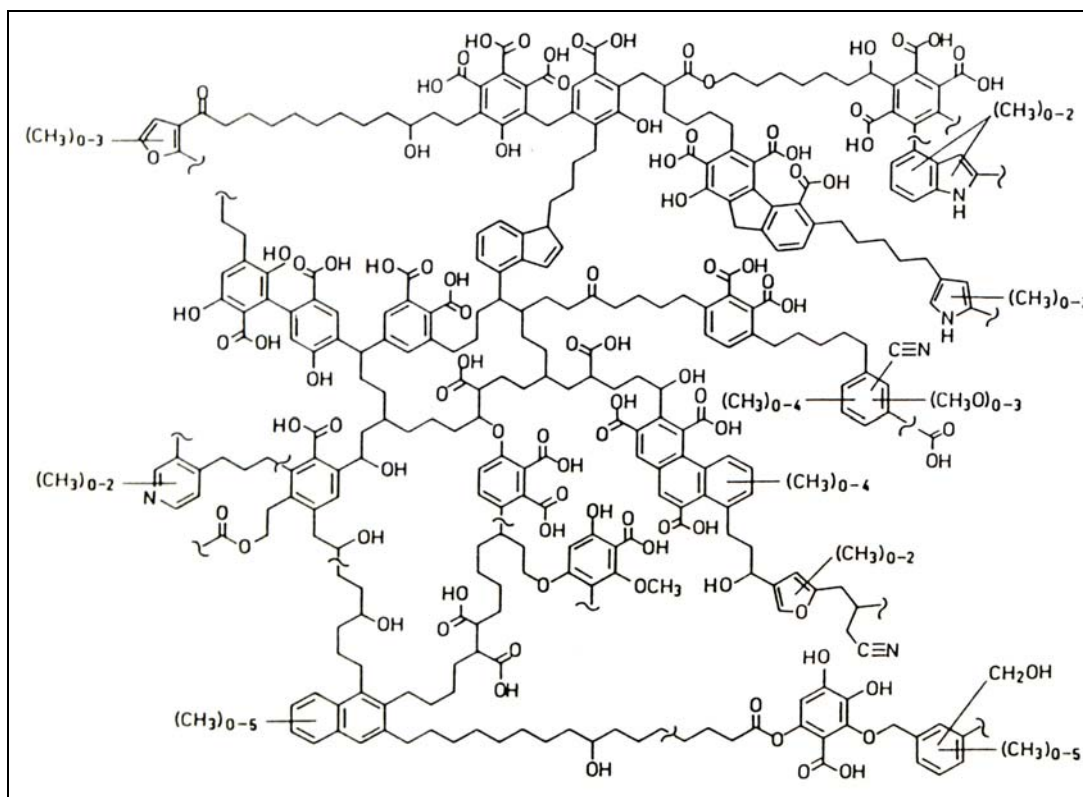


**Fig. 3.1:** Suggested structure of humic acid. Adopted from [32].

The molecular weight range of HS is not discrete due to possible variations in numbers and types of functional groups and structural elements [30]. Wolf et al. [33] measured the molecular size and mass distribution of different HS: natural HA and FA and synthetic HA by means of AFFFF (asymmetrical flow field-flow fractionation) and TOF-SIMS (time-of-flight secondary ion mass spectrometry), respectively. In AFFFF measurements related to polycarboxylic acids (PCA) standards, the FA showed the smallest size distribution with molecular sizes up to 3000 Da and all HA showed larger size distribution with molecular sizes up to 10 – 14 kDa.

Molecular masses in the range 150 – 3000 Da for natural HA and FA and 150 –1500 Da for synthetic HA resulted from TOF-SIMS measurements. The results showed that the molecular size of HS is not always correlated with their molecular mass and shows generally higher values.

In recent studies, Plancque [34] and Piccolo [35] proposed a supramolecular nature of HS, in which relatively small heterogeneous molecules (masses around 500 Da), deriving from degradation and decomposition of dead biological material, are self-assembled by hydrogen bonds, and also by weaker forces such as Van der Waals,  $\pi$ - $\pi$ , and CH- $\pi$  interactions into large assemblies of high molecular mass.

### ***Interaction of Humic Substances with Metal Ions***

HS have a very good ability to form stable complexes with polyvalent cations. The formation of these complexes promotes the mobilization, transport, segregation, and deposition of trace metals in soils, sediments, sedimentary rocks, and biogenic deposits of various types. Organic complexing agents play an important role in the chemical weathering of rocks and minerals, and they function as carriers of metal cations in natural waters [36].

The complex nature of the interactions between natural organic matter (NOM) and metal ions is given by the heterogeneous, polyelectrolytic and polydispersive character of HS. This characteristic is mainly determined by a variety of dissociated functional groups. Their ability to form complexes with metal ions can be attributed to their high content of oxygen containing functional groups, including carboxyl, phenolic, and enolic OH, and C=O structures of various types. Amino groups may also be involved, but carboxylate groups (COO<sup>-</sup>) play a prominent role in the complexing of metal ions by HA [28]. However, it was shown that phenolic hydroxyl groups can also contribute to the complex formation of metal ions already at low pH values [37]. The nature of binding is in the range from pure electrostatic, non-specific interactions of metal cation with total negative charge on the surface of HA macromolecule to the covalent, specific interactions as a formation of the chelates with ligands (functional groups of HS). Higher capability for metal binding is attributed to FA which can be caused by a general greater amount of oxygen functional groups compared with HA. These differences can be also found by comparing samples from different sources in the environment.

For the interpretation of equilibrium interactions of HS with metal ions, special models were suggested. Relatively often, models of discrete binding sites considering HA as a mixture of



a finite number of individual, independent ligands corresponding to different types of binding sites in macromolecule of HA are used, e.g., charge neutralization model developed by Kim and Czerwinski [38]. Using this model, they calculated the complexation constants of  $\text{UO}_2^{2+}$  and trivalent actinides with different HA (e.g.,  $\log \beta = 6.42 \pm 0.14$  for Am(III)/Cm(III) with HA-Aldrich, pH 6, I: 0.1 M  $\text{NaClO}_4$ ). The next group of models considers continuous distribution of HA functional groups corresponding to their dissociation and binding properties. They can be characterized by means of a distribution function (e.g., Gaussian) describing distribution of dissociation or complexation constants. Complexation measurements and calculations were performed by many authors under different conditions for a broad spectrum of metal ions and HS, e.g., Np(V) with HA-Aldrich at pH 7:  $\log \beta = 3.87 \pm 0.19$  and with HA type M42 at pH 7:  $\log \beta = 3.50 \pm 0.15$  [39], Th(IV) with HA-Aldrich at pH 3.98:  $\log \beta = 9.528 \pm 0.044$  [40]. U(VI) and Am(III) complexation constants are summarized in **Tab. 4.2** and **Tab. 9.2**, respectively.

### ***3.2. Characterization of Humic Acid Type M42***

As the representative of humic substances, the in-house synthesized HA type M42 was used in this work. Unlabeled HA type M42 [41], batch M145 [42], was applied in the EXAFS and TRLS measurements. In order to detect and to determine the fate of HA in the studied systems, the  $^{14}\text{C}$ -labeled HA type M42, batch M170, was used in the sorption and kinetic experiments. The basic synthesis of this HA and its characterization is described in detail in [41] and [42], thus, only short introduction will be given in this chapter.

The synthetic HA type M42, batch M145, was synthesized from the mixture of 33 g xylose, 22 g glutamic acid monohydrate and 60 mL water which was heated for 92 h at  $80 \pm 2^\circ\text{C}$  under reflux and inert gas. After expiration of the reaction time and cooling of the mixture, the formed solid melanoidin fraction was separated from the liquid fraction by centrifugation. Then, the solid product was washed and ground with ethanol and ether. The HA melanoidin fractions were extracted by stirring the solid product with 2 M NaOH under inert gas. The synthetic HA was precipitated from the alkaline solution with 2 M HCl. The resulting precipitate was washed, dialyzed using dialysis tubes against purified water and lyophilized.

$^{14}\text{C}$ -labeled synthetic HA type M42, batch M170, was synthesized according to the unlabeled HA, however, applying  $^{14}\text{C}$ -labeled [ $u\text{-}^{14}\text{C}$ ]glutamic acid as the starting material. The

specific activity of this synthesized HA was 2.38 MBq/g [42]. **Tab. 3.1** summarizes the elemental composition of HA type M42, batch M145 and the functional groups content of both synthesized HA types, M42, batch M145, and [<sup>14</sup>C]M42, batch M170 in comparison to natural HA from literature [43],[44].

**Tab. 3.1:** Characterization of HA type M42 and [<sup>14</sup>C]M42 [42] in comparison to natural HA [43],[44].

HA	Elemental composition					
	C (%)	H (%)	N (%)	O (%)	Ash (%)	Moisture (%)
Type M42 batch M145	56.1 ± 0.3	4.1 ± 0.1	4.4 ± 0.1	26.8 ± 0.3	0.11	8.4
Natural HA [43]	50 - 60	4 - 6	2 - 6	30 - 35		
	Functional groups					
	COOH (meq/g)		PEC <sup>a</sup> (meq/g)		Phenolic/acidic OH (meq/g)	
Type M42 batch M145	3.76 ± 0.09		3.51 ± 0.07		2.0 ± 0.2	
Type [ <sup>14</sup> C]M42 batch M170	3.63 ± 0.03		3.55 ± 0.05		not measured	
Natural HA [44]	1.5 – 5.7				2.1 – 5.7	

<sup>a</sup>Proton exchange capacity

Synthetic HA M42 shows an elemental composition similar to natural HA. The carboxyl group content and the proton exchange capacity (PEC) of synthetic HA type M42 are comparable to those of naturally occurring HA. In addition to that, HA type M42 shows U(VI) complexation behavior comparable to naturally occurring HA [41]. Also, in the FT-IR spectra there are almost no differences in terms of position of the IR absorption bands and the band intensities between natural HA, labeled HA and unlabeled HA M42 [42]. Compared to the natural HA, the synthetic HA shows a higher homogeneity, a simple overall structure, and a well defined functionality with the possibility of defined isotopic labeling (<sup>14</sup>C). Such labeled HA can then be directly measured because of its radioactivity and, therefore, it is well suited for use in the sorption and kinetic experiments performed in this work. Further advantage of labeled HA is that it can be detected at low concentrations.

## 4. U(VI)-Speciation in Aqueous Solution

In the following chapter, some basic chemical properties of uranium are described. Uranium was chosen as representative of actinides with the stable VI-oxidation state. Oxidation state can significantly affect the sorption and/or migration of actinides under aerobic and anaerobic conditions. Moreover, the U(VI) speciation is also influenced by different inorganic (e.g,  $\text{HCO}_3^-/\text{CO}_3^{2-}$ ) and organic (e.g., HA) ligands occurring in the solution. Therefore, oxidation state and U(VI) species distribution are properties which should be taken into account by interpretation of the sorption data and by the modeling of actinide migration.

### 4.1. Chemical Properties of Uranium

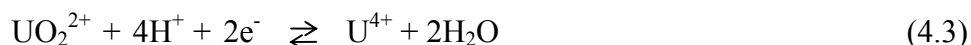
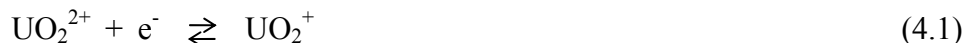
Some characteristic chemical properties of U are summarized in **Tab. 4.1**. The electronic configuration of U is  $[\text{Rn}] 5f^3 6d^1 7s^2$ . As it was already mentioned above, the most stable oxidation state of U in solution is U(VI) with the uranyl ion as the stable entity. The only known U ion in the U(V) oxidation state in aqueous solution is linear dioxouranium ion. Aqueous solutions containing U(IV) are stable in the absence of oxidation agents like dissolved oxygen. Aqueous solutions containing U(III) are rapidly oxidized under evolution of hydrogen.

**Tab. 4.1:** Chemical properties of uranium [45].

Atomic number	92
Electronic configuration	$[\text{Rn}] 5f^3 6d^1 7s^2$
Oxidation states	3, 4, 5, <u>6</u>
Ion types and colors	
$\text{U}^{3+}$	red
$\text{U}^{4+}$	green
$\text{UO}_2^+$	pale mauve
$\text{UO}_2^{2+}$	yellow
$\text{UO}_5^{3-}$	-
Stability in aqueous solution	
$\text{U}^{3+}$	aqueous solution evolve hydrogen on standing
$\text{U}^{4+}$	stable to water, slowly oxidized by air to $\text{UO}_2^{2+}$
$\text{UO}_2^+$	disproportionates to $\text{U}^{4+}$ and $\text{UO}_2^{2+}$
$\text{UO}_2^{2+}$	stable, difficult to reduce

Underlined oxidation number indicates the most stable oxidation state.

The relative stability of the various oxidation states is strongly dependent on the pH of the solution and on the presence of complexing ligands. The rate of the redox transformations between the different oxidation states of U is rapid, when there is no change in chemical compositions between the oxidized and reduced forms, otherwise it is very slow. This means that the reactions (4.1) and (4.2) are fast, while the reaction (4.3) is slow:



U is a strong Lewis acid and a hard electron acceptor in all its different oxidation states. This high Lewis acidity results in extensive hydrolysis of U that decreases in order  $\text{U(IV)} > \text{U(VI)} \gg \text{U(III)} > \text{U(V)}$  [46].

## ***4.2. U(VI) Speciation in Presence of Inorganic Ligands***

U also shows a strong capability of complex binding to inorganic and organic ligands. Strong hydrolysis of U(VI) occurs in aqueous solutions. Other complexing inorganic anions present in substantial amounts in natural waters, particularly in groundwaters, can be, for example,  $\text{HCO}_3^-/\text{CO}_3^{2-}$ ,  $\text{SO}_4^{2-}$  or  $\text{PO}_4^{3-}$ . Because of the omnipresence in nature and strong complexation properties of  $\text{CO}_3^{2-}$ , the carbonate complexation is one of the most important. In **Fig. 4.1** and **Fig. 4.2**, the distribution of U(VI) species in 0.1 M  $\text{NaClO}_4$  solution is demonstrated as a function of pH value for U(VI) concentrations  $1 \cdot 10^{-6}$  M and  $1 \cdot 10^{-5}$  M, respectively, in the (a) presence of  $\text{CO}_2$  ( $p\text{CO}_2 = 10^{-3.5}$  atm) and (b) absence of  $\text{CO}_2$  ( $\text{N}_2$ -atmosphere). The species distribution was calculated using the code EQ3/6 [47] based on the most recent compilation of U(VI) complex formation constants [48]. The speciation diagrams at  $I = 0.01$  M  $\text{NaClO}_4$  are not shown, because they do not differ significantly.

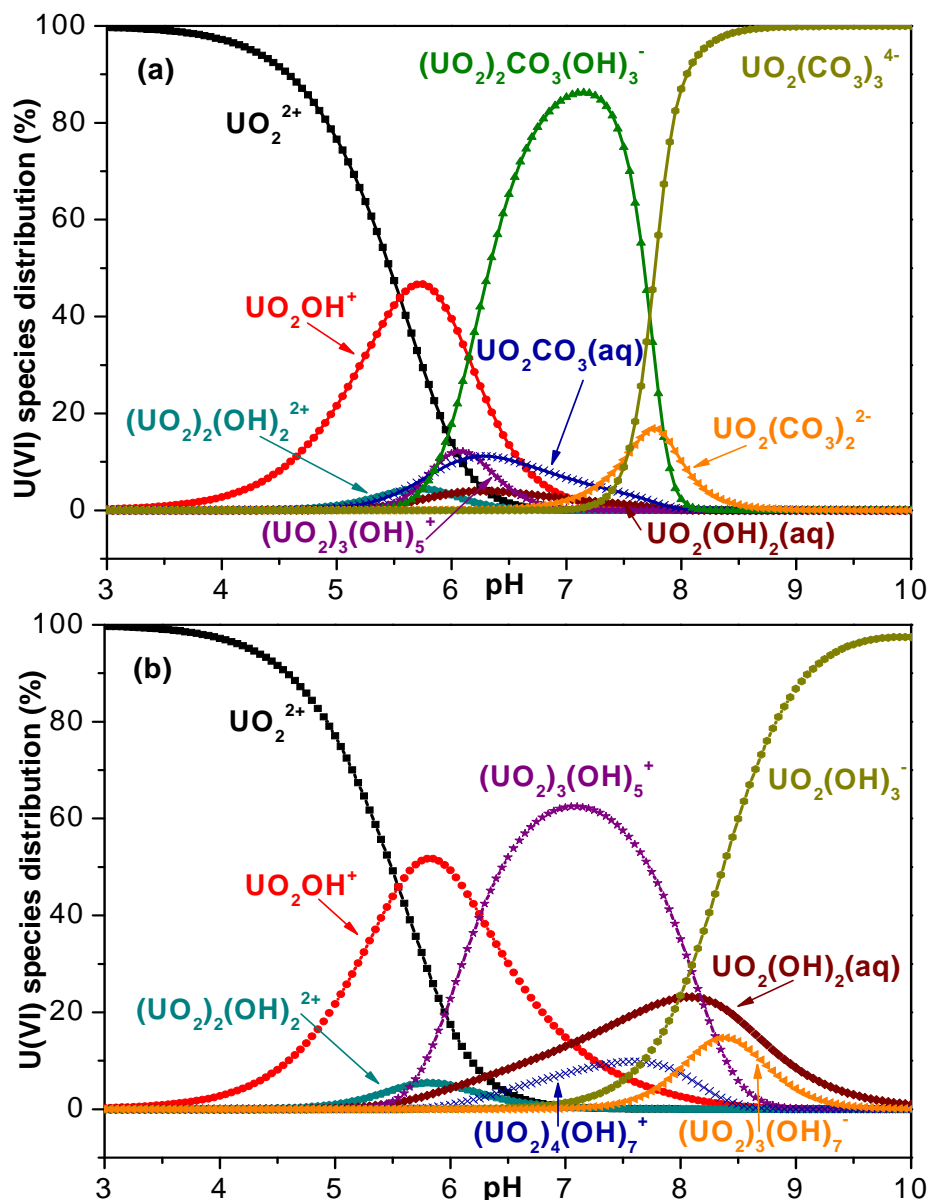


**Fig. 4.1:** U(VI) speciation in the (a) presence and (b) absence of CO<sub>2</sub> (I = 0.1 M NaClO<sub>4</sub>, [U(VI)] = 1·10<sup>-6</sup> M).

From the diagrams it becomes evident that at pH < 5 U(VI) prevails in solution as the free UO<sub>2</sub><sup>2+</sup> cation. At pH > 5 the U(VI) speciation is dominated by a series of hydrolyzed U(VI) species such as UO<sub>2</sub>OH<sup>+</sup>, (UO<sub>2</sub>)<sub>3</sub>(OH)<sub>5</sub><sup>+</sup>, UO<sub>2</sub>(OH)<sub>3</sub><sup>-</sup>, UO<sub>2</sub>(OH)<sub>2</sub>(aq), and (UO<sub>2</sub>)<sub>3</sub>(OH)<sub>7</sub><sup>-</sup>. In the presence of CO<sub>2</sub>, uranyl-carbonato complexes (UO<sub>2</sub>)<sub>2</sub>CO<sub>3</sub>(OH)<sub>3</sub><sup>-</sup>, UO<sub>2</sub>(CO<sub>3</sub>)<sub>3</sub><sup>4-</sup>, and UO<sub>2</sub>(CO<sub>3</sub>)<sub>2</sub><sup>2-</sup> become dominant at higher pH values (pH > 6.5).

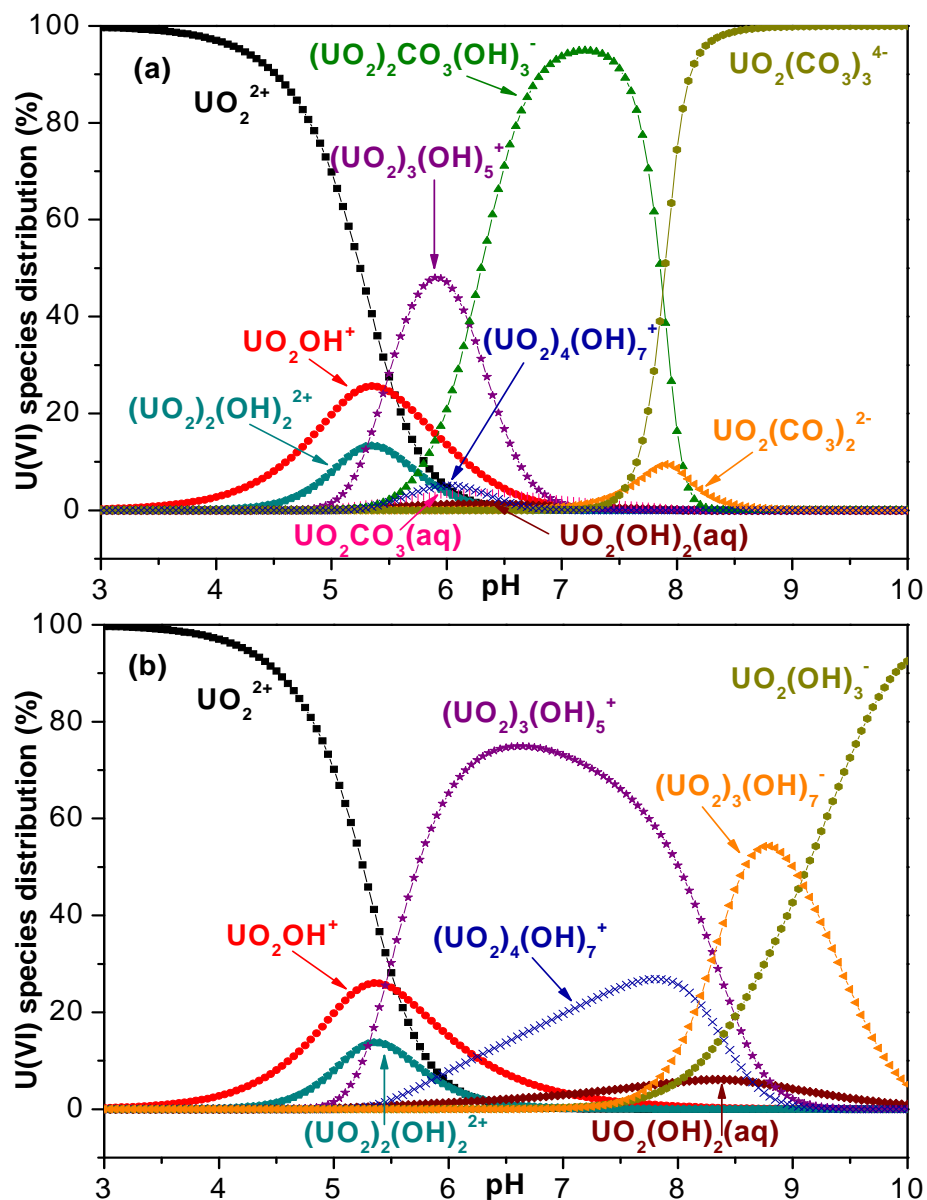


**Fig. 4.2:** U(VI) speciation in the (a) presence and (b) absence of CO<sub>2</sub> (I = 0.1 M NaClO<sub>4</sub>, [U(VI)] = 1·10<sup>-5</sup> M).

### ***4.3. U(VI) Speciation in Presence of Humic Acid***

The presence of HA can affect the U(VI) speciation significantly. Therefore, the knowledge of the interaction of U(VI) with HA is important for the speciation calculation and for the interpretation of the sorption experiments performed in this study. A short literature overview to the complexation of U(VI) with HA and results of U(VI) speciation calculations in presence of HA are given in this chapter.

#### ***Interaction of U(VI) with Humic Substances***

The formation of organic macromolecular actinide complexes could affect the sorption behavior in geological systems due to changes in the total solubility, formation of species with altered size and charge and with various organic groups available for complexation or hydrophobic interaction, formation of colloidal aggregates or interaction with other solid surfaces.

A large number of studies have been performed on the humate and fulvate complexation behavior of actinide ions in different oxidation states and a variety of methods have been applied, e.g., ion exchange or TRLFS [49].

The humate complexation of the  $\text{UO}_2^{2+}$  ion has been studied by a number of authors, interpreting the complexation reaction in different ways: formation of 1:1 and 1:2 uranyl-humate complexes without explicitly stating the number of ligands involved in such complex forms, and the formation of strong and weak complexes. At pH values  $\geq 5$ , where the amount of hydrolyzed uranyl species is not negligible, a part of the reaction products can be a mixed complex, i.e., uranyl-hydroxo-humate complex [50]. Selected complexation constants for U(VI)-HA complexation together with experimental conditions and methods used for their determination are summarized in **Tab. 4.2**. Besides the formation of these uranyl-humate or uranyl-hydroxo-humate complexes, the possible existence of a ternary uranyl-carbonato-humate complex ( $\text{UO}_2\text{CO}_3$ )HA in waters containing humic substances was reported by Glaus et al. [51]. However, its stability constant is quite low ( $\log \beta \approx 5$ ).

**Tab. 4.2:** Selected U(VI) complexation constants.

Material	Experimental Conditions	Method	Log $\beta$	Reference
Gohy-573	pH 4 0.1 M NaClO <sub>4</sub>	ultrafiltration anion exchange TRLFS	UO <sub>2</sub> HA(II) 6.16 ± 0.13	[50]
Suwannee River HA, FA	pH 4 and pH 5 0.1 M NaClO <sub>4</sub>	ion exchange	UO <sub>2</sub> FA(II) 5.37 ± 0.15 pH 4 5.13 ± 0.12 pH 5 UO <sub>2</sub> HA(II) 6.75 ± 0.15 pH 4 7.57 ± 0.14 pH 5	[54]
synthetic HA M42 Aldrich HA Fluka HA	pH ~ 4 0.1 M NaClO <sub>4</sub>	TRLFS	UO <sub>2</sub> HA(II) synthetic HA M42 6.16 ± 0.22 Fluka HA 6.04 ± 0.15 Aldrich HA 5.85 ± 0.22	[41]
Aldrich HA	pH 4 and pH 5 0.1 M NaClO <sub>4</sub>	anion exchange	UO <sub>2</sub> HA(II) 6.08 ± 0.15	[52]
Gohy-227	pH 1 – 4 0.1 M NaClO <sub>4</sub>	ultrafiltration anion exchange	UO <sub>2</sub> (OH)HA(I) 14.7 ± 0.5	[55]
Aldrich HA	pH 7	TRLFS fs-TRLFS	UO <sub>2</sub> (OH)HA(I) 14.89 ± 0.54	[53]
Gohy-573	pH 7.5 – 7.9 0.1 M NaClO <sub>4</sub>	solubility measurements of UO <sub>2</sub> (OH) <sub>2</sub> (s) in presence of HA	UO <sub>2</sub> (OH)HA(I) 14.6 ± 0.02	[56]

The speciation computations were performed for two cases: for solutions in equilibrium with atmospheric CO<sub>2</sub> (pCO<sub>2</sub> = 10<sup>-3.5</sup> atm) and in the absence of CO<sub>2</sub> by means of the modified geochemical speciation code EQ3/6 [42] with integrated metal ion charge neutralization model [38] for the description of the HA complexation ([U(VI)] = 1·10<sup>-6</sup> M, [HA] = 10 mg/L, I = 0.1 M NaClO<sub>4</sub>). Within the calculations, complexation data for two different types of U(VI)-humate complexes were considered: the binary UO<sub>2</sub>HA(II) complex (e.g., [37],[41],[52]) and the ternary complex UO<sub>2</sub>(OH)HA(I) ([53]). Ternary uranyl-carbonato-humate complexes were not included in the speciation calculations for the system with HA. **Fig. 4.3** shows the U(VI) speciation in solution in the presence of HA.



In the presence of HA, the free uranyl cation  $\text{UO}_2^{2+}$  predominates in the solution only at very low pH values ( $\sim \text{pH } 3$ ). The formation of  $\text{UO}_2\text{HA}(\text{II})$  starts very soon. This complex dominates the speciation in solution below pH 4. Then, both uranyl-humate species determine the speciation in solution in the pH range between pH 4.5 and pH 9 (absence of  $\text{CO}_2$ ) and pH 4.5 and 7.5 (presence of  $\text{CO}_2$ ). Next, the  $\text{UO}_2(\text{OH})\text{HA}(\text{I})$  complex is the prevailing species in solution. At higher pH values uranyl-carbonato and uranyl-hydroxo complexes become dominant in the presence and absence of  $\text{CO}_2$ , respectively.

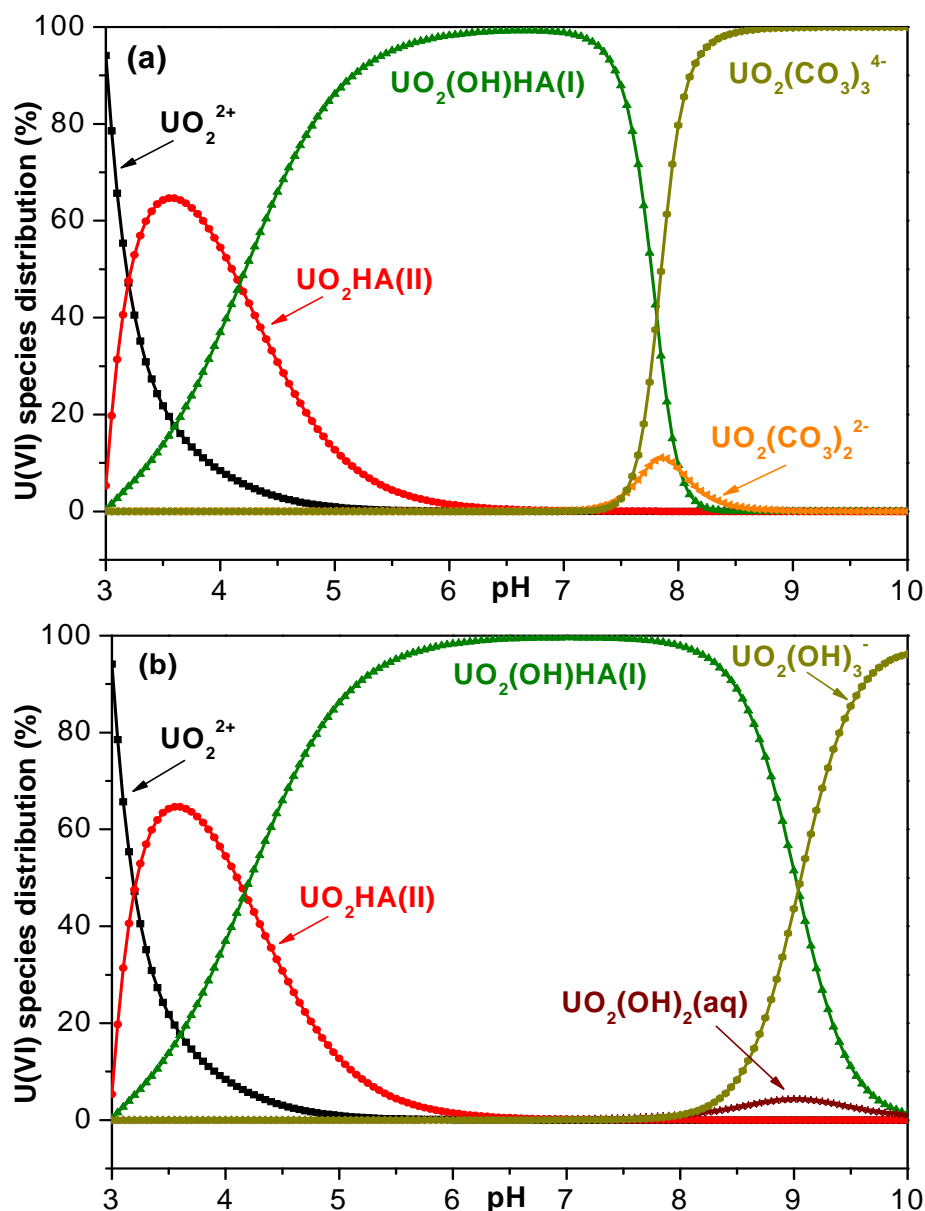


**Fig. 4.3:** U(VI) speciation in the presence of HA in the (a) presence and (b) absence of  $\text{CO}_2$  ( $I = 0.1 \text{ M NaClO}_4$ ,  $[\text{U(VI)}] = 1 \cdot 10^{-6} \text{ M}$ ,  $[\text{HA}] = 10 \text{ mg/L}$ ).

## 5. Humic Acid Sorption onto Kaolinite

To improve information on the influence of the HA on the U(VI) sorption, the sorption of HA onto kaolinite was studied. The HA sorption onto kaolinite can be affected by many factors. In this work, the influence of pH value, HA concentration, ionic strength of the solution, presence of CO<sub>2</sub>, and presence of U(VI) on HA sorption onto kaolinite were studied. Results of the HA sorption onto kaolinite under different experimental conditions are described in this chapter.

The experimental conditions of kinetic and sorption experiments used in this work were discussed and unified in the frame of joint project of BMWi No. 02E9673 “Migration of actinides in the system clay, humic substance, aquifer: characterization and quantification of the influence of humic substances”. Results of the HA and U(VI) kinetic and sorption experiments, presented in the following chapters, were published by Křepelová et al. [57].

The HA and U(VI) sorption experiments were carried out in this work. Namely therefore that results of the sorption experiments in individual systems HA-kaolinite and U(VI)-kaolinite are important for comparison with experiments in the investigated ternary system U(VI)-HA-kaolinite performed under comparable experimental conditions.

The sorption of HA onto clay minerals was also described in literature. The HA sorption can be affected by many factors, e.g., pH value, HA concentration, ionic strength of the solution or presence of CO<sub>2</sub>. Influence of *pH value* on HA sorption was studied in [58]-[67]. The sorption behavior of HA shows a general trend of decreasing HA sorption with increasing pH, as well as decreasing percentages of HA adsorbed with increasing HA initial concentration. Fairhurst et al. [63] reported that the sorption of HA onto kaolinite and montmorillonite is high at low pH for HA concentrations 2 – 10 mg/L with sorption dropping rapidly between pH 5 and pH 7. At higher HA concentration, 25 mg/L, the drop in percentage of sorbed HA occurs at lower pH (pH 3). The influence of *ionic strength* on the HA sorption was studied in [59] and [61]. Kretzschmar et al. [61] investigated the sorption of Portsmouth soil HA onto kaolinite as a function of pH and ionic strength. They found the strongest decrease in the HA sorption between pH 3 and pH 7. The HA sorption increased as the ionic strength increased from 0.001 M to 0.1 M, moreover, an increase of the HA sorption occurred between 0.01 M and 0.1 M. Schulthess and Huang [68] studied the HA and FA sorption by silicon and aluminum oxide surfaces on clay minerals. They

modeled the surface of clay minerals (mordenite, kaolinite, and montmorillonite) as mixtures of amorphous Al and Si oxides. The results showed a strong sorption of HA and FA by Al sites on the Al oxide and kaolinite and weak sorption by Si sites on the Si oxide, mordenite and montmorillonite.

### **5.1. Kinetics of Humic Acid Sorption onto Kaolinite**

Kinetic experiments were conducted to evaluate the time required to reach the sorption equilibrium. The initial concentration of HA was 10 mg/L and the ionic strength was kept at 0.01 M NaClO<sub>4</sub>. Detailed descriptions of experimental conditions and the sorption procedure are given in chapter 10.2.1.

**Fig. 5.1** shows the amount of sorbed HA as a function of contact time between HA and kaolinite for two pH values: pH 5 and pH 7.5. It becomes evident that the system reaches the sorption equilibrium quite fast. At pH 5 and pH 7.5, the amount of the sorbed HA does not change significantly after 50 h; thus, 60 h are sufficient to establish the sorption equilibrium in the system.

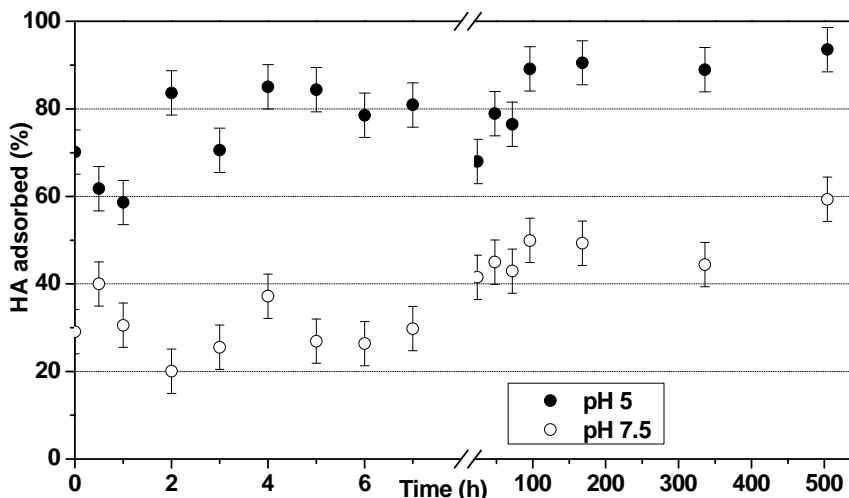


**Fig. 5.1:** Percentage of HA adsorbed from solution during kinetic experiments at pH 5 (filled symbols) and pH 7.5 (open symbols) ([HA] = 10 mg/L, I = 0.01 M NaClO<sub>4</sub>, pCO<sub>2</sub> = 10<sup>-3.5</sup> atm).

## 5.2. Sorption Capacity of Kaolinite for Humic Acid

The sorption capacity of kaolinite for HA was determined by measuring of the HA sorption onto kaolinite at different HA concentrations in the range between 10 mg/L and 50 mg/L and for different pH values. The results are depicted in **Fig. 5.2**. HA sorption is expressed as milligrams of HA sorbed onto 1 g of kaolinite. The maximal sorption of HA was achieved for HA concentration 20 mg/L at pH 5 – 8. The sorption at higher initial concentrations of HA onto kaolinite did not increase further. At pH 4, the maximal sorption was achieved for the initial HA concentration of 30 mg/L. The differences in HA amount adsorbed by various pH values arises from the dependence of HA sorption on pH value (see chapter 5.3).

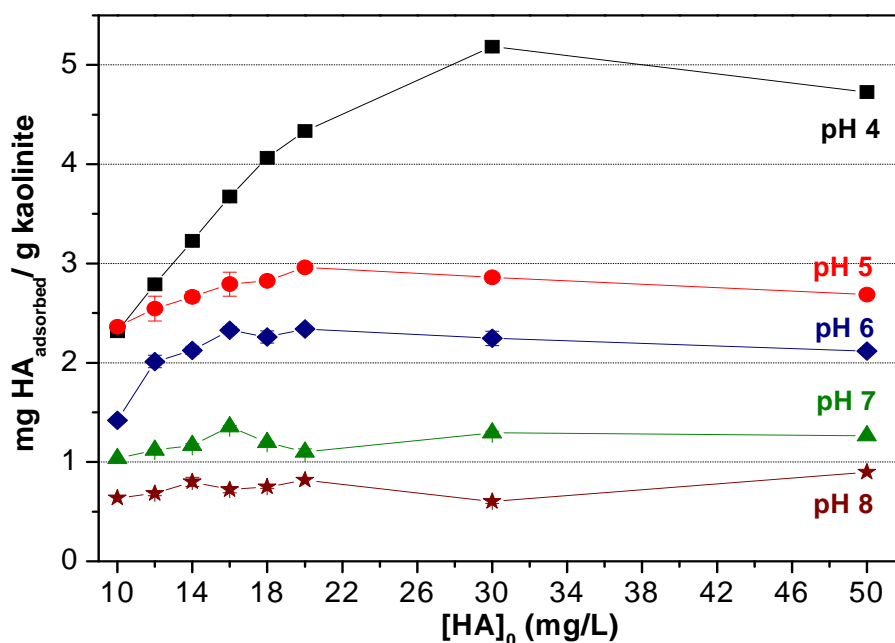


**Fig. 5.2:** Sorption of HA onto kaolinite as a function of pH and initial HA concentration ( $I = 0.01 \text{ M NaClO}_4$ ,  $p\text{CO}_2 = 10^{-3.5} \text{ atm}$ ).

## 5.3. Effect of pH and Humic Acid Concentration

The HA sorption experiments were performed in this work, since for evaluation of the experiments in the studied system U(VI)-HA-kaolinite, also binary systems HA-kaolinite and U(VI)-kaolinite must be investigated and described under comparable experimental conditions. Moreover, unlike other works,  $^{14}\text{C}$ -labeled synthetic HA was applied in these experiments.

HA uptake onto kaolinite as a function of pH and HA concentration at two different ionic strengths is shown in **Fig. 5.3**. The observed results are comparable to those of natural HA described in literature [58]-[67]. The sorption of HA decreases with increasing initial concentration and pH. More than 90 % of 10 mg/L HA is adsorbed onto kaolinite at pH 3. However, there is the possibility that a part of HA precipitates on the kaolinite surface at pH 3. There could be an overlapping of both processes, HA sorption and precipitation.

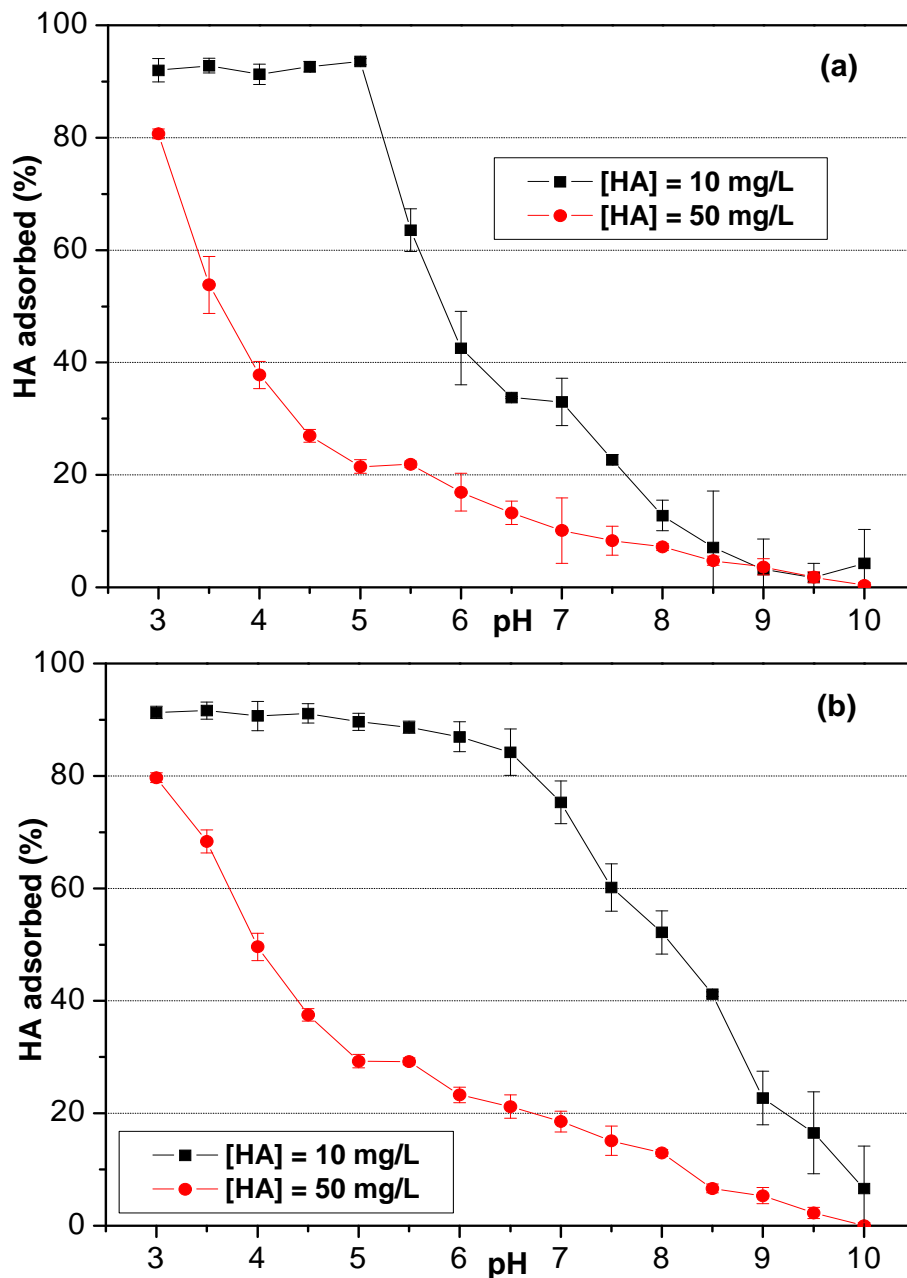


**Fig. 5.3:** HA sorption onto kaolinite as a function of pH and HA concentration (a)  $I = 0.01$  M  $\text{NaClO}_4$ , (b)  $0.1$  M  $\text{NaClO}_4$  ( $\text{pCO}_2 = 10^{-3.5}$  atm).

The percentage of HA sorbed decreases with increasing HA concentration due to saturation of binding sites of kaolinite (see chapter 5.2). Observed decrease of the HA sorption with increasing pH is regarded as the result of the electrostatic repulsions between carboxyl groups of HA and kaolinite surface. At  $\text{pH} > 3$ , carboxyl groups of HA are deprotonated resulting in a negative charge of the HA. Kaolinite is expected to feature a negative surface charge in this pH range (p.z.c. of kaolinite amounts to 6.0 [23] and p.z.n.p.c. is reportedly  $5.1 \pm 0.2$  [24] or  $4.99 \pm 0.03$  [25]).

Other factors contributing to the sorption behavior of HA would arise from specific site binding mechanisms such as ligand exchange and/or surface complexation reaction between -OH groups of kaolinite and anionic groups of HA. For instance, Murphy et al. [66] suggest that HA ligand exchange sorption reaction can occur in the following sequence: i) protonation of the surface hydroxyl  $\text{SOH} + \text{H}^+ \rightleftharpoons \text{SOH}_2^+$ , ii) outer-sphere complexation of the carboxylate group with the protonated hydroxyl group  $\text{SOH}_2^+ + \text{HuCOO}^- \rightleftharpoons \text{SOH}_2^+-\text{OOCHu}$ , and iii) ligand exchange to yield an inner-sphere complex  $\text{SOH}_2^+-\text{OOCHu} \rightleftharpoons \text{SOOCHu} + \text{H}_2\text{O}$ . SOH represents the surface hydroxyl group on the sorbent, and Hu-COO<sup>-</sup> represents the humic carboxyl groups.

Niitsu et al. [60] give a further example of a possible HA sorption reaction  $x(-\text{SOH}_2^+) + y\text{A}^- = (-\text{SOH}_2\text{A})_x \text{A}_{y-x}^{x-y}$ , where  $-\text{SOH}_2^+$  represents the positive sites on kaolinite available for carboxylate groups A<sup>-</sup> of HA. They suggest that also another interaction of colloidal HA with the mineral surface is possible. It could be described by DLVO (Derjaguin-Landau-Verwey-Overbeek) theory for colloids, based on van der Waals attractive interaction and electrical double layer repulsions.

The still significant sorption in the higher pH range (pH 6 – 8) can lead to the possible conclusion that HA reacts not only with silanol and aluminol groups of the surface but probably also interacts with organic components of clay via hydrogen bonds and hydrophobic attractions [69]. However, the TOC amount in kaolinite KGa-1b is quite low (see chapter 2.3), so in this studied system the contribution of organic components to HA sorption onto kaolinite can be neglected.

### 5.4. Influence of Ionic Strength

Fig. 5.4 depicts the sorption of HA in 0.01 M and 0.1 M NaClO<sub>4</sub> solutions for both studied HA concentrations. For HA concentration of 10 mg/L, between pH 3 and pH 5, the HA sorption at both ionic strengths is comparable and reaches almost 95 %. For HA concentration of 50 mg/L, the sorption is lower, starting at 80% at pH 3 and decreasing to near 0% at pH 10. In both cases, the 0.1 M NaClO<sub>4</sub> solution consistently shows higher sorption than the 0.01 M solution at higher pH values.

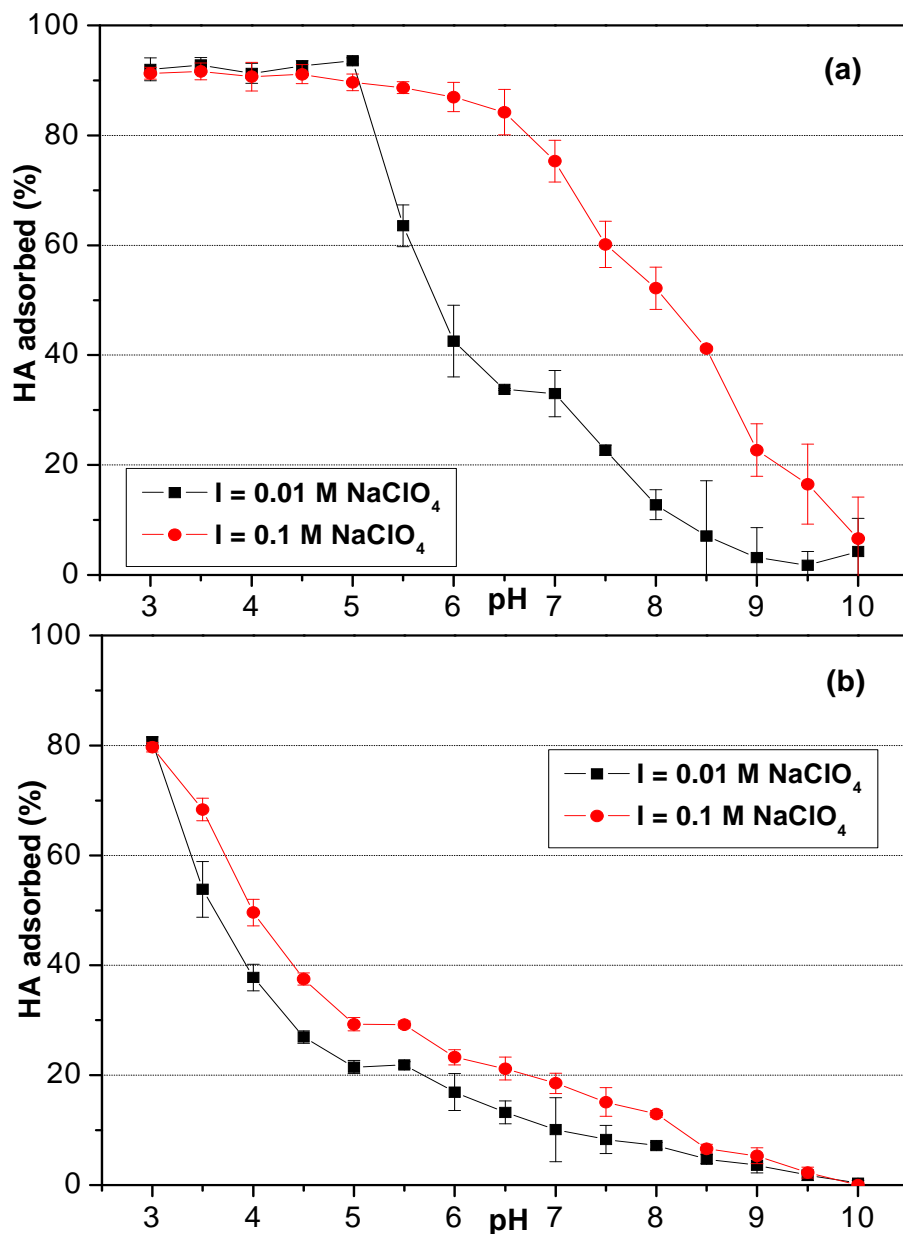


**Fig. 5.4:** Influence of the ionic strength on the HA sorption onto kaolinite (a) [HA] = 10 mg/L, (b) [HA] = 50 mg/L (pCO<sub>2</sub> = 10<sup>-3.5</sup> atm).

Strong differences in the amount of sorbed HA occur at pH > 5. The sorption of HA is increased at higher ionic strength. The maximal difference in the sorbed amount of HA between

both ionic strengths (almost 60%) was achieved at pH 6.5. An increase of the HA sorption with increasing ionic strength has been reported by some researches [59],[61]. The changes in the macromolecular configuration of HA as a function of the ionic strength are a possible explanation. At high ionic strength, the negative charges of HA macromolecules are well screened and consequently the HA wind up like random coils. Therefore, more HA can be adsorbed to the mineral surface [61].

At low ionic strength HA adopts a more linear or open configuration. Considered on a mole carbon basis, HA occupies a higher amount of mineral surface area than HA at high ionic strength [59], resulting in lower HA sorption on the surface. With an increase of HA concentration to 50 mg/L, the ionic strength loses its influence on the HA sorption.

### ***5.5. Effect of CO<sub>2</sub>-Presence***

**Fig. 5.5** shows the influence of carbonate on the HA sorption onto kaolinite for two HA concentrations: 10 and 50 mg/L. There are strong differences in both cases. In the system, where the initial HA concentration is 10 mg/L, the uptake of HA is comparable up to pH 5, whereas higher HA sorption onto kaolinite occurs in the absence of CO<sub>2</sub> at pH  $\geq$  5.5. The opposite effect is observed in the systems with initial HA concentration of 50 mg/L. The HA sorption is enhanced in the system without CO<sub>2</sub> in the pH range between pH 3 and pH 5, while at pH  $\geq$  5.5 the HA sorption is comparable in both systems. A possible explanation for this phenomenon could be the differences in the surface speciation on kaolinite in the presence and absence of CO<sub>2</sub>.



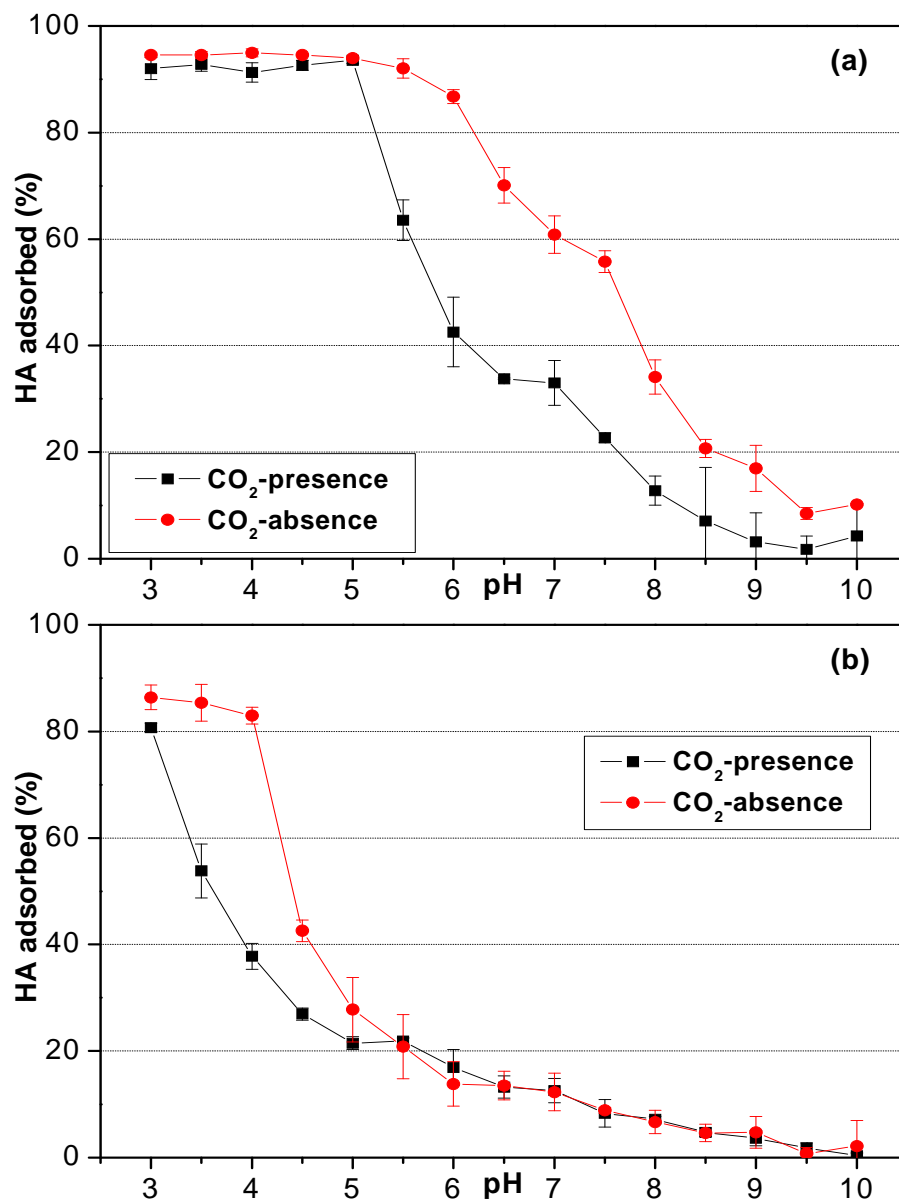


**Fig. 5.5:** Influence of CO<sub>2</sub> on the HA sorption onto kaolinite (a) [HA] = 10 mg/L, (b) [HA] = 50 mg/L (I = 0.01 M NaClO<sub>4</sub>).

### **5.6. Influence of U(VI)-Presence**

The presence of U(VI) has no influence on the HA sorption at 0.1 M ionic strength (**Fig. 5.6b**). However, in the 0.01 M solution the presence of U(VI) enhances the sorption of HA compared to the system without U(VI) at pH > 5.5 (**Fig. 5.6a**). This can be explained by the possible association between UO<sub>2</sub><sup>2+</sup> and HA on the kaolinite surface which is expected to be strongest in the pH range of increased U(VI) sorption onto kaolinite (see paragraph 6.3).

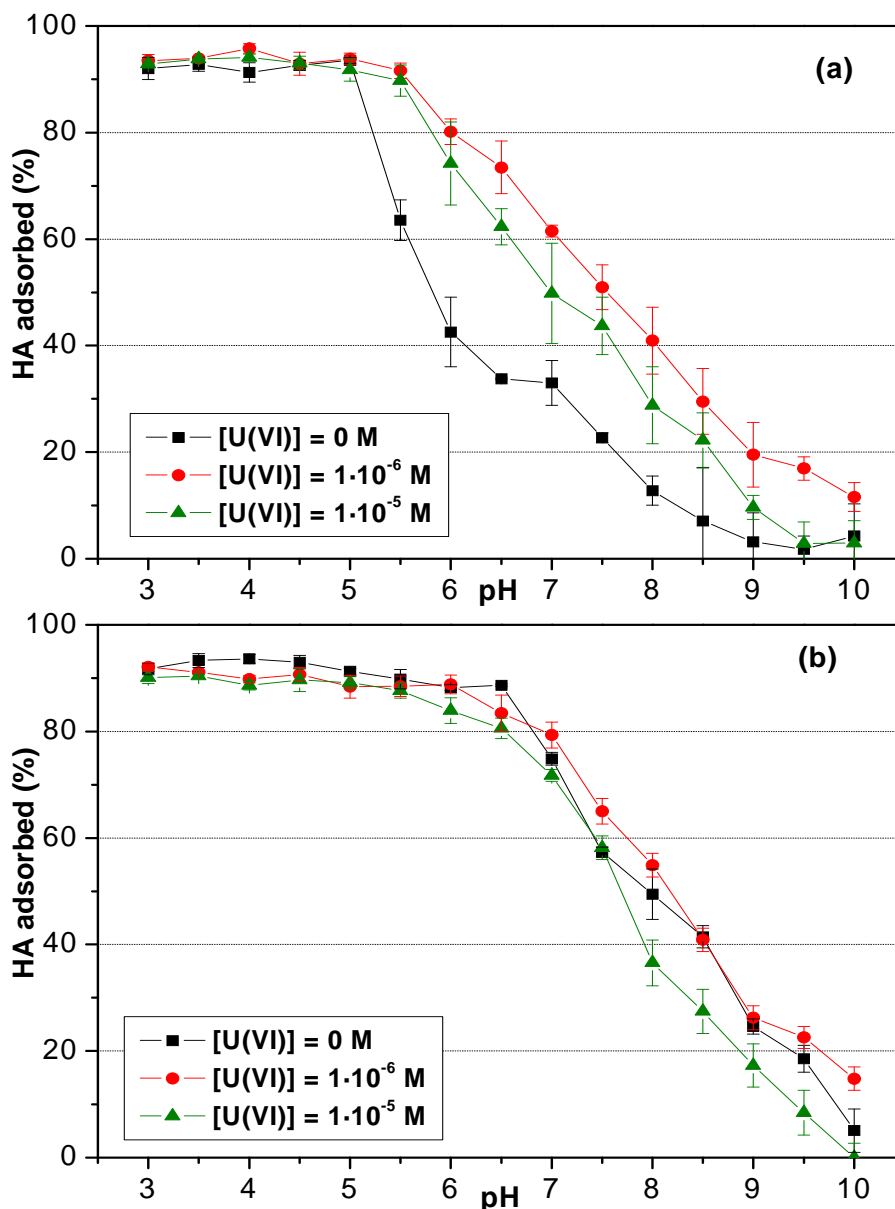


**Fig. 5.6:** Influence of the presence of U(VI) on the HA sorption onto kaolinite (a)  $I = 0.01$  M NaClO<sub>4</sub>, (b)  $I = 0.1$  M NaClO<sub>4</sub> ([HA] = 10 mg/L,  $p\text{CO}_2 = 10^{-3.5}$  atm).

Redden et al. [23] reported that U(VI) enhances the sorption of citrate onto kaolinite, when the citrate concentrations are comparable to those of U(VI). Schmeide et al. [70] explained a high HA sorption onto albite due to specific interactions of cations released into the aqueous phase due to mineral weathering and cation exchange processes with carboxylate groups of HA. These cations are able to form bridges between negatively charged surface species and HA carboxylate groups, thus, increasing the number of sorption sites for HA.

## 5.7. Binding of Humic Acid on Kaolinite Surface

To determine how HA interacts with the kaolinite surface, the X-ray photoelectron spectroscopy (XPS) was applied [71]. Three samples with different contents of HA were measured. Characterizations of the investigated samples are specified in **Tab. 5.1**.

**Tab. 5.1:** Sample characterization.

Sample	Characterization
RKS	Product of synthesis of HA M42 (R11/04KS) [72] in the presence of kaolinite, <b>9 mg HA/g kaolinite</b>
HA(4)	Kaolinite with sorbed HA (M42) at pH 4, 94% sorbed, <b>2.35 mg HA/g kaolinite</b>
HA(7.5)	Kaolinite with sorbed HA (M42) at pH 7.5, 45% sorbed, <b>1.18 mg HA/g kaolinite</b>

First, the overview spectra of all HA samples were recorded. The elements C, O, Al, Si, and minor amounts of Na were detected. Consecutively, the binding energies and relative intensities of the XPS lines of C, O, Al, and Si were determined. **Tab. 5.2** summarizes the obtained O 1s, Si 2s, Al 2s, Si 2p, and Al 2p binding energies and XPS lines. The binding energies of the HA-kaolinite samples agree within the experimental error with each other and with those of the untreated kaolinite sample. The uptake of HS by kaolinite and the relative intensities of XPS lines are given in **Tab. 5.3**.

**Tab. 5.2:** Binding energies of O 1s, Si 2s, Al 2s, Si 2p, and Al 2p XPS lines in eV. Standard error amounts to  $\pm 0.1$  eV.

Sample	O 1s	Si 2s	Al 2s	Si 2p	Al 2p
HA(4)	531.9	153.6	119.0	102.6	74.3
HA(7.5)	531.9	153.7	119.0	102.6	74.3
HA(7.5) <sup>a</sup>	531.8	153.5	119.4	102.5	74.6
RKS	532.0	153.7	119.0	102.7	74.3
KGa-1b <sup>b</sup>	532.2	153.9	119.3	102.9	74.6

a) after 10 min Ar<sup>+</sup> sputtering (4 kV, 10 – 15  $\mu$ A)

b) untreated kaolinite

Relatively small amounts of adsorbed hydrocarbons (i.e., approximately 1 atom% C) were detected on the untreated kaolinite surface. As can be seen from **Tab. 5.3**, the C 1s/Al 2p intensity ratio for all samples with sorbed HA is nearly constant. However, the difference between HA uptake by kaolinite in the samples varied by a factor of eight (9 mg/g – 1.2 mg/g).

**Tab. 5.3:** Relative XPS line intensities and uptake of HS by kaolinite. Experimental error amounts to  $\pm 5\%$ .

Sample	HS <sub>sorbed</sub> (mg/g)	C 1s/Al 2p	Si 2p/Al 2p	O 1s/Al 2p
HA(4)	2.4	0.61	1.60	20.6
HA(7.5)	1.2	0.47	1.62	20.1
HA(7.5) <sup>a</sup>	-	0.18	1.48	16.6
RKS	9.0	0.52	1.59	20.0
KGa-1b <sup>b</sup>	-	0.10	1.54	19.6
Calculated <sup>c</sup>	-	0	1.52	22.7

a) after 10 min Ar<sup>+</sup> sputtering (4 kV, 10-15  $\mu$ A)

b) untreated kaolinite, c) Al<sub>2</sub>(Si<sub>2</sub>O<sub>5</sub>)(OH)<sub>4</sub>

By XPS measurements it was found that the surface of the HA-kaolinite samples contains only approximately 5 atom% carbon. From this, the important conclusion that *the surface of the clay particles is not covered by a homogenous HA layer* can be made. It seems that part of HA must be distributed between the kaolinite particles. This means that *in the ternary system U(VI)-kaolinite-HA, U(VI) can interact with significant parts of the kaolinite surface that are not covered by HA*. Furthermore, all samples show comparable surface composition as the untreated kaolinite according to the amount of Si, Al, and O. Thus, it can be derived that the *chemical composition of the kaolinite surface was not altered by HA sorption or during HA synthesis*. The obtained experimental intensity ratios Si 2p/Al 2p and O 1s/Al 2p are in good agreement with the theoretical values that were calculated corresponding to the chemical composition of kaolinite, i.e., Al<sub>2</sub>(Si<sub>2</sub>O<sub>5</sub>)(OH)<sub>4</sub>. After sputtering of the sample HA(7.5) 10 min with Ar<sup>+</sup> ions, the C 1s/Al 2p intensity ratio decreased from 0.47 to 0.18 (cf. **Tab. 5.3**). This means that a significant amount of C could be removed from the surface of the kaolinite particles. Nevertheless, the C 1s/Al 2p intensity ratio of the sputtered HA-kaolinite sample was almost twice higher than that of the untreated kaolinite surface. This means that the remaining HA may not be bound to the kaolinite surface but could be located between the clay particles. It confirms the conclusion already resulted from above discussed comparable C 1s/Al 2p intensity ratios of all measured HA-kaolinite samples.

## 6. U(VI) Sorption onto Kaolinite

The influence of different experimental conditions such as pH value, ionic strength, CO<sub>2</sub>-presence and U(VI)-concentration onto U(VI) sorption was studied. Furthermore, the influence of size fractionation of kaolinite on U(VI) sorption was also determined. Albeit, the U(VI) sorption in the absence of HA onto different minerals is quite well described in literature [2],[4],[12],[23],[42],[70],[73]-[85], the sorption experiments in the binary system U(VI)-kaolinite were performed to have the complex information about the studied system U(VI)-HA-kaolinite and to have the data for the comparison of both systems, without and with HA, measured under the same experimental conditions. In this chapter, the literature overview to U(VI) sorption onto clay minerals and the obtained results of U(VI) sorption onto kaolinite are described.

In the experimental procedure, there are two steps which can influence the results of experiments: filtration of the samples and conditioning of the kaolinite with NaClO<sub>4</sub> solution. Therefore, experiments were performed where these two effects were investigated. Obtained results are discussed in chapters 6.7 and 6.8. The detailed description of the experimental conditions and sorption procedure is given in chapter 10.2.2.

### ***6.1. Actinide Interactions with Solid Surfaces***

The interaction of metal ions (e.g., actinides) in aqueous solution with the solid surfaces can be generally described as a mixture of at least three different, idealized processes [86]:

- (1) **Physical adsorption** is due to non-specific forces of attraction between sorbent and solute. This sorption process is rapid, reversible and rather concentration independent since the solute can form several consecutive layers on the sorbent. The process is non-selective and only slightly dependent on the ion exchange capacity of the solid. However, the speciation of the solute has major influence on this process.
- (2) **Electrostatic adsorption** (ion exchange) is due to coulombic attraction between charged solute species and the sorbent, which usually carries a net charge that is dependent on both pH and ionic strength. The process is rapid, often reversible and concentration dependent and highly influenced by the properties of the solid (exchange capacity) as well as of the ionic

strength (competing ions). Hydrolyzed and complexed actinides, and, in many systems, the uncomplexed dioxo, penta- and hexavalent actinyl ions, do not exhibit ideal ion exchange behavior on high-capacity solid sorbents like most layer silicates.

(3) **Chemisorption** (specific adsorption) is caused by the action of chemical forces between solute and sorbent, when the anions of the solid lattice could form strong complexes with the solute. This is often a fairly slow, partly irreversible and selective process that is dependent on the concentration of the trace element and requires a certain composition of the sorbent.

Other processes that would influence the apparent solubility of trace elements in solution include precipitation, co-precipitation and chemical substitution.

Sorption on solid surfaces is often quantitatively described in terms of sorption isotherms (total concentration in solution vs. total concentration in the adsorbent) or as distribution coefficient (the ratio of the concentration in the solid and solution phases under specified conditions, Eq. (6.1)).

The sorption of metal ions onto solid surfaces can be interpreted applying different models. For the modeling of sorption data, the surface complexation model (SCM) was often used, e.g., the sorption of U(VI) onto ferrihydrite [87],[88],[102], kaolinite [13],[88], Am(III) and U(VI) onto amorphous silica [85], and Eu(III) onto hematite [89]. Payne et al. [13] modeled the U(VI) sorption onto Georgia kaolinites with SCM model using code FITEQL. They assumed the presence of two types of surface sites: titanol ( $>TiOH$ ) and aluminol ( $>AlOH$ ). Another frequently used model is the diffuse double layer model (DDLDM) applied to study, e.g., the U(VI) and Se(IV) sorption onto Na-bentonite [90] and the U(VI) sorption onto phyllite [12],  $\alpha$ -alumina [82], montmorillonite [74], and quartz [1]. The triple-layer surface complexation model (TLSCM) was used to model the effects of carbonate on the sorption of Cr(II), Pb(II) and U(VI) onto goethite [91]. Bradbury et al. [92] developed and used 2 Site Protolysis Non Electrostatic Surface Complexation and Cation Exchange (2SPNE SC/CE) model to describe the sorption of 11 radionuclides with different valence states, e.g., Ni(II), Eu(III), Am(III), Th(IV), Np(V) and U(VI) on montmorillonite.

## **U(VI) Sorption onto Clay Minerals**

The sorption of actinides onto clay minerals is influenced by several factors such as pH, adsorbent concentration, actinide concentration, ionic strength, and temperature.

The *pH value* affects the speciation of actinides and it can also simultaneously influence the charge of adsorbent, especially by clay minerals (see chapter 2.2). Different forms of an element can be adsorbed with different mechanisms and the charge interactions between adsorbent and sorbate influence an extent of the sorption. Thus, pH can have a high impact on capture of trace elements. In the most cases, the sorption curve has a similar trend. At low pH value, the sorption is very low and it increases from a certain pH value (adsorption edge) to the maximum and stays constant with increasing pH value in the absence of carbonate or the sorption decreases at higher pH value in the presence of carbonate. A series of works dealt with the U(VI) sorption onto kaolinite [13],[23],[73],[88]. The U(VI) sorption edge was observed between pH 3 and pH 4 and the drop in the U(VI) sorption usually occurs at pH > 8. Also, the other works studying the U(VI) sorption onto montmorillonite [1],[74], smectite [75] and bentonite [90], chlorite and biotite [73] mostly show the typical U(VI) sorption curve described above with similar values of pH adsorption edges reaching different sorption maxima for different minerals. Two sorption maxima were observed in the study of the U(VI) sorption onto cypris clay [93].

The next parameter influencing the sorption of actinides from aqueous solutions onto *adsorbent* is its *concentration* expressed as the ratio  $m/V$ , where  $m$  is weight of the solid phase and  $V$  is volume of the aqueous phase. The effect of adsorbent concentration can be expressed by means of the distribution coefficient  $K_d$  (Eq. (6.1)) under consideration of validity of linear sorption isotherm, that is under consideration that  $K_d$  will not change with  $m/V$  ratio:

$$K_d = (m_a / m_r) \cdot (V / m), \quad (6.1)$$

where  $m_a$  is the equilibrium amount of sorbed trace element and  $m_r$  is the equilibrium amount of this element in the solution. Palaban et al. [1] reported that the percentage of U(VI) sorbed onto clinoptilolite and montmorillonite increases with an increasing  $m/V$  ratio, however, data replotted in term of  $K_d$  showed that changes in  $m/V$  have only little or no influence on  $K_d$ . Payne et al. [13] found an increase of percentage of the U(VI) uptake on kaolinite with an increase of mass loading of the solid system. Kilislioglu et al. [76] also observed the dependence of the U(VI) sorption on the amount of adsorbent in the study of the U(VI) sorption onto halloysite. The

percentage of sorbed U(VI) and the distribution coefficient increased with increasing amount of adsorbent. Beneš et al. [91] reported the dependence of position of two sorption maxima of U(VI) sorption onto cypris clay on the concentration of the clay. Payne et al. [88] observed an increase of the U(VI) uptake on kaolinite with increasing mass loading of the solid in the system.

The *initial concentration of actinides* in the solution also influences their sorption. Hyun et al. [74] studied the U(VI) sorption on montmorillonite. For comparison, the authors also presented results of the U(VI) sorption onto kaolinite and chlorite. In the kaolinite system, as the total U(VI) concentration increased, the sorption pH edge shifted to a higher pH region. In the chlorite system, differences in the U(VI) sorption can be found mainly in the pH range between pH 5 and pH 7. A significant concentration dependence of the U(VI) sorption on halloysite was observed by Kilislioglu et al. [76]. Percentage of the sorption and distribution coefficient decreased as the initial concentration of U(VI) increased. Payne et al. showed in the studies [13] and [88] a decrease of percentage of U(VI) sorbed onto kaolinite with increasing U(VI) concentration.

The influence of *ionic strength* belongs to important factors affecting the sorption of actinides. Increase of the sorption of U(VI) on smectite with decreasing ionic strength was observed in NaClO<sub>4</sub> electrolyte, whereas in Ca(ClO<sub>4</sub>)<sub>2</sub> electrolyte no effect was found [75]. An increase of *temperature* enhanced the sorption kinetics of U(VI) on halloysite in [76].



## 6.2. Kinetics of U(VI) Sorption onto Kaolinite

As in the case of HA, the kinetic experiments were conducted to determine the time which U(VI) required to establish the sorption equilibrium. The initial concentration of U(VI) was  $1 \cdot 10^{-6}$  M and the ionic strength was kept at 0.01 M NaClO<sub>4</sub>. The experiments were performed at two pH values: pH 5 and pH 7.5. Detailed descriptions of experimental conditions and the sorption procedure are given in chapter 10.2.1.

The amount of U(VI) sorbed onto kaolinite as a function of different contact times is illustrated in **Fig. 6.1**. U(VI) sorbed onto kaolinite amounts to ~ 70% at pH 5 and to almost 100% at pH 7.5. Similarly to HA (cf. section 5.1), kinetics of the U(VI) sorption onto kaolinite is very fast. The sorbed amount of U(VI) is stable after 50 h at pH 5 and even earlier at pH 7.5.

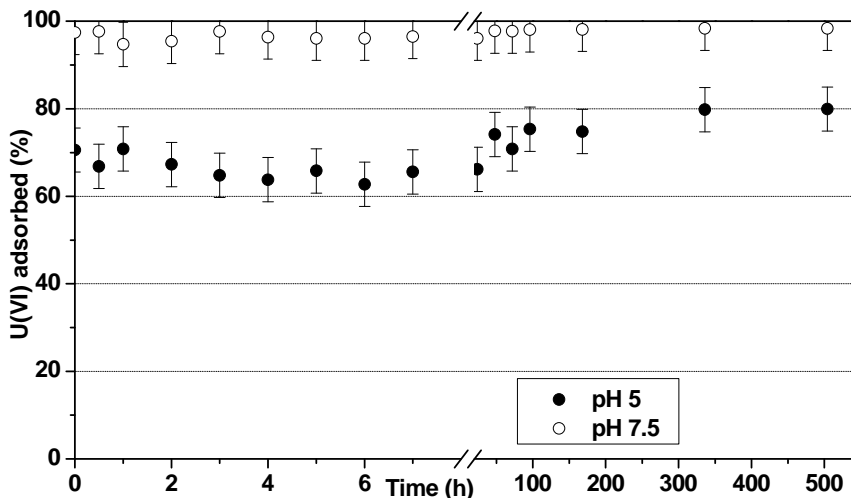


**Fig. 6.1:** Percentage of U(VI) adsorbed from solution during kinetic experiments at pH 5 (filled symbols) and pH 7.5 (open symbols) ( $[U(VI)] = 1 \cdot 10^{-6}$  M,  $I = 0.01$  M NaClO<sub>4</sub>,  $pCO_2 = 10^{-3.5}$  atm).

### **6.3. Effect of pH and U(VI) Concentration**

Results of the batch experiments for kaolinite and U(VI) as a function of pH and U(VI) concentration at two different ionic strengths are depicted in **Fig. 6.2**. They are consistent with those data previously reported in literature ([2],[4],[42],[70],[73]-[85]). In the presence of CO<sub>2</sub>, the percentage of the total U(VI) sorbed onto kaolinite increases from nearly zero at pH 3 to 97% between pH 6 and pH 8. Above pH 8, the U(VI) sorption decreases. The highest U(VI) sorption occurs in the pH range, where the U(VI) hydroxyl complexes are important. The positioning of the sorption edges at low pH values suggests the formation of relative strong actinide/surface site complexes. The formation of inner-sphere surface complexes was reported by several authors [23],[77],[94]. Reich et al. [94] proposed a structural model for the inner-sphere sorption of U(VI) on kaolinite based on the measured U-O and U-Si/Al distances. From their EXAFS investigations in this system it was concluded that U(VI) is possibly coordinated by edge sharing with [SiO<sub>4</sub>] tetrahedra and/or [AlO<sub>6</sub>] octahedra. On the contrary, T. Payne et al. [13] excluded the U(VI) sorption onto silanol sites. They assigned the U(VI) sorption onto kaolinite to aluminol and titanol sites, coming from accessory Ti phases (predominantly anatase) in the kaolinite sample. They modeled the U(VI)-kaolinite system as a combination of aluminol and titanol sites, using a simple non-electrostatic surface complexation model. However, no spectroscopic evidence was given for the U(VI) interaction with the titanol sites.

An increase of U(VI) initial concentration from  $1 \cdot 10^{-6}$  M to  $1 \cdot 10^{-5}$  M causes a shift of the sorption pH edge by one pH unit to higher pH values. The mass of U(VI) sorbed in the maximum of sorption curves is higher in the case of  $1 \cdot 10^{-5}$  M U(VI) concentration (e.g., pH 7: 532  $\mu$ g U(VI)/ 1 g kaolinite is sorbed) than in  $1 \cdot 10^{-6}$  M U(VI) concentration (pH 7: 59  $\mu$ g U(VI)/1 g kaolinite is adsorbed). However, the percentage of U(VI) sorbed onto kaolinite decreases due to the higher initial U(VI) concentration.

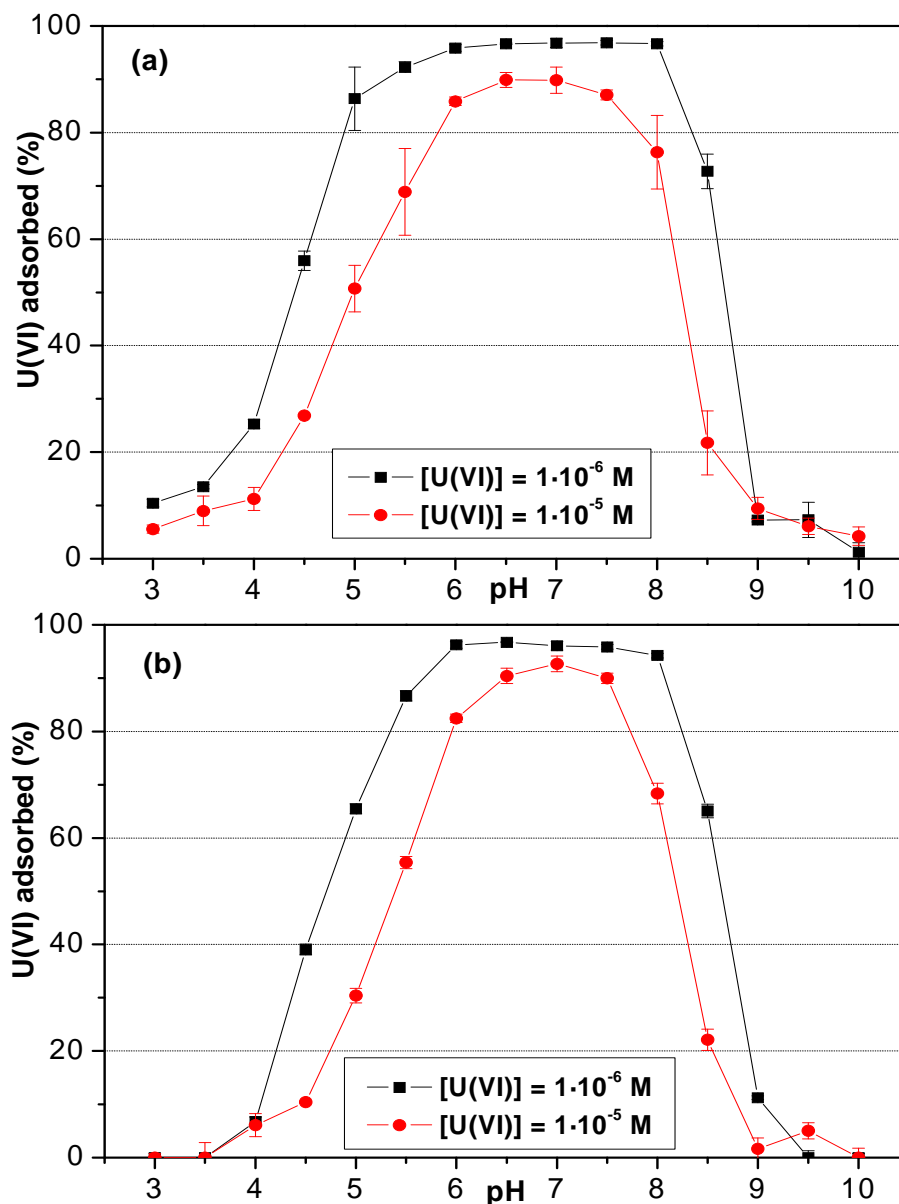


**Fig. 6.2:** U(VI) sorption onto kaolinite as a function of pH and U(VI) concentration (a)  $I = 0.01$  M  $\text{NaClO}_4$ , (b)  $I = 0.1$  M  $\text{NaClO}_4$  ( $p\text{CO}_2 = 10^{-3.5}$  atm).

### 6.4. Influence of Ionic Strength

The influence of ionic strength on the U(VI) sorption onto kaolinite is shown in **Fig. 6.3** for both studied U(VI) concentrations  $1 \cdot 10^{-6}$  M and  $1 \cdot 10^{-5}$  M in the presence of  $\text{CO}_2$ . The ionic strength has a small influence on the U(VI) sorption onto kaolinite in the pH range  $< 5.5$ . The differences in the sorption are more significant for the U(VI) concentration of  $1 \cdot 10^{-6}$  M than for the U(VI) concentration of  $1 \cdot 10^{-5}$  M. They reach a maximum of 20 % at pH 5. The influence of

ionic strength on the U(VI) sorption onto kaolinite becomes negligible at  $\text{pH} \geq 6$  for both studied U(VI) concentrations.

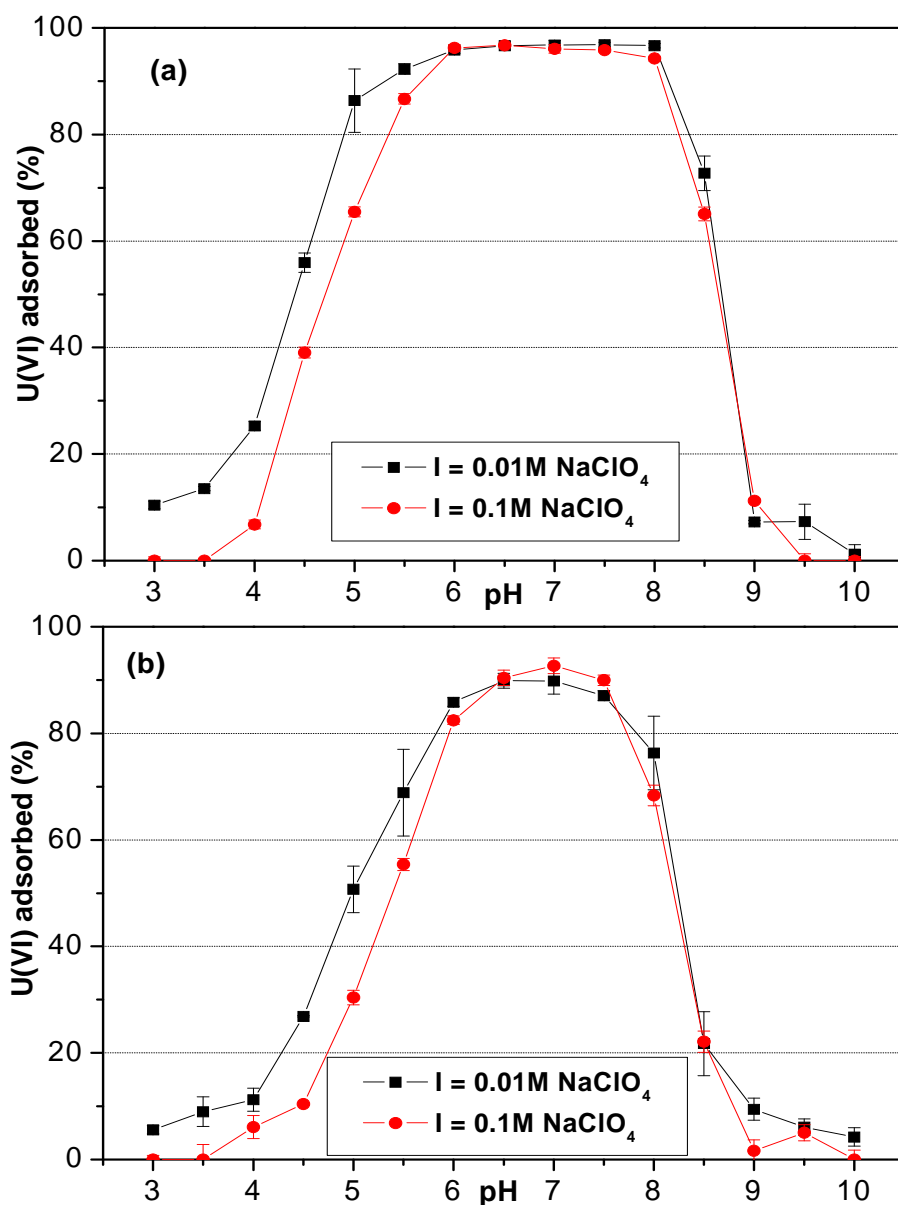


**Fig. 6.3:** Influence of the ionic strength on the U(VI) sorption onto kaolinite for U(VI) concentrations (a)  $1 \cdot 10^{-6}$  M and (b)  $1 \cdot 10^{-5}$  M ( $\text{pCO}_2 = 10^{-3.5}$  atm).

### 6.5. Effect of CO<sub>2</sub>-Presence

Fig. 6.4 illustrates the effect of CO<sub>2</sub>-presence on the U(VI) sorption onto kaolinite. The U(VI) sorption behavior is comparable in the systems with and without CO<sub>2</sub> in the pH range between pH 3 and pH 8.

At  $\text{pH} > 8$ , however, no sorption decrease was observed in the absence of  $\text{CO}_2$ . This behavior is a result of the U(VI) speciation in the solution. In the presence of  $\text{CO}_2$ , U(VI) forms negatively charged uranyl-carbonato complexes  $\text{UO}_2(\text{CO}_3)_3^{4-}$  ( $\log \beta = 21.0 \pm 0.3$  [95]) and  $(\text{UO}_2)_2\text{CO}_3(\text{OH})_3^-$  ( $\log \beta \approx 41$  [48]), cf. chapter 4. Under these conditions the kaolinite surface is also negatively charged. Therefore, the electrostatic repulsions between uranyl-carbonato complexes and kaolinite result in the low U(VI) sorption in this pH range.

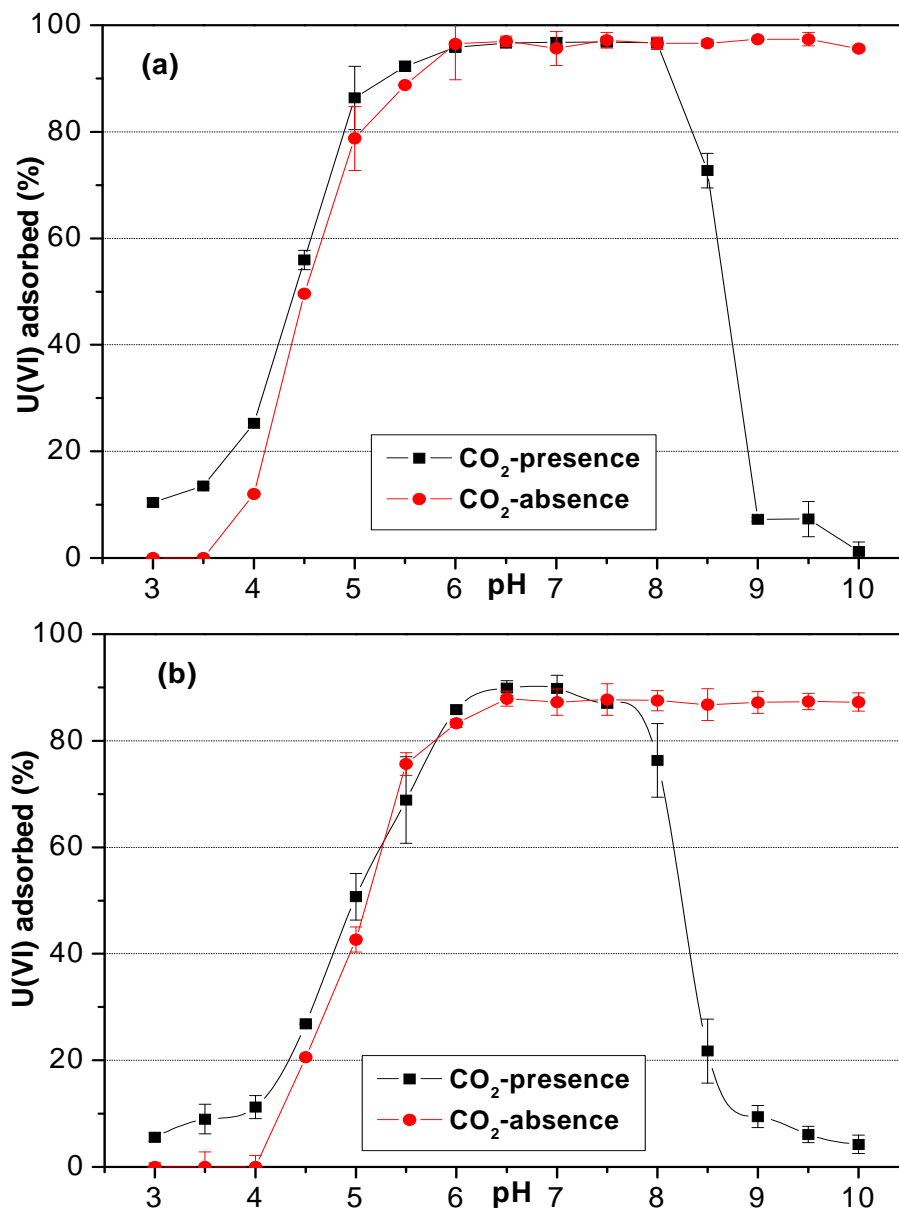


**Fig. 6.4:** U(VI) sorption onto kaolinite as a function of pH and  $\text{CO}_2$ -presence (a)  $[\text{U(VI)}] = 1 \cdot 10^{-6}$  M, (b)  $[\text{U(VI)}] = 1 \cdot 10^{-5}$  M ( $I = 0.01$  M  $\text{NaClO}_4$ ).

### 6.6. Effect of Size Fractionation of Kaolinite

The sorption of U(VI) onto size-fractionated (< 2 μm) and untreated kaolinite was studied for two U(VI) concentrations:  $1 \cdot 10^{-6}$  M and  $1 \cdot 10^{-5}$  M. The results are illustrated in **Fig. 6.5**.

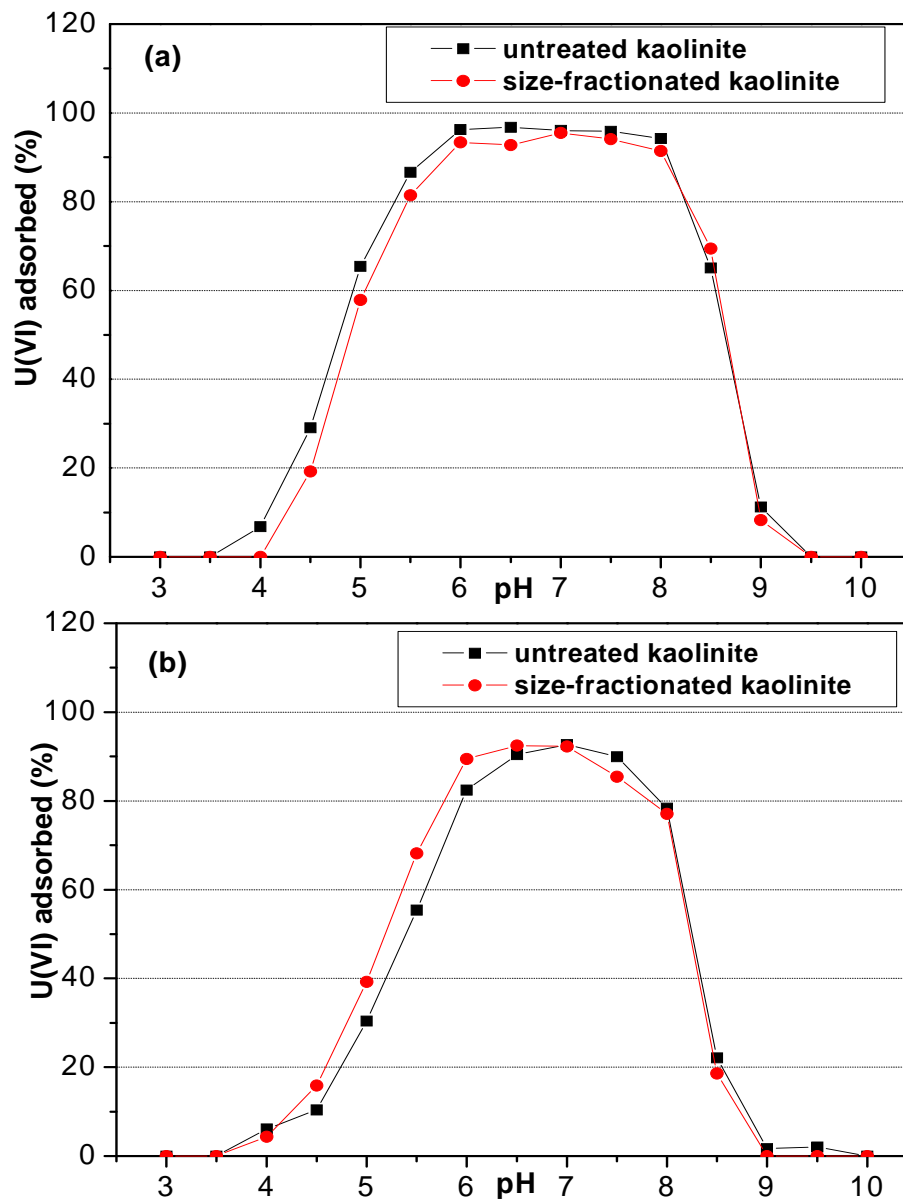


**Fig. 6.5:** U(VI) sorption onto untreated and size-fractionated kaolinite at U(VI) concentration (a)  $1 \cdot 10^{-6}$  M and (b)  $1 \cdot 10^{-5}$  M ( $I = 0.01$  M  $\text{NaClO}_4$ ,  $p\text{CO}_2 = 10^{-3.5}$  atm).

It can be seen that there are only small (pH 4.5 – 5.5.) or no (pH > 5.5) significant differences in the U(VI) sorption. Such results are not surprising when considering the values of

the surface areas of both types of kaolinite. The surface area of untreated and size-fractionated kaolinite KGa-1b amounts to 11.8 m<sup>2</sup>/g and 11.9 m<sup>2</sup>/g [26], respectively (cf. chapter 2.3.4).

### **6.7. Effect of Sample Filtration on the Results**

The influence of filtration on the U(VI) and HA sorption onto kaolinite was determined. Several experiments were performed, where the supernatants were analyzed by ICP-MS (for U(VI)) and LSC (for HA) either direct after centrifugation or after filtration. In the experiments with U(VI), the influence of filters with three different pore sizes 5 nm, 200 nm, and 450 nm was studied. An example of the obtained results is given in **Fig. 6.6** for a U(VI) concentration of 1·10<sup>-5</sup> M and an ionic strength of 0.01 M NaClO<sub>4</sub>. It can be seen that the filtration with used filters has no effect on the results of the U(VI) sorption in the pH range > pH 5.5. The difference in the U(VI) sorption at low pH values by filtration with 5 nm filter results from the U(VI) sorption on the filter material. For the other conditions used in sorption experiments similar conclusions can be made.

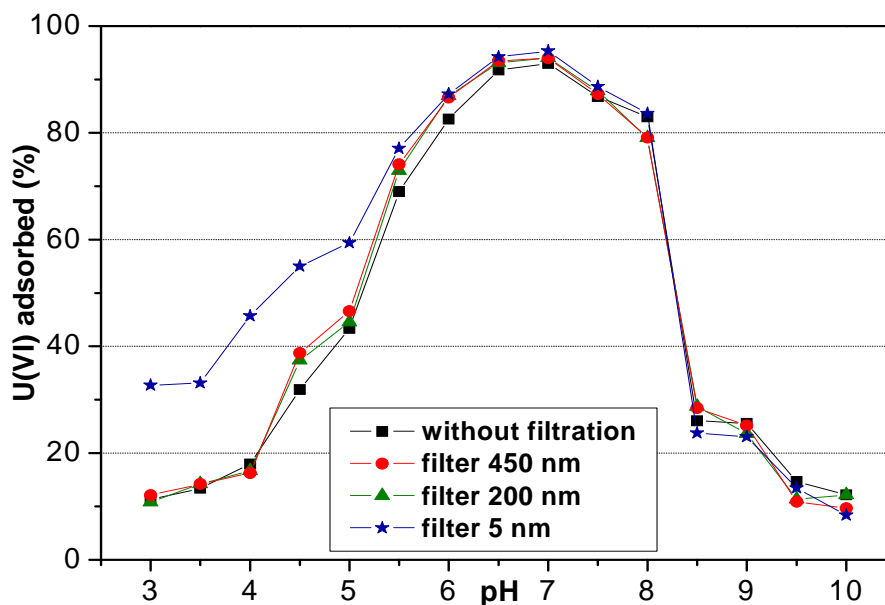


**Fig. 6.6:** Effect of filtration on U(VI) sorption onto kaolinite ([U(VI)] = 1·10<sup>-5</sup> M, I = 0.01 M NaClO<sub>4</sub>, pCO<sub>2</sub> = 10<sup>-3.5</sup> atm).

In the experiments with HA, the influence of filtration was studied with two different filter pore sizes: 200 nm and 450 nm. Also in the case of HA sorption, no effects of filtration were found comparing to the unfiltered samples. An example of such results is shown in **Fig. 6.7a** for

HA sorption in the absence of U(VI) and **Fig. 6.7b** for HA sorption in the presence of U(VI) for HA concentration 10 mg/L.

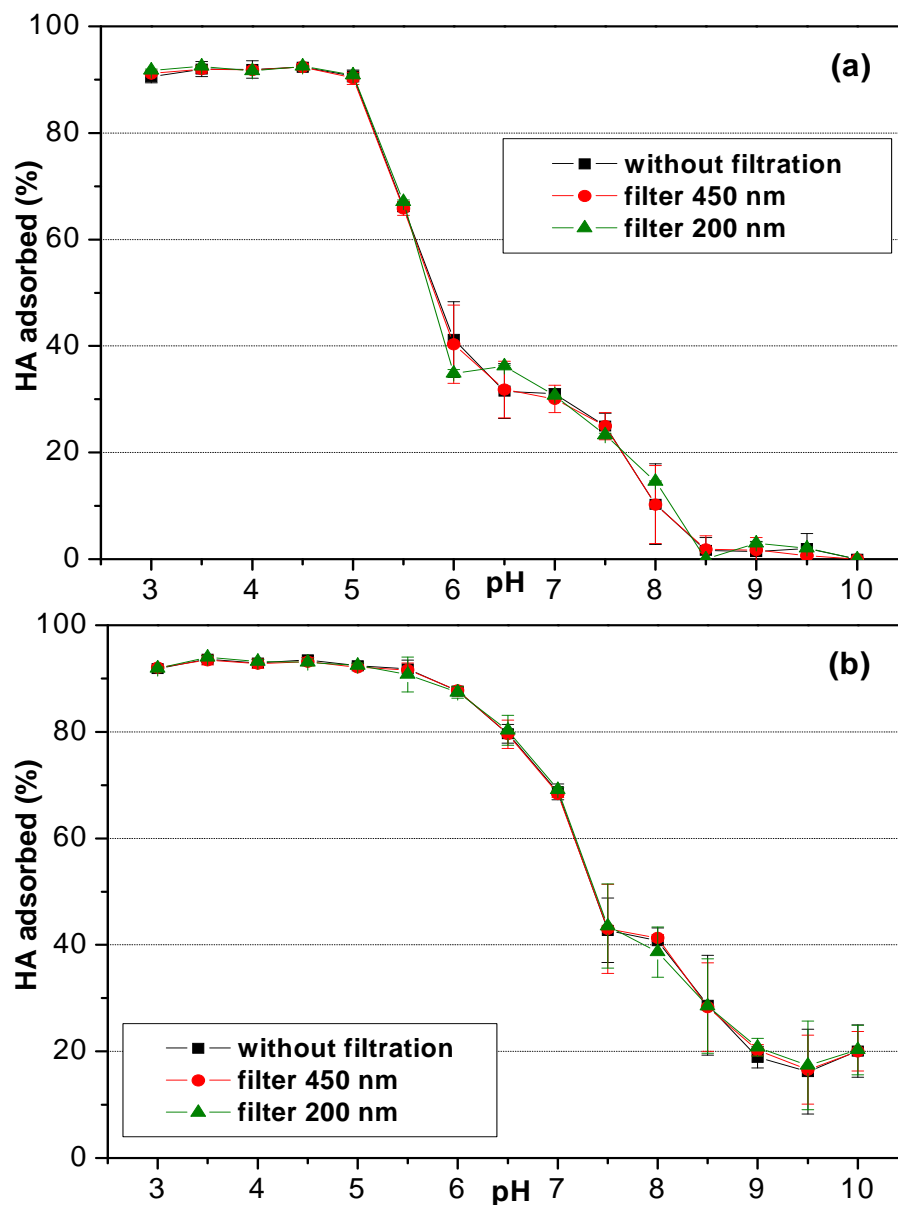


**Fig. 6.7:** Effect of the filtration on HA sorption onto kaolinite in the (a) absence and (b) presence of U(VI) ([HA] = 10 mg/L, [U(VI)] =  $1 \cdot 10^{-6}$  M, I = 0.01 M NaClO<sub>4</sub>).

### 6.8. Effect of Conditioning on the Kaolinite

In the kinetic and sorption experiments is kaolinite firstly pre-conditioned with NaClO<sub>4</sub> solution for 72 h and then it is next 60 h (contact time) shaken with the same solution after addition of U(VI) and/or HA. Therefore, the experiments described in this chapter were



performed to determine possible kaolinite structure changes or its dissolution during the kinetic and sorption experiments. Firstly, the evolution of the clay mineral structure and the formation of secondary phases were monitored by XRD. The XRD spectra of kaolinite were measured after one week of kaolinite conditioning with 0.01 M NaClO<sub>4</sub> at three different pH values – pH 4, pH 7, and pH 10. The spectra were then compared with the XRD spectrum of kaolinite without conditioning. The X-ray diagrams indicate no changes in XRD spectra during the course of the experiment for all studied pH values (**Fig. 6.8**). The formation of secondary phases was not observed.

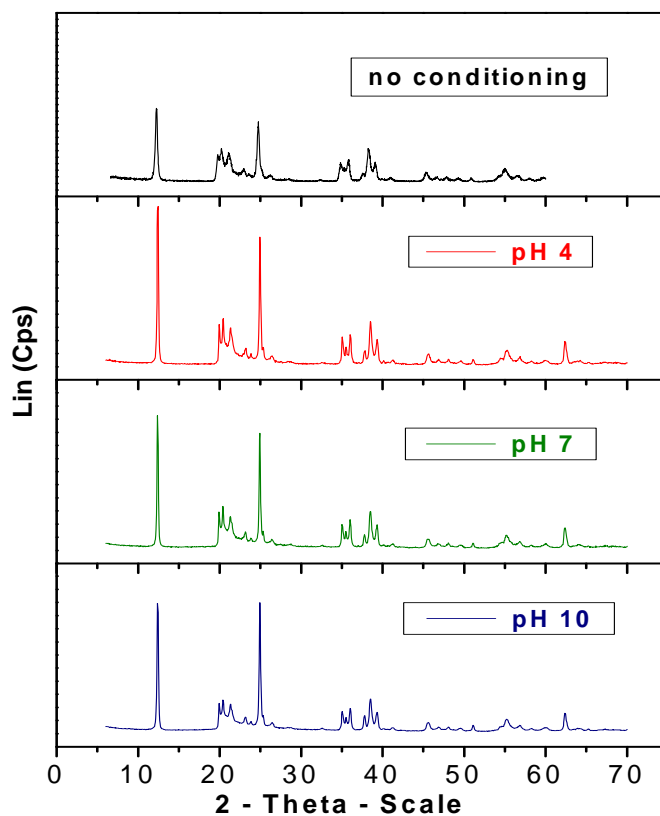


**Fig. 6.8:** XRD spectra of the kaolinite without and after conditioning.

Secondly, kaolinite expected dissolution during the experimental runs is reflected by the release of Si and Al into solution. The concentrations of these elements in the solution were measured after different contact times of kaolinite with the solution. The samples were measured by ICP-MS after 24, 72 (time of pre-conditioning of kaolinite with solution) and after next 60 h (contact time of kaolinite with activity). The obtained results are shown in **Fig. 6.9**. The highest measured Al concentration in the solution: 127 µg/L was achieved at pH 3, whereas at pH 5 and pH 10 the Al concentration did not exceed 42 µg/L. Si showed opposite behavior, the highest Si

dissolution: 6.5 mg/L was observed at pH 10, while its concentration at pH 3 and pH 5 did not exceed 0.4 mg/L. The concentration of dissolved Al ( $127 \mu\text{g/L} \cong 4.7 \cdot 10^{-6} \text{ M}$ ) or Si ( $42 \text{ mg/L} \cong 2.32 \cdot 10^{-4} \text{ M}$ ) can exceed the concentration of U(VI) ( $1 \cdot 10^{-6} \text{ M}/1 \cdot 10^{-5} \text{ M}$ ) in solution and, therefore, they could act as competing ions in sorption experiments.

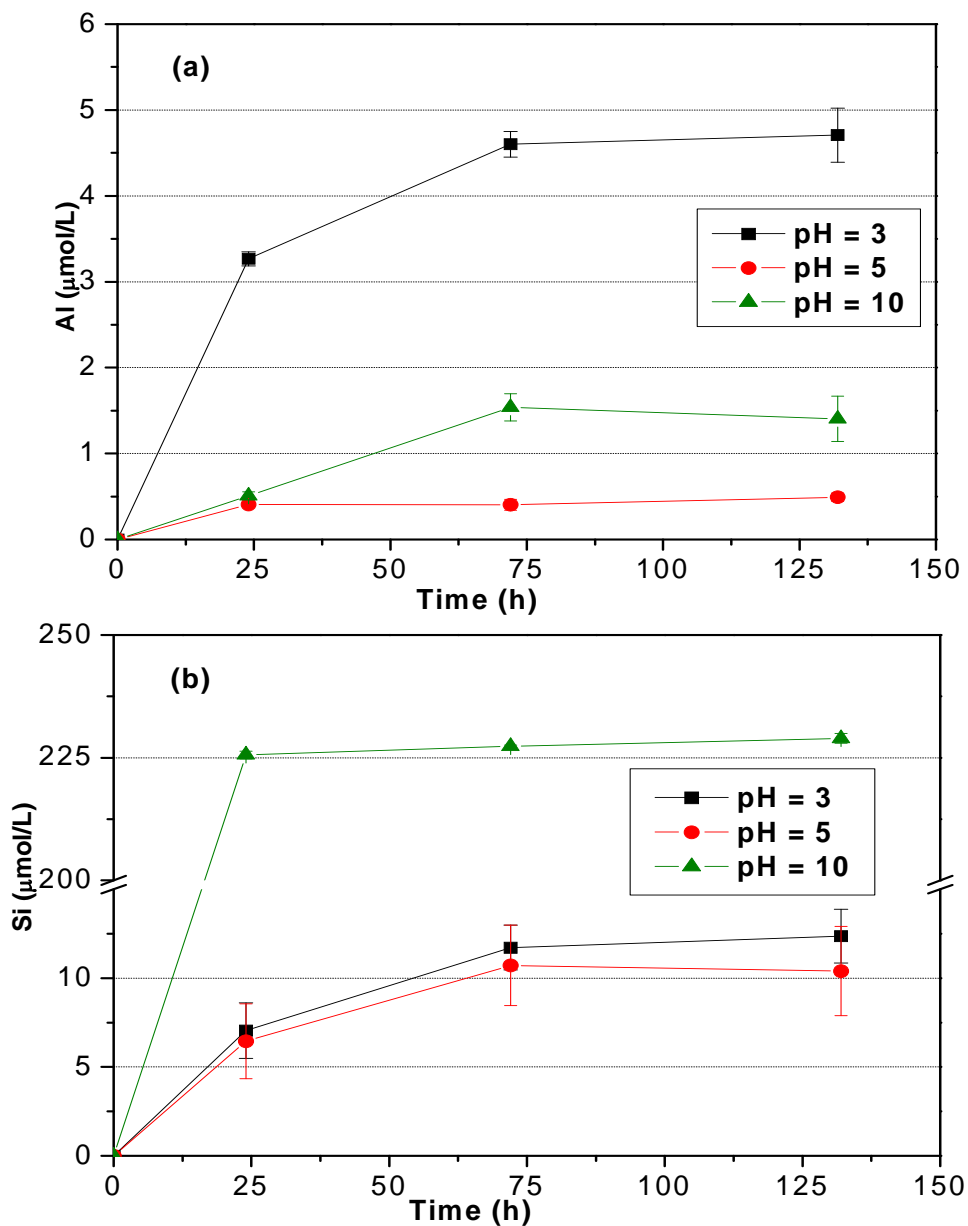


**Fig. 6.9:** Aqueous concentrations of (a) Al and (b) Si after different contact times of kaolinite with the solution ( $I = 0.01 \text{ M NaClO}_4$ ,  $p\text{CO}_2 = 10^{-3.5} \text{ atm}$ ).

However, the highest Al dissolution occurs in the pH range where no or only low U(VI) sorption onto kaolinite exists, thus, the effect of Al on the U(VI) sorption onto kaolinite could be

neglected. Also in the case of Si dissolution, the highest amount of dissolved Si occurs at pH 10 where U(VI) sorption is very low. Moreover, from kinetics experiments (cf. section 6.2) it is evident that the amount of sorbed U(VI) did not change with the time, so if there would be some effect of Si/Al ions on the U(VI) sorption, it has to be observable also in kinetic measurements.

From **Fig. 6.9** it also becomes obvious that the highest dissolution of both ions occurs within the first 72 h. These results suggest that the surface of clays minerals is affected by complex reactions and that the sorption occurs in a „dynamic“ process. However, the kinetics of the sorption mechanism is thought to be much faster than the dissolution reactions [96].

Cama et al. [97] studied the effect of pH and temperature on kaolinite (KGa-2) dissolution rate under acidic conditions. They have found that kaolinite dissolution rate increases with temperature and decreases with pH. They assigned the control of the rate of kaolinite dissolution at pH range between pH 0.5 and pH 4.5 to two independent parallel reaction paths consisting of fast sorption of a proton on a different surface site followed by a slow hydrolysis step. Huertas et al. [98] suggested that the two active sites that control the rate under acidic conditions are the edge and basal Al sites.

## 7. Influence of Humic Acid on the U(VI) Sorption onto Kaolinite

HA can influence the sorption of actinides due to the formation of soluble binary or ternary U(VI)-humate complexes. Therefore, the effect of HA on the U(VI) sorption onto kaolinite was determined in this work under different experimental conditions. The U(VI) sorption in the presence of HA was studied in batch experiments varying the U(VI) and HA concentrations as a function of pH in the presence and absence of CO<sub>2</sub>. In this chapter, results of the kinetic and sorption experiments are described and compared with literature.

The U(VI) sorption onto clay minerals in the presence of HA was investigated only by a few authors (e.g., [93],[99]). The U(VI) sorption onto iron, silica or aluminum oxides is studied more often. The influence of HA on the sorption of actinide ions onto a sorbent depends particularly on the *pH value*. At the low pH range generally an increase of actinide ions sorption with the addition of HA was observed, whereas at higher pH values a decrease or no effect was observed. The pH range, where the changes in sorption occur, depends on the type of sorbent and on other parameters, such as concentration ratio of HA and sorbent, HA and actinide, and ionic strength. Beneš et al. [93] reported that the sorption of U(VI) ( $[U(VI)] = 4.2 \cdot 10^{-5}$  M) onto cypris clay passes through two maxima and a minimum as the pH value increases (pH 2 – 12). The presence of humate ( $[HA] = 0.3, 3$  g/L) caused a shift of maxima, whereas the position of the sorption minimum remained unaffected for solid/liquid ratio of 5 g/L. No changes in maxima positions and a shift of sorption minimum were observed in the experiments with higher amount of cypris clay (50 g/L). The next parameters influencing actinides sorption in the presence of HA can also be the *ionic strength*, the *ratio of HA and sorbent* concentrations or the *sorption kinetics*. Schmeide et al. [100] studied the kinetics of the U(VI) and HA sorption onto muscovite. However, the equilibrium was not reached in the studied time of 312 h.

HA can influence the interaction of actinides with clay minerals, moreover, it can cause either their retardation or release in the environment. Therefore, it is important to study HA influence also on molecular level to predict the macroscopic processes.

## ***7.1. Kinetics of U(VI) Sorption onto Kaolinite in Presence of Humic Acid***

The kinetic experiments were conducted to determine the time which U(VI) required to establish the sorption equilibrium in the presence of HA. Furthermore, the influence of a sequence of U(VI) and HA addition to the kaolinite suspension on the sorption equilibrium was studied (for detailed description see section 10.2.1). Three different cases of U(VI) and HA addition were investigated: U(VI) and HA were preconditioned for 24 h (pH ~7) and then added to the kaolinite containing solution, U(VI) and HA were added simultaneously to the kaolinite containing solution and the kaolinite containing solution was preconditioned with HA for 60 h and then U(VI) was added. **Fig. 7.1** represents results of the kinetic experiments for the ternary system studied in this work. **Fig. 7.1a** shows the U(VI) sorption in presence of HA as a function of contact times at pH 5 and **Fig. 7.1b** illustrates the U(VI) sorption in presence of HA at different contact times at pH 7.5.

The results indicate that the system reaches a sorption equilibrium within few hours after addition of U(VI) and HA to the kaolinite suspension. Compared to pH 7.5, an increase of the U(VI) sorption in the presence of HA is observed at pH 5 (for explanation see paragraph 7.2). Although the sorption kinetics of U(VI) in the absence of HA is fast (cf. chapter 6.2), it seems that the presence of HA can still accelerate the U(VI) sorption onto kaolinite. The reason could be that the amount of surface sites is enhanced largely by HA [100].

Comparing the different pre-equilibration modes, no significant differences in the U(VI) sorption behavior can be derived. Therefore, it can be concluded that the pre-equilibration of the U(VI)-HA solution before the addition to the kaolinite suspension has no significant influence on the U(VI) sorption kinetic in the studied time scale.

Similarly, Schmeide et al. [100] studied the kinetics of the U(VI) and HA sorption onto phyllite, ferrihydrite, and muscovite. In agreement to the system studied in this work, U(VI) sorption onto ferrihydrite was rapid since the U(VI) and HA concentration in solution decreased significantly within 10 min. Also, no dependence of the U(VI) sorption on the order of addition of reactants was observed after 10 min. U(VI) kinetics onto phyllite exhibited a rapid U(VI) sorption in the first seconds, but the steady state was reached finally after 300 min. U(VI) sorption rate did not exhibit significant dependence on the sequence of addition of reactants. In

the case of the U(VI) uptake by muscovite, the equilibrium was not reached even after 13 days. The addition of HA and especially addition of uranyl-humate complexes resulted in a faster U(VI) sorption.

Reiller et al. [101] studied the influence of addition order and contact time on Th(IV) retention by hematite in the presence of HA. Th(IV) retention was hindered when HA and hematite were equilibrated beforehand during 24 h. However, when HA was added after a 24 h equilibration of the Th(IV)-hematite system, Th(IV) was barely desorbed from the iron oxide surface. Increasing contact time between components of the system only indicated slight Th(IV) retention variation.

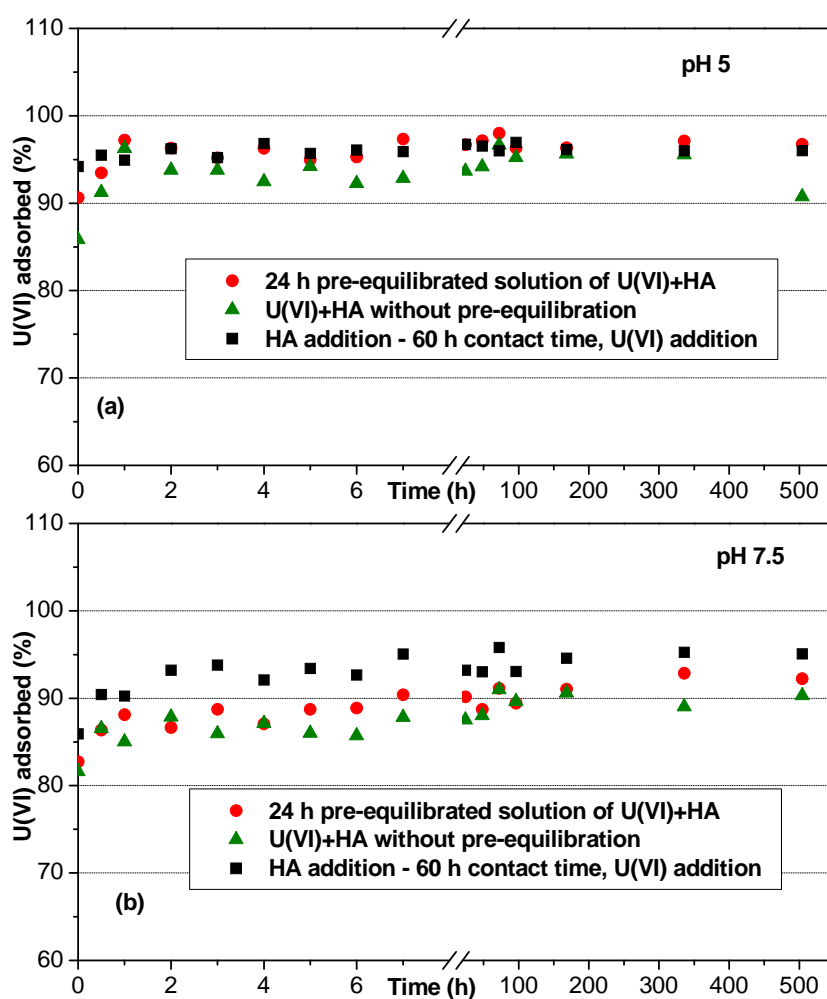


**Fig. 7.1:** U(VI) sorption kinetics in the presence of HA for three different types of U(VI) and HA additions at (a) pH 5 and (b) pH 7.5 ( $[U(VI)] = 1 \cdot 10^{-6}$  M,  $[HA] = 10$  mg/L,  $I = 0.01$  M  $NaClO_4$ ,  $pCO_2 = 10^{-3.5}$  atm). The standard error of all data points amounts to  $\pm 5\%$ .

## **7.2. U(VI) Sorption in Presence of Humic Acid**

The presence of HA significantly influences the sorption of U(VI) onto kaolinite in the whole studied pH range. The effect of HA onto U(VI) sorption as a function of pH and HA concentration at two different U(VI) concentrations shows **Fig. 7.2**. The sorption curve can be divided into three parts. In the first pH region, at  $\text{pH} < 5$ , an increase in the U(VI) uptake was observed compared to the HA-free system. From the above reported results of HA sorption onto kaolinite (see paragraph 5.3), it is evident that almost 100% of HA by initial HA concentration of 10 mg/L and 80% by initial HA concentration of 50 mg/L is adsorbed on the kaolinite surface in this pH range. A reduction in the U(VI) uptake was expected because of the competition between HA and U(VI) for available binding sites on the kaolinite surface. However, the adsorbed HA forms additional binding sites for U(VI), therefore, the U(VI) sorption can rise in its presence.

In the second part, there is a difference in the U(VI) sorption onto kaolinite at the U(VI) initial concentration of  $1 \cdot 10^{-6}$  M and  $1 \cdot 10^{-5}$  M in presence of 10 mg/L of HA. For the U(VI) initial concentration of  $1 \cdot 10^{-6}$  M, the U(VI) sorption is lower in the presence of HA compared to the system free of HA between pH 5 and pH 8.5. At pH 5, it starts desorption of HA from the kaolinite surface (see **Fig. 5.3**). It leads to a decrease of the U(VI) sorption onto kaolinite due to the formation of dissolved uranyl-humate complexes. Formation of binary complexes  $\text{UO}_2\text{HA}(\text{II})$  as well as mixed ternary uranyl-hydroxo-humate complexes  $\text{UO}_2(\text{OH})\text{HA}(\text{I})$  can occur (for the details see **Fig. 4.3**, chapter 4.3 for  $[\text{U}(\text{VI})] = 1 \cdot 10^{-6}$  M, the speciation diagrams for  $[\text{U}(\text{VI})] = 1 \cdot 10^{-5}$  M are not shown, because they do not differ significantly). Although, the HA (10 mg/L  $\approx 3.6 \cdot 10^{-5}$  M HA(I), calculated according to charge neutralization model [38]) concentration exceeds the U(VI) concentration ( $1 \cdot 10^{-6}$  M) in the solution, U(VI) uptake in the presence of HA is reduced only very slightly (about 10 %) compared to the system free of HA. It seems, that in spite of HA presence, U(VI) prefers sorption onto kaolinite before the complexation with HA in the solution. In the sorption experiments with the U(VI) initial concentration of  $1 \cdot 10^{-5}$  M, the difference in the initial concentrations of HA and U(VI) was very low ( $1 \cdot 10^{-5}$  M of U(VI) vs.  $3.6 \cdot 10^{-5}$  M of HA(I)). Thus, the sorption of U(VI) onto kaolinite is even more preferred before the complexation of U(VI) with HA than at lower U(VI) concentration. Consequently, HA has no influence on the U(VI) sorption onto kaolinite in the pH range between pH 6 and pH 8 at U(VI) concentration of  $1 \cdot 10^{-5}$  M. However, in the experiments carried out with higher HA concentration

- 50 mg/L - the U(VI) sorption is significantly lower than in the experiments conducted with only 10 mg/L for both U(VI) initial concentrations. The lower U(VI) sorption at higher initial HA concentration results from a higher amount of dissolved HA forming aqueous complexes with U(VI). Thus, the competition between uranyl-humate complex formation and surface complexation arises in the studied system. This can lead to an enhancement of the mobility of U(VI) in the environment.

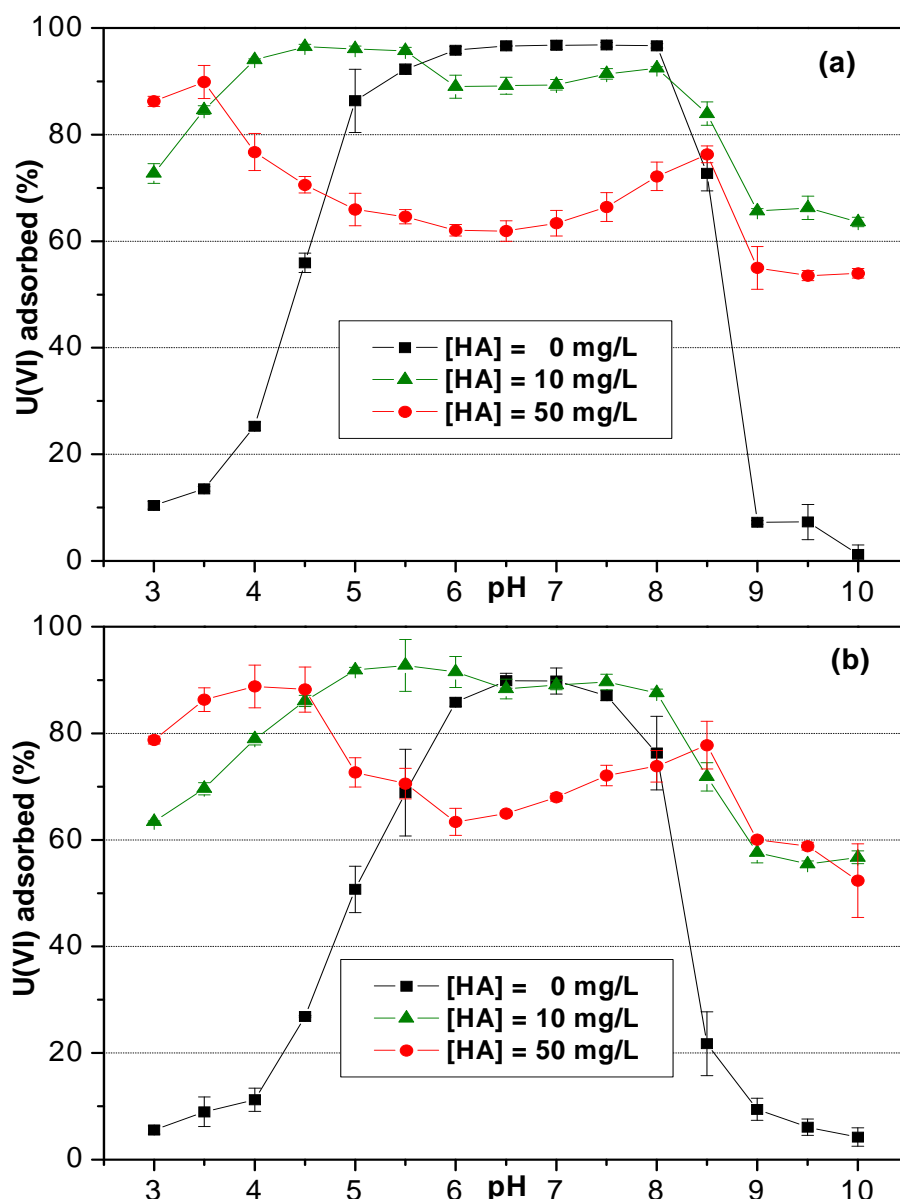


**Fig. 7.2:** Influence of HA on the U(VI) sorption for the U(VI) concentrations (a)  $1 \cdot 10^{-6}$  M and (b)  $1 \cdot 10^{-5}$  M ( $I = 0.01$  M  $\text{NaClO}_4$ ,  $p\text{CO}_2 = 10^{-3.5}$  atm).



In the third pH region, at  $\text{pH} > 8.5$ , in the presence of  $\text{CO}_2$  the sorption of U(VI) again increases in the presence of HA. HA is almost desorbed from the kaolinite surface (10 % of HA is adsorbed at  $\text{pH} 8.5$ ), one should expect reduced sorption of U(VI) onto kaolinite in the presence of HA. Notwithstanding, an enhancement of the U(VI) sorption occurs. From the comparison with the same system without  $\text{CO}_2$ , where no decrease of U(VI) sorption was observed in the presence of HA, one can conclude that carbonate must play a role by the U(VI) sorption onto kaolinite also in the presence of HA. It is possible that uranyl-carbonato-humate complexes are formed which can interact with the kaolinite surface and, therefore, enhance the U(VI) sorption onto kaolinite in the presence of HA in the alkaline pH region. Glaus et al. [51] reported the possible existence of the ternary uranyl-carbonato-humate complex  $(\text{UO}_2\text{CO}_3)\text{HA}$  in waters containing humic substances. Such sorption behavior in the alkaline pH range seems to be specific for the studied system and experimental conditions used. Murphy et al. [2] reported slightly lower sorption of U(VI) onto hematite in the presence of HA compared to the HA-free system in the alkaline pH region. Payne et al. [102] observed similar phenomena as [2] but for the sorption of U(VI) onto ferrihydrite. Schmeide et al. [70] reported also slight decrease of the U(VI) sorption onto phyllite in the presence of HA compared with the system without HA at  $\text{pH} > 8$ . Beneš et al. [93] studied the U(VI) sorption onto cypris clay in the presence of sodium humate. The presence of humate enhanced the sorption of U(VI) at  $\text{pH} < 4 - 7.5$  and suppressed it at  $\text{pH} > 4 - 8$ .

The influence of HA on the U(VI) sorption onto kaolinite in the absence of  $\text{CO}_2$  shows **Fig. 7.3**. At  $\text{pH} < 5$ , an increase of the U(VI) sorption was observed compared to the HA-free system. At  $\text{pH} > 5$  in the experiments with 10 mg/L of HA, HA has no influence on the U(VI) sorption onto kaolinite at U(VI) initial concentration of  $1 \cdot 10^{-6}$  M. It can be observed a slight increase of the U(VI) sorption at U(VI) initial concentration of  $1 \cdot 10^{-5}$  M, but it is not significant when considering the experimental error ( $1\sigma$ ). The U(VI) sorption decreases in the presence of 50 mg/L of HA compared to the HA-free system because of the formation of uranyl-humate and uranyl-hydroxo-humate complexes. The U(VI) sorption remains stable over the rest of pH range studied. There is no drop in the U(VI) sorption at higher pH ( $\text{pH} > 8.5$ ) due to formation of negative charged uranyl-carbonato complexes. As in the system in  $\text{CO}_2$ -presence, the U(VI) sorption decreases with increasing HA concentration.

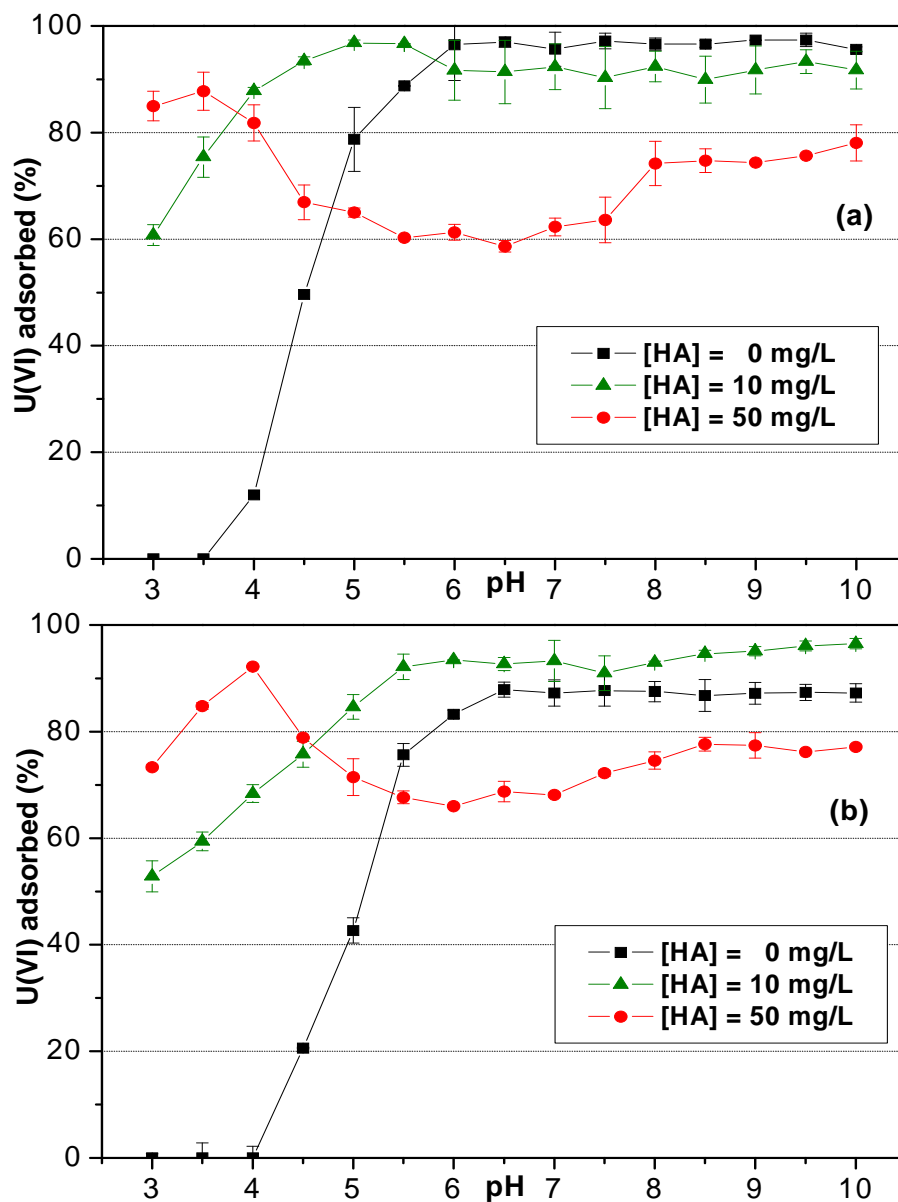


**Fig. 7.3:** Influence of HA on the U(VI) sorption for the U(VI) concentrations (a)  $1 \cdot 10^{-6}$  M and (b)  $1 \cdot 10^{-5}$  M in the absence of  $CO_2$  ( $I = 0.01$  M  $NaClO_4$ ).

## **8. Structure Determination of U(VI)-Kaolinite Surface Complexes in Absence and Presence of Humic Acid**

The sorption on clay minerals strongly affects the mobility of actinides in the geosphere. In order to model the sorption behavior of actinides in the environment, the knowledge of the structure of surface complexes of actinides is important. Different methods, e.g., attenuated total reflection - Fourier transform infrared spectroscopy (ATR-FTIR), X-ray absorption spectroscopy (XAS), time-resolved laser-induced fluorescence spectroscopy (TRLFS) or laser-induced photoacoustic spectroscopy (LIPAS), can be applied for characterization of the surface complexes of actinides. However, there is still a lack of information in literature about actinide complexation, especially in more complicated systems, e.g., in systems with solid surfaces and in the presence of different complexation ligands such as HS.

In this work, two spectroscopic methods were used to characterize surface species on kaolinite: XAS and TRLFS. For the first time, two methods were applied on the system U(VI)-HA-kaolinite under comparable experimental conditions. Their basic principles together with the results of the measurements are described in this chapter.

### ***8.1. U(VI)-Humic Acid-Kaolinite Surface Complexes Studied by EXAFS***

X-ray absorption spectroscopy, which includes X-ray absorption near-edge structure (XANES) and EXAFS, is a technique which can be used to determine the average local structure and oxidation state of an atom in chemical environments. EXAFS is a useful tool for determining local bond lengths and coordination numbers of neighboring atoms in order to distinguish between inner- and outer-sphere complexes and to analyze the complex structure [103]. Moreover, not only crystalline but also amorphous substances can be investigated by XAS. The theory given in this chapter is adopted from [104]-[106].

### 8.1.1. Principles of X-ray Absorption Spectroscopy

When X-rays hit a sample, the oscillating electric field of the electromagnetic radiation interacts with the electrons bound in an atom. Either the radiation will be scattered by these electrons or absorbed and excite the electrons (see **Fig. 8.1**). A narrow parallel monochromatic X-ray beam of intensity  $I_0$  will be reduced to intensity  $I$  after passing through a sample of thickness  $x$  according to the following expression:

$$\mu x = \ln(I_0 / I), \quad (8.1)$$

where  $\mu$  is the linear absorption coefficient which depends on the types of atoms and the density of the material.

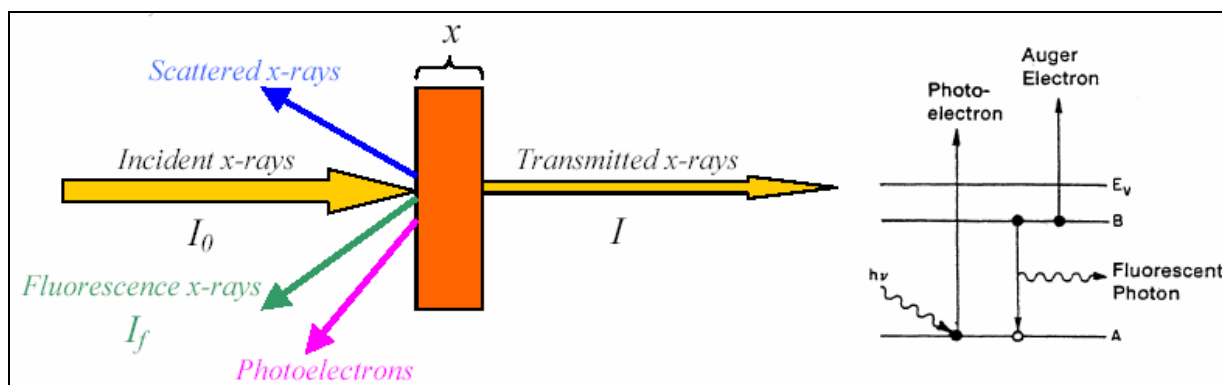


**Fig. 8.1:** Schematic diagram of XAS principles [104].

At certain energies, the absorption increases drastically and gives rise to an absorption edge. Each such edge occurs, when the energy of the incident photons is just sufficient to cause the excitation of a core electron of the absorbing atom to a continuum state, i.e., to produce a photoelectron. Thus, the energies of the absorbed radiation at these edges correspond to the binding energies of electrons in the K, L, M, etc., shells of the absorbing element. The absorption edges are labeled in the order of increasing energy, K, L<sub>I</sub>, L<sub>II</sub>, L<sub>III</sub>, M<sub>I</sub>,..., corresponding to the excitation of an electron from the 1s (<sup>2</sup>S<sub>1/2</sub>), 2s (<sup>2</sup>S<sub>1/2</sub>), 2p (<sup>2</sup>P<sub>1/2</sub>), 2p (<sup>2</sup>P<sub>3/2</sub>), or 3s (<sup>2</sup>S<sub>1/2</sub>),... orbitals, respectively.

When the photoelectron leaves the absorbing atom, its wave is backscattered by the neighboring atoms. The graphical representation of X-ray absorption as a function of photon energy  $E$  is called X-ray absorption spectrum. The U L<sub>III</sub>-edge XAS spectrum of U(VI) in CaUO<sub>4</sub> is shown in **Fig. 8.2** as an example.

### ***XANES and EXAFS***

An X-ray absorption spectrum is generally divided into two parts - XANES and EXAFS. The XANES range extends from several eV before the edge to approximately 50 eV above the edge. In the XANES region, transitions of core electrons to non-bound levels with close energy occur. Because of the high probability of such transition, a sudden raise of absorption is observed. In the absorption spectrum introduced in **Fig. 8.2**, the XANES region is characterized by an absorption maximum corresponding to an electron transfer from  $2p_{3/2}$  level to  $6d$  level. In the near-edge region, the ejected photoelectrons have usually low kinetic energy and experience strong multiple scattering (*MS*) (see **Fig. 8.2a**) by the first and even higher coordinating shells. The scattering happens in different directions in space. The scattered waves interfere with the outgoing photoelectron wave. Thus, the XANES spectrum results from these interferences between the scattered waves and outgoing photoelectron.

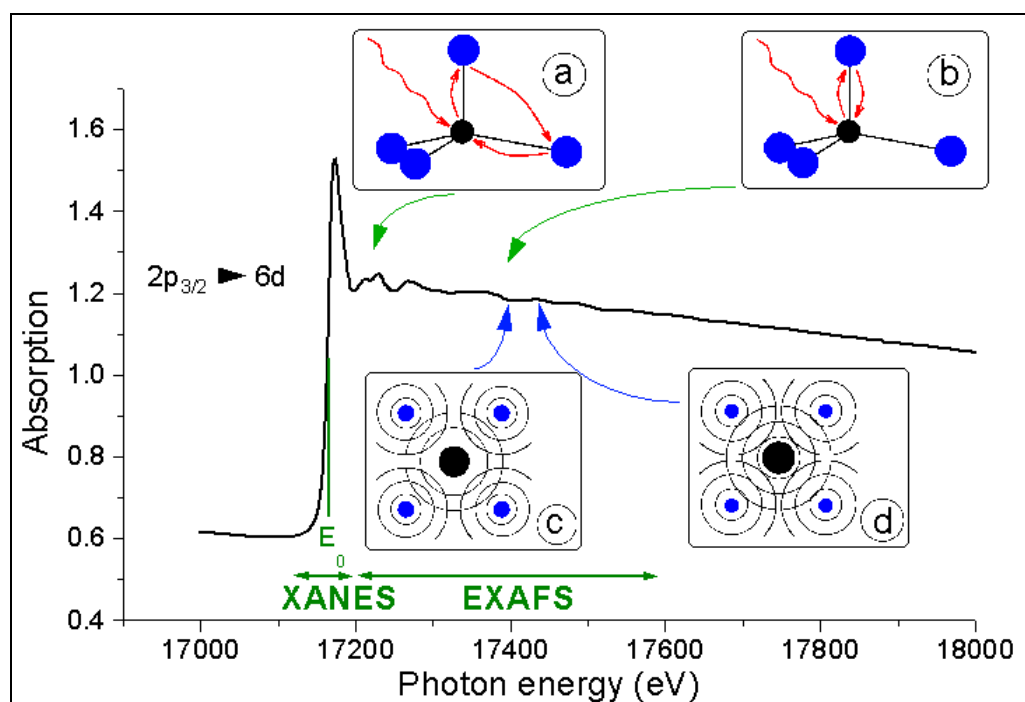


**Fig. 8.2:** XAS spectrum for the L<sub>III</sub>-edge of U(VI) in CaUO<sub>4</sub> [106]. The inserted figures show schematically a) multiple scattering, b) single-scattering, c) negative and d) positive interference of electron waves.

The XAS spectrum continues with the EXAFS region 50 – 1000 eV above the sorption edge. The photoelectrons have higher kinetic energy as in XANES region. Similarly to XANES range, the basic physical process resulting in oscillation of absorption in the EXAFS region is

backscattering of ejected photoelectron waves on the electron shells of the neighboring atoms. The single scattering (see **Fig. 8.2b**) by the nearest neighboring atoms normally dominates. The resulting interference of the outgoing photoelectron wave and backscattered wave, depending on their environment and distance traveled, causes either reinforcing (a maximum of the EXAFS oscillation, see **Fig. 8.2d**) or cancellation (a minimum of the EXAFS oscillation, see **Fig. 8.2c**) of each other. These interferences cause the sinusoidal progression curve of the dependence of absorption coefficient on the energy and/or wave number  $k$ :

$$k = \sqrt{\frac{2m}{\hbar^2}(E - E_0)}, \quad (8.2)$$

where  $\lambda = 2\pi/k$ ,  $\hbar = h/2\pi$ ,  $h$  is the Planck's constant,  $m$  is the electron mass,  $E$  is the incident photon energy and  $E_0$  is the threshold energy of the absorption edge. The variation of photon energy during the measurement of an X-ray spectrum causes a change of the kinetic energy and wavelength of backscattered photoelectron waves and leads as a result to oscillations which are reflected in the EXAFS spectrum. The frequency of these oscillations correlates with the distance between the absorbing atom and the neighboring atoms. The amplitude of the oscillations is related to the number of neighboring atoms. Thus, the atomic distances and coordination numbers can be determined. The whole EXAFS signal arises as a sum of the EXAFS oscillations of all neighboring atoms. By Fourier transformation of the EXAFS data, the individual contributions can be separated and the radial distribution function at the absorbing atom can be obtained.

For reasonably high energy (>60 eV) and moderate thermal or static disorders, the modulation of the absorption coefficient  $\chi(E)$  in EXAFS, normalized to the background absorption ( $\mu_0$ ) is given by:

$$\chi(E) = \frac{\mu(E) - \mu_0(E)}{\mu_0(E)} \quad (8.3)$$

In order to relate  $\chi(E)$  to structural parameters, it is necessary to convert the energy  $E$  into the photoelectron wavevector  $k$  via Eq. (8.2). This transformation of  $\chi(E)$  in  $E$  space gives rise to  $\chi(k)$  in  $k$  space:

$$\chi(k) = \sum_j N_j S_i(k) F_j(k) e^{-2\sigma_j^2 k^2} e^{-2r_j/\lambda_j(k)} \frac{\sin(2kr_j + \phi_{ij}(k))}{kr_j^2}, \quad (8.4)$$

where  $F_j(k)$  is the backscattering amplitude from each of the  $N_j$  neighboring atoms of the  $j$ -th type with a Debye-Waller factor of  $\sigma_j$  to account for thermal vibration (assuming harmonic vibration) and static disorder (assuming Gaussian pair distribution) and at a distance  $r_j$  away.  $\phi_{ij}(k)$  is the total phase shift experienced by the photoelectron. The term  $e^{-2r_j/\lambda_j(k)}$  is due to inelastic losses in scattering process (due to neighboring atoms and the medium in between) with  $\lambda_j$  being the electron mean free path.  $S_i(k)$  is the amplitude reduction factor due to many-body effects such as shake up/off processes at the central atom (denoted by  $i$ ). It is clear that each EXAFS wave is determined by the backscattering amplitude ( $N_j F_j(k)$ ), modified by reduction factors  $S_i(k)$ ,  $e^{-2\sigma_j^2 k^2}$ , and  $e^{-2r_j/\lambda_j(k)}$ , and the  $1/kr_j^2$ , and sinusoidal oscillation which is a function of the interatomic distances ( $2kr_j$ ) and the phase shift ( $\phi_{ij}(k)$ ).

While the amplitude function  $F_j(k)$  depends only on the type of the backscatters, the phase function contains contributions from both, the absorber and backscatter. The Debye-Waller factor  $\sigma$  plays an important role in EXAFS spectroscopy. It contains important structural and chemical information, which is difficult to obtain, yet it comes as a bonus to the EXAFS determination of interatomic distances.

Transmission is just one of several modes of EXAFS measurements. The fluorescence technique involves the measurement of the fluorescence radiation (over some solid angle) perpendicular to the incident beam. This method removes the “background” absorption due to other constituents, thereby improving the sensitivity by orders of magnitude. **Fig. 8.3** illustrates the two experimental set-ups for XAS measurements.

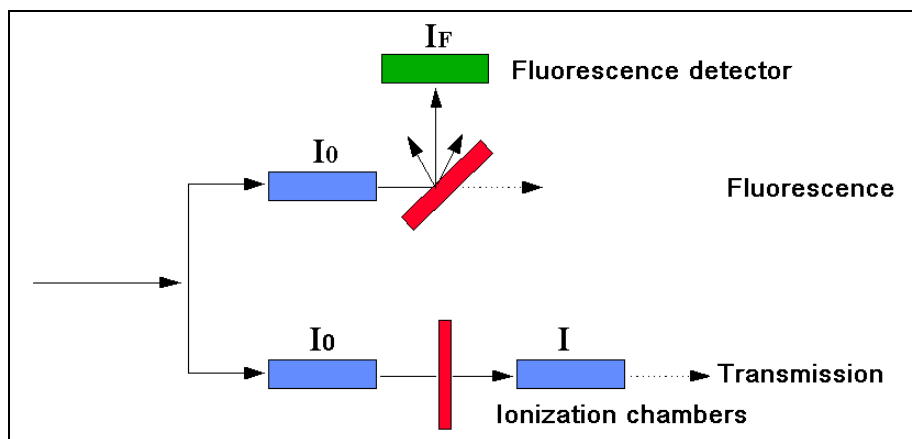


**Fig. 8.3:** Schema for XAS measurements.

Numerous publications, where the EXAFS technique was applied to study the actinide speciation, prove that this technique is a powerful tool for obtaining basic molecular-level information. This technique was applied, for example, to study the complexation of actinides with organic substances such as HA [107]-[110]. EXAFS was also used in many investigations of the surface complexation of U(VI) on different minerals, e.g., silica [111]-[113], alumina [112], kaolinite [77],[94] montmorillonite [103],[112], ferrihydrite [111], goethite [114] or pristine and albite [115].

In this work, results of the EXAFS measurements in the system U(VI)-HA-kaolinite are interpreted and compared with the binary systems U(VI)-kaolinite [94] and U(VI)-HA [107],[108] to obtain information on the influence of HA on the near-neighbor surrounding of U(VI) in kaolinite surface complexes.

### **8.1.2. Sample Preparation**

For the EXAFS measurements the samples were prepared in the form of wet paste. U(VI) and HA (unlabeled HA type M42) were adsorbed onto 200 mg of kaolinite, as described in chapter 10.2.2, the supernatants were removed and measured by ICP-MS. The wet pastes (kaolinite with sorbed U(VI) and HA) were immediately filled into special polyethylene sample holders. These sample holders were then sealed with Kapton polyamide tape and heat-sealed in two layers of polyethylene foil to avoid moisture loss during analysis and to provide several layers of containment of the radioactive sample (**Fig. 8.4**).



**Fig. 8.4:** Sample prepared for EXAFS measurement.

To have the possibility to compare the results of the ternary system, the samples were prepared and measured under the same experimental conditions as those of the binary system



[94]. Two series of samples were prepared and measured to examine the reproducibility of the EXAFS measurements. In the first series, prepared and measured in November 2004, six samples were prepared and labeled U4-134 – U4-140. In the second series, prepared and measured in February 2006, seven samples were prepared (six under the same conditions as for the first series and one additional) and labeled U6-06 – U6-11. **Tab. 8.1** summarizes the sample preparation conditions, the U(VI) and HA concentrations, pH values and amount of adsorbed U(VI). Only the pH values were varied. The concentrations of U(VI) and HA were the same for all samples:  $1 \cdot 10^{-5}$  M and 10 mg/L, respectively. One sample was prepared in a N<sub>2</sub>-box to avoid the presence of CO<sub>2</sub>. In addition, one sample was prepared without HA to prove the accuracy of the samples preparation by comparing the results with [94].

**Tab. 8.1:** Samples for EXAFS measurements ( $[U(VI)] = 1 \cdot 10^{-5}$  M, I = 0.1 M NaClO<sub>4</sub>).

Sample	[HA] <sub>0</sub> (mg/L)	pH <sub>start</sub>	pH <sub>end</sub>	U(VI) <sub>sorbed</sub> (%)	CO <sub>2</sub> /N <sub>2</sub>
U4-134	10	<b>5.06</b>	<b>4.95</b>	90.51	CO <sub>2</sub>
U4-135	10	<b>6.07</b>	<b>6.06</b>	97.44	CO <sub>2</sub>
U4-136	10	<b>7.06</b>	<b>6.93</b>	96.93	CO <sub>2</sub>
U4-137	10	<b>8.58</b>	<b>8.41</b>	66.61	CO <sub>2</sub>
U4-138	10	<b>8.66</b>	<b>8.55</b>	97.79	N <sub>2</sub>
U4-140	—	<b>7.08</b>	<b>7.01</b>	92.06	CO <sub>2</sub>
U6-06	10	<b>3.01</b>	<b>3.03</b>	57.53	CO <sub>2</sub>
U6-07	10	<b>5.04</b>	<b>5.03</b>	89.62	CO <sub>2</sub>
U6-08	10	<b>6.06</b>	<b>6.04</b>	97.04	CO <sub>2</sub>
U6-09	10	<b>7.05</b>	<b>7.00</b>	97.55	CO <sub>2</sub>
U6-10	10	<b>8.59</b>	<b>8.52</b>	62.04	CO <sub>2</sub>
U6-11	10	<b>8.65</b>	<b>8.51</b>	97.79	N <sub>2</sub>
U6-13	—	<b>7.05</b>	<b>7.03</b>	91.36	CO <sub>2</sub>

### 8.1.3. EXAFS Analysis

EXAFS data reduction was performed using EXAFSPAK [116] following standard procedures. The  $\chi(k)$  function was extracted from the raw data by fitting a linear function to the pre-edge region and a spline function to the post-edge region and normalizing the edge jump to unity. The energy axis (eV) was converted to photoelectron wave vector units ( $\text{\AA}^{-1}$ ) by assigning the origin  $E_0$  to the first inflection point of the adsorption edge.  $E_0$  was corrected for each spectrum in the fitting procedure ( $E_0 = 17.2$  keV). The resulting  $\chi(k)$  functions were weighted

with  $k^3$  to compensate for the dampening of the EXAFS amplitude with increasing  $k$  and were Fourier transformed to obtain the radial structure functions (RSF). The four major peaks below  $3.5 \text{ \AA}^{-1}$  in the Fourier transforms (FT) were isolated and back-transformed. These back transformed peaks were fit in  $k$ -space. Structural parameters were extracted with fits to the standard EXAFS equation (Eq. (8.4), chapter 8.1.1). Then, multi-shell fitting was done in  $k$ -space using the same parameters. Ab initio U-Si/Al, U-O<sub>ax</sub> and U-O<sub>eq</sub> scattering paths were generated using the FEFF 8.20 [117] code from the binary system fitting. The amplitude reduction factor,  $S_0^2$ , was equal to 1.0. The  $k$ -range was always started at  $3.1 \text{ \AA}$  and the extend of the range was dependent on the quality of each spectrum, therefore, the  $k_{max}$  value for each sample is always given in the table with the obtained structural parameters. The energy shift  $\Delta E_0$  and the values of coordination numbers ( $N$ ) were kept fixed during the fit procedure, whereas the values of bond distances ( $R$ ) and Debye-Waller factors ( $\sigma^2$ ) were allowed to adjust freely. The structural model for fitting the EXAFS oscillations was derived from the EXAFS investigation of the binary system U(VI)-kaolinite KGa-1b [94].

As a first approximation to fit the U L<sub>III</sub>-edge  $k^3$ -weighted EXAFS oscillations of the samples, only the main components, i.e., oxygen atoms in the axial (O<sub>ax</sub>,  $N = 2$ ) and equatorial (O<sub>eq</sub>,  $N = 5$ ) coordination shells coordinated to the uranyl ion and the multiple scattering (MS) along the uranyl unit [118], were considered. All samples exhibit similar EXAFS oscillations and FTs, therefore the U L<sub>III</sub>-edge  $k^3$ -weighted EXAFS oscillation and the corresponding FT (not corrected for the phase shift) are shown in **Fig. 8.5** only for one sample (U6-09) as an example.

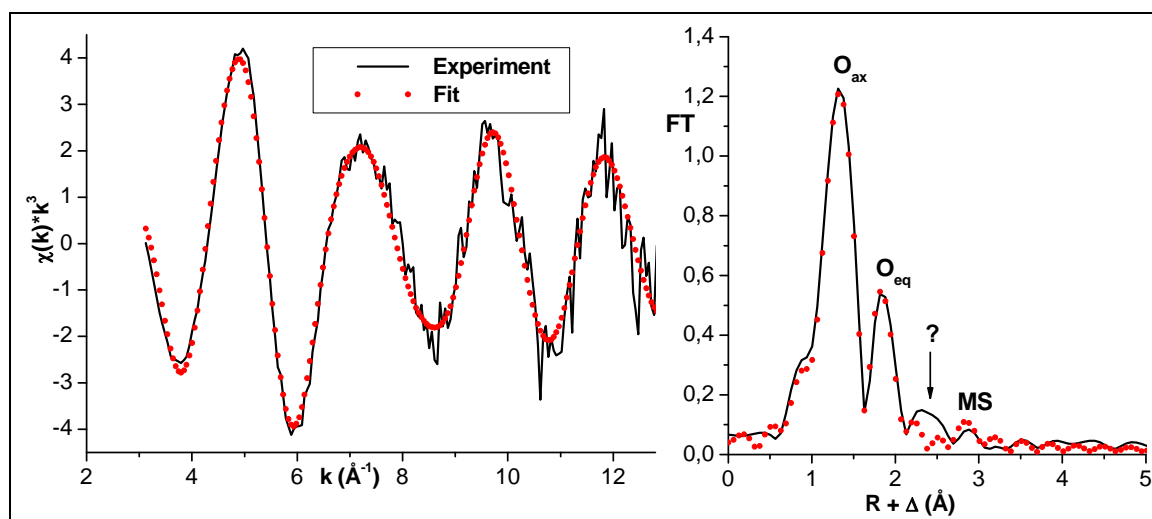


**Fig. 8.5:** EXAFS oscillation and FT and the first fit of the sample U6-09.

The first and the second peak in FT diagram represent the oxygen atoms coordinated to the uranyl unit in the axial and equatorial shells. The last one contains the contribution from MS along the uranyl ion. It becomes evident that the fit is not ideal, especially the FT shows some residual structure in the spectrum which means that the fitting model must be improved.

**Tab. 8.2** summarizes the structural parameters for the samples obtained from the first fit. From the table it can be seen that the structural parameters for all samples are comparable, there are no remarkable differences. From the fitting of the sample U6-06 a very high reduced error resulted. It is caused by the low U(VI) signal and the high signal noise.

**Tab. 8.2:** The results of the first fit.

pH	Sample	$k_{\max}$ ( $\text{\AA}^{-1}$ )	U-O <sub>ax</sub> (N=2)		U-O <sub>eq</sub> (N=5)		$\Delta E$ (eV)	Red. error
			R ( $\text{\AA}$ )	$\sigma^2$ ( $\text{\AA}^2$ )	R ( $\text{\AA}$ )	$\sigma^2$ ( $\text{\AA}^2$ )		
3	U6-06	10.4	1.75	0.0014	2.36	0.0114	-13.0	1.49
5	U6-07	11.4	1.77	0.0027	2.35	0.0130	-13.5	0.47
	U4-134	12.5	1.77	0.0031	2.35	0.0131	-12.6	0.19
6	U6-08	11.4	1.77	0.0024	2.35	0.0128	-12.8	0.11
	U4-135	11.4	1.77	0.0033	2.34	0.0128	-12.3	0.14
7	U6-09	12.3	1.78	0.0022	2.36	0.0126	-11.9	0.17
	U4-136	12.2	1.77	0.0041	2.33	0.0132	-13.0	0.23
7	U6-13	12.2	1.79	0.0023	2.36	0.0123	-10.9	0.22
	U4-140	11.2	1.78	0.0027	2.35	0.0112	-11.7	0.20
8.5	U6-10	10.2	1.79	0.0035	2.37	0.0098	-10.4	0.37
	U4-137	11.2	1.79	0.0036	2.35	0.0119	-11.0	0.25
8.5	U6-11	12.1	1.79	0.0025	2.35	0.0127	-11.0	0.24
	U4-138	12.1	1.78	0.0040	2.33	0.0134	-11.8	0.12

$$\Delta R: \pm 0.02 \text{ \AA}, \Delta \sigma^2: \pm 0.001 \text{ \AA}^2$$

However, one conclusion can already be made. The U(VI) did not adsorb onto kaolinite at pH 3 at all and HA caused an enhancement of U(VI) sorption by forming additional binding sites for U(VI) as described in chapter 7. It means that U(VI) is in this case adsorbed onto kaolinite via the HA and, therefore, the average atomic distance between U(VI) and its equatorial oxygen atoms of 2.36  $\text{\AA}$  corresponds to the atomic distance between U(VI) and oxygen atoms of sorbed HA. Moreover, it confirms that U(VI) interacts with HA on the kaolinite surface. Because of the low U(VI) signal, the fitting was complicated and also the  $k$ -range had to be reduced to 10.4  $\text{\AA}^{-1}$ . Therefore, no fit improvement could be obtained and the sample was not included in the next fitting procedure.

In the next step, it was assumed that U(VI) is by the sorption onto kaolinite coordinated also to Si/Al atom of the kaolinite edge. By the next fitting, additionally to the oxygen atoms in axial and equatorial shells and MS, one Si/Al shell was considered with one Si/Al atom at the distance of 2.71 or 3.1 Å. The resulted structural parameters of the fits are summarized in **Tab. 8.3**. The distances between the U-O<sub>ax</sub> pair vary only very slightly between 1.76 Å and 1.79 Å. The differences in obtained U-O<sub>eq</sub> distances are by this fit more significant, they vary between 2.32 Å and 2.37 Å. The obtained distances U-Si/Al from the Si/Al shell fitting are not very consistent. Some samples show better fit with resulting shorter U-Si/Al distance, some samples with longer U-Si/Al distance and some samples could not be fitted with this additional Si/Al shell, mostly because of high signal noise was too high and the *k*-range had to be reduced. Compared to the results of the first fit, there are no significant differences in the obtained values of U-O<sub>eq</sub> and U-O<sub>ax</sub> distances and Debye-Waller factors, however, the decreasing of reduced errors of the fits is an evidence of the fit improvement.

**Tab. 8.3:** The results of the fit with Si/Al atom.

pH	Sample	k <sub>max</sub> (Å <sup>-1</sup> )	U-O <sub>ax</sub> (N=2)		U-O <sub>eq</sub> (N=5)		U-Si/Al (N=1)		ΔE (eV)	Red. error
			R (Å)	σ <sup>2</sup> (Å <sup>2</sup> )	R (Å)	σ <sup>2</sup> (Å <sup>2</sup> )	R (Å)	σ <sup>2</sup> (Å <sup>2</sup> )		
5	U6-07	11.4	1.76	0.0024	2.34	0.0142	-	-	-13.5	0.19
	U4-134	12.5	1.76	0.0032	2.33	0.0149	<b>2.73</b>	0.0108	-12.5	0.15
6	U6-08	11.4	1.77	0.0024	2.34	0.0140	-	-	-12.8	0.11
	U4-135	11.4	1.77	0.0033	2.34	0.0139	<b>3.10</b>	0.0113	-12.2	0.14
7	U6-09	12.3	1.78	0.0033	2.35	0.0136	<b>3.07</b>	0.0081	-11.8	0.16
	U4-136	12.2	1.77	0.0041	2.32	0.0147	<b>2.72</b>	0.0092	-12.8	0.16
7	U6-13	12.2	1.79	0.0023	2.37	0.0133	<b>3.09</b>	0.0091	-10.8	0.21
	U4-140	11.2	1.78	0.0030	2.34	0.0137	<b>2.69</b>	0.0088	-11.5	0.1
8.5	U6-10	10.2	1.79	0.0036	2.37	0.0109	-	-	-10.4	0.37
	U4-137	11.2	1.78	0.0038	2.34	0.0142	<b>2.70</b>	0.0086	-11.0	0.23
8.5	U6-11	12.1	1.79	0.0025	2.35	0.0138	<b>3.09</b>	0.0070	-11.0	0.22
	U4-138	12.1	1.78	0.0040	2.33	0.0145	<b>3.08</b>	0.0085	-11.8	0.14

ΔR: ± 0.02 Å, Δσ<sup>2</sup>: ± 0.001 Å<sup>2</sup>

**Fig. 8.6** shows the U L<sub>III</sub>-edge k<sup>3</sup>-weighted EXAFS oscillations and the corresponding FTs for the samples prepared at pH 7 in the presence of HA: U6-09 and U6-136 as the example of fit results, where the difference in obtained distances of U-Si/Al occurred. It is obvious that the fitting model still does not fit the measured data satisfactorily.

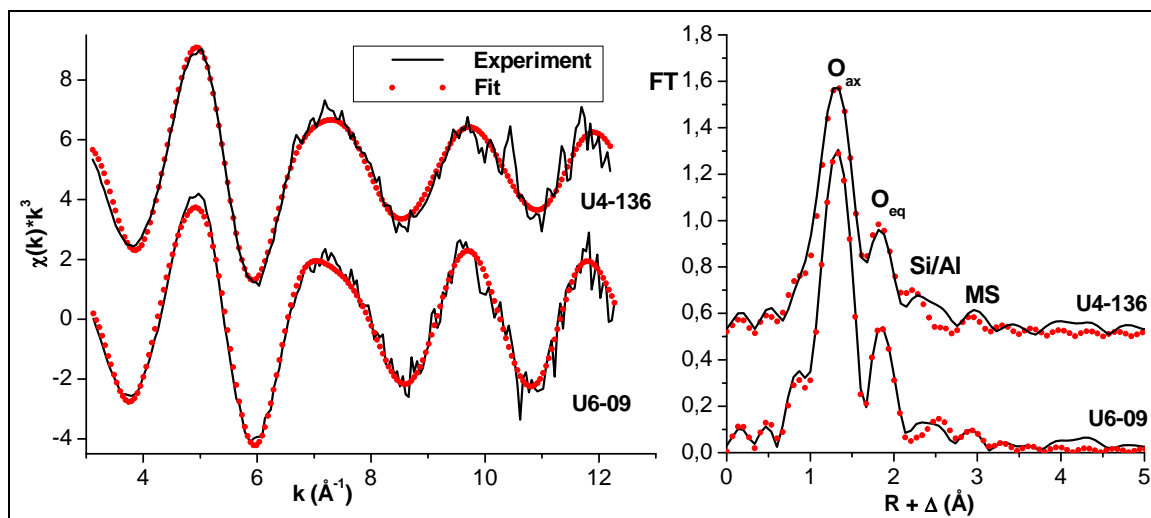


**Fig. 8.6:** EXAFS oscillations and corresponding FTs of the samples U4-136 and U6-09.

Therefore, the structure residuals corresponding to the U-Si/Al signal were subtracted from the EXAFS oscillations, FT filtered, separately fitted, then again brought together to the EXAFS spectrum and the whole spectrum was fitted again. However, this fit also did not match the experimental data properly. Hence, the fit of residual subtraction was performed again, but with the consideration of two Si/Al atoms with U-Si/Al distances at 3.1  $\text{\AA}$  and 3.3  $\text{\AA}$  as the initial values. Next figure (**Fig. 8.7**) shows the result of such fit for the sample U6-09.

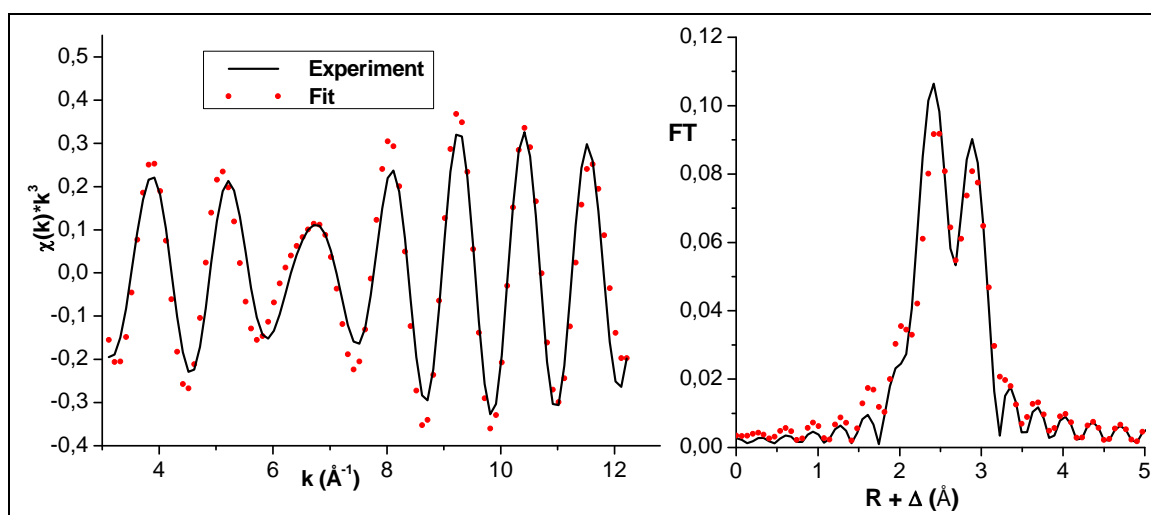


**Fig. 8.7:** Residual subtraction and fitting with two Si/Al atoms (sample U6-09).

From the comparison of both residual fitting resulted that the fit with two Si/Al atoms matches the experimental data much better than the fit with only one Si/Al atom. So, the same fitting procedure was then applied on all samples. The results of the fitting of the subtracted

residual for all samples are summarized in **Tab. 8.4**. The obtained U-Si/Al distances are comparable for all fitted samples.

**Tab. 8.4:** The results of the fitting of subtracted residuals with two Si/Al atoms.

pH	Sample	$k_{\max}$ ( $\text{\AA}^{-1}$ )	U-Si <sub>1</sub> /Al <sub>1</sub> (N=1)		U-Si <sub>2</sub> /Al <sub>2</sub> (N=1)		$\Delta E$ (eV)
			R ( $\text{\AA}$ )	$\sigma^2$ ( $\text{\AA}^2$ )	R ( $\text{\AA}$ )	$\sigma^2$ ( $\text{\AA}^2$ )	
5	U6-07	11.4	3.089	0.00631	3.308	0.00380	-13.5
	U4-134	12.5	3.094	0.00442	3.301	0.00477	-12.6
6	U6-08	11.4	3.085	0.00574	3.307	0.00695	-12.8
	U4-135	11.4	3.096	0.00569	3.315	0.00652	-12.3
7	U6-09	12.3	3.080	0.00599	3.310	0.00687	-11.9
	U4-136	12.2	3.080	0.000394	3.290	0.00455	-13.0
7	U6-13	12.2	3.085	0.00527	3.292	0.00697	-10.9
	U4-140	11.2	3.076	0.00559	3.274	0.00752	-11.7
8.5	U6-10	10.2	not determinable				-10.4
	U4-137	11.2	3.089	0.00435	3.293	0.00572	-11.0
8.5	U6-11	12.1	3.100	0.00593	3.330	0.00767	-11.0
	U4-138	12.1	3.090	0.00560	3.310	0.00556	-11.8

$\Delta R: \pm 0.02 \text{ \AA}$ ,  $\Delta \sigma^2: \pm 0.001 \text{ \AA}^2$

Finally, the EXAFS spectra of all samples were fitted considering oxygen atoms in the axial ( $N = 2$ ) and equatorial ( $N = 5$ ) coordination shells coordinated to the uranyl ion, MS along the uranyl unit and two coordination shells each with one Si/Al ( $N_{1,2} = 1$ ) atom coordinated to the uranyl ion. The U L<sub>III</sub>-edge  $k^3$ -weighted EXAFS oscillations and corresponding FTs for the samples U6-09 and U4-136 as an example are shown in **Fig. 8.8**.

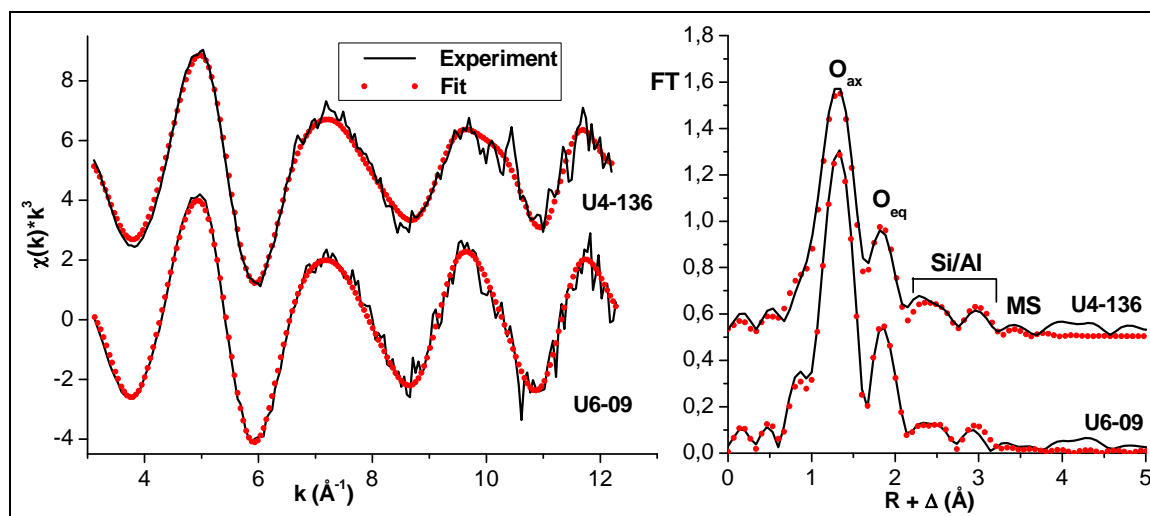


**Fig. 8.8:** Final fit of the EXAFS oscillations and FTs of samples U6-09 and U4-136.

The obtained structural parameters are summarized in **Tab. 8.5**. There are no significant differences in the obtained structural parameters of the samples. The distances between the U-O<sub>ax</sub> pair amount to 1.76 Å – 1.79 Å. The differences in U-O<sub>eq</sub> distances vary between 2.33 Å and 2.37 Å. The obtained distances U-Si/Al are in the range 3.06 Å – 3.10 Å for the first Si/Al atom and 3.26 Å – 3.31 Å for the second Si/Al atom. No U-U and U-Ti interactions were detected in all samples. From the comparison with the results of fitting with only one Si/Al atom, summarized in **Tab. 8.3**, it can be concluded that the fits were improved as results from lowering of reduced errors of the fits.

**Tab. 8.5:** The obtained structural parameters of the samples.

pH	Sample	k <sub>max</sub> (Å <sup>-1</sup> )	U-O <sub>ax</sub> (N=2)		U-O <sub>eq</sub> (N=5)		U-Si <sub>1</sub> /Al <sub>1</sub>		U-Si <sub>2</sub> /Al <sub>2</sub>		ΔE (eV)	Red. error
			R (Å)	σ <sup>2</sup> (Å <sup>2</sup> )	R (Å)	σ <sup>2</sup> (Å <sup>2</sup> )	R (Å)	σ <sup>2</sup> (Å <sup>2</sup> )	R (Å)	σ <sup>2</sup> (Å <sup>2</sup> )		
<b>5</b> <b>HA</b>	U6-07	11.4	<b>1.76</b>	0.0024	<b>2.35</b>	0.0142	<b>3.09</b>	0.0048	<b>3.30</b>	0.0033	-13.5	0.148
	U4-134	12.5	<b>1.76</b>	0.0031	<b>2.34</b>	0.0144	<b>3.10</b>	0.0035	<b>3.30</b>	0.0036	-12.6	0.114
<b>6</b> <b>HA</b>	U6-08	11.4	<b>1.77</b>	0.0025	<b>2.35</b>	0.0140	<b>3.08</b>	0.0042	<b>3.30</b>	0.0051	-12.8	0.072
	U4-135	11.4	<b>1.77</b>	0.0033	<b>2.34</b>	0.0140	<b>3.10</b>	0.0048	<b>3.31</b>	0.0056	-12.3	0.071
<b>7</b> <b>HA</b>	U6-09	12.3	<b>1.78</b>	0.0023	<b>2.35</b>	0.0137	<b>3.08</b>	0.0050	<b>3.30</b>	0.0060	-11.8	0.127
	U4-136	12.2	<b>1.77</b>	0.0041	<b>2.33</b>	0.0145	<b>3.08</b>	0.0030	<b>3.29</b>	0.0032	-13.0	0.113
<b>7</b> <b>No HA</b>	U6-13	12.2	<b>1.79</b>	0.0024	<b>2.37</b>	0.0135	<b>3.08</b>	0.0029	<b>3.27</b>	0.0036	-10.9	0.174
	U4-140	11.2	<b>1.77</b>	0.0030	<b>2.34</b>	0.0123	<b>3.06</b>	0.0040	<b>3.26</b>	0.0042	-12.6	0.155
<b>8.5</b> <b>CO<sub>2</sub></b>	U6-10	10.2	<b>1.79</b>	0.0035	<b>2.37</b>	0.0107	<b>3.09</b>	0.0056	<b>3.32</b>	0.0137	-10.4	0.311
	U4-137	11.2	<b>1.78</b>	0.0037	<b>2.35</b>	0.0130	<b>3.08</b>	0.0027	<b>3.27</b>	0.0036	-11.3	0.230
<b>8.5</b> <b>N<sub>2</sub></b>	U6-11	12.1	<b>1.78</b>	0.0025	<b>2.35</b>	0.0140	<b>3.10</b>	0.0043	<b>3.32</b>	0.0054	-11.0	0.200
	U4-138	12.1	<b>1.78</b>	0.0040	<b>2.33</b>	0.0147	<b>3.09</b>	0.0035	<b>3.30</b>	0.0033	-11.8	0.097

ΔR: ± 0.02 Å, Δσ<sup>2</sup>: ± 0.001 Å<sup>2</sup>

### 8.1.4. Effect of pH

The obtained U L<sub>III</sub>-edge  $k^3$ -weighted EXAFS oscillations and corresponding FTs of the samples prepared at different pH values in the presence of HA are depicted in **Fig. 8.9**. As it can be seen from the figure, all examined samples exhibit comparable EXAFS oscillations and FTs with no remarkable differences at different pH values.

The results of the fitting procedure are summarized in **Tab. 8.5**. The obtained structural parameters show no significant differences. The radial distances between uranyl ion and axial oxygens vary only slightly, between 1.76 Å and 1.78 Å, but this difference are within the experimental error. Also the distances between uranyl ion and equatorial oxygens do not change significantly, the values amount to 2.33 Å – 2.35 Å. U-Si/Al atom distances differ with different pH values in a narrow range 3.08 Å – 3.10 Å and 3.27 Å – 3.31 Å.

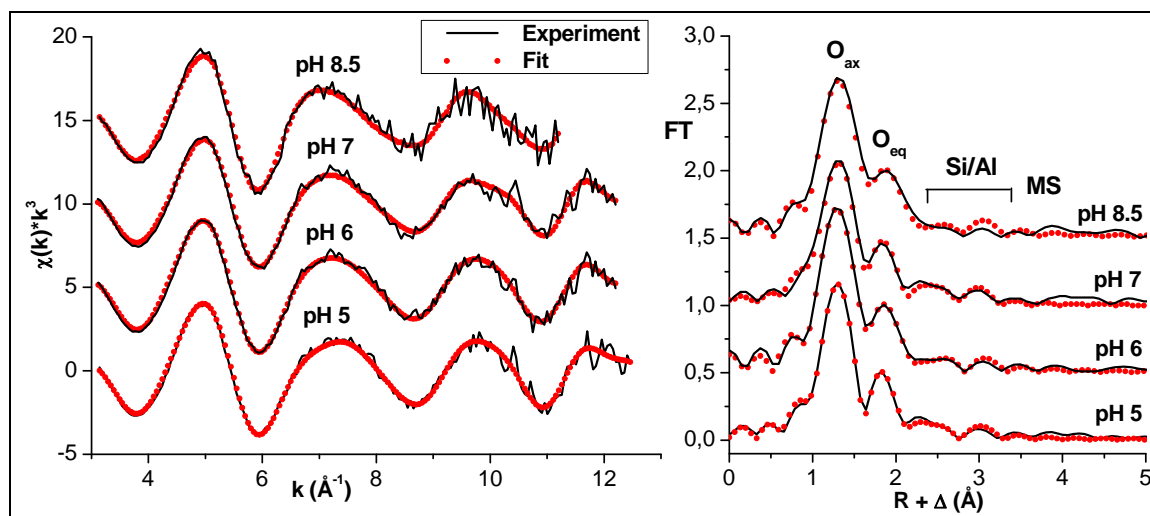


**Fig. 8.9:** EXAFS oscillation and FTs of the samples prepared at different pH values.

In the binary system, Reich et al. [94] observed an increase of U-O<sub>eq</sub> bond distances with increasing pH value from 2.36 Å to 2.41 Å probably due to the formation of ternary surface uranyl complexes with carbonate. This effect was not found in ternary system studied in this work, presumably because the uranium forms uranyl-hydroxyl-humate complexes and the effect of carbonate on the U-O<sub>eq</sub> atom distance is suppressed in the presence of HA. It can be concluded that pH value has no influence on structural parameters in the studied system.



### 8.1.5. Influence of CO<sub>2</sub> at pH 8.5

Two samples were prepared to study the effect of CO<sub>2</sub> at pH 8.5 on the U(VI) coordination environment in the surface complexes in the presence of HA. Also in this case the obtained U L<sub>III</sub>-edge k<sup>3</sup>-weighted EXAFS oscillations and corresponding FTs are comparable for both samples, see **Fig. 8.10**. It is obvious that the fit of the sample prepared on air is more problematic than that for the sample prepared in a nitrogen atmosphere. It is due to higher signal noise, therefore, the *k*-range had to be reduced to 11.2 Å<sup>-1</sup>.

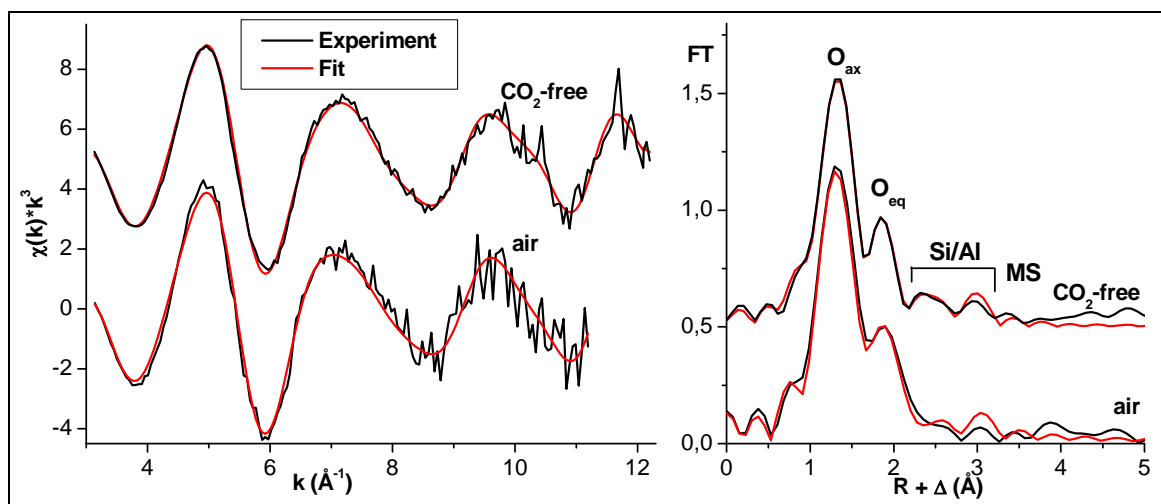


**Fig. 8.10:** EXAFS oscillation and FTs of the samples with different CO<sub>2</sub> concentration.

The resulted structural parameters for these two samples are given in **Tab. 8.5**. There is a small observable drop from 2.35 Å to 2.33 Å of the bond distance between U(VI) and equatorial oxygen atoms in the absence of CO<sub>2</sub> compared to the system with CO<sub>2</sub> presence. From this it could be derived that U(VI) adsorbed on the kaolinite surface interacts with carbonate, but the obtained difference is too small and it is not significant under consideration of the experimental error. However, such effect was also observed by Reich et al. [94] in the binary system U(VI)-kaolinite, where the decrease of the U-O<sub>eq</sub> distance was more significant, from 2.41 Å to 2.36 Å. But then, the U-O<sub>eq</sub> distance in [UO<sub>2</sub>(CO<sub>3</sub>)<sub>3</sub>]<sup>4-</sup> amounts to 2.44 Å, so it can not be concluded definitely that there is an influence of carbonate on the near-neighbor surrounding of U(VI) in the kaolinite surface complexes.

### 8.1.6. Effect of Humic Acid Presence

**Fig. 8.11** illustrates the U L<sub>III</sub>-edge  $k^3$ -weighted EXAFS oscillations and corresponding FTs of the samples with and without HA prepared at the same pH value (pH ~ 7). Again, the samples exhibit comparable EXAFS oscillations and FTs with no significant differences.

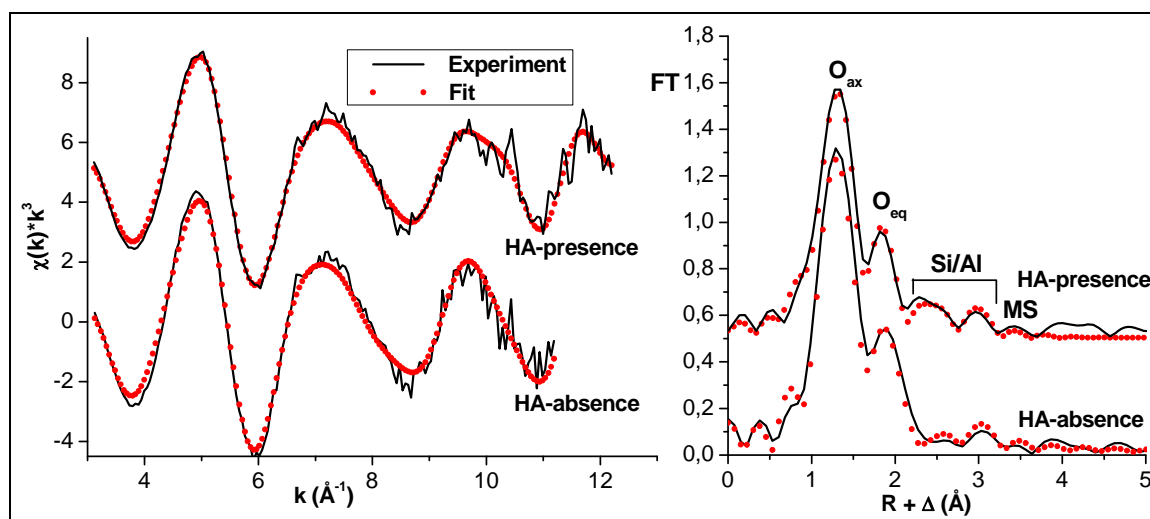


**Fig. 8.11:** EXAFS oscillation and FTs of the samples with and without HA.

The obtained structural parameters (see **Tab. 8.5**) are also in this case very similar. The U-O<sub>ax</sub> distances amount to 1.77 Å for both samples, independently on the presence of HA. Also other distances, i.e., distance between U and Si/Al atoms and U and O<sub>eq</sub> are comparable. The U-Si/Al distances are slightly shortened from 3.08 Å and 3.29 Å in the presence of HA to 3.06 Å and 3.26 Å in the absence of HA. The U-O<sub>eq</sub> distances are almost identical: 2.33 Å for the sample with HA and 2.34 Å for the sample without HA. It leads to the conclusion that HA has no influence on the near-neighbor surrounding of U(VI) in the kaolinite surface complexes. However, this conclusion could be also given by the limitation of the EXAFS method. As described above, from the measuring of the sample prepared at pH 3 resulted that the observed atomic distance between U and equatorial oxygen atom at 2.36 Å corresponds to the atomic distance between U and oxygen atom of adsorbed HA. From the measurements of other samples resulted that the distance between U and equatorial oxygen of kaolinite surface varies in the range between 2.33 Å and 2.37 Å. So, it is not possible to distinguish the oxygen atoms of HA and of kaolinite surface, therefore, the influence of HA must be evaluated carefully and it has to be studied with some additional methods. So, TRLS measurements in the systems U(VI)-kaolinite and U(VI)-kaolinite-HA were performed (see chapter 8.2).

### 8.1.7. Comparison of EXAFS Results of the Binary and the Ternary Systems

The EXAFS analysis of the ternary system was compared with the EXAFS analysis of the binary system U(VI)-kaolinite performed by Reich et al. [94]. They studied the effect of pH, CO<sub>2</sub>-presence, and U(VI)-concentration on the U(VI) sorption onto kaolinite by means of combination of batch sorption experiments and EXAFS measurements.

For the EXAFS analysis they used two different tools. Firstly, the EXAFS analysis was performed using EXAFSPAK [116]. The following conclusions have resulted: No U-U interactions were observed, therefore, U(VI) forms only mononuclear surface complexes. The U-O<sub>eq</sub> distances increased with increasing pH values. U-Si/Al interactions at 3.1 Å and 3.3 Å were found, this points to inner-sphere sorption of UO<sub>2</sub><sup>2+</sup> by edge-sharing with SiO<sub>4</sub>-tetrahedra and/or AlO<sub>6</sub>-octahedra.

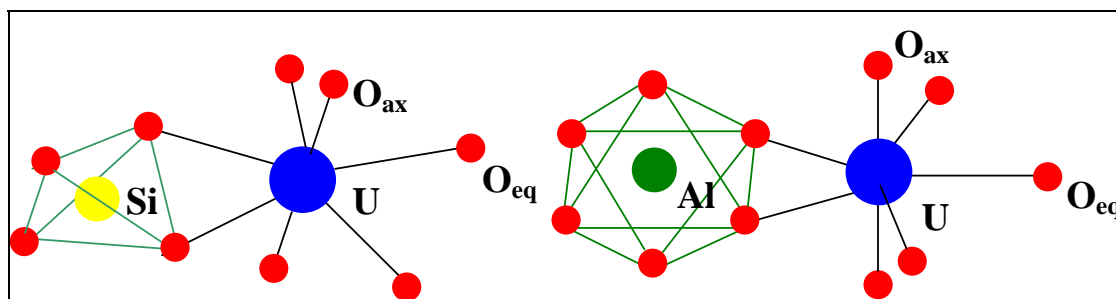


**Fig. 8.12:** Illustration of possible uranyl-kaolinite surface interactions according to [94].

Secondly, the Tikhonov regularization method [119] was used, which has been proposed for EXAFS analysis as an alternative to the analysis of EXAFS spectra by conventional shell fitting. An improved algorithm that utilizes a priori information about the sample has been developed and applied to the analysis of U L<sub>III</sub>-edge spectra of U(VI) adsorbed onto kaolinite [94]. The relative position of different pairs of atoms in a sample can be described by partial radial distribution function (RDF)  $g_f(r)$ . A priori information about sample is used to address the problem of non-uniqueness of the solutions. The U L<sub>III</sub>-edge EXAFS spectrum calculated agreed well with experimental data. Two peaks at 1.79 Å and 2.35 Å with N equal 1.9 (O<sub>ax</sub>) and 5.1 (O<sub>eq</sub>), respectively, were obtained. Approximately 0.7 Si/Al atoms at 3.06 Å and 0.4 Å atoms at 3.26 Å were found to surround the U(VI) atom.

**Tab. 8.6** shows the comparison of results from this work and the structural parameters derived from EXAFS analysis of the binary system U(VI)-kaolinite. Furthermore, the comparison

of system U(VI)-HA-kaolinite studied in this work with other binary model systems such as U(VI)-silica or U(VI)-montmorillonite is shown in **Tab. 8.7**. Finally, comparison of the ternary system U(VI)-HA-kaolinite with the binary system U(VI)-HA is given in **Tab. 8.8**.

**Tab. 8.6:** Comparison of the obtained structural parameters of different kaolinite systems.

System	R(U-O <sub>ax</sub> ) (Å) N = 2	R(U-O <sub>eq</sub> ) (Å) N = 5	R(U-Si/Al) (Å) N = 1 or 2	Reference
<b>Kaolinite KGa-1b</b>	1.80	2.36 – 2.41	3.1/3.3	[94]
<b>Kaolinite KGa-2</b>	1.80	2.40	3.3	[77]
<b>Kaolinite KGa-1b-HA</b>	1.77	2.35 ± 0.02	3.1/3.3	This work

The U-O<sub>ax</sub> distances obtained for both binary kaolinite systems KGa-1b and KGa-2 are the same, while in the presence of HA this distance was shortened. In [94], an increase of U-O<sub>eq</sub> with pH from 2.36 to 2.41 Å was observed which did not occur in the ternary system. The system with kaolinite KGa-2 (weighted average of samples prepared at pH 6.2 – 7.1) gave the value for U-O<sub>eq</sub> distance comparable to those obtained for the binary system with kaolinite KGa-1b. The value obtained for the ternary system is also slightly lower. In [77] only one U-Si/Al distance was obtained, but this distance is the same as the longer U-Si/Al distance found for the systems with kaolinite KGa-1b.

**Tab. 8.7:** Comparison of the obtained structural parameters of different model binary systems with the ternary system studied in this work.

System	R(U-O <sub>ax</sub> ) (Å)	N	R(U-O <sub>eq</sub> ) (Å)	N	R(U-Si/Al) (Å)	N	Reference
<b>Silica</b>	1.79	2	2.26	3	2.72	1	[111]
<b>Silica</b>	1.76	2	2.33	5.17	3.08	1	[112]
<b>UO<sub>2</sub>SiO<sub>4</sub>H<sub>2</sub></b>	1.80		2.14		2.88		[113]
<b>Montmorillonite</b>	1.78	2	2.36	5.94	3.42	1	[103]
<b>Kaolinite KGa-1b-HA</b>	1.77	2	2.35 ± 0.02	5	3.1/3.3	2	This work

Comparison of the systems with different minerals is more complicated. Here, similar systems with samples prepared under similar conditions have been chosen from literature. However, there is no unified fitting manner. Values of axial U-O distances are in good agreement for all systems; they are in the range 1.76 Å – 1.80 Å. More significant are the differences in obtained equatorial U-O and U-Si/Al distances. The values of equatorial U-O distances were found to be in a quite broad range 2.14 Å – 2.36 Å. U-Si/Al distances obtained for silica systems

are lower than those for kaolinite or montmorillonite systems. Only in this work and the work of Reich et al. [94], the best fitting of EXAFS data was obtained considering two U-Si/Al distances.

**Tab. 8.8:** Comparison of the obtained structural parameters for the ternary system with those of the binary systems U(VI)-HA from literature.

System	R(U-O <sub>ax</sub> ) (Å) N = 2	R(U-O <sub>eq</sub> ) (Å) N = 5	R(U-Si/Al) (Å) N = 2	Reference
UO <sub>2</sub> -natural HA	1.78	2.39	-	[108]
UO <sub>2</sub> -synthetic HA	1.78	2.39	-	
UO <sub>2</sub> -natural HA	1.78	2.37	-	[107]
UO <sub>2</sub> -synthetic HA-kaolinite	1.77	2.35 ± 0.02	3.1/3.3	This work

In all UO<sub>2</sub>-HA samples, the axial U-O distances of 1.78 Å and five equatorial oxygen atoms at distances 2.37 – 2.39 Å were found. The U-O<sub>eq</sub> distances are the same, within the experimental error, for both synthetic and natural uranyl humates. The equatorial distances for the uranyl humates indicate predominantly monodentate coordination of the HA carboxylate groups to U(VI) [107],[108]. The shorter U-O<sub>eq</sub> distance in the system with kaolinite can indicate changes in the U(VI) binding, when also kaolinite is present in the system. It can mean that U(VI) prefers direct binding onto kaolinite surface than the complexation with HA.

It is hard to distinguish between U(VI) bound to HA or to kaolinite or other minerals because of very similar values of axial and equatorial U-O distances as described in previous chapter. Generally, the obtained values of structural parameters of the system U(VI)-HA-kaolinite studied in this work are similar or they lie in the range of the obtained values of other systems. Therefore, it could be concluded that HA has *no effect on the EXAFS structural parameters in the system U(VI)-HA-kaolinite*. Moreover, it seems that in spite of the presence of HA, *U(VI) prefers to adsorb rather directly onto kaolinite than via HA*, otherwise no U-Si/Al interactions could be observed.

## ***8.2. U(VI) Surface Complexation in the Systems U(VI)-Kaolinite and U(VI)-Humic Acid-Kaolinite Studied by TRLFS***

The time-resolved laser-induced fluorescence spectroscopy (TRLFS) was applied as the second method to study the kind of U(VI) surface complexes onto kaolinite. These investigations were performed at different pH values in the absence and presence of HA. TRLFS provides information on both lifetime and spectral characteristic of adsorbed species, which allows to derive information on the number of different species and their spectral identity. This method may, therefore, provide information complementary to EXAFS spectroscopy and other techniques [115]. Together with EXAFS investigations and further complementary methods (e.g., XPS), TRLFS technique can supply new insight into actinide surface complexation and, therefore, it can contribute to an improved knowledge of actinide behavior in the environment

### **8.2.1. Laser Fluorescence Spectroscopy**

TRLFS is increasingly used to study the speciation of fluorescent actinides or their complexation with organic (e.g., HA) and inorganic ligands (e.g., sulfate, carbonate, phosphate). Recently, the application of this method was spread to study the character of adsorbed actinides species onto solid matter [120]-[125]. TRLFS as one fluorescence spectroscopic method was performed to study the U(VI) sorption, for example, onto gibbsite [122], muscovite [126] or silica [121].

The major advantages of TRLFS over other techniques (such as EXAFS) are i) its enhanced sensitivity and its combined information on ii) concentrations (based on intensities), iii) molecular structure (based on emission wave numbers and lifetimes) [121]. Further benefits are that TRLFS is a non-invasive and in-situ method for the direct investigation of solutions, solids and also sorbates. A drawback is the limited number of fluorescent species, thus, TRLFS is not a universal method. The measurements are dependent on temperature and strongly influenced by apparatus properties. Maximally four species can be identified and the laser dispersion peak can occur, therefore, it must be either filtered during measurements or the obtained spectrum must be corrected.

### ***Principles of Fluorescence Spectroscopy***

Luminescence is the emission of light from any substance and occurs in electronically excited states. Luminescence is formally divided into two categories, *fluorescence* and *phosphorescence*, depending on the nature of the excited state. In excited singlet states, the electron in the excited orbital is paired (of opposite spin) to the second electron in the ground state orbital. Consequently, return to the ground state is spin-allowed and occurs rapidly by emission of a photon. Phosphorescence is emission of light from triplet excited states in which the electron in the excited orbital has the same spin orientation as the ground state electron [127].

The processes, which occur between the absorption and emission of light, are usually illustrated by a Jabłoński diagram [128]. A typical Jabłoński diagram is shown in **Fig. 8.13**. The singlet ground, first, and second electronic states are depicted by S0, S1, and S2, respectively. At each of these electronic energy levels the fluorophores can exist in a number of vibrational energy levels, denoted by 0, 1, 2, etc.

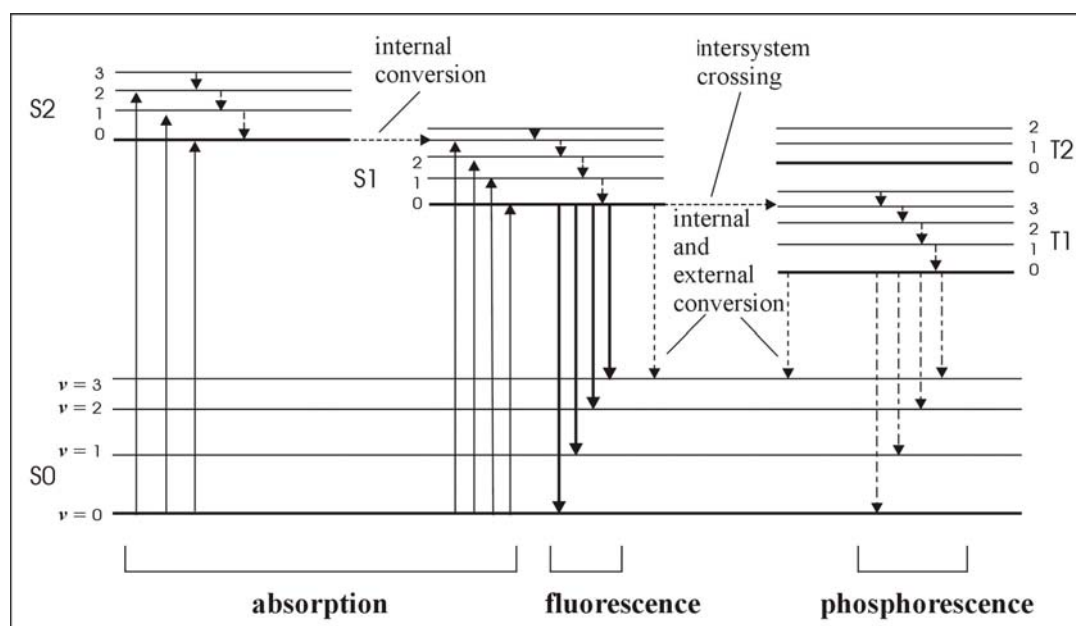


**Fig. 8.13:** The Jablonski-schema of the most significant absorption and emission processes in the molecules [128].

Absorption typically occurs from molecules with the lowest vibrational energy. Following light absorption, several processes can occur. A fluorophore is usually excited to some higher vibrational level of either S1 or S2. With some rare exceptions, molecules in condensed phases rapidly relax to the lowest vibrational level of S1. This process is called *internal conversion*.

Return to the ground state typically occurs to a higher excited state of vibrational ground state level, which then quickly reaches thermal equilibrium. An interesting consequence of emission to higher vibrational ground states is that the emission spectrum is typically a mirror image of the absorption spectrum of the  $S_0 \rightarrow S_1$  transition. Molecules in the  $S_1$  state can also undergo a spin conversion to the first triplet state,  $T_1$ . Emission from  $T_1$  is termed phosphorescence and conversion of  $S_1$  to  $T_1$  is called *intersystem crossing* [127].

The fluorescence of the molecule is characterized by the spectral distribution of the emitted light, fluorescence lifetime and fluorescence quantum yield. The fluorescence spectrum results from the spectral decomposition of the fluorescence light of the sample and from the expression of fluorescence intensity as a function of the wavelength. The *fluorescence lifetime* is the decay time in which the fluorescence intensity decreases to proportion of  $1/e$  of its initial value. The fluorescence decay is usually expressed as exponential function of the rate constants of emitted ( $k_a$ ) and non-radiative ( $k_b$ ) transitions and the function of wavelength ( $I$ ). The time law for the fluorescence decay is expressed as [129]:

$$\frac{dI}{dt} = -(k_a + k_b) \cdot I = -k_c \cdot I \quad (8.5)$$

The integration over the time  $t = 0 - t$  yields the fluorescence decay function:

$$I = I_0 \cdot e^{-k_c \cdot t} = I_0 \cdot e^{-\frac{t}{\tau}}, \quad (8.6)$$

where  $I$ ,  $I_0$  are the fluorescence intensities at the time  $t$  and  $t_0$ ;  $k_c$  is the intrinsic decay constant,  $t$  is the time after fluorescence excitation,  $\tau$  is the intrinsic fluorescence lifetime.

Different molecules have different fluorescence spectra and different fluorescence lifetimes, whereby different species in the solution can be determined. Such differences are significant enough to be observable. The *fluorescence quantum yield* gives the efficiency of the fluorescence process. It is defined as the number of emitted photons relative to the number of adsorbed photons [128],[129].

Fluorescence measurements can be broadly classified into two types of measurements, *steady-state* and *time-resolved*. Steady-state measurements are performed with constant illumination and observation. The sample is excited with a continuous beam of light and the intensity of the emission spectrum is recorded. The second type of measurements, time-resolved measurement, is used for measuring intensity decays or anisotropy decays [127]. Time-resolved



measurement allows setting the time of excitation, moreover, the spectra can be recorded at given times after the excitation of laser pulse. In this manner, more species with different fluorescence lifetimes occurring together in the solution or on a solid phase can be detected due to time fluorescence discrimination. The lifetimes of these species can be then calculated from exponential decay function, which has for  $i$  species the following form:

$$Y = \sum_i A_i \cdot e^{-\frac{t_x}{\tau_i}}, \quad (8.7)$$

where  $Y$  is measured fluorescence intensity at the time  $x$ ,  $A_i$  is fluorescence intensity of the  $i$ -th species at the time 0,  $\tau_i$  is the fluorescence lifetime of  $i$ -th species.

### ***Spectroscopic Properties of the Uranyl Ion***

Uranium belongs to the 5f-elements. It possesses in the gaseous form the following electronic configuration:  $5f^3 6d 7s^2$  [45]. The schematic overview of the fluorescence transitions for uranium is depicted in **Fig. 8.14**. Theoretical models for the uranyl ion usually consider a triplet excited state, and most comparisons of models with spectral data require the consideration of  $\pi$ -bonding. The combined UV and visible spectra are composed of seven major electronic bands which consist of 24 single bands and represent transitions to progressively higher lying orbitals.

The fluorescence spectrum is divided into 6 fluorescence emission bands. The five lowest energy bands have an average spacing of  $855 \pm 20 \text{ cm}^{-1}$ , which points to the symmetric vibration of the uranyl ion in its ground state. However, the emission band at  $21270 \text{ cm}^{-1}$  is only  $768 \text{ cm}^{-1}$  from the next lower energy band and is probably of an origin different from the other five emission bands. The positions of the first two absorption bands correspond quite closely with the positions of these two highest energy fluorescence bands. Thus, there are two energy levels from which the excited uranyl ion releases energy i) the emission energy level at  $20502 \text{ cm}^{-1}$ , which corresponds to the first absorption level,  $20582 \text{ cm}^{-1}$ , is affected by five symmetric vibrations of the uranyl ion in the ground state; and ii) the emission energy level at  $21270 \text{ cm}^{-1}$ , which corresponds to the second absorption level,  $21329 \text{ cm}^{-1}$  is not noticeably affected by the ground state vibrations [130].

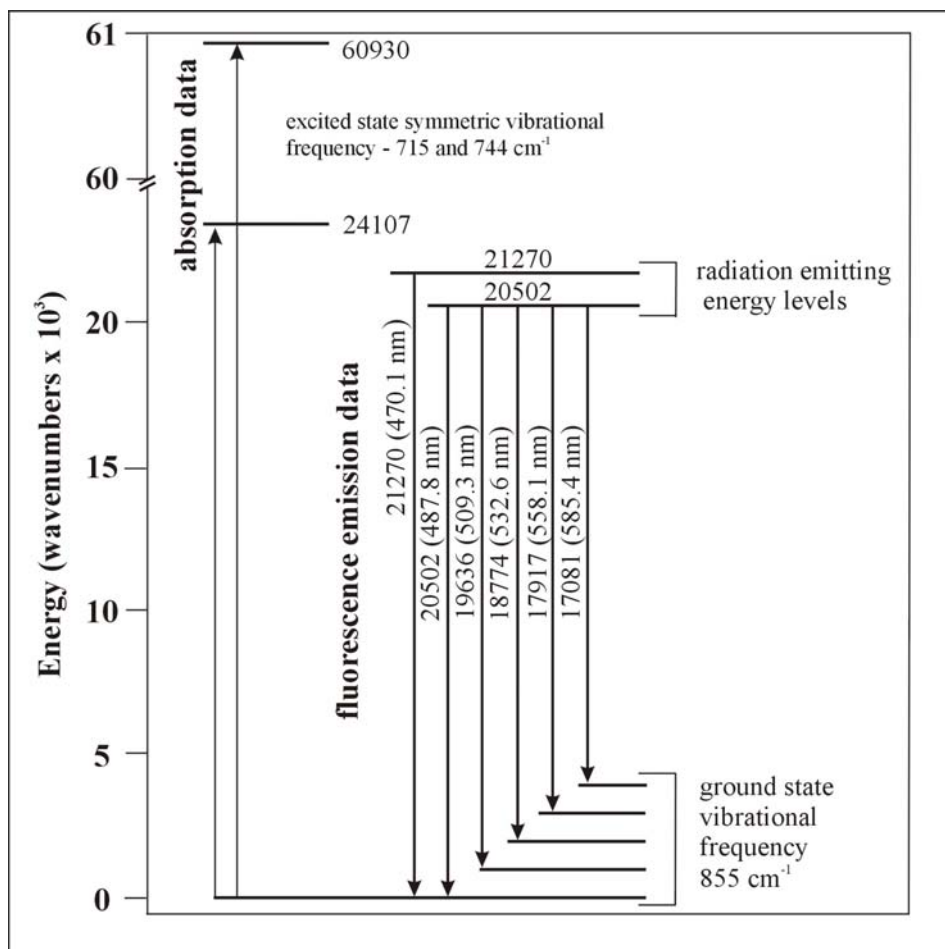


**Fig. 8.14:** Scheme of the excited terms of the uranyl ion [130].

The broad character of uranyl emission bands indicates that the electronic transitions are not metal orbital metal orbital transitions which are usually distinguished by sharp intense bands for ions of the heavy elements. The transitions probably result from electron transfers within, or from, the covalent O-U-O bonds, which would be expected to have a significant  $\pi$ -bond contribution. **Fig. 8.15** shows the typical fluorescence emission spectrum of the free uranyl ion ( $[U(VI)] = 1 \cdot 10^{-5}$  M) in the 0.01 M NaClO<sub>4</sub> solution measured at pH = 1.0. Six characteristic fluorescence emission bands were measured corresponding to the scheme in **Fig. 8.14**. **Fig. 8.16** introduces also uranyl emission spectrum, but this spectrum was measured at pH value comparable to the measurements in this work. The difference in the spectrum shape results from the U(VI) speciation in the solution (cf. chapter 4). At low pH values, the U(VI) is present in the solution as free UO<sub>2</sub><sup>2+</sup> ion, while the uranyl-hydroxo and uranyl-carbonato complexes occur at higher pH values and, therefore, the ideal fluorescence spectrum of free uranyl ion is changed.

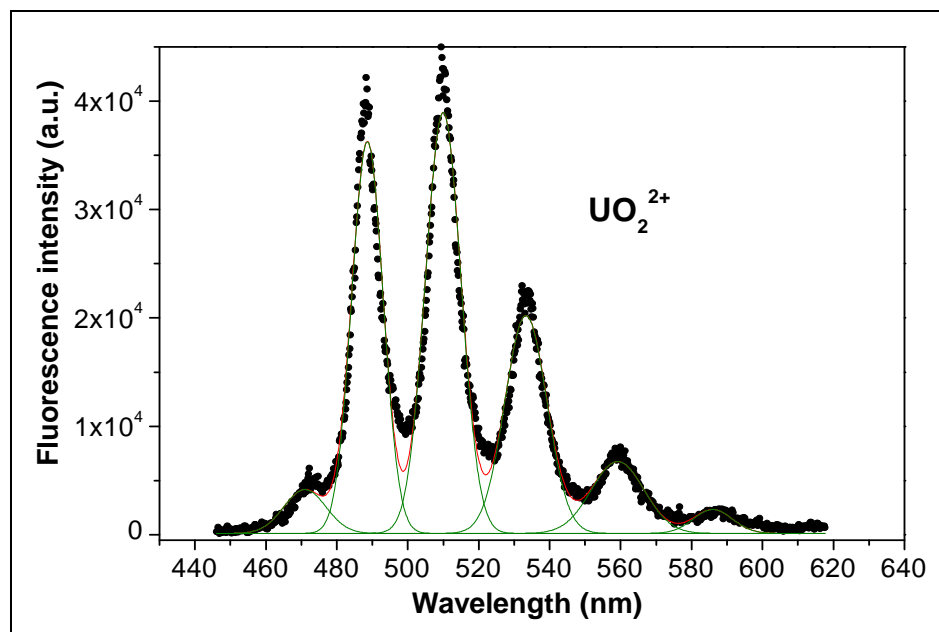


**Fig. 8.15:** Fluorescence emission spectrum of the free uranyl ion in 0.01 M NaClO<sub>4</sub> ([U(VI)] = 1·10<sup>-5</sup> M, pH 1.0).

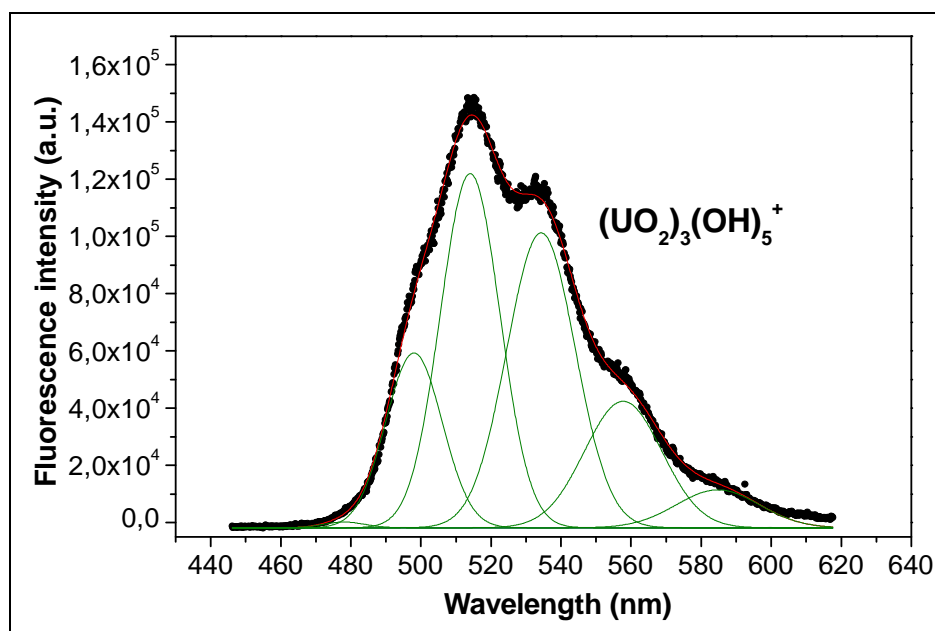


**Fig. 8.16:** Fluorescence emission spectrum of U(VI) in 0.1 M NaClO<sub>4</sub> ([U(VI)] = 5.63·10<sup>-6</sup> M, pH 6.69) [53].

Baumann et al. [122] used TRLFS in combination with batch experiments to study the U(VI) sorption onto gibbsite. They identified two adsorbed U(VI) surface species in the pH range between pH 5 and pH 8.5 with different fluorescence lifetimes of 330 and 5600 ns, respectively. The detected fluorescence spectra were described by six characteristic fluorescence emission

bands, whose maxima were shifted relative to the values for the free uranyl ion in perchlorate medium by 9.6 – 0.4 nm. Arnold et al. [126] found two adsorbed U(VI) surface species on edge-surface of muscovite. The two species showed different positions of the fluorescence emission bands and different lifetimes indicating a different coordination environment for the two species.

### **8.2.2. Sample Preparation and Data Evaluation**

The TRLFS data were collected for two systems. The binary system consists of U(VI) adsorbed onto kaolinite, whereas in the ternary system also HA was present. U(VI) or U(VI)-HA were adsorbed as described in chapter 10.2.2 under the following experimental conditions: U(VI) and HA (unlabeled HA type M42) initial concentrations were  $1 \cdot 10^{-5}$  M and 10 mg/L, respectively, ionic strength was kept at 0.1 M NaClO<sub>4</sub>, pH values were adjusted between pH 5 and pH 8, solid/solution ratio was 4 g/L. After phases separation, the supernatants were analyzed by ICP-MS for U(VI) final concentrations. For the spectroscopic investigation, kaolinite samples from the batch experiments were first re-suspended in 10 mL of a solution with pH and ionic strength being identical to the original solution (without U(VI) and HA). This ascertained that only fluorescence signals caused from originally sorbed U(VI) would be detectable, eliminating the dissolved U(VI) fraction. Time-resolved spectra of this kaolinite suspension were then recorded at permanent stirring. The re-distribution of fluorescent U(VI) species between solid and solution phase after the first centrifugation was negligible. To verify this, kaolinite was separated again from the solution after the first TRLFS measurement. The supernatants were measured by ICP-MS for U(VI) concentration. The results of these analysis confirmed that U(VI) was not desorbed from kaolinite during TRLFS measurements. To be sure that also HA does not desorb from kaolinite during TRLFS measurements in ternary system, one series of measurements in ternary system was performed using <sup>14</sup>C-labeled HA type M42. The supernatants were analyzed by LSC for HA concentration. As for U(VI), the results of these analysis corroborated that HA was not desorbed from kaolinite during TRLFS measurements. **Tab. 8.9** shows the experimental conditions of sample preparation, the U(VI) and HA concentrations, pH values and amount of adsorbed U(VI). The measuring system is thoroughly described in chapter 10.3.10.

**Tab. 8.9:** Samples for TRLFS measurements ( $[U(VI)] = 1 \cdot 10^{-5}$  M,  $I = 0.1$  M  $NaClO_4$ ,  $pCO_2 = 10^{-3.5}$  atm).

Sample	[HA] <sub>0</sub> (mg/L)	pH <sub>start</sub>	pH <sub>end</sub>	U(VI) <sub>sorbed</sub> (%)
U5	-	<b>5.05</b>	<b>5.03</b>	42.28
U6	-	<b>6.06</b>	<b>6.03</b>	87.32
U7	-	<b>7.05</b>	<b>7.06</b>	91.44
U8	-	<b>8.08</b>	<b>8.03</b>	81.43
U-HA5	10	<b>5.06</b>	<b>5.01</b>	97.79
U-HA6	10	<b>6.05</b>	<b>6.05</b>	98.08
U-HA7	10	<b>7.04</b>	<b>7.04</b>	98.16
U-HA8	10	<b>8.07</b>	<b>8.01</b>	75.34

The lifetimes of U(VI) fluorescence species were determined from bi-exponential fit analysis of obtained data indicating at least two surface species. An example of the lifetime analysis for the sample of U(VI) adsorbed onto kaolinite at pH ~7 is shown in **Fig. 8.17**.

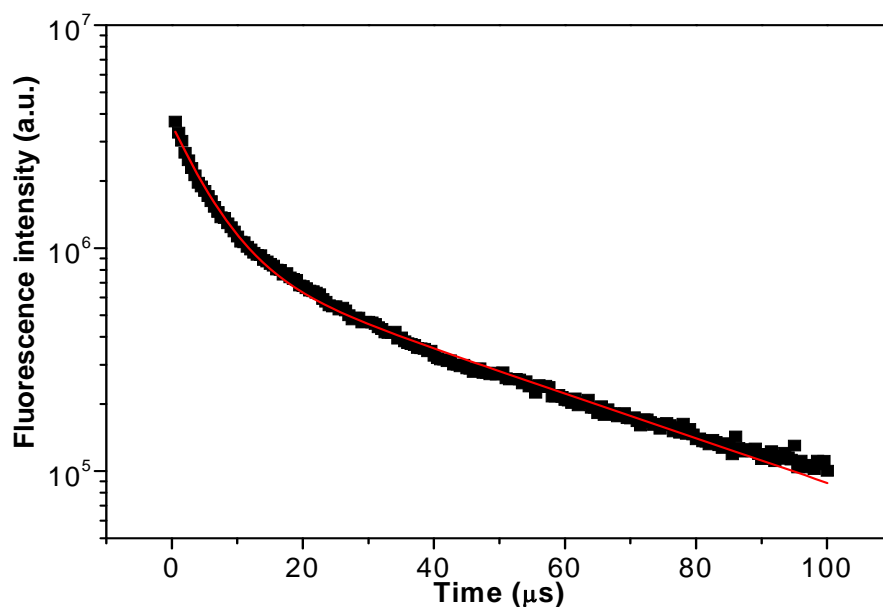


**Fig. 8.17:** Bi-exponential fluorescence decay behavior of the sample adsorbed at pH ~ 7 (U7).

By this analysis, one point in the decay curve represents the value of fluorescence intensity integrated for all wavelengths at a given delay time. The fluorescence lifetimes of two U(VI) surface species were calculated from Eq. (8.8):

$$y = y_0 + A_1 e^{-(x-x_0)/t_1} + A_2 e^{-(x-x_0)/t_2} \quad (8.8)$$

The lifetime analysis and the generation of the graphics utilized OriginPro 7.5G software (OriginLab Corp., Northampton, MA).

Another possibility to determine the fluorescence lifetimes is shown in **Fig. 8.18** left. Firstly, the fluorescence intensities, contrary to previous case, were integrated for each wavelength at a given delay time. The respective fluorescence decay curve was fitted to a sum of exponential decay terms. The resulted values of the fluorescence decay lifetime were then depicted as a function of wavelength and the average value of the decay lifetime with standard deviation was determined. In the case of bi-exponential decay, the spectral contributions of both species have to be extracted from the measured sum spectrum. **Fig. 8.18** right shows the spectral contributions of single species for the sample of U(VI) adsorbed onto kaolinite at pH ~ 7 as an example.

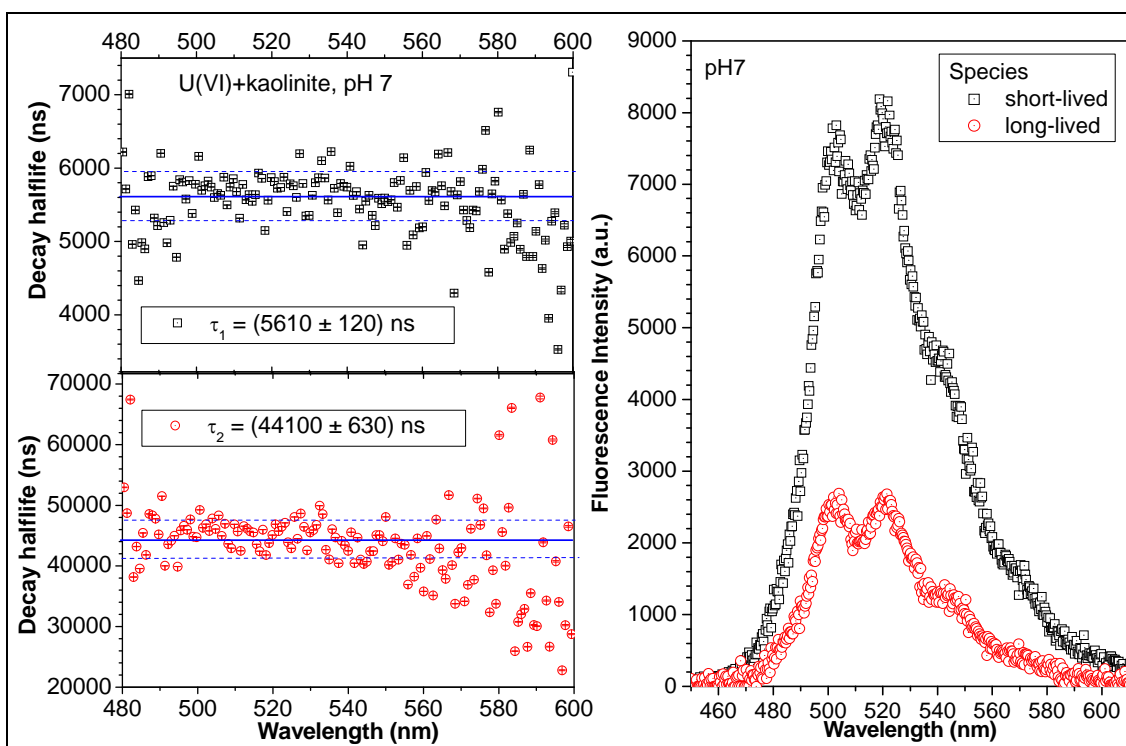


**Fig. 8.18:** Fluorescence decay lifetimes of U(VI) adsorbed onto kaolinite at pH ~ 7 (left) and respective single component spectra (right). The evaluation of the spectroscopic data was performed with in-house software by Brendler et al. [131] to obtain the fluorescence lifetimes and the single component spectra.

### 8.2.3. Surface Complexation of U(VI) on Kaolinite in Absence of Humic Acid

TRLFS measurements provide two kinds of characteristic information: the position of fluorescence emission bands and the fluorescence lifetimes. The positions of fluorescence bands are primary attributes of TRLFS spectrum, whereas the fluorescence lifetime is a secondary feature, because of its dependence on the sample preparation and temperature of experiment. The fluorescence lifetimes vary depending on the number of neighboring water molecules surrounding the U(VI) atom [132]. Such characteristic spectral information is useful for the identification of fluorescent aqueous uranium species, as well as U(VI) surface species adsorbed onto kaolinite.

The samples were excited with the laser beam (266 nm) and the fluorescence spectra were recorded at different times (0.03 – 100.03  $\mu$ s) after excitation by laser pulse. **Fig. 8.19** shows the dependence of the fluorescence intensity on the delay time. The original spectra of all samples with U(VI) adsorbed onto kaolinite at different pH values are comparable, thus, only the original TRLFS spectrum of U(VI) adsorbed onto kaolinite at pH ~ 7 is shown as an example.

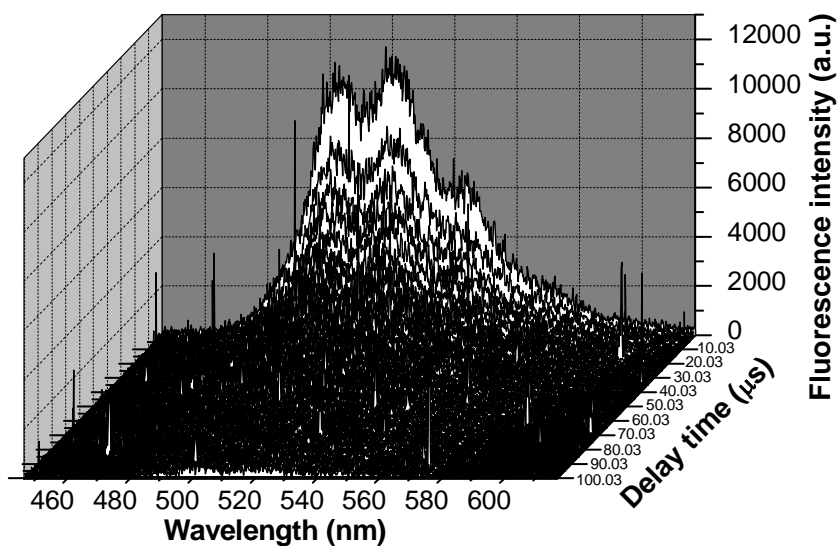


**Fig. 8.19:** TRLFS spectrum of U(VI) adsorbed onto kaolinite at pH ~ 7.

The TRLFS spectra of the sorbed U(VI) surface species on kaolinite suspensions indicated at least two surface species with two different fluorescence lifetimes, i.e., one short- and one long- lived species. The calculated average fluorescence lifetimes of the short- and long-lived species are  $\tau_1 = 5870 \pm 690$  ns and  $\tau_2 = 42480 \pm 1670$  ns, respectively, with the errors

representing one standard deviation ( $1\sigma$ ). The results of fluorescence lifetime determinations for all measured samples are summarized in **Tab. 8.10**. The values of fluorescence lifetimes of both species demonstrate no dependence on pH value.

**Tab. 8.10:** Fluorescence lifetimes of the U(VI) species sorbed onto kaolinite, errors represent  $1\sigma$ .

Sample	pH	$\tau_1$ (ns)	$\tau_2$ (ns)
U5	5	$5640 \pm 150$	$40800 \pm 440$
U6	6	$6880 \pm 150$	$41300 \pm 470$
U7	7	$5610 \pm 120$	$44100 \pm 630$
U8	8	$5330 \pm 160$	$43700 \pm 730$
Mean lifetime		$5870 \pm 690$	$42480 \pm 1670$

By means of the internal fitting module of the program OriginPro 7.5G, the fluorescence emission bands can be determined. Six fluorescence emission bands were obtained for the fluorescence spectra of all measured samples which can be described by a set of six absorption peaks in accordance with the work of Bell and Biggers [130]. An example of such deconvoluted fluorescence spectra of single species with their characteristic positions of the fluorescence emission bands is illustrated in **Fig. 8.20** for U(VI) surface species adsorbed onto kaolinite at pH  $\sim 7$ . As it can be seen, the deconvoluted fluorescence spectra reveal six characteristic fluorescence emission bands that are almost identical for both U(VI) surface species.

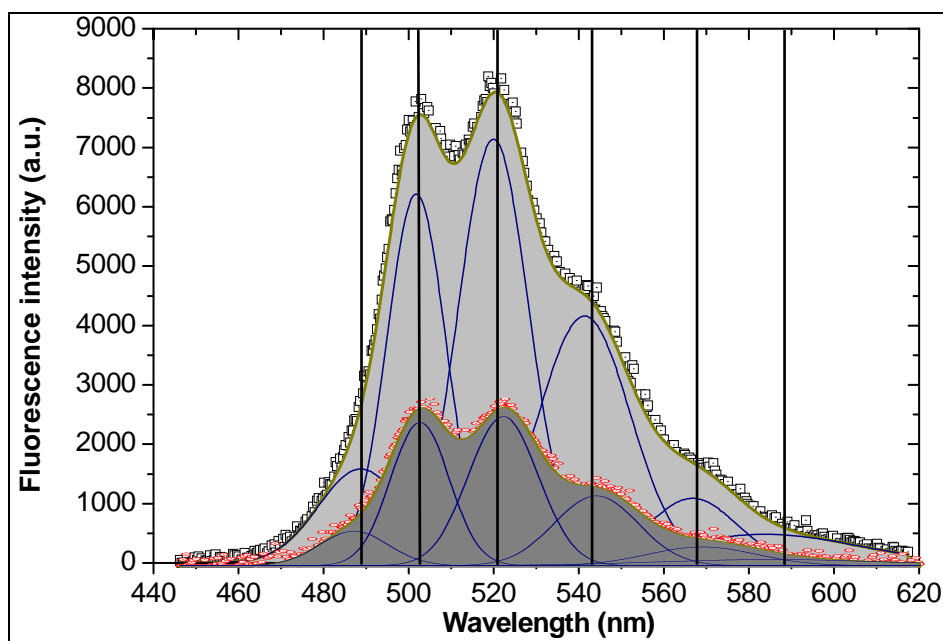


**Fig. 8.20:** Deconvoluted fluorescence spectra with characteristic positions of the fluorescence emission bands for the sample measured at pH  $\sim 7$ .



The peak maxima are situated at  $486.9 \pm 0.9$ ,  $501.8 \pm 0.6$ ,  $520.6 \pm 0.9$ ,  $541.7 \pm 0.7$ ,  $567.8 \pm 1.5$ , and  $583.3 \pm 0.6$  nm, for details see **Tab. 8.11**. For further discussion only the first five peaks will be considered, because the sixth emission band is very low and broad and, therefore, rather uncertain. The positions of peak maxima are shifted significantly to higher wavelengths relative to the values for the free uranyl ion in perchlorate medium (see [130] or **Tab. 8.11**). The shifts range from 16.8 nm for the first peak to 9.7 nm for the fifth one.

**Tab. 8.11:** Wavelengths of peak maxima positions (in nm) for two fluorescent components.

Sample	pH	1 <sup>st</sup> peak	2 <sup>nd</sup> peak	3 <sup>rd</sup> peak	4 <sup>th</sup> peak	5 <sup>th</sup> peak	6 <sup>th</sup> peak
Short-lived species							
U5	5	486.7	502.9	521.9	541.5	568.5	583.9
U6	6	486.2	501.1	519.0	541.1	570.7	583.9
U7	7	488.7	501.8	520.0	541.4	566.8	583.9
U8	8	486.8	501.3	519.9	540.8	566.7	583.6
Long-lived species							
U5	5	486.8	501.3	521.3	542.0	569.1	582.4
U6	6	486.2	502.4	521.1	541.5	566.2	582.6
U7	7	486.5	501.8	521.0	542.5	567.1	583.4
U8	8	487.7	501.9	520.5	542.8	567.3	583.0
Weighted average of all peak maxima with standard deviation							
		$486.9 \pm 0.9$	$501.8 \pm 0.6$	$520.6 \pm 0.9$	$541.7 \pm 0.7$	$567.8 \pm 1.5$	$583.3 \pm 0.6$
Peak maxima of free $\text{UO}_2^{2+}$ ion in perchlorate medium							
$\text{UO}_2^{2+}$		470.1	487.8	509.3	532.6	558.1	585.4

Due to the coincidence of all the fluorescence peaks, these two adsorbed U(VI) surface species, i.e., the short-lived and the long-lived, are assumed to be similar in coordination environment throughout the investigated pH range. They should thus have identical numbers of hydroxyl groups in their first coordination sphere, as different numbers of hydroxyl group cause changes in the spectral features [122]. Shorter fluorescence lifetimes indicate more water molecules in the coordination environment of the respective adsorbed U(VI) surface species, because water molecules quench the fluorescence lifetime [126]. On this basis, it can be concluded that *U(VI) forms two surface species on kaolinite, which differ in the amount of water molecules in their coordination environment.*

### 8.2.4. Surface Complexation of U(VI) on Kaolinite in Presence of Humic Acid

The original TRLFS spectrum of U(VI) sorbed on kaolinite in the presence of HA at pH ~ 7 is shown in **Fig. 8.21** as representative of the original spectra of all samples with U(VI) adsorbed onto kaolinite in the presence of HA at different pH values.

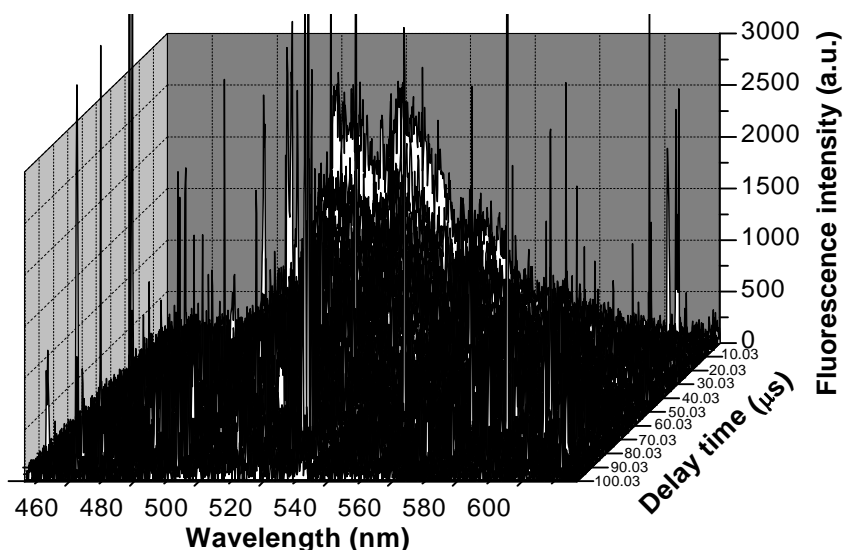


**Fig. 8.21:** TRLFS spectrum of U(VI) adsorbed onto kaolinite in the presence of HA at pH ~ 7.

Obviously, compared to the original TRLFS spectrum of U(VI) sorbed onto kaolinite in the absence of HA at the same pH value, the presence of HA drastically reduces the signal-noise ratio. This effect is typical for the whole pH range investigated within the present work. Therefore, the lifetime analysis and also the detection of emission bands were more complicated and resulted in higher standard deviations.

The lifetimes of U(VI)-HA fluorescence species were determined as described in chapter 8.2.2 from bi-exponential fit analysis of obtained data. Comparable to the binary system, two different surface species with two different fluorescence lifetimes were indicated. The bi-exponential decay curve of the sample of U(VI) adsorbed onto kaolinite in the presence of HA at pH ~ 7 is depicted in **Fig. 8.22**.

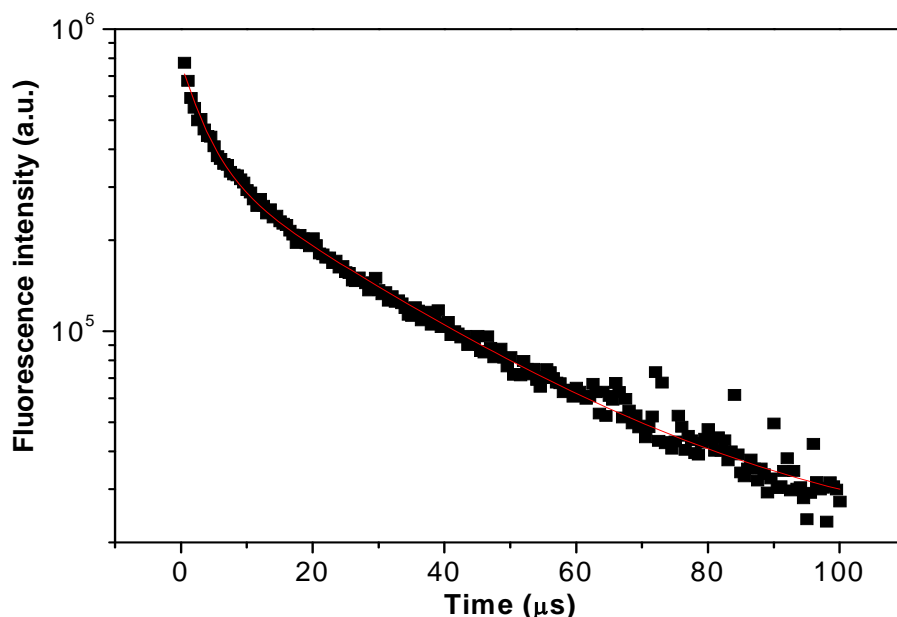


**Fig. 8.22:** Bi-exponential fluorescence decay behavior of the sample U-HA7.

In the case of these samples, the lifetime analysis was more problematic due to the rather noisy spectra. Therefore, it was performed only in the shortened wavelength range: 480 nm – 600 nm. The average fluorescence lifetimes were calculated from Eq. (8.8.). They amount to  $\tau_1 = 4380 \pm 570$  ns and  $\tau_2 = 31300 \pm 3580$  ns for the short- and long-lived species, respectively. The results of fluorescence lifetime determinations are summarized in **Tab. 8.12**. The obtained fluorescence lifetimes of long-lived species are not as consistent as in the binary system.

**Tab. 8.12:** Fluorescence lifetimes of the U(VI) species sorbed onto kaolinite in the presence of HA.

Sample	pH	$\tau_1$ (ns)	$\tau_2$ (ns)
U-HA5	5	$3540 \pm 490$	$26300 \pm 410$
U-HA6	6	$4770 \pm 370$	$31400 \pm 1400$
U-HA7	7	$4540 \pm 220$	$32700 \pm 450$
U-HA8	8	$4680 \pm 450$	$34700 \pm 2980$
Mean lifetime		$4380 \pm 570$	$31300 \pm 3580$

Due to a lower quality of the spectra and the shortening of the evaluated wavelength range, the detection of fluorescence emission bands was limited. As in the binary system, six peaks were assumed to describe satisfactorily the measured spectra, but the position of the last peak was very uncertain and, thus, only the positions of the first five peaks were found. The peak maxima are situated at  $486.6 \pm 1.1$ ,  $501.1 \pm 2.2$ ,  $520.5 \pm 1.5$ ,  $542.2 \pm 2.6$ , and  $566.7 \pm 3.6$ , the peak positions

of each U(VI) sample adsorbed onto kaolinite in the presence of HA are summarized in **Tab. 8.13**.

**Tab. 8.13:** Wavelengths of peak maxima positions (in nm) for two fluorescent components.

Sample	pH	1 <sup>st</sup> peak	2 <sup>nd</sup> peak	3 <sup>rd</sup> peak	4 <sup>th</sup> peak	5 <sup>th</sup> peak
Short-lived species						
U-HA5	5	486.4	504.9	523.3	540.9	564.0
U-HA6	6	485.2	501.7	519.5	538.6	571.8
U-HA7	7	488.8	500.1	519.5	544.1	566.8
U-HA8	8	485.9	503.1	521.5	542.9	566.9
Long-lived species						
U-HA5	5	486.7	498.7	518.8	546.1	567.1
U-HA6	6	486.7	499.8	521.2	544.4	559.8
U-HA7	7	487.2	501.8	520.1	541.9	570.4
U-HA8	8	485.7	498.9	519.9	539.1	566.9
Weighted average of all peak maxima with standard deviation						
		486.6 ± 1.1	501.1 ± 2.2	520.5 ± 1.5	542.2 ± 2.6	566.7 ± 3.6
Peak maxima of free UO <sub>2</sub> <sup>2+</sup> ion in perchlorate medium						
UO <sub>2</sub> <sup>2+</sup>		470.1	487.8	509.3	532.6	558.1

Two different obtained lifetimes indicate, as in the binary system, formation of at least two different surface complexes. The interpretation of these two complexes is, however, more complicated due to the presence of HA. Comparison of TRLFS results measured in the binary and ternary system will be the subject of the following chapter.

### 8.2.5. Comparison of Results of the Binary and the Ternary Systems

**Tab. 8.4** shows the comparison of the fluorescence intensities and the amounts of the U(VI) sorbed onto kaolinite of the samples prepared at pH ~ 7 in the presence and absence of HA. It can be seen that the U(VI) sorption onto kaolinite is comparable in both cases, i.e., in the absence and presence of HA. The difference in the sorbed amounts is 7%, while the fluorescence intensity is almost five times lower in the presence of HA than in its absence. It is obvious that HA decreases the measured fluorescence intensity of the samples. This points to differences in surface speciation induced by HA.

**Tab. 8.14:** Comparison of relative fluorescence intensity and amount of U(VI) adsorbed onto kaolinite of the samples prepared at pH ~ 7 in the absence and presence of HA.

pH ~ 7	U(VI)adsorb. (%)	RFI*
HA-absence	91	12000
HA-presence	98	2500

\* Relative fluorescence intensity

From previous paragraphs it resulted that minimally two different surface species can be identified in both systems. **Tab. 8.15** shows the comparison of the mean values of the respective fluorescence lifetimes obtained in the presence and absence of HA. In the presence of HA, the fluorescence lifetimes of both species are significantly shorter. Shorter fluorescence lifetimes indicate HA in the coordination environment of the adsorbed U(VI) surface species, because HA quenches the fluorescence lifetime. This means that in the presence of HA the hydration shell of uranyl ions is partly displaced by HA.

**Tab. 8.15:** Comparison of fluorescence lifetimes in the absence and presence of HA.

pH 5 - 8	$\tau_1$ (ns)	$\tau_2$ (ns)
HA-absence	5900 ± 700	42500 ± 1700
HA-presence	4400 ± 600	30900 ± 3600

In **Fig. 8.23** the obtained lifetimes of the surface species identified in the presence and absence of HA as a function of pH values are depicted. It becomes evident that pH values have no significant influence on fluorescence lifetimes of U(VI) surface species in the binary as well as in the ternary system.

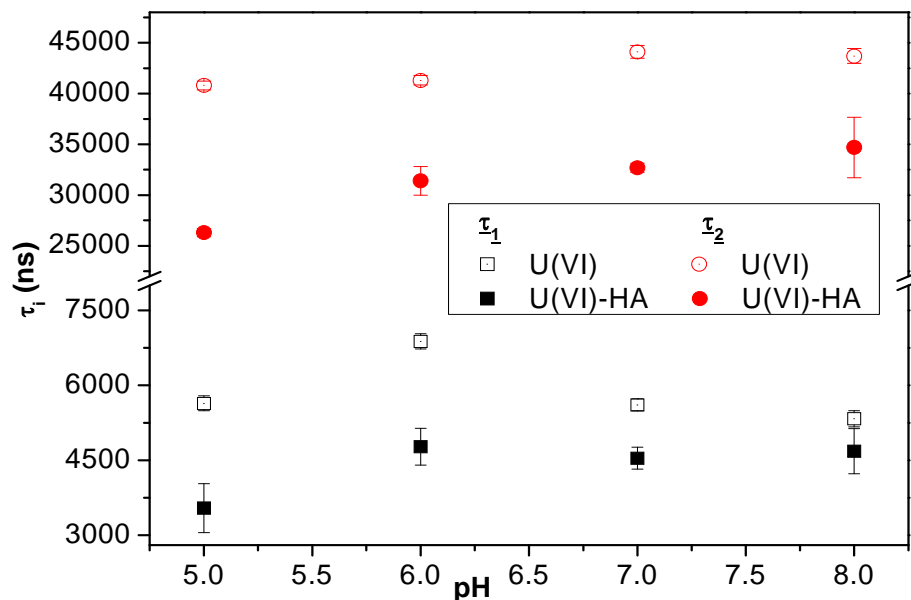


**Fig. 8.23:** Fluorescence lifetimes as a function of pH values.

Six fluorescence emission bands were obtained for the fluorescence spectra of all measured samples of U(VI) adsorbed onto kaolinite in the absence of HA. In the presence of HA, only five peaks were found due to lower quality of spectra. The comparison of mean values of identified peak positions for the samples in the absence and presence of HA is given in **Tab. 8.16**. No differences in peak positions were observed. It can be, therefore, concluded that HA does not influence the peak positions of both species.

**Tab. 8.16:** Comparison of absorption peak positions in the absence and presence of HA.

pH 5 - 8	1 <sup>st</sup> peak	2 <sup>nd</sup> peak	3 <sup>rd</sup> peak	4 <sup>th</sup> peak	5 <sup>th</sup> peak	6 <sup>th</sup> peak
HA-absence	486.9 ± 0.9	501.8 ± 0.6	520.6 ± 0.9	541.7 ± 0.7	567.8 ± 1.5	583.3 ± 0.6
HA-presence	486.6 ± 1.1	501.1 ± 2.2	520.5 ± 1.5	542.2 ± 2.6	566.7 ± 3.6	-

### 8.2.6. Comparison of Results with Model Systems

Spectroscopic techniques were used to obtain detailed information about U(VI) interaction with kaolinite. They should help to identify on which of possible binding sites of kaolinite (silanol, aluminol groups), U(VI) would prefer to adsorb. Unfortunately, in EXAFS it is not possible to distinguish between Al and Si atoms. To decide between aluminol and silanol groups, TRLS measurements of the system U(VI)-kaolinite were compared with the systems U(VI)-gibbsite [133] and U(VI)-silica gel [134] systems. Gibbsite, Al(OH)<sub>3</sub>, was chosen as a

model mineral for aluminol sites and silica gel, SiO<sub>2</sub>, represents silanol binding groups. **Tab. 8.17** compares the mean values of fluorescence lifetimes obtained for the U(VI)-kaolinite system with these model systems. In all systems, at least two fluorescence lifetimes were identified. The calculated average fluorescence lifetimes of the short- and long-lived species were 2400 ± 200 ns and 13200 ± 2500 ns, respectively, for U(VI)-gibbsite system, 138 ± 53 μs and 362 ± 103 μs, respectively, for U(VI)-silica gel system and 5900 ± 700 ns and 42500 ± 1700 ns, respectively, for U(VI)-kaolinite system.

**Tab. 8.17:** Comparison of mean values of fluorescence lifetimes obtained for the systems studied in this work with model systems UO<sub>2</sub>-gibbsite and UO<sub>2</sub>-silica gel.

System	$\tau_1$ (ns)	$\tau_2$ (ns)	Reference
UO <sub>2</sub> -gibbsite	2400 ± 200	13200 ± 2500	[133]
UO <sub>2</sub> -silica gel	138400 ± 52900	361800 ± 103200	[134]
UO <sub>2</sub> -kaolinite	5900 ± 700	42500 ± 1700	This work
UO <sub>2</sub> -HA-kaolinite	4400 ± 600	30900 ± 3600	This work

It becomes evident that the values of fluorescence lifetimes of both fluorescence species on kaolinite lie in the range between values obtained for gibbsite and for silica gel, nevertheless, the fluorescence lifetimes of species on kaolinite are closer to those on gibbsite than on silica gel. It seems that U(VI) adsorbs on both kinds of available sites but not equally. It is not easy to identify in which ratio they are represented or which binding sites are more occupied by U(VI). However, aluminol binding sites are assumed to control the sorption of U(VI). From scanning electron microscopy of kaolinite particles, the ratio between planes and edges of kaolinite particles was calculated to be about 0.72 which indicates a higher amount of edges relative to basal planes. Similarly, Brady et al. [14] reported higher percentage of edges relative to basal plane of the kaolinite KGa-1 resulting from scanning force microscopy. They also reported elevated reactivity of Al edge sites, relative to Si, and a weak sorption on basal planes resulting from their molecular modeling. This supports the idea that Al binding sites govern the U(VI) sorption onto kaolinite in the system studied in this work. Finally, an excess of Al<sub>2</sub>O<sub>3</sub> was found by chemical analysis in untreated kaolinite (cf. **Tab. 2.1**).

### **8.3. Surface Speciation Model Development**

In this work, the interaction of HA and/or U(VI) with kaolinite was studied by XPS, EXAFS and TRLFS. In this chapter, results of these measurements are interpreted together and an attempt is made to describe the U(VI) surface speciation on kaolinite in the absence and presence of HA.

#### **8.3.1. System U(VI)-Kaolinite**

From TRLFS investigations it resulted that U(VI) forms at least two surface species on kaolinite, which differ in the amount of water molecules in their coordination environment. From EXAFS measurements of U(VI) sorption onto kaolinite [94] it was concluded that U(VI) forms inner-sphere surface complexes, moreover, two U-Si/Al interactions were found, which means that these surface complexes are bidentate. Thus, U(VI) is associated by edge-sharing with SiO<sub>4</sub>-tetrahedra and/or AlO<sub>6</sub>-octahedra. Nevertheless, unlike TRLFS measurements, in EXAFS measurements two surface species were not identify. This is given by the limitation of the EXAFS technique which determines only the average values of all bond distances. Baumann et al. [122] and Arnold et al. [126] studied the U(VI) sorption on gibbsite ([U(VI)]: 1·10<sup>-5</sup> M, pH: 5 – 8.5, I: 0.1 M NaClO<sub>4</sub>) and muscovite ([U(VI)]: 1·10<sup>-5</sup> M, pH: 7, I: 0.01 M NaClO<sub>4</sub>), respectively, by TRLFS. Baumann et al. [122] attributed the surface species with the shorter fluorescence lifetime to the bidentate mononuclear inner-sphere surface complex in which U(VI) is bound to two reactive hydroxyl groups at the broken edge linked to one Al. Arnold et al. [126] ascribed the surface species with the shorter fluorescence lifetime to an inner-sphere bidentate surface complex in which U(VI) binds to aluminol groups of edge-surfaces of muscovite. Both interpreted the surface species with the significantly longer fluorescence lifetimes as an amorphous U(VI) condensate or nanosized clusters of polynuclear uranyl surface species. This conclusion was made on the basis of findings by Thompson [77] and Sylwester [112]. From their EXAFS measurements, performed in the systems U(VI)-kaolinite KGa-2 [77], U(VI)-silica and U(VI)- $\gamma$ -alumina [112], resulted a U-U interaction at near-neutral pH range, which indicates the formation of polynuclear surface species. This could not be concluded for the second surface species identified in the system studied in this work, because in EXAFS spectra (see chapter 8.1.3) no U-U interactions were detected, therefore, U(VI) forms only mononuclear surface



complexes on kaolinite. This is supported by works of Reich [111] and Gabriel [121]. Reich et al. [111] measured EXAFS of U(VI) adsorbed onto silica gel. Several samples were measured. One of them was prepared using experimental conditions similar to this work ([U(VI)]:  $2 \cdot 10^{-5}$  M, pH: 4.5, I: 0.1 M NaClO<sub>4</sub>, U(VI) sorption: 99%). They did not observe any distinct peak which could be attributed to backscattering from U neighbors. From all their measurements resulted that U(VI) forms inner-sphere, mononuclear complexes at the silica gel surface. Gabriel et al. [121] studied the uranyl surface speciation on silica particles by means of TRLFS under following experimental conditions: [U(VI)]:  $1 \cdot 10^{-5}$  M,  $1 \cdot 10^{-6}$  M, pH: 4 – 9, I: 0.01 M NaNO<sub>3</sub>. They identified two fluorescent uranyl surface complexes described as mononuclear (1:1) complexes with release of two and three protons, respectively. In combination with the constant capacitance model they finally identified three surface complexes, postulated as  $\equiv\text{SiO}_2\text{UO}_2^0$ ,  $\equiv\text{SiO}_2\text{UO}_2\text{OH}^-$ , and  $\equiv\text{SiO}_2\text{UO}_2\text{OHCO}_3^{3-}$ . However, from the values of fluorescence lifetimes measured in this work and from other above mentioned reasons, it is assumed for the system studied in this work that U(VI) bind preferably to aluminol binding sites of kaolinite.

### **8.3.2. U(VI)-Humic Acid-Kaolinite System**

EXAFS measurements of the U(VI) sorption onto kaolinite in the presence of HA showed that HA has no influence on the U(VI) EXAFS structural parameters in the kaolinite surface complexes. Therefore, it can be proposed that U(VI) forms inner-sphere bidentate surface complexes in the ternary as well as in the binary system. Moreover, it was found that even if HA is present, U(VI) prefers to adsorb rather directly onto kaolinite than via HA. This is indicated by the detection of U-Si/Al interactions.

From TRLFS measurements performed in the ternary system it resulted that HA decreases the fluorescence intensity and the fluorescence lifetimes of U(VI) surface species. Thus, shorter fluorescence lifetimes indicate the presence of HA in the coordination environment of the sorbed U(VI) surface species. This means that the hydration shell of uranyl ions is partly displaced by HA. In the presence of HA, the energy absorbed by U(VI) is apparently only partly released as a fluorescence. Partly, this energy is lost due to quenching properties of HA. Uranyl-humate complexes themselves do not show any fluorescence at all [53] under the applied measuring conditions. So, if U(VI) would be bound on kaolinite predominantly via HA, no U(VI) fluorescence of the prepared samples U(VI)-HA-kaolinite should be measured. This leads to the

conclusion that U(VI) is not bound to kaolinite via HA, but it is sorbed directly as the uranyl-humate complex.

The result of XPS measurements of HA sorption onto kaolinite matches very well with these observations in TRLFS and EXAFS measurements. As it is described in chapter 5.7, the surface of the kaolinite particles is not covered by a homogenous HA layer. Part of HA must be distributed between the kaolinite particles. This means that in the ternary system, U(VI) can interact with significant parts of the kaolinite surface that are not covered by HA.

### **8.3.3. Conclusions**

Two adsorbed fluorescence U(VI) species on kaolinite were identified in the binary (U(VI)-kaolinite) as well as in the ternary (U(VI)-HA-kaolinite) system in TRLFS measurements. Both surface species can be attributed to adsorbed bidentate mononuclear surface complexes in which two equatorial coordinated oxygen atoms of the uranyl ion are bound to two Al and/or Si (preferentially to Al) atoms of aluminol octahedra and/or silicon tetrahedral. They likely differ in the number of water molecules in their coordination environment. In the ternary system, U(VI) prefers direct binding to the kaolinite than via HA which is distributed between kaolinite particles. The hydration shell of the U(VI) surface complex is partly displaced by complexed HA.

## 9. Influence of Humic Acid on the Am(III) Sorption onto Kaolinite

In addition to the studies with U(VI), the first comparative experiments were performed in this work to determine the influence of HA on the Am(III) sorption onto kaolinite. In this chapter, the first results of kinetic, sorption and laser fluorescence measurements in the systems Am(III)-kaolinite and Am(III)-HA-kaolinite are described. Am(III) was chosen as an analogue for trivalent actinides. The experiments were performed similarly to U(VI) in order to compare the obtained results with those gained from similar investigations with U(VI).

### 9.1. Americium Chemistry in Solution

The electronic configuration of Am is  $[\text{Rn}] 5f^7 7s^2$ . Am may exist in different oxidation states in acidic aqueous media such as: Am(III), Am(IV), Am(V) and Am(VI). In a highly alkaline solution Am(VII) is produced. Am(II) was observed only in solid compounds. The most stable oxidation state is Am(III), which is produced by the dissolution of a metal or Am oxides in acids and by the reduction of other oxidation states [45]. Some basic chemical properties of Am are shown in **Tab. 9.1**.

**Tab. 9.1:** Chemical properties of americium [45].

Atomic number	95
Electronic configuration	$[\text{Rn}] 5f^7 7s^2$
Oxidation states	(2), <u>3</u> , 4, 5, 6
Ion types and colors	
Am <sup>3+</sup>	pink or yellow
Am <sup>4+</sup>	pink or red
AmO <sub>2</sub> <sup>+</sup>	yellow
AmO <sub>2</sub> <sup>2+</sup>	lemon yellow
AmO <sub>5</sub> <sup>3-</sup>	dark green
Stability in aqueous solution	
Am <sup>3+</sup>	stable, difficult to oxidize
Am <sup>4+</sup>	known in solution only as complex fluoride or carbonate ions
AmO <sub>2</sub> <sup>+</sup>	disproportionates in strong acid to Am <sup>3+</sup> and AmO <sub>2</sub> <sup>2+</sup>
AmO <sub>2</sub> <sup>2+</sup>	easy to reduce

Underlined oxidation number indicates the most stable oxidation state.

Similar to U(VI), the hydrolysis reactions and carbonate complexation are important properties of the Am(III) ion in the solution. **Fig. 9.1** depicts the relative Am(III) species distribution in the model solution.

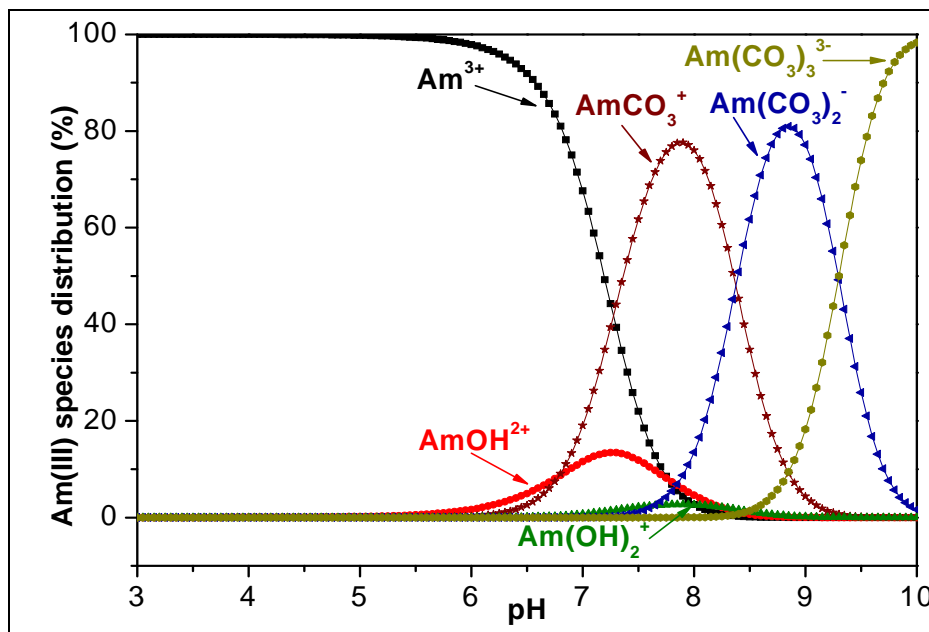


**Fig. 9.1:** Relative species distribution of Am(III) in 0.1 M NaClO<sub>4</sub> solution. [Am(III)] = 1·10<sup>-6</sup> M, pCO<sub>2</sub> = 10<sup>-3.5</sup> atm, t = 25°C).

As for U(VI), the speciation distribution was calculated using the code EQ3/6 [47] based on the most recent compilation of Am(III) complex formation constants [48]. Am(III) speciation was calculated for Am(III) concentration 1·10<sup>-6</sup> M in 0.1 M NaClO<sub>4</sub> solution. Equilibrium of the system with atmospheric CO<sub>2</sub> was assumed. The speciation diagram of Am(III) in 0.01 M NaClO<sub>4</sub> solution does not differ, therefore, only one speciation diagram (0.1 M) as an example is shown. From the diagram it is obvious that only two Am(III) species are significant at lower pH values. Am(III) prevails in solution as the free Am<sup>3+</sup> cation up to pH 7. Between pH 6 and pH 8.5 also the AmOH<sup>2+</sup> cation is important. AmCO<sub>3</sub><sup>+</sup> prevails between pH 7.5 and pH 8.5. The negatively charged Am(III)-carbonato complexes Am(CO<sub>3</sub>)<sub>2</sub><sup>-</sup> and Am(CO<sub>3</sub>)<sub>3</sub><sup>3-</sup> dominate at higher pH values (pH > 8.5). Moreover, AmOHCO<sub>3</sub> (am) can precipitate between pH 8 and pH 8.7 under the considered experimental conditions.

### ***Interaction of Am(III) with Humic Substances***

The complexation of trivalent actinides with HA has been investigated by numerous laboratories. Investigations have been conducted on effect of pH, HA of different origin, and different experimental methods [135]. **Tab. 9.2** summarizes some selected results of the complexation constants determinations for Am(III) with HA together with experimental conditions and applied methods. On this place, it should be mentioned that Panak et al. [136] reported the formation of a Cm-carbonato-humate complex  $\text{Cm}(\text{CO})_3\text{HA}$  with  $\log \beta = 12.4 \pm 0.2$  determined by TRLFS in the natural groundwater from Gorleben area (Gohy-573). Formation of such carbonato-humate complex can also be expected for Am(III), however, the formation of such Am(III)-carbonato-humate complex was not yet reported.

**Tab. 9.2:** Selected americium complexation constants.

<b>Material</b>	<b>Experimental Conditions</b>	<b>Methods</b>	<b>Log <math>\beta</math></b>	<b>Reference</b>
Lake Bradford HA Aldrich HA	pH 5 - 6 0.1 M, 1 M $\text{NaClO}_4$	LIPAS UV spectroscopy ultrafiltration	Am(III)HA(III) Bradford HA $6.27 \pm 0.04$ Aldrich HA $6.36 \pm 0.14$	[137]
red earth HA, FA	pH 5.2 – 5.7 0.02 M, 0.1 M $\text{NaClO}_4$	cation exchange	Am(III)HA(III) 8.04 (pH 5.7, I:0.02) 6.91 (pH 5.4, I: 0.1) Am(III)FA(III) 8.88 (pH 5.2, I: 0.02) 7.32 (pH 5.2, I: 0.1)	[138]
HA Aldrich	pH 4 - 6 0.1 M $\text{NaClO}_4$	cation exchange solvent extraction	Am(III)-HA 1:1 $6.9 \pm 0.11$ Am(III)-HA 1:2 $10.7 \pm 1.9$	[139]
Gohy-573	pH 6 – 10 0.1 M $\text{NaClO}_4$	UV/Vis TRLFS	Am(OH)HA(II) $12.71 \pm 0.17$ Am(OH) <sub>2</sub> HA(I) $17.40 \pm 0.21$	[140]

## **9.2. Kinetics of Am(III) Sorption onto Kaolinite**

In the present work, kinetic experiments were performed to evaluate the time which Am(III) requires to reach constant distribution ratio. The experimental conditions were the same as in the kinetic experiments with U(VI) or HA (see paragraph 10.2.1). The initial concentration of Am(III) was  $1 \cdot 10^{-6}$  M and the kinetic curve was obtained at pH 5.

**Fig. 9.2** illustrates the results of the kinetic experiments for Am(III) adsorbed onto kaolinite from the solution. It becomes evident that the system reaches the sorption equilibrium very fast. Am(III) exhibits high sorption onto kaolinite, 98% of Am(III) is adsorbed already after half an hour and the amount of Am(III) adsorbed does not change significantly within the time.

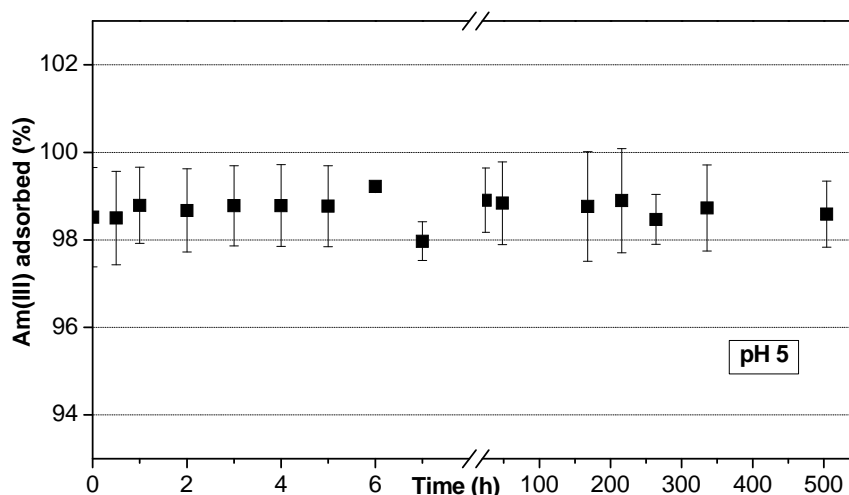


**Fig. 9.2:** Percentage of Am(III) adsorbed from solution during kinetic experiments at pH 5 ( $[Am(III)] = 1 \cdot 10^{-6}$  M,  $I = 0.01$  M  $NaClO_4$ ,  $pCO_2 = 10^{-3.5}$  atm).

## **9.3. Am(III) Sorption onto Kaolinite in Absence and Presence of Humic Acid**

As already mentioned in chapter 6, the sorption of actinides onto clay minerals can be influenced by pH, adsorbent and actinide concentrations, ionic strength or temperature. The Am(III) sorption dependence on *pH value* observed, for example, Murali et al. [141]. They showed a monotone increase of Am(III) uptake onto bentonite from pH 3.2 to pH 7.5. Samadfam et al. [58] observed an increase of the sorption coefficients of Am(III) onto kaolinite with pH over the whole pH range studied (nitrogen atmosphere). Variation of the bentonite/water ratio did not cause any changes in  $K_d$  at pH 2.9 for Am(III) sorption on bentonite [141]. The influence of

ionic strength on the Am(III) sorption onto kaolinite and montmorillonite was reported in [62]. An increase of the ionic strength from 0.02 to 0.1 M suppressed the sorption of Am(III) onto kaolinite and montmorillonite, it shifted the sorption to higher pH values. At the ionic strength of 0.1 M the sorption started to grow at pH 3, while at 0.02 M the sorption increased already from pH 1.5.

The influence of HA on the Am(III) sorption onto clay minerals was studied only rarely [58],[62],[142]. The effect of ionic strength in the presence of HA studied, for example, Takahashi et al. [142]. They determined the Am(III) sorption onto kaolinite and silica gel in the presence of HA. They observed an increase of the sorption with increasing ionic strength from 0.02 M (NaClO<sub>4</sub>) over 0.1 M up to 0.7 M in contrast to the sorption of Am(III) in the system without HA, where the opposite effect was observed.

In the case of Am(III), only the influence of pH value and the presence of HA onto Am(III) sorption was studied. The sorption experiments were carried out for a Am(III) concentration of  $1 \cdot 10^{-6}$  M and a HA concentration of 10 mg/L in 0.01 M NaClO<sub>4</sub> solutions. The experiments were performed as described in chapter 10.2.1.

The results are depicted in **Fig. 9.3**. In the absence of HA, Am(III) exhibits very strong sorption onto kaolinite which is almost independent on the pH value. The percentage of sorbed Am(III) amounts to 98% at pH 3 and to almost 100% at higher pH values. Neither the positive charge of the Am<sup>3+</sup> ion as the main species at pH < 7, nor the presence of negatively charged carbonate complexes in the solution at higher pH values influence the Am(III) sorption onto kaolinite under the studied conditions. Samadfam et al. [58] studied the Am(III) sorption onto kaolinite in the absence of CO<sub>2</sub> in 0.1 M NaClO<sub>4</sub> solution. Contrary to findings in this work, the sorption coefficients of Am(III) increased with pH over the whole pH range. The difference in the Am(III) sorption at low pH values can not be ascribed to the absence of CO<sub>2</sub>, because the Am(III) speciation does not differ for the system with and without CO<sub>2</sub> at low pH values. Takahashi et al. [62] observed the sorption edge for Am(III) sorption onto kaolinite at pH 1.5 (I: 0.02 M NaClO<sub>4</sub>) above which the sorption of Am(III) increased with pH. The reason for no observation of a sorption edge at lower pH values in this work is presumably the high solid/solution ratio used in the sorption experiments. The solid/solution ratio in the experiments in this work was 4 g/L, whereas Takahashi et al. [62] reported a solid/solution ratio of 2 g/L and Samadfam et al. [58] an even lower solid/solution ratio of 1 g/L. The difference between [58] and

this work in Am(III) sorption onto kaolinite at low pH values can be also caused by the different ionic strengths of the solutions. Wang et al. [143] studied the Eu(III) sorption onto illite at different ionic strengths (0.02 M – 1 M). They showed that Eu(III) sorption at low pH values decreases with increasing ionic strength. Similarly to this work, the percentage of Eu(III) sorbed onto illite at I: 0.02 M amounts to 80% at pH 3 and it increases with pH to 100% at pH 5.5, whereas at I: 0.5 or 1 M the amount of Eu(III) adsorbed at pH 3 was 10%.

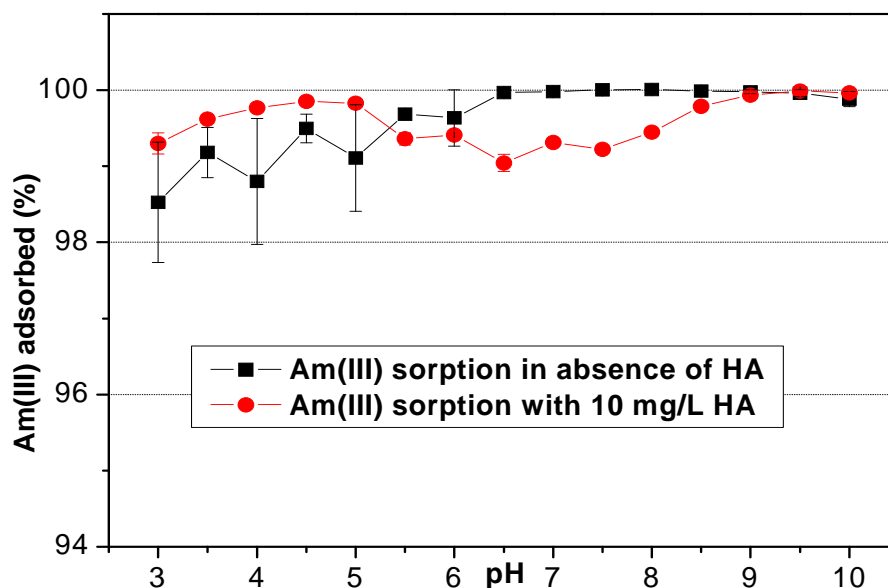


**Fig. 9.3:** Comparison of Am(III) sorption onto kaolinite in the absence and presence of HA ( $I = 0.01 \text{ M NaClO}_4$ ,  $[\text{Am(III)}] = 1 \cdot 10^{-6} \text{ M}$ ,  $[\text{HA}] = 10 \text{ mg/L}$ ,  $p\text{CO}_2 = 10^{-3.5} \text{ atm}$ ).

In the presence of HA (**Fig. 9.3**), there are small changes in the Am(III) sorption in comparison to the system without HA. At pH values  $< 5$ , HA very slightly enhances the sorption of Am(III). Conversely, at pH values  $\geq 5.5$  the presence of HA decreases the sorption of Am(III) in comparison to the system without HA due to the formation of americium-humate complexes. The formation of binary Am(III)-humate complex with the stability constant of  $\log \beta 6.27 \pm 0.04$  was reported by Kim et al. [137]. Moreover, the formation of ternary Am-hydroxo-humate complexes -  $\text{Am(OH)HA}$  or  $\text{Am(OH)}_2\text{HA}$  - with stability constants of  $\log \beta = 12.71 \pm 0.17$  and  $\log \beta = 17.40 \pm 0.21$ , respectively, was reported by Morgenstern et al. [140]. However, the drop of Am(III) sorption onto kaolinite observed in this study is very small around 1%. One can assume that with increasing concentration of HA, the Am(III) sorption will further decrease similarly to the system U(VI)-HA-kaolinite (see paragraph 7.2). Samadfam et al. [58] reported a



decrease of the Am(III) sorption onto kaolinite with increasing HA concentration from 5 to 20 ppm at pH > 5.5. Generally, the trend in sorption behavior of Am(III) in the presence of HA is consistent with the results reported in literature for trivalent actinides [58],[62],[63],[144],[145] - at low pH values the sorption was enhanced by the presence of HA, while at high pH the presence of HA lowered the sorption. At pH > 8.5, the HA has no influence on Am(III) sorption onto kaolinite, which reaches almost 100% as in the system without HA.

The influence of filtration on Am(III) sorption onto kaolinite was determined. Two series of measurements were performed where the supernatants were analyzed by LSC either direct or after filtration using filter of pore sizes of 450 nm. As in the case of U(VI) and HA, the filtration with used filters had no effect on the results of Am(III) sorption in the studied pH range.

### **9.3.1. Comparison of Am(III) and U(VI) Sorption Results**

The sorption experiments in the systems with Am(III) and U(VI) were performed under the same experimental conditions to have the possibility to compare the sorption behavior of the actinides with different oxidation state. From the comparison of **Fig. 6.2a** and **Fig. 9.3** showing the sorption curves as a function of pH value in the absence of HA, it is obvious that under applied conditions the U(VI) sorption onto kaolinite is dependent on pH, while Am(III) sorption is in principle unaffected by pH value. Also, the effect of carbonate, which was observable in sorption experiments with U(VI) (cf. **Fig. 6.4a**), is suppressed in the case of Am(III). No decrease of the Am(III) sorption, as in the system with U(VI), at higher pH values was observed. This is caused by a different speciation of both compared actinides. U(VI) forms stronger and more negative carbonate complexes than Am(III) (cf **Fig. 4.1** and **Fig. 9.1**). However, similar effects of HA on sorption of U(VI) (see **Fig. 7.2a**) and Am(III) (cf. **Fig. 9.3**) were observed. In both systems, the sorption of U(VI) and Am(III) increased at low pH values in the presence of HA compared to the system without HA. At higher pH values, the sorption of U(VI) and Am(III) decreases in the presence of HA due to the formation of soluble U(VI)- and Am(III)-humate complexes. At pH > 8.5, no influence of HA on Am(III) sorption onto kaolinite was observed, while U(VI) sorption was enhanced again compared to the system without HA.

## ***9.4. Surface Complexation of Am(III) on Kaolinite in Absence and Presence of Humic Acid***

Laser-induced fluorescence spectroscopy was applied to study the surface complexation of Am(III) on kaolinite. Because of the short lifetimes of the Am(III) fluorescence species (e.g.,  $1.2 \cdot 10^{-5}$  M of Am(III) in H<sub>2</sub>O:  $24.6 \pm 0.6$  ns [146]) no time-resolved spectra were measured in this study. The fluorescence properties of Am(III) surface complexes on kaolinite were studied at different pH values in the absence and presence of HA. Up to now, TRLFS measurements of Am(III) were performed very rarely, e.g., Thouvenot et al. [147] compared Am(III) fluorescence spectra in solid and liquid media and Stumpf et al. [148] measured fluorescence emission spectra of Am(III) in calcite. More often the sorption of Cm(III) or Eu(III), as the analogues of trivalent actinides, was studied, e.g., Cm(III) sorption onto kaolinite and smectite [125] and calcium silicate hydrate [123] or Eu(III) sorption onto  $\gamma$ -alumina [124].

### ***Spectroscopic Properties of Americium***

Americium belongs to the 5f-elements. In the gaseous form it has the following electronic configuration:  $5f^7 7s^2$  [45]. The absorption spectra of trivalent ions possess a unique sharpness. The luminescence of Am(III) was studied much less than that of U(VI). Yusov, et al. [149] reported that the luminescence spectrum consists of four bands in the range between 570 and 1100 nm. The luminescence intensity of Am(III) depends very strongly on the solvent. Stover et al. [150] measured the absorption spectrum of Am(III) in perchloric acid solution in the wavelength range 220 to 1000 nm. The spectrograms show marked similarity to those of rare earth solutions, but Am(III) absorption was much more intense. The absorption in the 500 nm region was especially strong and was found to persist at very low concentrations.

Thouvenot et al. [147] compared the Am(III) fluorescence spectra in solid (ThO<sub>2</sub>) and liquid (K<sub>2</sub>CO<sub>3</sub>) media. In aqueous complexing media the Am(III) excitation spectrum exhibited one single broad band centered around 510 nm, and corresponding to <sup>7</sup>F<sub>0</sub> → <sup>5</sup>L<sub>6</sub> transition. The energy level scheme of Am(III) in ThO<sub>2</sub> including the most important states involved in the excitation and emission spectra are shown in **Fig. 9.4**. The luminescence spectrum at room temperature consists of two main groups of lines in the ranges 670 – 750 nm, and 800 – 850 nm corresponding to transitions from <sup>5</sup>D<sub>1</sub> towards <sup>7</sup>F<sub>1</sub> and <sup>7</sup>F<sub>2</sub>.

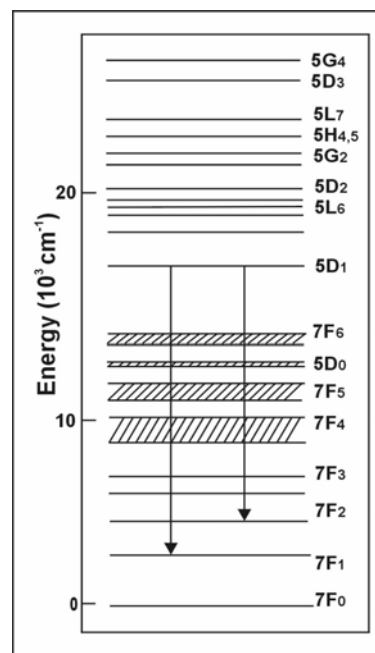


**Fig. 9.4:** Energy level scheme of Am(III) in ThO<sub>2</sub> [147].

Geipel and Stumpf [151] measured the time-resolved laser fluorescence spectra of Am(III) (1·10<sup>-5</sup> M) in 0.1 M NaClO<sub>4</sub> diluted with increasing amounts of pure D<sub>2</sub>O. Samples were excited with a 503.2 nm laser pulse. An example of a Am(III) spectrum in 88% D<sub>2</sub>O is shown in **Fig. 9.5**. They observed a fluorescence emission at 690.8 nm and they found the relationship between the fluorescence lifetime of Am(III) species and the amount of water molecules in the solvation shell of Am(III).

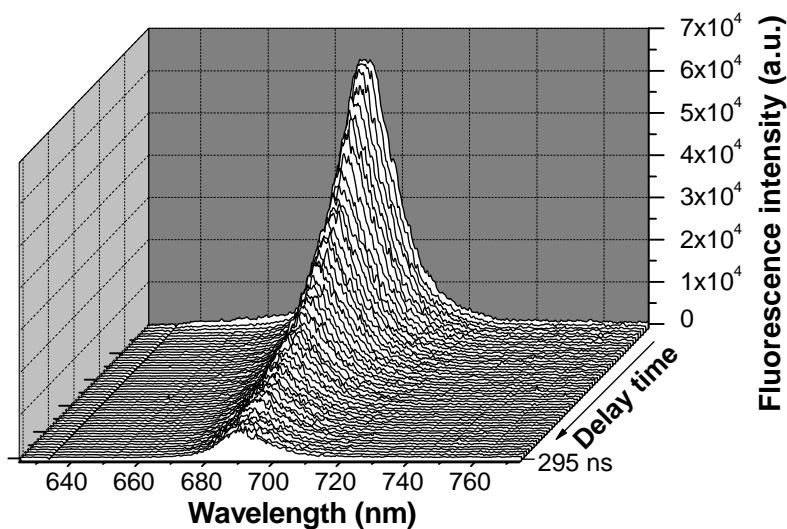


**Fig. 9.5:** Time-resolved fluorescence spectrum of Am(III) in 88% D<sub>2</sub>O [151].

### 9.4.1. Sample Preparation and Data Evaluation

Am(III) or Am(III)-HA were sorbed as described in chapter 10.2.2 under the following experimental conditions: Am(III) and HA (unlabeled HA type M42) initial concentrations were  $1 \cdot 10^{-6}$  M and 10 mg/L, respectively, ionic strength was kept at 0.01 M NaClO<sub>4</sub>, pH values were adjusted between pH 5 and pH 8, solid/solution ratio was 4 g/L. After phases separation, the supernatants were given to LSC for Am(III) final concentration measurements. For the spectroscopic investigation, kaolinite samples from the batch experiments were first re-suspended in 10 mL of a solution with pH and ionic strength being identical to the original solution (without Am(III) and HA). The fluorescence spectra of kaolinite suspension were then recorded at permanent stirring. **Tab. 9.3** shows the experimental conditions of sample preparation, the Am(III) and HA concentrations, the pH values and the amount of adsorbed Am(III). The measuring system is described in chapter 10.3.10.

The evaluation of the spectroscopic data was performed with OriginPro 7.5G software (OriginLab Corp., Northampton, MA).

**Tab. 9.3:** Samples for laser-induced fluorescence measurements ( $[Am(III)] = 1 \cdot 10^{-6}$  M,  $I = 0.01$  M NaClO<sub>4</sub>,  $pCO_2 = 10^{-3.5}$  atm).

Sample	[HA] <sub>0</sub> (mg/L)	pH <sub>start</sub>	pH <sub>end</sub>	Am <sub>adsorbed</sub> (%)
Am5	-	<b>5.07</b>	<b>5.04</b>	99.56
Am6	-	<b>6.05</b>	<b>6.08</b>	99.69
Am7	-	<b>7.01</b>	<b>6.98</b>	99.60
Am8	-	<b>8.02</b>	<b>8.03</b>	99.95
Am-HA5	10	<b>5.04</b>	<b>5.03</b>	99.54
Am-HA6	10	<b>6.00</b>	<b>6.02</b>	99.01
Am-HA7	10	<b>7.08</b>	<b>7.05</b>	99.07
Am-HA8	10	<b>8.04</b>	<b>7.99</b>	99.34

### 9.4.2. Results of Fluorescence Measurements

The samples were excited with an excitation wavelength of 526 nm. **Fig. 9.6** shows the dependence of the relative fluorescence intensity on the wavelength for the samples prepared without HA at pH values between pH 6 and 8.

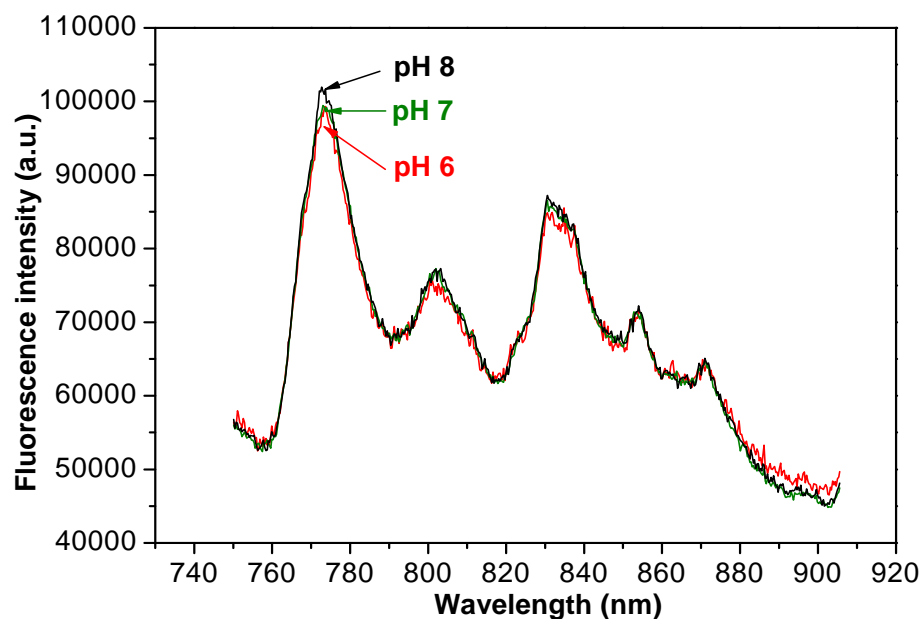


**Fig. 9.6:** Fluorescence spectra of Am(III) adsorbed onto kaolinite at pH 6, 7, 8 in HA-absence.

First of all, the shape of the measured fluorescence spectrum of Am(III) adsorbed onto kaolinite is somewhat unexpected. Only one emission peak of Am(III) in solution was observed in literature (see paragraph 9.4). Therefore, similarly to the observations in the systems with U(VI), a shift in the position of this peak was assumed in the system with solid matter compared to the solution system. The different shape of fluorescence spectrum could be a result of the formation of different complexes on the surface of solid matter than in the solution. It is possible that water molecules from the first solvation shell of Am(III) are released and, therefore, the fluorescence properties of Am(III) were changed, especially the fluorescence lifetimes. Similar effect observed Stumpf et al. [148]. They measured fluorescence emission spectra of Am(III) in calcite at various excitation wavelengths (501 – 506 nm) and at 18 K. The spectra differ with the variation of the excitation wavelength indicating different Am(III)-calcite species. They observed peak maxima at 685.7, 688.0, and 709.5 nm in all spectra, further emission peaks at 690.5 and 697.7 nm appeared at excitation wavelengths  $\geq 503$  nm. They suggest that the peaks at 685.7, 688.0, 690.5, and 709.5 nm belong to Am(III) incorporated into the calcite bulk structure and that

one at 697.7 nm to Am(III) sorbed onto the calcite surface. Furthermore, they measured also the decay of Am(III) fluorescence emission. The measured lifetimes of  $414 \pm 16$  ns and  $1875 \pm 45$  ns can be attributed to the sorbed Am-calcite species and to the incorporated Am(III) ion, respectively.

To be sure that the measured fluorescence comes from Am(III) and not from kaolinite or HA, the fluorescence spectra of a kaolinite suspension (without Am(III) and HA) and of a kaolinite suspension with adsorbed HA (without Am(III)) were measured. Nevertheless, no fluorescence signals were detected and, therefore, no sensible spectra were observed. Moreover, the fluorescence spectrum of Am(III) in the solution (without kaolinite and HA) was measured ( $[Am(III)] = 1 \cdot 10^{-5}$  M, pH 3). The result of this measurement is illustrated in **Fig. 9.7**. It is obvious that the fluorescence emission peak expected at around 690 nm is very uncertain. It is caused by the quite low Am(III) concentration in solution and by water molecules in the solvation shell of Am(III) quenching the fluorescence signal. Geipel and Stumpf [151] and Kimura and Choppin [152] reported that the fluorescence lifetime of Am(III) and Cm(III) depends on the amount of water molecules in the first solvation shell of Am(III) and Cm(III), respectively. The more water molecules are associated to Am(III) and Cm(III) the shorter fluorescence lifetimes of Am(III) and Cm(III) species were measured. This can be also the reason why it was difficult to measure the fluorescence spectrum of Am(III) in the solution.

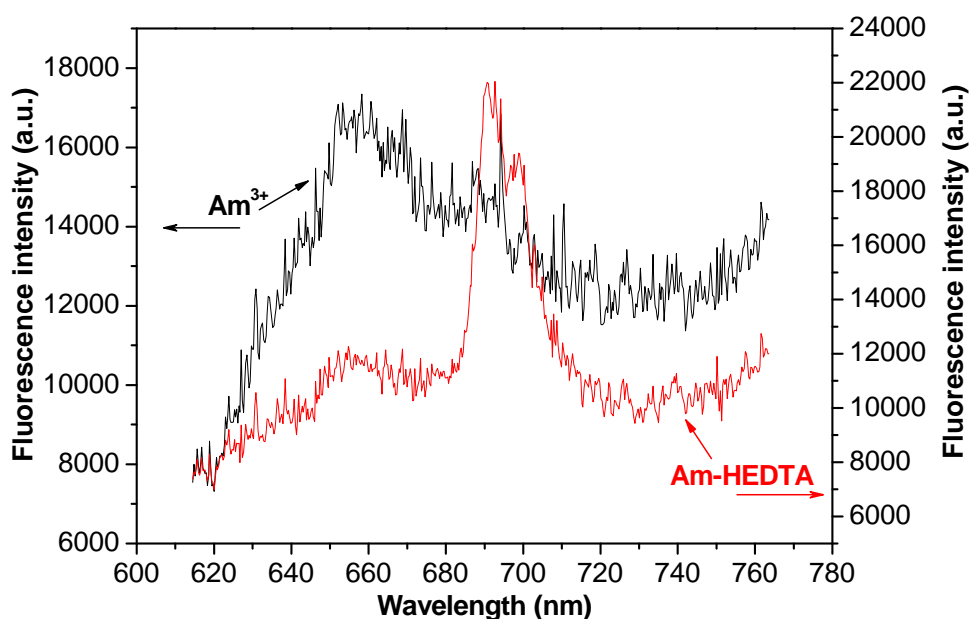


**Fig. 9.7:** Fluorescence spectra of Am(III) ion and Am-HEDTA complex in 0.01 M NaClO<sub>4</sub> solution ( $[Am(III)] = 1 \cdot 10^{-5}$  M,  $[EDTA] = 2 \cdot 10^{-5}$  M, pH = 3, excitation wavelength 508 nm).

To avoid these mentioned complications, sodium salt of ethylenediaminetetraacetic acid ( $\text{Na}_4\text{EDTA}$ ) was given to the solution of Am(III) and the fluorescence spectrum of the Am-HEDTA complex was measured. By addition of EDTA to the solution, the water molecules in Am(III) solvation shell are exchanged with  $\text{HEDTA}^{3-}$  ligands. Consequently, the fluorescence intensity and fluorescence lifetimes of Am(III) increased and, therefore, the expected fluorescence emission peak of Am(III)-HEDTA complex was detected at around 690 nm as shown in **Fig. 9.7**. Thus, it was proved that the measured fluorescence signal should belong only to Am(III) species. However, it is clear that the interpretation of the measured fluorescence emission peaks of Am(III) sorbed onto kaolinite is not possible up to now. It can be assumed, based on the report of Stumpf et al. [148], that Am(III) is not only sorbed onto the kaolinite surface, but it could be incorporated into the kaolinite structure, for example, due to an exchange with Al atoms. Therefore, further investigations are required to satisfactorily explain the causes of such changes in fluorescence spectra in the studied systems.

Further, the samples show no dependence on the pH value of sample preparation which should not be surprising under consideration that almost the same amount of Am(III) is sorbed onto kaolinite at different pH values (cf. **Tab. 9.3**). However, at pH 5 no reasonable spectrum of Am(III) species sorbed onto kaolinite was measured, although the amount of Am(III) adsorbed does not differ from other measured pH values. This result points to changes in surface speciation of Am(III) on kaolinite by the transition from pH 5 to higher pH values, although no differences occur in the Am(III) speciation in the solution between pH 5 and pH 6 (see **Fig. 9.1**).

The fluorescence spectra of Am(III) sorbed onto kaolinite in the presence of HA at pH values 6 – 8 are depicted in **Fig. 9.8**. Similarly to previous observation in the system without HA, the fluorescence spectrum of Am(III) sorbed at pH 5 could not be measured. Contrary to the determinations in the binary system, a dependence of the fluorescence intensities on the pH values of sample preparation is observed in the ternary system. This phenomenon can be a result of HA quenching effect and changes in the Am(III) surface speciation in HA-presence. The formation of Am(III)-humate surface complexes on kaolinite is expected at pH 6 and, therefore, a quenching effect of HA was measured. With increasing pH value, mixed ternary surface Am(III)-hydroxo-humate and Am(III)-carbonato-humate complexes can arise (see chapter 9.1). Thus, HA in the Am(III)-humate surface complex can be substituted by these other ligands. It leads then to the release of HA into the solution and to a decrease of the HA quenching effect.

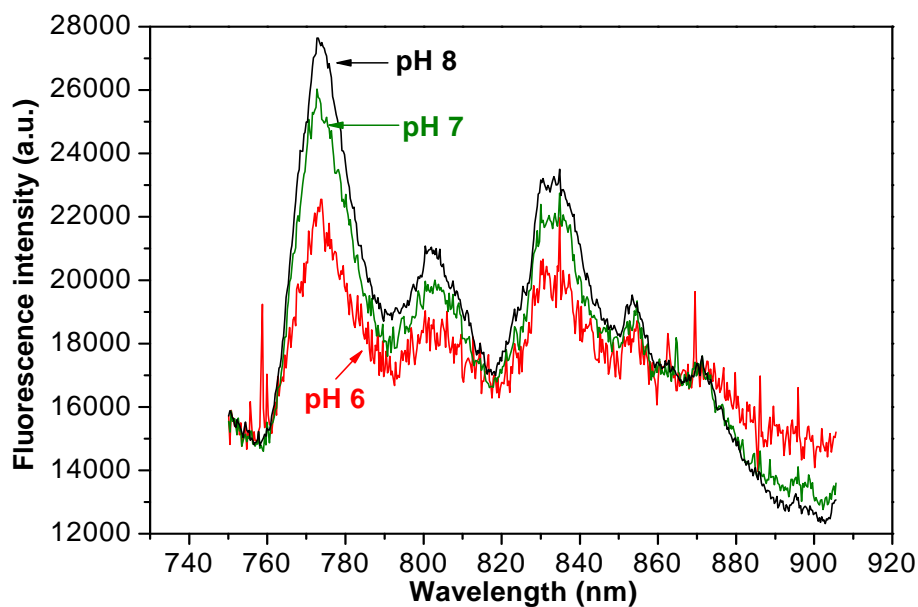


**Fig. 9.8:** Fluorescence spectra of Am(III) adsorbed onto kaolinite at pH 6, 7, 8 in HA-presence.

From the comparison of the fluorescence spectra at the same pH values in the absence and presence of HA resulted that, as in the case of U(VI)-kaolinite and U(VI)-HA-kaolinite systems, the HA decreases the fluorescence intensity of the samples. This indicates differences in surface speciation in both systems. In the presence of HA, no differences in the peak positions were observed comparing to the binary system. An example for the samples prepared in the absence and presence of HA at pH 6 is given in **Fig. 9.9**.

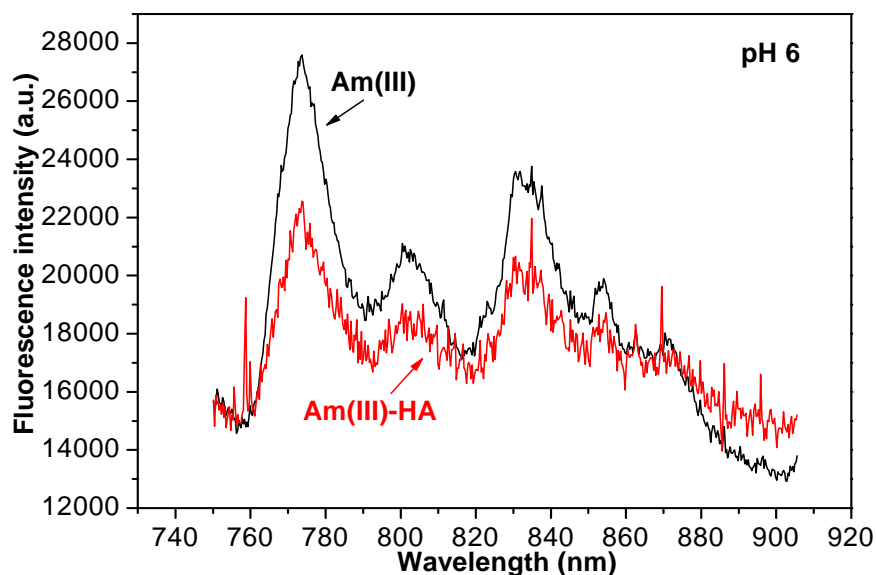


**Fig. 9.9:** Comparison of fluorescence spectra of Am(III) adsorbed onto kaolinite in the absence and presence of HA at pH 6.



## 10. Experimental Part

### 10.1. Materials

(1) **Kaolinite:** Kaolinite KGa-1b (IN: 47907-2054) from the Clay Minerals Society Source Clays Repository (Washington County Georgia) [22] was chosen as model mineral.

Kaolinite was used in the experiments without any pre-treatment. The only exceptions were measuring of XRD spectra and two sets of batch experiments, where also size-fractionated kaolinite was used. A. Bauer from FZK-INE performed the treatment according to [153].

(2) For the preparation of solutions deionized water with a resistivity of  $> 18 \text{ M}\Omega\cdot\text{cm}^{-1}$  produced by the Milli-RO/Milli-Q-System (Millipore, Schwalbach, Germany) was used. For the experiments performed under inert-gas ( $\text{N}_2$ ) atmosphere, the deionized water was boiled for approximately 1.5 h to remove the carbonate.

(3) For the study of the chemical interaction of U(VI),  $\text{U}_{\text{nat}}$  in the form of  $1.08\cdot 10^{-3} \text{ M UO}_2(\text{ClO}_4)_2$  was used as stock solution in all experiments. For the preparation of this stock solution, 0.5 mL of a 0.1 M U(VI) solution was diluted with 0.01 M  $\text{HClO}_4$  (Merck, Darmstadt, Germany) to 50 mL.

(4) For the sorption experiments with HA and U(VI)-HA  $^{14}\text{C}$ -labeled synthetic HA type M42, batch M170 [42] was applied. For the preparation of the stock solution (5 g/L) 50 mg HA was weighed, diluted with 1720  $\mu\text{L}$  of 0.1 M NaOH (Merck, Darmstadt, Germany) and filled up to the volume of 10 mL with 0.1 M  $\text{NaClO}_4$  (Merck, Darmstadt, Germany). The activity of the HA stock solution was measured by LSC.

(5) For the study with Am(III), 100  $\mu\text{L}$  of a solution  $^{243}\text{Am(III)}$  in  $\text{H}_2\text{O}/\text{D}_2\text{O}$  (8 mg) with the activity of  $1.8\cdot 10^7 \text{ Bq}$  was diluted with  $\text{H}_2\text{O}$  to 5 mL. This diluted solution was then used as the stock solution for the experiments with Am(III). 1  $\mu\text{L}$  of this solution possesses the activity of 160 Bq corresponding to 0.022  $\mu\text{g}$  of Am. The stock solution contains  $^{243}\text{Am}$  in the equilibrium with  $^{239}\text{Np}$  ( $1.9\cdot 10^{-8} \mu\text{g}$  in 1  $\mu\text{L}$ ).

(6) For the experiments with Am(III)-HA synthetic HA type M42, batch M145 [42] was used. 50 mg of HA was weighted, diluted with 1720  $\mu\text{L}$  of 0.1 M NaOH and filled up to the

volume of 10 mL with 0.1 M NaClO<sub>4</sub>. Unlabeled HA was applied to avoid the overlapping of the measured signal of <sup>239</sup>Np (β-emitter, decay product of <sup>243</sup>Am) with <sup>14</sup>C in LSC measurements.

(7) For the pH adjustment solutions of 1 M, 0.1 M, 0.01 M HClO<sub>4</sub> (Merck, Darmstadt, Germany) and 1 M, 0.1 M, 0.01 M NaOH (Merck, Darmstadt, Germany) were used.

(8) For the adjustment of ionic strength solutions of 0.1 M or 0.01 M NaClO<sub>4</sub> were prepared by dissolution of NaClO<sub>4</sub>·H<sub>2</sub>O (Merck, Darmstadt, Germany) in the appropriate volume of distilled (ambient atmosphere experiments) or CO<sub>2</sub> – free (inert gas experiments) water.

(9) 1 M NaHCO<sub>3</sub> solution was prepared by dissolution of 8.4 mg NaHCO<sub>3</sub> (Merck, Darmstadt, Germany) in 100 mL of distilled water.

(10) To determine the vial wall sorption of U(VI) and Am(III) 1 M HNO<sub>3</sub> (Riedel de Haën, Seelze, Germany) was applied. To measure the HA vial wall sorption 1 M NaOH (Merck, Darmstadt, Germany) was used.

(11) For the sorption and kinetic experiments 5 and 15 mL polypropylene (PP) centrifuge tubes were applied (Cellstar, Greiner Bio-One, Kremsmünsterand, Austria).

(12) The solutions were prepared and stored in glass and polyethylene vessels. For their preparation and dosing automatic pipettes from different producers were used.

(13) For LSC measurements of HA concentration in solutions the scintillation cocktail Ultima Gold (Perkin Elmer, Boston, USA) was applied.

(14) All the chemicals used for the preparation of experimental solutions were p. a. quality.

## ***10.2. Experimental Procedures***

### **10.2.1. Kinetic Experiments**

All kinetic experiments were performed under ambient atmosphere (pCO<sub>2</sub> = 10<sup>-3.5</sup> atm). In the case of Am(III), the experiments were carried out in a glove box due to high α-radioactivity of the samples. 40 mg of kaolinite were weighed into 15 mL PP centrifuge tubes, 10 mL of 0.01 M NaClO<sub>4</sub> were added subsequently. The pH values of the samples were adjusted at pH 5 (kinetics of U(VI), Am(III) and HA sorption) and pH 7.5 (kinetics of U(VI) and HA sorption) by addition of dilute HClO<sub>4</sub> or NaOH. For kinetic experiments at pH 7.5, 2.15 μL of NaHCO<sub>3</sub> were added to accelerate the equilibrium process with atmospheric CO<sub>2</sub>. The kaolinite

was pre-equilibrated with NaClO<sub>4</sub> for 72 h by the continuous shaking on a horizontal shaker. After pre-equilibration, 9.26 μL of U(VI) stock solution, 20 μL of HA stock solution or 112 μL of diluted Am(III) stock solution were added to the kaolinite suspension to obtain the final concentrations of 1·10<sup>-6</sup> M, 10 mg/L and 1·10<sup>-6</sup> M of U(VI), HA or Am(III), respectively. After addition of U(VI), HA or Am(III), the pH values were readjusted immediately. The samples were shaken and taken after different contact times: 0, 0.5, 1, 2, 3, 4, 5, 6, 7, 24, 48, 72, 96, 168, 336, and 504 h. The phases were separated by centrifugation (4000 rpm, 30 min). Then, the supernatants of the samples were filtered (450 nm). The filtrates were analyzed for the final U(VI), HA, and Am(III) concentrations. Finally, the U(VI), HA, and Am(III) sorption onto vial walls was investigated. The amount of U(VI)/HA/Am(III) adsorbed on the mineral surface was calculated as the difference between the initial U(VI)/HA/Am(III) concentration and the sum of the amounts of U(VI)/HA/Am(III) remaining in solution and U(VI)/HA/Am(III) sorbed onto the vial walls.

Moreover, in the case of U(VI) and HA, the effect of the pre-equilibration time of the U(VI) and HA solution as well as the influence of the sequence of U(VI) and HA addition to the kaolinite suspension on the sorption equilibrium were studied. Three experimental modes were applied to study the kinetics of U(VI) sorption onto kaolinite in the presence of HA: i) U(VI) and HA were preconditioned for 24 h (pH ~7) and then added to the kaolinite containing solution, ii) U(VI) and HA were added simultaneously to the kaolinite containing solution, iii) the kaolinite containing solution was preconditioned with HA for 60 h and then U(VI) was added.

### **10.2.2. Sorption Experiments**

The sorption experiments with U(VI) and HA were carried out under ambient atmosphere (pCO<sub>2</sub> = 10<sup>-3.5</sup> atm) and under inert gas conditions (N<sub>2</sub>-box). The sorption experiments with Am(III) were performed only under ambient atmosphere in a glove box. 40 mg of kaolinite were weighed into 15 mL PP centrifuge tubes, afterward 10 mL of 0.1 M NaClO<sub>4</sub> (sorption experiments with U(VI) and HA) or 0.01 M NaClO<sub>4</sub> (sorption experiments with U(VI), Am(III), and HA) were added. The desired pH values of the samples were adjusted between pH 3 and pH 10 by addition of dilute HClO<sub>4</sub> or NaOH. For studies at pH values above pH 7 in the presence of CO<sub>2</sub>, a calculated amount of NaHCO<sub>3</sub> was added to accelerate the equilibrium process with atmospheric CO<sub>2</sub>. For pre-equilibration the samples were continuously shaken on a horizontal

shaker and the pH values were controlled and readjusted. The conditioning time of kaolinite was 72 h and 4 – 5 weeks in the presence and absence of CO<sub>2</sub>, respectively. After pre-equilibration, 9.26 or 92.6 μL U(VI) stock solution were added to the kaolinite suspension for the investigation of U(VI) sorption onto kaolinite. The final concentration of U(VI) in the solution was 1·10<sup>-6</sup> M or 1·10<sup>-5</sup> M. To determine the HA sorption onto kaolinite, 20 or 100 μL HA stock were added to the kaolinite suspension. The final concentration of HA in the solution was 10 or 50 mg/L. For investigation of the U(VI) sorption onto kaolinite in the presence of HA, pre-equilibrated U(VI)-HA solution (equilibration time: 24 h, pH ~7) was added. The final concentrations of U(VI) and HA in the solution were 1·10<sup>-5</sup> M or 1·10<sup>-6</sup> M and 10 or 50 mg/L, respectively. In the sorption experiments with Am(III), 112 μL of diluted stock solution were added to achieve the initial concentration of 1·10<sup>-6</sup> M of Am(III). After addition of U(VI), HA, U(VI)-HA, Am(III) or Am(III)-HA solutions, the pH values were readjusted immediately. The samples were shaken on the horizontal shaker for 60 h to equilibrate. After shaking, the final pH values of the samples were measured and the samples were then centrifuged. The supernatants of single samples were filtered (450 nm). Prior to filtering, the filters were rinsed with 1 mL of sample solution. The filtrates were analyzed for the final U(VI), HA, and Am(III) concentration.

Finally, the U(VI), HA, and Am(III) sorption onto vial walls was investigated. The vials were washed with water and dried. Then, 7 mL 1 M HNO<sub>3</sub> or 1 M NaOH were added and the vials were shaken for 2 days. The maximal vial wall sorption of U(VI) was observed between pH 6 and 7.5 and reached values up to 5%. In acidic range the vial wall sorption was maximal 3%, above pH 8 the vial wall sorption was negligible. HA and Am(III) vial wall sorption was negligible in the entire pH range.

The amount of U/HA/Am(III) adsorbed on the mineral surface was calculated as the difference between the initial U(VI)/HA/Am(III) concentration and the sum of the amounts of U(VI)/HA/Am(III) remaining in solution and U(VI)/HA/Am(III) adsorbed onto the vial walls.

## ***10.3. Instruments and Methods***

### **10.3.1. Analysis of U(VI) Concentration**

The U(VI) concentration in solution was determined by ICP-MS (Inductive Coupled Plasma-Mass Spectrometry) using mod. ELAN 6000 (Perkin Elmer, Boston, USA). All samples

were acidified with 15  $\mu\text{L}$  of concentrated  $\text{HNO}_3$ . Prior to the measurement of the U(VI) concentrations in the samples in the presence of HA, HA was removed by digestion with  $\text{HNO}_3$  in a microwave oven mod. mls 1200 mega (MLS, Leutkirch im Allgäu, Germany) in order to avoid any disturbing effects of HA during ICP-MS measurements.

### **10.3.2. Analysis of Humic Acid and Am(III) Concentration**

HA and Am(III) concentration in solution were measured by liquid scintillation counting using LSC counters mod. LS 6000LL (Beckman Coulter, Krefeld, Germany) and mod. 1414 Wallac Win Spectral Liquid Scintillator Counter (Perkin Elmer, Boston, USA), respectively. For HA concentration measurements, a quantity of 1 mL of the filtered solution was mixed with 5 mL Ultima of Gold. In the case of Am(III), 0.5 mL of the solution was mixed with 5 mL of Ultima Gold.

### **10.3.3. Speciation Calculations**

The speciation computations were performed by V. Brendler with the program EQ3/6 [47] based on the complex formation constants compiled in NEA database [48].

### **10.3.4. Structure Analysis of Kaolinite by Infrared Spectroscopy**

The FTIR spectra were obtained using a Perkin-Elmer Mod 2000 FTIR spectrometer equipped with an IR source, KBr beam splitter, and DTGS KBr detector for the measurements in the spectral range  $4000 - 400 \text{ cm}^{-1}$ . Samples of 2 and 0.5 mg were dispersed in 200 mg of KBr to record optimal spectra in the regions of  $4000 - 3000$  and  $4000 - 400 \text{ cm}^{-1}$ , respectively. The pellet with 0.5 mg sample was measured immediately after pressing, whereas the disc with 2 mg of sample was heated overnight at  $150^\circ\text{C}$  to minimize the amount of adsorbed water.

### **10.3.5. Structure Analysis of Kaolinite by X-Ray Diffraction Spectroscopy**

Powder XRD data were collected for the pre-treated and untreated kaolinite KGa-1b on a Bruker-AXS D5005 powder X-ray diffractometer in  $\theta$ - $\theta$  geometry with curved PG-secondary monochromator using  $\text{CaK}\alpha$  radiation, incident and diffracted beam Soller slits, and a Kevex solid-state Si(Li) detector. Data were collected from  $5$  to  $70^\circ 2\theta$  using a step size of  $0.05^\circ 2\theta$  and

a count time of 5 – 20 s per step. The samples were analyzed as random (backpacked) mounts. The data were analyzed by means of EVA code (Bruker-AXS) and the peak analysis was performed by means of Peak Fit Code (Jandel Scientific).

### **10.3.6. X-Ray Photoelectron Spectroscopy Measurements**

X-ray photoelectron spectroscopy (XPS) measurements were performed by T. Reich in University of Mainz, Institute for Nuclear Chemistry. The samples were measured in the form of dry powders pressed into indium foil without further pretreatment. XPS spectra were excited by Mg K $\alpha$  radiation (1253.6 eV). The analyzer pass energy was 50 eV and the vacuum during the measurements was set to  $2 \cdot 10^{-8}$  mbar. The electrostatic charging of the sample surface was corrected by setting the C 1s binding energy to 285.0 eV.

### **10.3.7. Cation Exchange Capacity Measurement**

The cation exchange capacity (CEC) of untreated kaolinite KGa-1b was measured by the compulsive exchange method [154]. By this method the clay mineral is saturated with BaCl<sub>2</sub> and then brought to an equilibrium solution ionic strength similar to that of the original clay mineral solution. The Ba<sup>2+</sup> cation is then exchanged by Mg<sup>2+</sup> by addition of MgSO<sub>4</sub> which precipitates BaSO<sub>4</sub>. After readjustment of the ionic strength to a value comparable to that of the clay mineral solution, the quantity of Mg<sup>2+</sup> adsorbed is estimated as a loss of Mg<sup>2+</sup> from the MgSO<sub>4</sub> added.

### **10.3.8. Kaolinite Surface Area Measurement**

The surface area of kaolinite was determined from the amount of adsorbed nitrogen at monolayer coverage from a BET (Brunauer-Emmet-Teller) plot of sorption isotherm data. Knowing the projected cross sectional area per molecule in a monolayer, the surface area is calculated from the monolayer coverage. The measurement was performed using the surface area analyzer SA 3100 (Beckman Coulter, Krefeld, Germany).

### **10.3.9. EXAFS Measurements**

EXAFS data were collected at the Rossendorf Beamline (ROBL) [155] at the ESRF, Grenoble, France. The uranium L<sub>III</sub>-edge absorption spectra were recorded in fluorescence mode at room temperature. The ionization potential of the uranium L<sub>III</sub>-edge was defined as 17 185 eV.

Multiple scans (5 – 8) were measured for all samples. The EXAFS spectra were analyzed according to standard procedures including statistical weighting of the 13 fluorescence channels and their dead-time correction using the suite of programs EXAFSPAK [116]. Theoretical scattering phases amplitudes were calculated with the scattering code FEFF 8.20 [117].

### **10.3.10. Laser Fluorescence Measurements**

Laser fluorescence data were collected for two systems. Binary system, which consists of U(VI) or Am(III) adsorbed on the kaolinite, and ternary system, where also HA was presented. Am(III) or U(VI) or U(VI)-HA or Am(III)-HA were adsorbed as described above (cf. 10.2.2): initial concentrations of U(VI), Am(III) and HA were  $1 \cdot 10^{-5}$  M,  $1 \cdot 10^{-6}$  M and 10 mg/L, respectively, ionic strength was 0.1 M NaClO<sub>4</sub> (U(VI), U(VI)-HA) and 0.01 M NaClO<sub>4</sub> (Am(III), Am(III)-HA), pH values were adjusted between pH 5 and pH 8, solid/solution ratio was 4 g/L. After phase separation, the supernatants were analyzed by ICP-MS or LSC for U(VI) and Am(III) final concentrations. For the spectroscopic investigation, kaolinite samples from the batch experiments were first re-suspended in 10 mL of a solution with pH and ionic strength being identical to the original solution (without U(VI), Am(III), HA). Time-resolved spectra of this kaolinite suspension were recorded at permanent stirring.

*For the systems U(VI)-kaolinite and U(VI)-HA-kaolinite* the used TRFLS system consists of a Nd:YAG diode laser (mod. SL 401-20, Spectron Laser Systems, Rugby, United Kingdom) with subsequent 4<sup>th</sup> harmonic generation. The wavelength of 266 nm was used for the excitation of the samples providing a maximized signal-to-noise ratio. Time-resolved spectra were recorded with ICCD-camera (Roper Scientific GmbH, Ottobrun, Germany) in the wavelength range between 446 nm and 617 nm. The delay time after the excitation laser pulse ranges from 0.03  $\mu$ s to 100.03  $\mu$ s, pulse energy was 0.3 mJ. Each spectrum was measured three times. For each spectrum 100 laser shots were averaged. 201 spectra at equidistant delay time were collected totally for one time-resolved spectrum.

The solution in the cuvette was excited by the applied laser pulse. Using a spectrograph (Roper Industries, Inc., USA) the fluorescence light from the sample was resolved into its intensities depending on the wavelength. To detect these intensities an array of photodiodes was used, which allowed the detection of the complete fluorescence spectrum simultaneously. To expose the diode array only during a definite and adjustable time, a gated intensifier was located





### **10.3.11. Measuring of pH**

pH values of the samples were measured using laboratory pH-Meter inoLab pH 720 (WTW, Weilheim, Germany) with BlueLine 16pH microelectrode (Schott Instruments, Mainz, Germany). The calibration was performed by means of standard buffers (WTW, Weilheim, Germany).

### **10.3.12. Experiments under CO<sub>2</sub>-Free Atmosphere**

The experiments, where the presence of CO<sub>2</sub> was excluded, were performed in the inert gas glove box (MBraun, Inertgas-Systeme GmbH, Garching, Germany) with nitrogen atmosphere (O<sub>2</sub> < 1 ppm).

### **10.3.13. Shaking of the Samples**

The samples were shaken on a horizontal shaker mod. Promax 2020 (Heidolph Instruments, Schwalbach, Germany).

### **10.3.14. Centrifugation of the Samples**

For the phases separation, the samples were centrifuged with Megafuge 1.0 (Heraeus Sepatech, Osterode/Harz, Germany) for 30 minutes by 4000 rpm.

### **10.3.15. Filtration of the Samples**

The supernatants of the samples were filtered using Minisart N membrane filters (Sartorius, Goettingen, Germany) with a pore size of 200 and/or 450 nm. Prior to the filtering, the filters were rinsed with 1 mL of sample solution. For study of the effect of the U(VI) sample filtration on the results, 5 nm filters from Microsep centrifugal devices (Pall GmbH, Dreieich, Germany) were additionally applied.

## 11. References

- [1] Palaban, R.T., Turner, D.R., Bertetti, E.P., Prikryl, J.D.: Uranium(VI) Sorption onto Selected Mineral Surfaces. Key Geochemical Parameters. In: *Adsorption of metals by geomedia: variables, mechanisms, and model applications* (Jenne, E.A., ed.). Academic Press, San Diego, 99 – 130 (1998).
- [2] Murphy, R.J., Lenhart, J.J., Honeyman, B.D.: The sorption of thorium(IV) and uranium(VI) to hematite in the presence of natural organic matter. *Coll. Surf. A: Physicochem. Eng. Asp.* **157**, 47 – 62 (1999).
- [3] McGraw-Hill Encyclopedia of Science and Technology. The McGraw-Hill Companies, Inc. <http://www.answers.com>.
- [4] Galán, E.: Genesis of clay minerals. Chapter 14. In: *Handbook of Clay Science. Developments in Clay Science, Vol. 1* (Bergaya, F., Theng, B.K.G., Lagaly, G., ed.). Elsevier Scientific Publishing Company, Amsterdam, London, New York, 1129 – 1162 (2006).
- [5] Clay Minerals. Academic classes. University of Minnesota, Department of Soil, Water, and Climate. <http://www.soils.umn.edu/academics/classes/soil2125/doc/s12chap1.htm>.
- [6] Bergaya, F., Lagaly, G.: General introduction: clays, clay minerals, and clay science. Chapter 1. In: *Handbook of Clay Science. Developments in Clay Science, Vol. 1* (Bergaya, F., Theng, B.K.G., Lagaly, G., ed.). Elsevier Scientific Publishing Company, Amsterdam, London, New York, 1 – 18 (2006).
- [7] Brigatti, M.F., Galán, E., Theng, B.K.G.: Structures and mineralogy of clay minerals. Chapter 2. In: *Handbook of Clay Science. Developments in Clay Science, Vol. 1* (Bergaya, F., Theng, B.K.G., Lagaly, G., ed.). Elsevier Scientific Publishing Company, Amsterdam, London, New York, 19 – 86 (2006).
- [8] Lagaly, G., Ogawa, M., Dékány, I.: Clay mineral organic interactions. Chapter 7.3. In: *Handbook of Clay Science. Developments in Clay Science, Vol. 1* (Bergaya, F., Theng, B.K.G., Lagaly, G., ed.). Elsevier Scientific Publishing Company, Amsterdam, London, New York, 309 – 377 (2006).

- [9] Claret, F., Schäfer, T., Bauer, A., Buckau, G.: Generation of humic and fulvic acid from Callovo-Oxfordian clay under high alkaline conditions. *Sci. Tot. Environ.* **317**, 189 – 200 (2003).
- [10] Claret, F., Bauer, A., Schäfer, T., Griffault, L., Lanson, B.: Experimental investigation of the interaction of clays with high-pH solutions: A case study from the Callovo-Oxfordian formation, Meuse-Haute Marne underground laboratory. *Clays Clay Miner.* **50**, 633 – 646 (2002).
- [11] Weaver, CH.E., Pollard, L.D.: The Chemistry of Clay Minerals. In: *Developments in Sedimentology*. Elsevier Scientific Publishing Company, Amsterdam, London, New York (1973).
- [12] Arnold, T., Zorn, T., Bernhard, G., Nitsche, H.: Sorption of uranium(VI) onto phyllite. *Chem. Geol.* **151**, 129 – 141 (1998).
- [13] Payne, T.E., Davis, J.A., Lumpkin, G.R., Chisari, R., Waite, T.D.: Surface complexation of uranyl sorption on Georgia kaolinite. *Appl. Clay Sci.* **26**, 151 – 162 (2002).
- [14] Brady, P.V., Cygan, R.T., Nagy, K.L.: Surface Charge and Metal Sorption to Kaolinite. In: *Adsorption of metals by geomeidia: variables, mechanisms, and model applications* (Jenne, E.A., ed.). Academic Press, San Diego, 371 – 382 (1998).
- [15] Moll, Jr., W.F.: Baseline studies of the clay minerals society source clays: Geological origin. *Clays Clay Miner.* **49**, 374 – 380 (2001).
- [16] Mermut, A.R., Cano, A.F.: Baseline studies of the clay minerals society source clays: Chemical analyses of major elements. *Clays Clay Miner.* **49**, 381 – 386 (2001).
- [17] Chipera, S.J., Bish, D.L.: Baseline studies of the clay minerals society source clays: Powder X-ray diffraction analyses. *Clays Clay Miner.* **49**, 398 – 409 (2001).
- [18] Wu, W.: Baseline studies of the clay minerals society source clays: Colloid and surface phenomena. *Clays Clay Miner.* **49**, 446 – 452 (2001).
- [19] Madejová, J., Komadel, P.: Baseline studies of the clay minerals society source clays: Infrared methods. *Clays Clay Miner.* **49**, 410 – 432 (2001).
- [20] Kogel, J.E., Lewis, S.A.: Baseline studies of the clay minerals society source clays: Chemical analysis by inductively coupled plasma-mass spectroscopy (ICP-MS). *Clays Clay Miner.* **49**, 387 – 392 (2001).

- [21] Borden, D., Giese, R.F.: Baseline studies of the clay minerals society source clays: Cation exchange capacity measurements by the ammonia-electrode method. *Clays Clay Miner.* **49**, 444 – 445 (2001).
- [22] Pruet, R.J., Webb, H.L.: Sampling and analysis of KGa-1b well-crystallized kaolin source clay. *Clays Clay Miner.* **41**, 514 – 519 (1993).
- [23] Redden, G.D., Jinhe, L., Leckie, J.: Adsorption of U(VI) and Citric Acid on Goethite, Gibbsite, and Kaolinite. Comparing results for Binary and Ternary Systems. In: *Adsorption of metals by geomedial: variables, mechanisms, and model applications* (Jenne, E.A., ed.). Academic Press, San Diego, 291 – 315 (1998).
- [24] Sutheimer, S.H., Maurice, P.A., Zhou, Q.: Dissolution of well and poorly crystallized kaolinites: Al speciation and effects of surface characteristics. *Am. Mineral.* **84**, 620 – 628 (1999).
- [25] Schroth, B.K., Sposito, G.: Surface charge properties of kaolinite. *Clays Clay Miner.* **45**, 85 – 91 (1997).
- [26] Sachs, S.: Personal communication.
- [27] Bauer, A.: Personal communication.
- [28] Gaffney, J.S., Marley, N.A., Clark, S.B.: Humic and Fulvic Acids. Isolation, Structure, and Environmental Role. In: *ACS Symposium Series 651*, American Chemical Society, Washington, DC, 2 – 16 (1996).
- [29] Aiken, G.R., McKnight, D.M., Werhaw, R.L., MacCarthy, P.: An Introduction to Humic Substances in Soil, Sediment, and Water. In: *Humic Substances in Soil, Sediment, and Water*. John Wiley & Sons, USA (1985).
- [30] Choppin, G.R.: The Role of Natural Organics in Radionuclide Migration in Natural Aquifer Systems. *Radiochim. Acta* **58/59**, 113 – 120 (1992).
- [31] Choppin, G.R., Allard, B.: Complexes of actinides with naturally occurring organic compounds. Chapter 11. In: *Handbook on the Physics and Chemistry of the Actinides* (Freeman, A.J., Keller, C., ed.). Elsevier Publishers B.V., 407 – 429 (1985).
- [32] Schulten, H.-R., Schnitzer, M.: A State of the Art Structural Concept for Humic Substances. *Naturwissenschaften* **80**, 29 – 30 (1993).

- [33] Wolf, M., Szymczak, W., Chanel, V., Buckau, G.: Molecular size and mass distribution of humic substances measured by AFFFF and TOF-SIMS. In: *Humic Substances in Performance Assessment of Nuclear Waste Disposal: Actinide and Iodine Migration in the Far-Field*. Second Technical Progress Report (Buckau, G., ed.). Forschungszentrum Karlsruhe, Institut für Nukleare Entsorgung. Wissenschaftliche Berichte, FZKA **6969**, 95 – 110 (2004).
- [34] Plancque, G., Amekraz, B., Moulin, V., Toulhoat, P., Moulin, Ch.: Molecular structure for fulvic acids by electrospray with quadrupole time-of-flight mass spectrometry. *Rapid Commun. Mass Spectrom.* **15**, 827 – 835 (2001).
- [35] Piccolo, A.: The Supramolecular Structure of Humic Substances. *Soil Sci.* **166**, 810 – 832 (2001).
- [36] Stevenson, F.J.: Organic matter reactions involving metal ions in soil. Chapter 16. In: *Humus Chemistry: Genesis, Composition and Reactions*. Second edition. John Wiley & Sons, New York (1994).
- [37] Pompe, S., Schmeide, K., Bubner, M., Geipel, G., Heise, K.H., Bernhard, G., Nitsche, H.: Investigation of humic acid complexation behavior with uranyl ions using modified synthetic and natural humic acids. *Radiochim. Acta* **88**, 553 – 558 (2000).
- [38] Kim, J.I., Czerwinski, K.R.: Complexation of Metal Ions with Humic Acid: Metal Ion Charge Neutralization Model. *Radiochim. Acta* **73**, 5 – 10 (1996).
- [39] Sachs, S., Bernhard, G.: NIR spectroscopic study of the complexation of neptunium(V) with humic acids: influence of phenolic OH groups on the complex formation. *Radiochim. Acta* **93**, 141 – 145 (2005).
- [40] Nash, K.L., Choppin, G.R.: Interaction of Humic and Fulvic Acids with Th(IV). *J. Inorg. Nucl. Chem.* **42**, 1045 – 1050 (1980).
- [41] Pompe S., Brachmann, A., Bubner, M., Geipel, G., Heise, K.H., Bernhard, G., Nitsche, H.: Determination and comparison of uranyl complexation constants with natural and model humic acids. *Radiochim. Acta* **82**, 89 – 95 (1998).
- [42] Sachs, S., Schmeide, K., Brendler, V., Křepelová, A., Mibus, J., Geipel, G., Heise, K.-H., Bernhard, G.: Synthesis and characterization of humic acids with specific functional properties. In: *Investigation of the Complexation and the Migration of Actinides and Non-*

*radioactive Substances with Humic Acids under Geogenic Conditions: Complexation of Humic Acids with Actinides in the Oxidation State IV Th, U, Np.* Forschungszentrum Rossendorf, Institute of Radiochemistry, Wissenschaftlich-Technische Berichte. FZR **399**, 3 – 19 (2004).

- [43] Stevenson, F.J.: *Humus Chemistry*. 1<sup>st</sup> ed., John Wiley & Sons, New York (1982).
- [44] Grauer, R.: Zur Koordinationschemie der Huminstoffe. Paul Scherrer Institut, Switzerland, Report No. 24, p.7 (1989).
- [45] Seaborg, G.T.: Overview of the Actinide and Lanthanide (the *f*) Elements. *Radiochim. Acta* **61**, 115 – 122 (1993).
- [46] Grenthe, I., Drożdżyński, J., Fujino, T., Buck, E.C., Albrecht-Schmitt, T.E., Wolf, S.F.: Uranium. Chapter 5. In: *The Chemistry of the Actinide and Transactinide Elements*. Third edition. Volume 1. (Moss, L.R., Edelstein, N.M., Fuger, J. ed.). Springer, Netherlands (2006).
- [47] Wolery, T.J.: EQ3/6, a Software Package for the Geochemical Modeling of Aqueous Systems. *UCRL-MA-110662 Part I*, Lawrence Livermore National Laboratory (1992).
- [48] Guillaumont, R., Fanghänel, T., Neck, V., Fuger, J., Palmer, D. A., Grenthe, I., Rand, M.H.: *Update on the Chemical Thermodynamics of Uranium, Neptunium, Plutonium, Americium and Technetium*. Elsevier, Amsterdam (2003).
- [49] Kim, J.I., Rhee, D.S., Wimmer, H., Buckau, G., Klenze, R.: Complexation of trivalent actinide ions ( $\text{Am}^{3+}$ ,  $\text{Cm}^{3+}$ ) with humic acid: A Comparison of different experimental methods. *Radiochim. Acta* **62**, 35 – 43 (1993).
- [50] Czerwinski, K.R., Buckau, G., Scherbaum, F., Kim, J.I.: Complexation of the uranyl ion with aquatic humic acid. *Radiochim. Acta* **65**, 111 – 119 (1994).
- [51] Glaus, M. A., Hummel, W., Van Loon, L. R.: Stability of Mixed-Ligand Complexes of Metal Ions with Humic Substances and Low Molecular Weight Ligands. *Environ. Sci. Technol.* **29**, 2150 – 2153 (1995).
- [52] Montavon, G., Mansel, A., Seibert, A., Keller, H., Kratz, J.V., Trautman, N.: Complexation Studies of  $\text{UO}_2^{2+}$  with Humic Acid at low Metal Ion Concentrations by Indirect Speciation Methods. *Radiochim. Acta* **88**, 17 – 24 (2000).

- [53] Sachs, S., Brendler, V., Geipel, G.: Uranium(VI) complexation by humic acid under neutral pH conditions studied by laser-induced fluorescence spectroscopy. *Radiochim. Acta* **95**, 103 – 110 (2007).
- [54] Lenhart, J.J., Cabaniss, S.E., MacCarthy, P., Honeyman, D.: Uranium(VI) complexation with citric, humic and fulvic acids. *Radiochim. Acta* **88**, 345 – 353 (2000).
- [55] Zeh, P., Czerwinski, K. R., Kim, J.I.: Speciation of uranium in Gorleben groundwaters. *Radiochim. Acta* **76**, 37 – 44 (1997).
- [56] Pashalidis, I.: U(VI) Mono-Hydroxo Humate Complexation. In: *Humic Substances in Performance Assessment of Nuclear Waste Disposal: Actinide and Iodine Migration in the Far-Field*. Second Technical Progress Report (Buckau, G., ed.). Forschungszentrum Karlsruhe, Institut für Nukleare Entsorgung. Wissenschaftliche Berichte, FZKA **6969**, 319 – 330 (2004).
- [57] Křepelová, A., Sachs, S., Bernhard, G.: Uranium(VI) sorption onto kaolinite in the presence and absence of humic acid. *Radiochimica Acta* **94**, 825 – 833 (2006).
- [58] Samadfam, M., Jintoku, T., Sato, S., Ohashi, H., Mitsugashira, T., Hara, M., Suzuki, Y.: Effects of humic acid on the sorption of Am(III) and Cm(III) on kaolinite. *Radiochim. Acta* **88**, 717 – 721 (2000).
- [59] Murphy, E.M., Zachara, J.M., Smith, S.C., Phillips, J.L.: The sorption of humic acids to mineral surfaces and their role in contaminant binding. *Sci. Tot. Environ.* **117/118**, 413 – 423 (1992).
- [60] Niitsu, Y., Sato, S., Ohashi, H., Sakamoto, Y., Nagao, S., Ohnuki, T., Muraoka, S.: Effects of humic acid on the sorption on neptunium(V) on kaolinite. *J. Nucl. Mat.* **248**, 328 – 332 (1997).
- [61] Kretzschmar, R., Hesterberg, D., Sticher, H.: Effects of Adsorbed Humic Acid on Surface Charge and Flocculation of Kaolinite. *Soil Sci. Soc. Am. J.* **61**, 101 – 108 (1997).
- [62] Takahashi, Y., Minai, Y., Kimura, T., Tominaga, T.: Adsorption of europium(III) and americium(III) on kaolinite and montmorillonite in the presence of humic acid. *J. Radioanal. Nucl. Chem.* **234**, 277 – 282 (1998).
- [63] Fairhurst, A.J., Warwick, P., Richardson, S.: The Effect of pH on Europium-Mineral Interactions in the Presence of Humic Acid. *Radiochim. Acta* **69**, 103 – 111 (1995).

- [64] Sakuragi, T., Tokuyama, A., Sato, S., Kozaki, T., Mitsugashira, T., Hara, M., Suzuki, Y.: Effects of calcium ions on the sorption of Am(III) and Eu(III) onto kaolinite in the presence of humic acid. *J. Nucl. Sci. Technol.* **3**, 520 – 523 (2002).
- [65] Murphy, E.M., Zachara, J.M., Smith, S.C., Phillips, J.L., Wietsma, T.W.: Interaction of hydrophobic organic compounds with mineral-bound humic substances. *Environ. Sci. Technol.* **28**, 1291 – 1299 (1994).
- [66] Murphy, E.M., Zachara, J.M.: The role of sorbed humic substances on the distribution of organic and inorganic contaminants in groundwater. *Geoderma* **67**, 103 – 124 (1995).
- [67] Murphy, E.M., Zachara, J.M., Smith, S.C.: Influence of mineral-bound humic substances on the sorption of hydrophobic organic compounds. *Environ. Sci. Technol.* **24**, 1507 – 1516 (1990).
- [68] Schulthess, C. P., Huang, C. P.: Humic and fulvic acid adsorption by silicon and aluminum oxide surfaces on clay minerals. *Soil Sci. Soc. Am. J.* **55**, 34 – 42 (1991).
- [69] Hizal, J., Apak, R.: Modeling of copper(II) and lead(II) adsorption on kaolinite-based clay minerals individually and in the presence of humic acid. *J. Coll. Interf. Sci.* **295**, 1 – 13 (2006).
- [70] Schmeide, K., Pompe, S., Bubner, M., Heise, K.-H., Bernhard, G., Nitsche, H.: Uranium(VI) sorption onto phyllite and selected minerals in the presence of humic acid. *Radiochim. Acta* **88**, 723 – 728 (2000).
- [71] Reich, T., Drebert, J., Křepelová, A., Sachs, S.: XPS Study of humic acid/kaolinite interaction. Forschungszentrum Rossendorf, Institute of Radiochemistry, Annual Report 2005. *FZR* **443**, p. 46 (2006).
- [72] Sachs, S., Bernhard, G.: Study of the humic acid synthesis in the presence of kaolinite and of the U(VI) adsorption onto a synthetic humic substance-kaolinite sorbate. Forschungszentrum Rossendorf, Institute of Radiochemistry, Annual Report 2004. *FZR* **419**, p. 49 (2005).
- [73] Ticknor, K.V.: Uranium Sorption on Geological Materials. *Radiochim. Acta* **64**, 229 – 236 (1994).



- [74] Hyun, S.P., Cho, Y.H., Hahn, P.S., Kim, S.J.: Sorption mechanism of U(VI) on a reference montmorillonite: Binding to the internal and external surfaces. *J. Radioanal. Nucl. Chem.* **250**, 55 – 62 (2001).
- [75] Turner, G.D., Zachara, J.M., McKinley, J.P. Smith, S.C.: Surface-charge properties and  $\text{UO}_2^{2+}$  adsorption of a subsurface smectite. *Geochim. Cosmochim. Acta* **60**, 3399 – 3414 (1996).
- [76] Kilislioglu, A., Bilgin, B.: Adsorption of uranium on halloysite. *Radiochim. Acta* **90**, 155 – 160 (2002).
- [77] Thompson, H.A., Parks, G.A., Brown, Jr., G.E.: Structure and Composition of Uranium(VI) Complexes at the Kaolinite-Water Interface. In: *Adsorption of metals by geomeidia: variables, mechanisms, and model applications* (Jenne, E.A., ed.). Academic Press, San Diego, 349 – 370 (1998).
- [78] McKinley, J.P., Zachara, J.M., Smith, S.C, Turner, G.D.: The influence of uranyl hydrolysis and multiple site-binding reactions on adsorption of U(VI) to montmorillonite. *Clays Clay Minerals* **43**, 586 – 598 (1995).
- [79] Rosentreter, J.J., Quarder, H.S., Smith, R.W., McLing, T.: Uranium Sorption onto Natural Sands as a Function of Sediment Characteristics and Solution pH. In: *Adsorption of metals by geomeidia: variables, mechanisms, and model applications* (Jenne, E.A., ed.). Academic Press, San Diego, 181 – 192 (1998).
- [80] Hongxia, Z., Zuyi, T.: Sorption of uranyl ions on silica: Effects of contact time, pH, ionic strength, concentration and phosphate. *J. Radioanal. Nucl. Chem.* **254**, 103 – 107 (2002).
- [81] Davis, J.A., Meece, D.E., Kohler, M., Curtis, G.P.: Approaches to surface complexation modelling of uranium(VI) adsorption on aquifer sediments. *Geochim. Cosmochim. Acta* **68**, 3621 – 3641 (2004).
- [82] Prikryl; J.D., Palaban, R.T., Turner, D.R., Leslie, B.W.: Uranium Sorption on  $\alpha$ -Alumina: Effects of pH and Surface-Area/Solution–Volume Ratio. *Radiochim. Acta* **66/67**, 291 – 296 (1994).
- [83] Ames, L.L., McGarrah, J.E., Walker, B.A.: Sorption of uranium and radium by biotite, muscovite, and phlogopite. *Clays Clay Miner.* **31**, 343 – 351 (1983).

- [84] Ames, L.L., McGarrah, J.E., Walker, B.A.: Sorption of trace constituents from aqueous solutions onto secondary minerals. I. Uranium. *Clays Clay Miner.* **31**, 321 – 334 (1983).
- [85] Labonne-Wall, N., Moulin, V., Vilarem, J.-P.: Retention Properties of Humic Substances onto Amorphous Silica: Consequences for the Sorption of Cations. *Radiochim. Acta* **79**, 37 – 49 (1997).
- [86] Beneš, P., Majer, V.: Trace chemistry of aqueous solutions: general chemistry and radiochemistry. Academia, Prague, 1980.
- [87] Waite, T.D., Davis, J.A., Payne, T.E., Waychunas, G.A., Xu, N.: Uranium(VI) adsorption to ferrihydrite: Application of a surface complexation model. *Geochim. Cosmochim. Acta* **58**, 5465 – 5478 (1994).
- [88] Payne, T.E., Lumpkin, G.R., Waite, T.D.: Uranium<sup>VI</sup> Adsorption on Model Minerals. Controlling Factors and Surface Complexation Modeling. In: *Adsorption of metals by geomedia: variables, mechanisms, and model applications* (Jenne, E.A., ed.). Academic Press, San Diego, 75 – 79 (1998).
- [89] Rabung, Th., Geckeis, H., Kim, J.I., Beck, P.: The Influence of Anionic Ligands on the Sorption Behaviour of Eu(III) on Natural Hematite. *Radiochim. Acta* **82**, 243 – 248 (1998).
- [90] Boulton, K.A., Cowper, M.M., Heath, T.G., Sato, H., Shibutani, T., Yui, M.: Towards an understanding of the sorption of U(VI) and Se(IV) on sodium bentonite. *J. Contamin. Hydrol.* **35**, 141 – 150 (1998).
- [91] Villalobos, M., Trotz, M.A., Leckie, J.O.: Surface Complexation Modeling Carbonate Effects on the Adsorption of Cr(VI), Pb(II), and U(VI) on Goethite. *Environ. Sci. Technol.* **35**, 3849 – 3856 (2001).
- [92] Bradbury, M.H., Baeyens, B.: Modelling the sorption of Mn(II), Co(II), Ni(II), Zn(II), Cd(II), Eu(III), Am(III), Sn(IV), Th(IV), Np(V) and U(VI) on montmorillonite: Linear free energy relationships and estimates of surface binding constant for some selected heavy metals and actinides. *Geochim. Cosmochim. Acta* **69**, 875 – 892 (2005).
- [93] Beneš, P., Kratzer, K., Vlčková, Š., Šebestová, E.: Adsorption of Uranium on Clay and the Effect of Humic Substances. *Radiochim. Acta* **82**, 367 – 373 (1998).
- [94] Reich, T. Ye., Kokrshunov, M.E., Antonova, T. V., Ageev, A.L., Moll, H., Reich, T.: New Regularization Method for EXAFS Analysis. *AIP Proceedings XAFS 13*, in press.

- [95] Pashalidis, I., Czerwinsky, K., R., Fanghänel, Th., Kim, J.I.: Solid-Liquid Phase Equilibria of Pu(VI) and U(VI) in Aqueous Carbonate Systems. Determination of Stability Constants. *Radiochim. Acta* **76**, 55 – 62 (1997).
- [96] Coppin, F., Berger, G., Bauer, A., Castet, S., Loubet, M.: Sorption of lanthanides on smectite and kaolinite. *Chem. Geol.* **182**, 57 – 68 (2002).
- [97] Cama, J., Metz, V., Ganor, J.: The effect of pH and temperature on kaolinite dissolution rate under acidic conditions. *Geochim. Cosmochim. Acta* **66**, 3912 – 3926 (2002).
- [98] Huertas, F.J., Chou, L., Wollast, R.: Mechanism of kaolinite dissolution at room temperature and pressure. Part II: Kinetic study. *Geochim. Cosmochim. Acta* **63**, 3261 – 3275 (1999).
- [99] Kornilovich, B., Pshinko, G., Spasenova, L., Kovalchuk, I.: Influence of Humic Substances on the Sorption Interactions between Lanthanide and Actinide Ions and Clay Minerals. *Adsorption Sci. Technol.* **18**, 873 – 880 (2000).
- [100] Schmeide, K., Brendler, V., Pompe, S., Bubner, M., Heise, K.H. Bernhard, G.: Kinetic Studies of the Uranium(VI) and Humic Acid Sorption onto Phyllite, Ferrihydrite and Muscovite. In: *Effects of Humic Substances on the Migration of Radionuclides: Complexation and Transport of Actinides*. Third Technical Progress Report (Buckau, G., ed.). Forschungszentrum Karlsruhe, Institut für Nukleare Entsorgung. Wissenschaftliche Berichte, FZKA **6524**, 149 – 169 (2000).
- [101] Reiller, P., Casanova, F., Moulin, V.: Influence of Addition Order and Contact Time on Thorium(IV) Retention by Hematite in the Presence of Humic Acids. *Environ. Sci. Technol.* **39**, 1641 – 1648 (2005).
- [102] Payne, T. E., Davis, J.A., Waite, T.D.: Uranium adsorption on ferrihydrite – effects of phosphate and humic acid. *Radiochim. Acta* **74**, 239 – 243 (1996).
- [103] Hennig, C., Reich, T., Dähn, R., Scheidegger, A. M.: Structure of uranium sorption complexes at montmorillonite edge sites. *Radiochim. Acta* **90**, 653 – 657 (2000).
- [104] Farideh, J.: X-Ray Absorption Spectroscopy.  
<http://www.chem.ucalgary.ca/research/groups/faridehj/xas.pdf>.
- [105] Teo, B.K.: EXAFS: Basic Principles and Data Analysis. In: *Inorganic Chemistry Concepts*. Vol. 9. Springer-Verlag, Berlin (1986).

- [106] Behrens, P.: X-ray absorption spectroscopy in chemistry. I. Extended X-ray absorption fine structure. *Trends Anal. Chem.* **11**, 218 – 222 (1992).
- [107] Denecke, M. A., Pompe, S., Reich, T., Moll, H., Bubner, M., Heise, K.-H., Nicolai, R., Nitsche, H.: Measurements of the Structural Parameters for the Interaction of Uranium(VI) with Natural and Synthetic Humic Acids using EXAFS. *Radiochim. Acta* **79**, 151 – 159 (1997).
- [108] Schmeide, K., Sachs, S., Bubner, M., Reich, T., Heise, K.-H., Bernhard, G.: Interaction of uranium(VI) with various modified and unmodified natural and synthetic humic substances studied by EXAFS and FTIR spectroscopy. *Inorg. Chim. Acta* **351**, 133 – 140 (2003).
- [109] Sachs, S., Schmeide, K., Reich, T., Brendler, V., Heise, K.H., Bernhard, G.: EXAFS study on neptunium(V) complexation by various humic acids under neutral pH conditions. *Radiochim. Acta* **93**, 17 – 25 (2005).
- [110] Schmeide, K., Reich, T., Sachs, S., Brendler, V., Heise, K.-H., Bernhard, G.: Neptunium(IV) complexation by humic substances studied by X-ray absorption fine structure spectroscopy. *Radiochim. Acta* **93**, 187 – 196 (2005).
- [111] Reich, T., Moll, H., Arnold, T., Denecke, M.A., Hennig, C., Geipel, G., Bernhard, G., Nitsche, H., Allen, P.G., Bucher, J. J., Edelstein, N.M., Shuh, D.K.: An EXAFS study of uranium(VI) sorption onto silica gel and ferrihydrite. *J. El. Spectr. Rel. Phenom.* **96**, 237 – 243 (1998).
- [112] Sylwester, E. R., Hudson, E. A., Allen, P. G.: The structure of uranium (VI) sorption complexes on silica, alumina, and montmorillonite. *Geochim. Cosmochim. Acta* **64**, 2431 – 2438 (2000).
- [113] Wheaton, V., Majumdar, D., Balasubramanian, K., Chauffe, L, Allen, P.G.: A comparative theoretical study of uranyl silicate complexes. *Chem. Phys. Letters* **371**, 349 – 359 (2003).
- [114] Moyes, L.N., Parkman, R.H., Charnock, J.M., Vaughan, D.J., Livens, F.R., Hughes, C.R., Braithwaite, A.: Uranium Uptake from Aqueous Solution by Interaction with Goethite, Lepidocrocite, Muscovite, and Mackinawite: An X-ray Absorption Spectroscopy Study. *Environ. Sci. Technol.* **34**, 1062 – 1068 (2000).

- [115] Walter, M., Arnold, T., Geipel, G., Scheinost, A., Bernhard, G.: An EXAFS and TRLFS investigation on uranium(VI) sorption to pristine and leached albite surfaces. *J. Coll. Interf. Sci.* **282**, 293 – 305 (2005).
- [116] George, G.N., Pickering, I.J.: EXAFSPAK: A Suite of Computer Programs for Analysis of X-ray Absorption Spectra. Stanford Synchrotron Radiation Laboratory, Stanford, CA, USA (1995).
- [117] Ankudinov, A. L. et al.: Parallel calculation of electron multiple scattering using Lanczos algorithms. *Phys. Rev. B* **65**, 104107 (2002).
- [118] Hudson, E.A., Rehr, J.J., Bucher, J.J.: Multiple-Scattering Calculations of the Uranium L<sub>III</sub>-edge X-ray Absorption Near-Edge Structure. *Phys. Rev. B* **52**, 13815 – 13826 (1995).
- [119] Babanov, Yu.A., Vasin, V.V., Ageev, A.L., Ershov, N.V.: A New Interpretation of EXAFS Spectra in Real Space. 1. General Formalism. *Phys. Stat. Sol (B)* **105**, 747 – 754 (1981).
- [120] Stumpf, Th., Bauer, A., Choppin, F., Fanghänel, Th., Kim, J.I.: Inner-sphere, outer-sphere and ternary surface complexes: a TRLFS study of the sorption process of Eu(III) onto smectite and kaolinite. *Radiochim. Acta* **90**, 345 – 349 (2002).
- [121] Gabriel, U., Charlet, L., Schläpfer, C.W., Vial, J. C., Brachmann, A., Geipel, G.: Uranyl surface speciation on silica particles studies by time-resolved laser-induced fluorescence spectroscopy. *J. Coll. Interf. Sci.* **239**, 358 – 368 (2001).
- [122] Baumann, N., Brendler, V., Arnold, T., Geipel, G., Bernhard, G.: Uranyl sorption onto gibbsite studied by time-resolved laser-induced fluorescence spectroscopy (TRLFS). *J. Coll. Interf. Sci.* **290**, 318 – 324 (2005).
- [123] Tits, J., Stumpf, T., Rabung, T., Wieland, E., Fanghänel, T.: Uptake of Cm(III) and Eu(III) by calcium silicate hydrates: A solution chemistry and time-resolved laser fluorescence spectroscopy study. *Environ. Sci. Technol.* **37**, 3568 – 3573 (2003).
- [124] Rabung, Th., Stumpf, Th., Geckeis, H., Klenze, R., Kim, J.I.: Sorption of Am(III) and Eu(III) onto  $\gamma$ -alumina: experiment and modelling. *Radiochim. Acta* **88**, 711 – 716 (2000).
- [125] Stumpf, T., Bauer, A., Choppin, F., Kim, J.I.: Time-resolved laser fluorescence spectroscopy study of the sorption of Cm(III) onto smectite and kaolinite. *Environ. Sci. Technol.* **35**, 3691 – 3694 (2001).

- [126] Arnold, T., Utsunomiya, S., Geipel, G., Ewing, R.C., Baumann, N., Brendler, V.: Adsorbed U(VI) Surface Species on Muscovite Identified by Laser Fluorescence Spectroscopy and Transmission Electron Microscopy. *Environ. Sci. Technol.* **40**, 4646 – 4652 (2006).
- [127] Lakowicz, J.R. *Principles of Fluorescence Spectroscopy*. 2<sup>nd</sup> Edition. Kluwer Academics / Plenum Publishers. New York (1999).
- [128] Otto, M.: *Analytische Chemie*, VCH Verlagsgesellschaft, Weinheim, New York, Basel, Cambridge, Tokyo (1995).
- [129] Perkampus, H.-H.: *Lexikon Spektroskopie*, VCH Verlagsgesellschaft, Weinheim (1993).
- [130] Bell, J.T., Biggers, R.E.: Absorption Spectrum of the Uranyl Ion in Perchlorate Media. III. Resolution of the Ultraviolet Band Structure; Some Conclusions Concerning the Excited State of  $\text{UO}_2^{2+}$ . *J. Mol. Spectr.* **25**, 312 – 329 (1968).
- [131] Brendler, V., Brachmann, A., Geipel, G.: Software to compute fluorescence lifetimes from time-resolved laser-induced fluorescence spectroscopy (TRLFS) studies, exploiting the full spectrum. *Forschungszentrum Rossendorf, Institute of Radiochemistry, Annual Report 1996*. *FZR* **180**, 13 – 14 (1997).
- [132] Geipel, G., Bernhard, G., Rutsch, M., Brendler, V., Nitsche, H.: Spectroscopic properties of uranium(VI) minerals studied by time-resolved laser-induced fluorescence spectroscopy (TRLFS). *Radiochim. Acta* **88**, 757 – 762 (2000).
- [133] Křepelová, A., Brendler, V., Sachs, S., Baumann, N., Bernhard, G.: New TRLFS measurements of U(VI) sorption onto gibbsite. *Forschungszentrum Dresden-Rossendorf, Institute of Radiochemistry, Annual Report 2006*, in press.
- [134] Trepte, P.: Sorption von Radionukliden an Tongestein: Spektroskopische Referenzdaten. Diploma thesis, University of Applied Science, Dresden (2006).
- [135] Czerwinski, K.R., Kim, J.I., Rhee, D.S., Buckau, G.: Complexation of trivalent actinide ions ( $\text{Am}^{3+}$ ,  $\text{Cm}^{3+}$ ) with humic acid: The effect of ionic strength. *Radiochim. Acta* **72**, 179 – 187 (1996).
- [136] Panak, P., Klenze, R., Kim, J.I.: A Study of Ternary Complexes of Cm(III) with Humic Acid and Hydroxide of Carbonate in Neutral pH Range by Time-Resolved Laser Fluorescence Spectroscopy. *Radiochim. Acta* **74**, 141 – 146 (1996).

- [137] Kim, J.I., Buckau, G., Bryant, E., Klenze, R.: Complexation of americium(III) with humic acid. *Radiochim. Acta* **48**, 135 – 143 (1989).
- [138] Wenming, D., Hongxia, Z., Meide, H., Zuyi, T.: Use of the ion exchange method for determination of stability constants of trivalent metal complexes with humic and fulvic acids. Part I:  $\text{Eu}^{3+}$  and  $\text{Am}^{3+}$  complexes in weakly acidic conditions. *Appl. Radiation Isotopes* **56**, 959 – 965 (2002).
- [139] Sakuragi, T., Sawa, S., Sato, S., Kozaki, T., Mitsugashira, T., Hara, M., Suzuki, Y.: Complexation of americium(III) with humic acid by cation exchange and solvent extraction. *J. Radioanal. Nucl. Chem.* **26**, 309 – 314 (2004).
- [140] Morgenstern, M., Klenze, R., Kim, J.I.: The formation of mixed-hydroxo complexes of Cm(III) and Am(III) with humic acid in the neutral pH range. *Radiochim. Acta* **88**, 7 – 16 (2000).
- [141] Murali, M.S., Mathur, J.N.: Sorption characteristics of Am(III), Sr(II) and Cs(I) on bentonite and granite. *J. Radioanal. Nucl. Chem.* **254**, 129 – 136 (2002).
- [142] Takahashi, Y., Minai, Y., Kimura, T., Meguro, Y., Tominaga, T.: Formation of actinide(III)-humate and its influence on adsorption on kaolinite. In: *Mat. Res. Soc. Symp. Proc.* **353**, Materials Research Society, 189 – 196 (1995).
- [143] Wang, L., Maes, A., De Canniere, P., van der Lee, J.: Sorption of Europium on Illite (Silver Hill Montana). *Radiochim. Acta* **82**, 233 – 237 (1998).
- [144] Sakuragi, T., Seichi, S., Kozaki, T., Mitsugashira, T., Hara, M., Suzuki, Y.: Am(III) and Eu(III) uptake on hematite in the presence of humic acid. *Radiochim. Acta* **92**, 697 – 702 (2004).
- [145] Samadfam, M., Sato, S., Ohashi, H.: Effect of Humic Acid on the Sorption of Eu(III) onto Kaolinite. *Radiochim. Acta* **82**, 361 – 365 (1998).
- [146] Kimura, T., Kato, Y.: Luminescence study on determination of the inner-sphere hydration number of Am(III) and Nd(II). *J. Alloys Comp.* **271 – 273**, 867 – 871 (1998).
- [147] Thouvenot, P., Hubert, S., Moulin, C., Decambox, P., Mauchien, P.: Americium trace determination in aqueous and solid matrices by time-resolved laser-induced fluorescence. *Radiochim. Acta* **61**, 15 – 21 (1993).

- [148] Stumpf, T., Marques Fernandes, M., Walther, C., Dardenne, K., Fanghänel, Th.: Structural characterization of Am(III) incorporated into calcite: A TRLS and EXAFS study. *J. Coll. Interf. Sci.* **302**, 240 – 245 (2006).
- [149] Yusov, A.B.: Luminiscence of transplutonium elements in solutions and its application. *Radiochem.* **35**, 1 – 14 (1993).
- [150] Stover, B.J., Conway, J.G., Cunningham, B.B.: The solution absorption spectrum of americium. *J. Am. Chem. Soc.* **73**, 491 – 492 (1951).
- [151] Geipel, G., Stumpf, Th.: Determination of the hydration number of the first solvation shell of Am<sup>3+</sup>. Forschungszentrum Rossendorf, Institute of Radiochemistry, Annual Report 2004, FZR **419**, p. 18 (2005).
- [152] Kimura, T., Choppin, G.R.: Luminescence study on determination of the hydration number of Cm(III). *J. Alloys Comp.* **213/214**, 313 – 317 (1994).
- [153] Chipera, S.J., Guthrie, G.D., Bish, D.L.: Preparation and purification of mineral dusts. In: *Health Effects of Mineral Dusts* (Guthrie, G.D., Mossman, B.T., ed.). Mineralogical Society of America, Reviews in Mineralogy **28**, p. 235 – 249 (1993).
- [154] Sumner, M.E., Miller, W.P.: Cation Exchange Capacity and Exchange Coefficients. Chapter 40. In: *Methods of Soil Analysis. Part 3: Chemical Methods* (Bigham, J.M., ed.). Soil Science Society of America, Inc., USA, 1201 – 1229 (1996).
- [155] Matz, W., Schell, N., Bernhard, G., Prokert, F., Reich, T., Claussner, J., Oehme, W., Schlenk, R., Dienel, S., Funke, H., Eichhorn, F., Betzl, M., Prohl, D., Strauch, U., Huttig, G., Krug, H., Neumann, W., Brendler, V., Reichel, P., Denecke, M.A., Nitsche, H.: ROBL - a CRG beamline for radiochemistry and materials research at the ESRF. *J. Synchrotron Rad.* **6**, 1076 – 1085 (1999).
- [156] Geipel, G., Brachmann, A., Brendler, V., Bernhard, G., Nitsche, H.: Uranium(VI) Sulfate Complexation Studied by Time-Resolved Laser-Induced Fluorescence Spectroscopy (TRLFS). *Radiochim. Acta* **75**, 199 – 204 (1996).



## Acknowledgements

First and foremost, I would like to thank Prof. Dr. G. Bernhard for the possibility to work on this interesting scientific task and to accomplish the thesis in the Institute of Radiochemistry of Forschungszentrum Dresden-Rossendorf. As well I would like to thank Dr. K.-H. Heise for the invitation and initial collaboration and for his support by applying for the Ph.D. position.

I would like to express my great appreciation to my supervisor Dr. S. Sachs for the scientific guidance through my Ph.D. study and for the time spent by the discussions. I would also like to thank for being so patient with reading the dissertation and last but not least for helping me to improve my German language.

I would like to appraise the discussions and support of Prof. Dr. T. Reich by the EXAFS analysis; I spent two really exciting days by EXAFS in Mainz.

I want to thank Dr. V. Brendler for helpful and fruitful consultations by TRLFS analysis and for the speciation calculation and Dr. G. Geipel for Am laser fluorescence measurements and the discussion of TRLFS analysis.

Furthermore, I want to express my gratitude to:

Dr. J. Mibus for his advices, remarks, and enthusiasm given to me.

R. Ruske and M. Meyer for their help in lab and useful advices by experimental work.

Dr. A. Scheinost, Dr. H. Funke, Dr. H. Hennig, and Dr. A. Roßberg for EXAFS measurements and Dr. A. Roßberg also for his help by EXAFS analysis.

ESRF and ROBL for providing the beam time.

Dr. N. Baumann for the performance of TRLFS, C. Eckardt for BET measurements, C. Nebelung for  $\alpha$ - and  $\gamma$ -spectroscopy and LS spectra deconvolution, Dr. A. Bauer for kaolinite size fractionation, Prof. Dr. T. Reich for XPS measurements and K. Muschter, U. Schaefer, and A. Scholz for IR, ICP-MS, and XRD measurements, respectively.

All my colleagues, which made so pleasant, dynamic and creative working atmosphere during my doctoral study.

Finally, most thanks to my great parents and my wonderful husband for the welfare and patience.

I also acknowledge the financial support of this work by German Federal Ministry of Economics and Technology projects No. 02E9673 and 02E10156 and EU project FUNMIG.



## **Erklärung**

Die Vorliegende Arbeit entstand im Institut für Radiochemie des Forschungszentrums Dresden-Rossendorf, e.V. unter der wissenschaftlichen Betreuung von Herrn Prof. Dr. Gert Bernhard. Die Betreuung der Arbeit unterlag außerdem Frau Dr. Susanne Sachs.

Es haben bisher keine weiteren Promotionsverfahren stattgefunden.

Ich erkenne die Promotionsordnung der Fakultät für Mathematik und Naturwissenschaften der Technischen Universität Dresden vom 20.03.2000 in der Fassung vom 16.4.2003 an.

## **Versicherung**

Hiermit versichere ich, dass ich die vorliegende Arbeit ohne unzulässige Hilfe Dritter und ohne Benutzung anderer als der angegebenen Hilfsmittel angefertigt habe; die aus fremden Quellen direkt oder indirekt übernommenen Gedanken sind als solche kenntlich gemacht. Die Arbeit wurde bisher weder im Inland noch im Ausland in gleicher oder ähnlicher Form einer anderen Prüfungsbehörde vorgelegt.

Dresden, den 02.02.2007

Adéla Křepelová